# Secure Visible Light Communication Systems Based on the Position of the User

**Farag Ibrahim Khalifa Mousa**

PhD

2017

# Secure Visible Light Communication Systems Based on the Position of the User

by

**Farag Ibrahim Khalifa Mousa**

A thesis submitted in partial fulfilment of the requirements of the University of Northumbria at Newcastle for the degree of Doctor of Philosophy

Research undertaken in the School of Computing, Engineering and Information Sciences

September 2017

I dedicate this work to my family

# Declaration

I hereby declare that I composed this work contained in this thesis which is to assessment on the programme of study leading to the award of PhD has not been submitted for any other award and that it is all my own work unless a precise reference in this regard to the work of others.

**I declare that the Word Count of this Thesis is 37,931 words**

Name: Farag Ibrahim Khalifa Mousa

Signature:… *Farag Mousa*

Date:……05/06/2018

# Acknowledgment

First and foremost, I would like to thank my principal supervisor Professor Krishna Busawon for providing me endless support, guidance and encouragement throughout my research work. Krishna offered his full confidence, enthusiasm and showed a lot of patience toward me at every turn. I am grateful to Professor Ahmed Bouridane as my second supervisor for always providing me his extensive and fruitful discussions, guidance and continuous supports usually at the expense of his own time. I will be forever indebted to him.

I wish to express my gratitude to Northumbria University, Mathematics, Physics and Electrical Engineering, English language centre and all wonderful people who I met during this journey, especially my colleagues from our area zone in EBE building who are friendly and scientific. I also would like to thank Azzaytuna University; Libya, Ministry of Higher Education and Scientific Research and Libyan government.

I wish to thank my previous supervision team, Dr Hoa Le-Minh and Dr Xuewu Dai as well as I am also grateful for all help from Optical Communication Research Group (ORCG) members.

Last but not the least, I hereby would like to offer my heartfelt thanks to my family and friends, especially to my mother and sisters. They never left my back and removed the happy encouraging smile from their faces.

# Abstract

In the past few decades, there has been a growing demand for bandwidth in wireless communication systems due to an increase in the number of mobile users, computer network applications and high speed internet access and services. Visible light communication (VLC) is a newly emerging technology in optical wireless communication (OWC) systems to provide both illumination and high-speed data communication. In addition, it can also be used for indoor positioning or localization with wide applications that has merited a number of attractive research studies. However, security in wireless communications has become a matter of concern due to the possibility of unauthorised access to transmitted data.

This thesis investigates received optical power (ROP) distribution to achieve illumination requirements for both optimal and sub-optimal Lambertian order in single and four cell configurations. Furthermore, it proposes VLC-based indoor positioning by using the received optical power levels from the emitting LEDs. Both scenarios of line-of-sight (LOS) and line-of-sight with non-line-of-sight (LOSNLOS) positioning are considered. The performance of the proposed system is evaluated under both noisy and noiseless channel cases and the impact of different location codes on the positioning error is also investigated. An analytical model of the system with noise and the corresponding numerical evaluation for a range of signal to noise ratios (SNRs) are presented. The results show that an accuracy of 8 cm in average is achievable at an SNR of 15 dB in the LOSNLOS scenario. We also introduce a novel approach for recovering 4×4 MIMO–VLC data with partial channel state information (CSI) knowledge both in noisy and noiseless cases. In addition, the proposed indoor localization system utilizing two visible light emitting diodes for different environments offering less complexity for both LOS and LOSNLOS scenarios is offered. The results of the scheme is compared with existing trilateration techniques and the

performance of the proposed system is evaluated with a reported accuracy of less than 20 cm for SNR values of greater than 13 dB.

This thesis also proposes a new secure single input single output (SISO) VLC system and investigates the bit error rate (BER) performance with and without encryption in the Media Access Control (MAC) layer and physical layer for both the LOS and LOSNLOS scenarios. For a BER of $10^{-3}$, the results show that there is 1 to ~ 3.5 dB power penalties for the secured VLC system for data rates of up to 10 Mbps. The key length impact on the error propagation is also investigated.

Finally, this thesis proposes a secure MIMO VLC system that relies on the position of the user by incorporating a new modified version of the Rivest-Shamir-Adleman (RSA) technique for encrypting the transmitted data in the MAC layer. Furthermore, the ability of the proposed system to control the size of the encrypted cell depending on the application environment is demonstrated.

# Table of Contents

# List of Figures

# List of Tables

# Glossary of Abbreviations

| | |
|---|---|
| 1D | One Dimension |
| 2D | Two Dimension |
| 3D | Three Dimension |
| 4G | Fourth Generation |
| 5G | Fifth Generation |
| AES | Advance Encryption Standard |
| AOA | Angle of Arrival |
| APD | Avalanche Photodiode |
| AWGN | Additive White Gaussian Noise |
| BER | Bit Error Rate |
| CAP | Carrier Amplitude Power |
| CDMMC | Combined Deterministic and Modified Monte Carlo |
| CIA | Confidentiality, Integrity, Availability |
| COEC | Centre of Encrypted Cell |
| CORA | Centre of the Receiver |
| CRB | Cramer Rao Bound |
| CSI | Channel State Information |
| CSR | Correlation Sum Ratio |
| DC | Direct Current |
| DES | Data Encryption Standard |
| DMT | Discrete Multitones |
| DSSS | Direct Sequence Spread Spectrum |
| DTMF | Dual Tone Multi Frequency |
| ECC | Elliptic Curve Cryptography |
| ER | Extinction Ratio |
| EVM | Error Vector Magnitude |
| FHSS | Frequency Hopping Spread Spectrum |
| FOV | Field of View |
| FPGA | Field Programmable Gate Array |
| FSO | Free Space Communication |

| | |
|---|---|
| GaN | Gallium Nitride |
| gcd | Greatest Common Divisor |
| GNFS | Generalized Number Field Sieve |
| GPS | Global Positioning System |
| IEEE | Institute of Electrical and Electronic Engineers |
| IM/DD | Intensity Modulation/ Direct Detection |
| INS | Inertial Navigation System |
| IoT | Internet of Things |
| IPS | Indoor Positioning Services |
| IR | Infra-red |
| ISI | Intersymbol Interference |
| ISO | International for Organization Standardization |
| LAN | Local Area Network |
| LD | Laser Diode |
| LEC | Length of Encrypted Cell |
| LED | Light Emitting Diode |
| Li-Fi | Light Fidelity |
| LOS | Line of Sight |
| LOSNLOS | Line of sight and non-line of sight |
| LMMSE | Least minimum mean square error |
| L-PPM | L-Pulse Position Modulation |
| LS | Least Square |
| MAC | Media Access Control |
| MHz | Mega Hertz |
| MIMO | Multi Input Multiple Output |
| ML | Maximum Likelihood |
| MMSE | Minimum Mean Square Error |
| M-PAM | M-ary Pulse Amplitude Modulation |
| MPUED | Maximum Percentage of Unencrypted Data |
| NLOS | Non Line of Sight |
| NRZ | Non Return to Zero |
| OFDM | Orthogonal Frequency Division Multiplexing |
| OFDMA | Orthogonal Frequency Division Multiplexing Access |
| OLO | Optimum Lambertian Order |
| OMIMO | Optical Multi Input Multiple Output |

| | |
|---|---|
| OOC | Optical Orthogonal Codes |
| OOK | On Off Keying |
| OTK | One Time Key |
| OWC | Optical Wireless Communication |
| P/S | Parallel to Serial |
| PD | Photodetector |
| PI | Pseudo-Inversion |
| PIN | Positive-Intrinsic Negative |
| PRBS | Pseudo Random Bit Stream |
| PS | Pilot Signal |
| PSD | Power Spectral Density |
| QAM | Quadrature Amplitude Modulation |
| QKD | Quantum Key Distribution |
| QoS | Quality of Service |
| RF | Radio Frequency |
| RFID | Radio Frequency Identification |
| RGB | Red-Green-Blue |
| RLS | Received Light Signal |
| RMSED | Root Mean Square Error Distance |
| ROP | Received Optical Power |
| RSA | Rivest-Shamir Adleman |
| RSSI | Received Signal Strength Indication |
| RSSR | Received Signal Strength Ratio |
| Rx | Receiver |
| RZ | Return to Zero |
| S/P | Serial to Parallel |
| SIMO | Single Input Multiple Output |
| SISO | Single Input Single Output |
| SNFS | Special Number Field Sieve |
| SNR | Signal to Noise Ratio |
| SQL | Structured Query Language |
| SwERP | Switching Estimated Receiver Position |
| TDM | Time Division Multiplexing |
| TDOA | Time Difference of Arrival |
| THz | Tera Hertz |

| | |
|---|---|
| TOA | Time of Arrival |
| Tx | Transmitter |
| VLC | Visible Light Communication |
| WDM | Wavelength Division Multiplexing |
| Wi-Fi | Wireless Fidelity |
| Wi-Max | Worldwide Interoperability for Microwave Access |
| WLAN | Wireless Local Area Network |
| WPLED | White Phosphor Light Emitting Diode |
| WSN | Wireless Sensor Network |
| YAG | Yitrium Aluminium |
| ZF | Zero Forcing |

# Glossary of Symbols

| | |
|---|---|
| $E_i$ | Energy |
| $h$ | Planck's constant (eVs) |
| $f$ | Frequency of light waves |
| $c$ | Speed of light waves |
| $\lambda$ | Wavelength of light waves |
| $\Phi$ | Luminous flux |
| $\Phi_e$ | Energy flux |
| $V(\lambda)$ | Luminous efficiency |
| $k_m$ | The maximum visibility |
| $\Lambda$ | Photodetector sensitivity |
| $\Re$ | The responsivity of photodetector |
| $y(t)$ | Photocurrent, |
| $x(t)$ | Transmitted optical power |
| $n(t)$ | Channel noise |
| $\otimes$ | The convolution process |
| $h(t)$ | Impulse response of optical channel |
| $t_0$ | Minimum delay |
| $P_{max}$ | Average power requirement for eye safety requirements |
| $\theta$ | Irradiance light angle |
| $R_0(\theta)$ | Angular distribution |
| $m_l$ | Lambertian emission |
| $\theta_{1/2}$ | Semi-angle at half luminance of the LED |
| $S(\theta)$ | Radiant intensity |
| $A_r$ | Active area of the photodetector |
| $\psi$ | Incident light angle |
| $A_{\text{eff}}(\psi)$ | Effective collection area of the photodetector |
| $n$ | Refractive index |
| $g(\psi)$ | Gain of an optical filter |
| $\mathrm{T_s}(\psi)$ | Optical gain of the concentrator |
| $L$ | Distance between the transmitter and receiver |

| | |
|---|---|
| $\mathrm{H_{ch,LOSi}}(0)$ | DC gain of the OWC channel |
| $P_{\mathrm{r\_LOS}}$ | Received optical power from LOS scenario |
| $P_t$ | Transmitted optical power |
| $\mathrm{H_{ch,ref}}(0)$ | DC gain for single multipath |
| $\rho$ | Reflectance factor |
| $\mathrm{dA_{wall}}$ | Reflective area of the small region |
| $\mathrm{L_1}$ | Distance between LED and a reflective point |
| $\mathrm{L_2}$ | Distance between a reflective point and a receiver |
| $\alpha_{\mathrm{r}}$ | Angle of incidence from multipath |
| $\beta_{\mathrm{r}}$ | Radiance angle to a reflective point from multipath |
| $I_p$ | Average photocurrent |
| $P_p$ | Incident optical power |
| $q$ | Electronic charge |
| $\eta_i$ | Quantum efficiency of the device in electrons per photon |
| $hv$ | Photon energy |
| $v$ | Photon frequency (m/s) |
| $R_f$ | Reflectivity at the entrance face of the photodiode |
| $\alpha$ | Absorption coefficient |
| $\eta_B$ | Efficiency of bandwidth |
| $B$ | Bandwidth of the IR transceiver |
| $\gamma$ | Average duty cycle |
| $E_{pulse}$ | Pulse energy |
| $E_B$ | Average energy per bit |
| $T_b$ | Bit duration |
| $\emptyset_{OOK}(t)$ | OOK signal |
| $PSD_{OOK,NRZ}\ (f)$ | Electrical power spectral density(PSD) of OOK-NRZ. |
| $PSD_{OOK,RZ(\gamma=0.5)}\ (f)$ | Electrical power spectral density(PSD) of OOK-RZ. |
| $\delta()$ | Dirac delta function |
| $\eta_P$ | Power efficiency |
| $\gamma$ | Duty cycle |
| $I_d$ | Dark current |
| $I_{\mathrm{l}}$ | Surface leakage current |
| $B_n$ | Equivalent noise bandwidth |
| $M$ | Gain factor |

| | |
|---|---|
| $I_T$ | Average of the total output current |
| $I_P$ | Principal photocurrent |
| $\sigma_{shot}^2$ | Total variance of shot noise |
| $I_{bg}$ | Photocurrent from background radiation |
| $P_{r-signal}$ | Received optical power |
| $P_{rISI}$ | Desired received power from multipath. |
| $R_L$ | Load resistance |
| $g_m$ | FET transconductance |
| $\kappa$ | Boltzmann's constant |
| $C_{\mathrm{pd}}$ | Fixed capacitance of photodetector per unit area |
| $T_e$ | Absolute temperature |
| $G_{oL}$ | Open-loop voltage gain |
| $\Gamma$ | FET channel noise factor |
| $I_2, I_3$ | Noise-bandwidth factors |
| $M$ | Number of the transmitters |
| $T_{xj}$ | Optical transmitters (i.e. LED or LEDs array) |
| $R_{xi}$ | Optical receivers (i.e. PDs) |
| $h_{ij}$ | Channel coefficient between the $j^{th}$ transmitter and the $i^{th}$ receiver |
| Y | Received signal vector |
| $H$ | Channel matrix for MIMO VLC system |
| $X$ | Transmitted signal vector |
| $n$ | AWGN vector |
| $H^{-1}$ | Inverse of matrix $H$ |
| $H^H$ | Hermitian of matrix $H$ |
| $H^T$ | Transpose of matrix $H$ |
| $H^\dagger$ | Pseudo inverse of matrix $H$ |
| $P_d$ | Power of the transmitted signal |
| $\sigma_n^2$ | Power of the noise at the receiver |
| $t_{dif}$ | Difference of time between the two signals arrival |
| $v_1$ and $v_2$ | Propagation speeds of signals |
| $(x_u, y_u)$ | Position of the user |
| $(x_{\mathrm{Tx}i}, y_{\mathrm{Tx}i})$ | Transmitter's position |
| $\phi_i$ | Angle between the transmitter and the user |

| | |
|---|---|
| $d_{\mathrm{Tx}i,u}$ | Distance between the user and the transmitter |
| $t_{propagation}$ | Propagation time of signal |
| $P_{\mathrm{rx}}$ | Received signal power |
| $P_{\mathrm{tx}}$ | Transmitted signal power |
| $G_{\mathrm{rx}}$ | Receiver gain |
| $d\Omega$ | Solid angle |
| $dP_i$ | Optical power radiated into $d\Omega$ |
| $\theta_{max}$ | Maximum irradiance angle |
| $d_{max}$ | Maximum distance between the transmitter and the receiver |
| $\theta_{1/2\_\mathrm{opt}}$ | Optimum semi-angle at half power |
| $m_{\mathrm{opt}}$ | Optimum Lambertian order |
| $C$ | Per-LED constant related to the maximum emission power |
| $\frac{\tau}{T}$ | Current duty cycle of the LED |
| $V_1$ and $V_0$ | High and low voltage values |
| $\mathrm{C}_{\mathrm{otp}}$ | Optical constant related to the parameters of the VLC environment |
| $P_{RFi}$ | RF received power |
| $P_{diff,t}$ | Difference in transmitted power between 0s and 1s at the transmitter side |
| $P_{diff,r}$ | Difference in transmitted power between 0s and 1s at the receiver side |
| $h_{LED}(t)$ | Impulse response of LED |
| $h_{Ch}(t)$ | Impulse response of VLC channel |
| $h_{Ch,LOS_i}(t)$ | Impulse response of VLC channel in LOS scenario |
| $h_{Ch,NLOS_i}(t)$ | Impulse response of VLC channel in NLOS scenario |
| $h_{Ch,LOSNLOS_i}(t)$ | Impulse response of VLC channel in LOS and NLOS scenarios |
| $h_{\mathrm{PD}}(t)$ | Impulse response of the PD |
| $n(t)$ | An additive white Gaussian noise (AWGN) |
| $P_{\mathrm{Rx},L_i}(\theta_{L_i})$ | Received power level at the distance, $L_i$ |
| $P_{\mathrm{Rx},h}(0)$ | Received power level at the distance, $h$, underneath Tx |
| $R_{0,LOS}(\phi)$ | Transmitter radiant intensity for the LOS scenario |
| $A_{eff,LOS}(\psi)$ | Effective signal collection for the LOS scenario |

| | |
|---|---|
| $\gamma$ | Path-loss exponent correction factor |
| $(x_{Rx}, y_{Rx})$ | Position of the receiver. |
| $\Delta\theta_{L_i}$ | Angular error |
| $\Delta d_i$ | Horizontal distance error |
| $X_{est}$ | Estimated original signal |
| $< n_i^2 >$ | Noise power at the receiver position |
| $< n_o^2 >$ | Noise power underneath the transmitter |
| $\mathrm{N}(\mu, \sigma)$ | AWGN |
| $\mu$ | Mean of noise |
| $\sigma$ | Variance of noise |
| $C_y$ | Cryptogram, ciphertext or unreadable text. |
| $E_y$ | Encryption algorithm |
| $K_e$ | Encryption key |
| $M_t$ | Transmitted message or plaintext |
| $M_r$ | Received message |
| $D_y$ | Decryption algorithm |
| $KU_b$ | Public key of public-key cryptosystem |
| $KR_b$ | Private key of public-key cryptosystem |
| $p$ and $q$ | Prime numbers |
| $\emptyset(n)$ | Euler Totient function |
| $(d, n)$ | Private key of RSA algorithm |
| $(e, n)$ | Public key of RSA algorithm |
| $\Delta P$ | Power penalty |
| $(x_{\mathrm{PD}_j}, y_{\mathrm{PD}_j})$ | Coordinates of the photodetector in the receiver array |
| $(x_{\mathrm{CORA}}, y_{\mathrm{CORA}})$ | Coordinates of the centre of the receiver (CORA) |
| $\big(P(:), Q(:)\big)$ | Prime number vectors |
| $K_l$ | Encrypted block length or the encrypted frame length |
| $(e(:), n(:), K_l)$ | Public key vectors |
| $(d(:), n(:), K_l)$ | Private key vectors |

# Chapter One

# Introduction

## 1.1. Research Fundamentals and Motivation

Nowadays, there is an exponentially growing demand for data transfer between the increasing number of the networks' users. As a result, the current communication systems, which are represented in Radio Frequency (RF) communication, are facing significant challenges to achieve this target due to the limitation of RF bandwidth, RF license fees, high implementation costs and spectrum overcrowding. The spectrum overcrowding problem of the present UK RF allocation chart is depicted in Fig. 1.1. From this chart, it can be seen that the highly restrictive bandwidth problem opens the prospect for optical wireless technology as an alternative to current wireless communication network such as Wi-Fi and Wi-Max.

Indeed, there has already been a number of research efforts and demonstrations focusing on optical wireless communication (OWC) technologies such as free-space optical (FSO) communication, infra-red (IR) and visible light communication (VLC) [1-4]. In this work, we focus on the VLC alternative. In the next sub-section, an overview of VLC technologies will be given.

### 1.1.1. Overview on Visible Light Communication

In recent years, VLC systems have emerged as new and competitive area in an OWC technology as a sequel to RF technology gathering significant research attention. The VLC is an emerging technology that aims to achieve high data rate using the visible range of the electromagnetic spectrum (i.e. visible light wavelengths between ~370 nm to ~ 780 nm). VLC technology, which referred to as light fidelity (Li-Fi) networks as well, has received

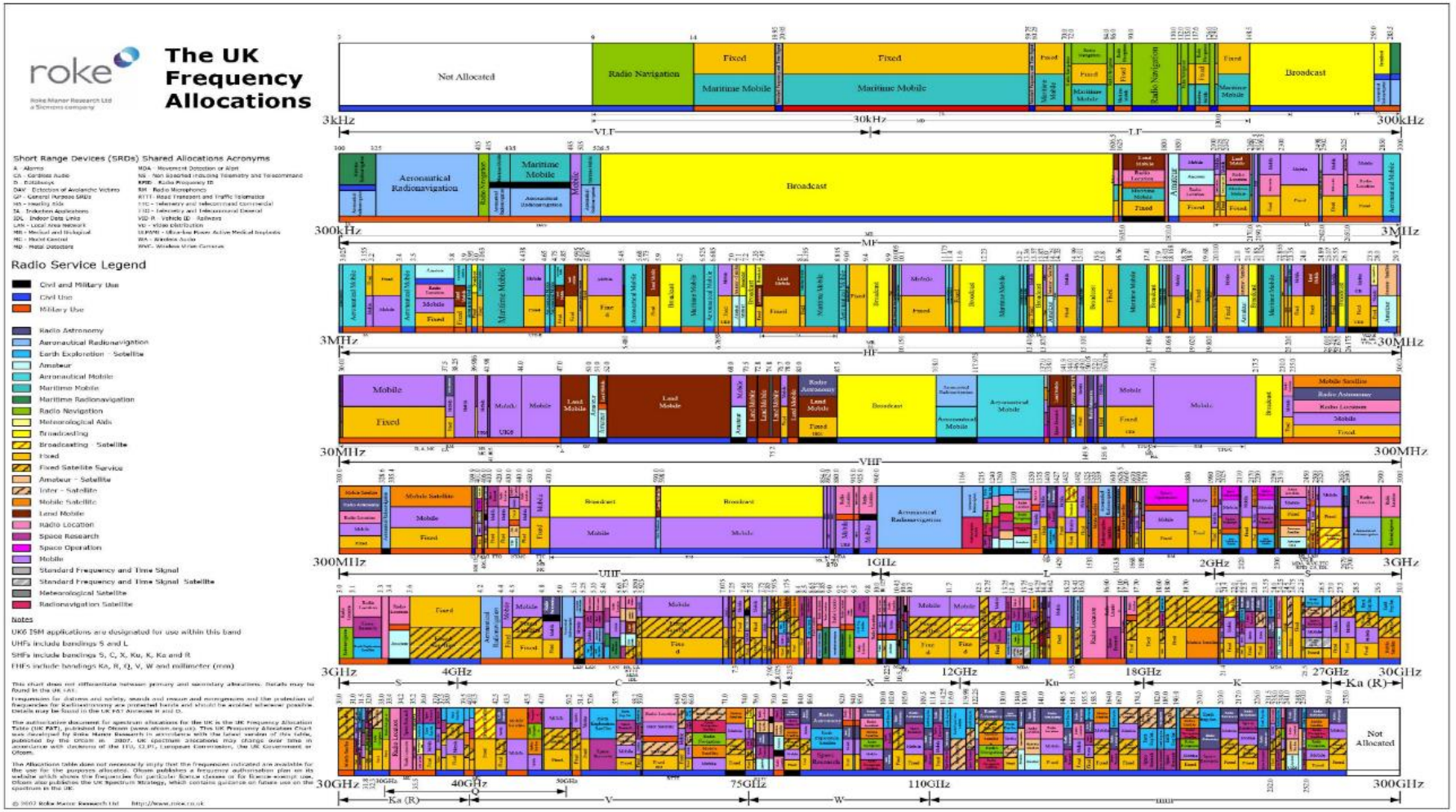


Fig. 1. 1 the UK radio frequency spectrum allocations chart to show overcrowding problem [4].

increasing research attention in two last decades due to their capability of providing two simultaneous functions; illumination and data transmission. Furthermore, the technology offers huge bandwidth of approximately ~ 400 THz, which is 10,000 times larger than the RF bandwidth (as shown in Fig. 1.2). In 2004, Toshihiko Komine proposed VLC as an emerging area in optical systems using white light emitting diodes (LEDs) in Japan. The white phosphor LEDS (WPLEDs) are the most popular type of inorganic LEDs which offer modulation bandwidth up to hundreds of MHz using several equalizers. However, there are a number of serious challenges associated with VLC technologies. For instance, those challenges include optimal spectra allocation, high capacity broadband links, power consumption, quality of service (QoS), mobility, indoor positioning and security. The contributions of this work will focus on the last two challenges, namely indoor positioning and security [5-14].

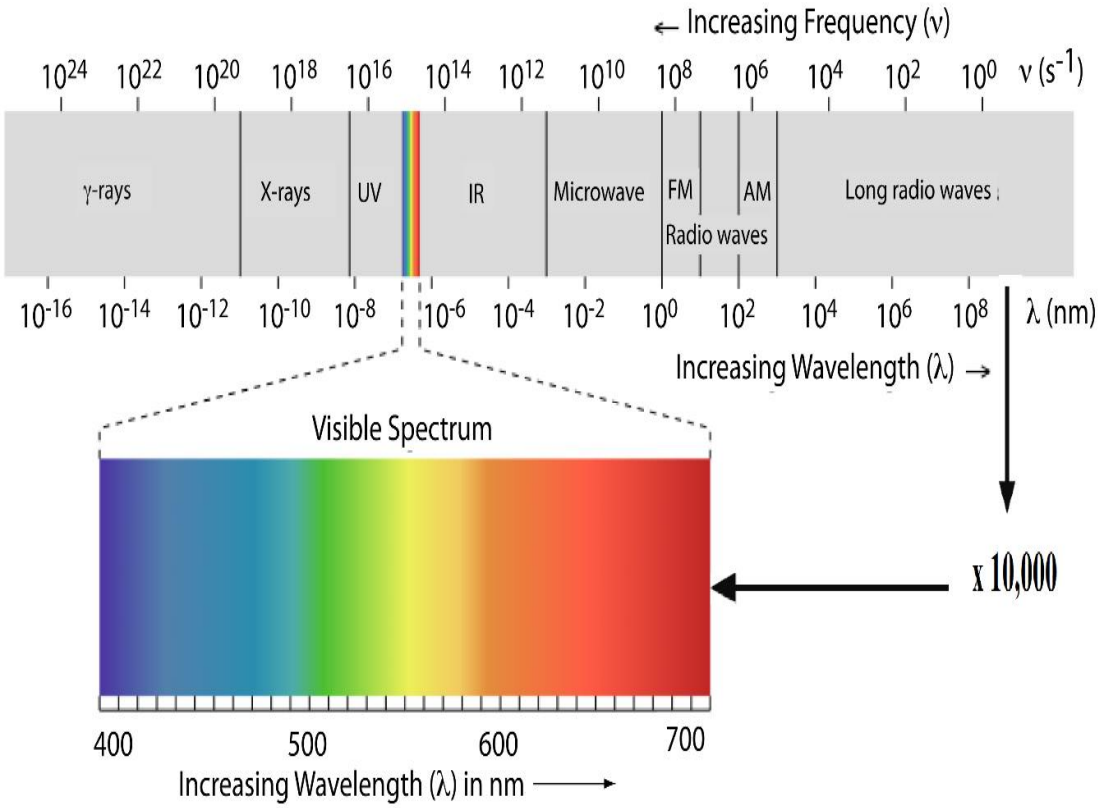


Fig. 1. 2 The visible light range in the electromagnetic spectrum to show the difference between the RF bandwidth and the visible light bandwidth [4].

## 1.1.2. Positioning in OWC Systems

Satellite based positioning methods such as global positioning systems (GPS) offer very accurate location measurements. However, these methods are incapable of providing the same positioning accuracy in indoor areas. Furthermore, they are expensive and suffer from high power consumption [12, 15-21]. Finding the location of a smart device using lighting equipment is still a challenging task. Both Bluetooth and Wi-Fi 802.1lx use the common 2.4 GHz unlicensed frequency; as a result, concerns about interference between them. Depending on the usage environment, Wi-Fi or Bluetooth based positioning systems can offer location accuracies within the range of 1-10 m [22, 23] In WLAN, the localization systems use a joint clustering technique for location estimation with an accuracy of more than 90% within a range of ~2.1m (7 feet) [24]. A grid based Bayesian location scheme within building with localization and tracking capability within 1.5 m is reported in [25, 26]. A tracking based positioning system, which determines the positions of users using the access points and tags attach to mobile terminals/users in order to determine their positions was developed for real-time locating system for Wi-Fi networks as reported in [27]. Furthermore, a real time tracking system for Wi-Fi networks based on trilateration determined from the RSSI values was developed to operate in a passive mode, with no need for mobile users to be related or send specific data to the positioning server application [26]. However, radio frequency based technologies are affected by the electromagnetic interference and background noise[28, 29]. In some applications, the positioning systems are mostly designed for tracking a small number of objects [30], thus designing an accurate indoor positioning system is challenging.

On the other hand, VLC systems are able to transmit localization information. For instance, Cossu et al. proposed a localization algorithm that uses low frequency tones to provide tracking information to the receiver [31]. Furthermore, Jung et al. [32] proposed an optical wireless indoor localization which used LEDs-based ceiling lamps, the signal phase

difference and the time difference of arrival (TDOA) localization algorithm where they have achieved an indoor localization accuracy of less than one cm in the space of 5m×5m×3m. Biagi and Vegni [33] also proposed a simple method utilising infrared LED devices for indoor positioning service (IPS). That method relied on comparisons to the impulse responses of power and time samples of a room map to estimate the location of a mobile device. Jia [16] proposed a method which is a hybrid between the VLC-based positioning method and the conventional received signal strength indication (RSSI) for indoor wireless sensor network (WSN) to achieve accurate positioning and lower power consumption. Kim et al. [34] developed an adjustment method to reduce the positioning error to within few centimetres. Moreover, Won et al. [35] proposed a new indoor 3D positioning technique that utilises location codes and a spatial distribution map and obtained a positioning error of less than 3 cm.

### 1.1.3. Security in OWC Systems

Security is an important factor in wireless networks. Authentication and encryption are two processes that are utilised to provide the security in WLAN. There exist various ways to improve security requirements and quantum cryptography, which utilises techniques such as quantum key distribution (QKD) is useful technique [36-39]. Zhiqiang et al. [40] proposed a new design scheme that uses a digital chaotic encryption core and relies on FPGA and Wi-Fi technology. On the other hand, security in optical wireless communication also represents a challenge. Jose et al. proposed new techniques for improving the security level for OWC networks. The method used modulation schemes based on the spread spectrum theory to encrypt data in the modulation process. These schemes are: Direct Sequence Spread Spectrum (DSSS) and Frequency Hopping Spread Spectrum (FHSS) [41].

Cryptography is a technique in which information can be hidden in ciphers and later used by authorized users employing a secret key. It refers to the science that studies algorithms to hide plaintext in a cipher-text using secret keys and sending an encrypted signal through the

unsecure communication channel. At the receiver side, only users (authorised or otherwise) who possess the secret keys are able to decrypt ciphertext and obtain the original message. Using the technique, it is either impossible or computationally infeasible for a hacker to crack the code. Therefore, cryptography can protect data during transmission from four general categories of attack: interruption, interception, modification and fabrication. There are three main units in a typical cryptography system: a data encryption unit, a data decryption unit and a key management unit as shown in Fig. 1.3. The key management unit manages the generation, distribution, recognition, and reception of the cryptographic keys [42, 43].

Cryptography techniques are generally divided into two categories of ciphers. The first one relates to symmetric ciphers known as conventional encryption or shared-key encryption which uses the same key for both encryption and decryption and are employed in such techniques as Data Encryption Standard (DES), Advance Encryption Standard (AES), and One Time Key (OTK) [44, 45]. On the other hand, the second technique is asymmetric cipher known as public-key cryptography which uses the different keys for encryption and decryption (e.g.; RSA algorithm, Diffie-Hellman key Exchange, and Elliptic curves cryptography). The summary of the issues, existing solutions and original contributions for the indoor VLC system in this thesis are outlined in Fig. 1.4. However, Fig. 1.5 explains the block diagram of the work which has been done in VLC positioning system in this thesis. On the other hand, the RSSI technique has been used to obtain the location of the user using

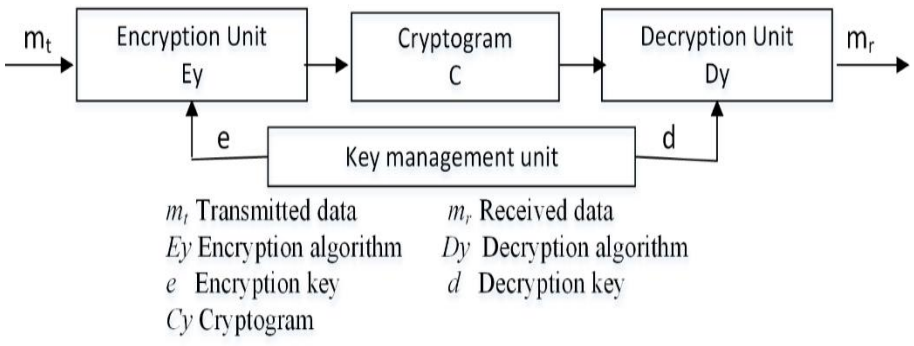


Fig. 1. 3 General cryptographic units [35].

three and two transmitters for an indoor positioning system. In each of the two indoor positioning system, we have implemented the positioning algorithm using ROP distributions and real system approaches as well as we have considered LOS and LOSNLOS scenarios for noisy and noiseless cases.

## 1.2. Aims and Objectives

The main aims of this work are to propose and design a novel secure SISO VLC system and a novel secure MIMO VLC system based on the position of the user and utilising cryptographic techniques. As a result, the objectives of this thesis are:

- To understand the VLC system and investigate its performance for SISO-TDM and MIMO.
- To develop and implement the positioning techniques for the VLC system.
- To develop and implement the security for the SISO VLC system.
- To develop and implement the security for the MIMO VLC system based on the VLC positioning system.

## 1.3. Original Contributions

An outline of the main contributions of this thesis are:

➢ In Chapter Three

- A comprehensive investigation of the received optical power (ROP) distributions and comparison between the ROP with and without optimum Lambertian order for single and four cell configurations is carried out.

  A novel 2-D indoor VLC positioning system using three transmitters and received signals indication (RSSI) for the LOS and the LOSNLOS scenarios using the ROP approach and an end-to-end system is designed. A comparison is also made with previous research work and this work has published in [46] (see Fig.1.5).

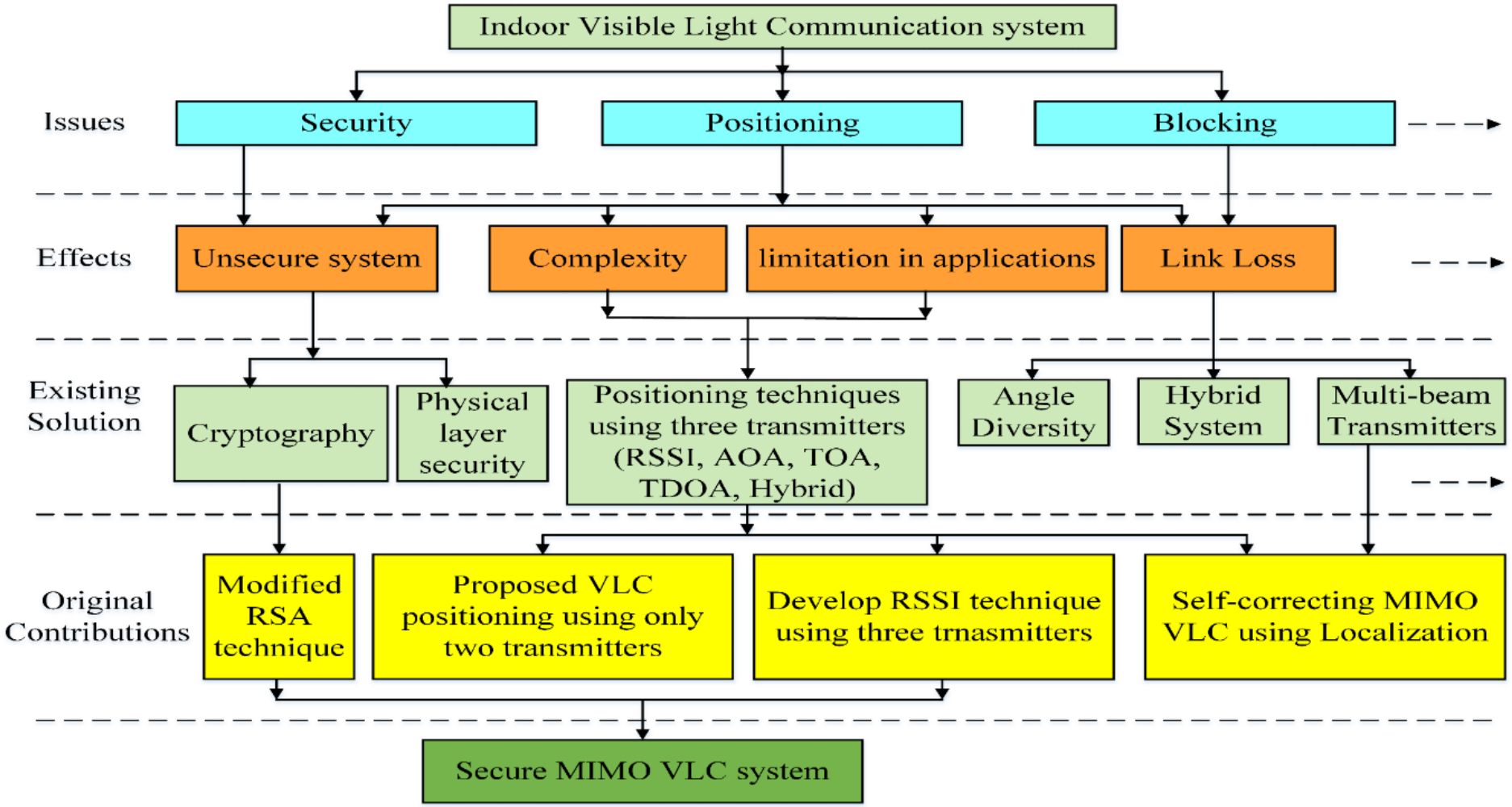


Fig. 1. 4 Summary of the issues, existing solution and original contributions for indoor VLC system in this dissertation.

- A novel approach for recovering the 4 × 4 MIMO VLC data with a partial channel state information (CSI) knowledge in both noisy and noiseless cases is designed and this work has published in [47].

➢ In Chapter Four

- We have proposed, designed, implemented and evaluated a novel 2D indoor VLC positioning what using only two transmitters using two approaches: the ROP distributions approach and end-to-end system for both LOS and LOSNLOS scenarios with ideal and noisy conditions (see Fig.1.5).
- We have derived and verified the mathematical model of the noise and the impact of noise on angular error and distance error. A comparison with a conventional trilateration method is also made in this Chapter and this work has published in [48] (see Fig.1.5).

➢ In Chapter Five

- We have proposed, designed and simulated a secure SISO VLC system using RSA technique for encryption and decryption for both LOS and LOSNLOS scenarios. Furthermore, investigation of the power penalty induced as a result of encrypted block length is conducted. This work has published in [49].

➢ In Chapter Six

- We have designed a novel secure MIMO VLC system based on the location of user and the RSA technique.
- We have developed a mathematical modelling of positioning in MIMO VLC systems.
- We have developed a secure RSA encryption and decryption at the MAC layer for secure MIMO VLC system, with no extra data needed. Generating the public and private keys is carried out at the receiver side and only the public key is sent in unsecure VLC channel.

.

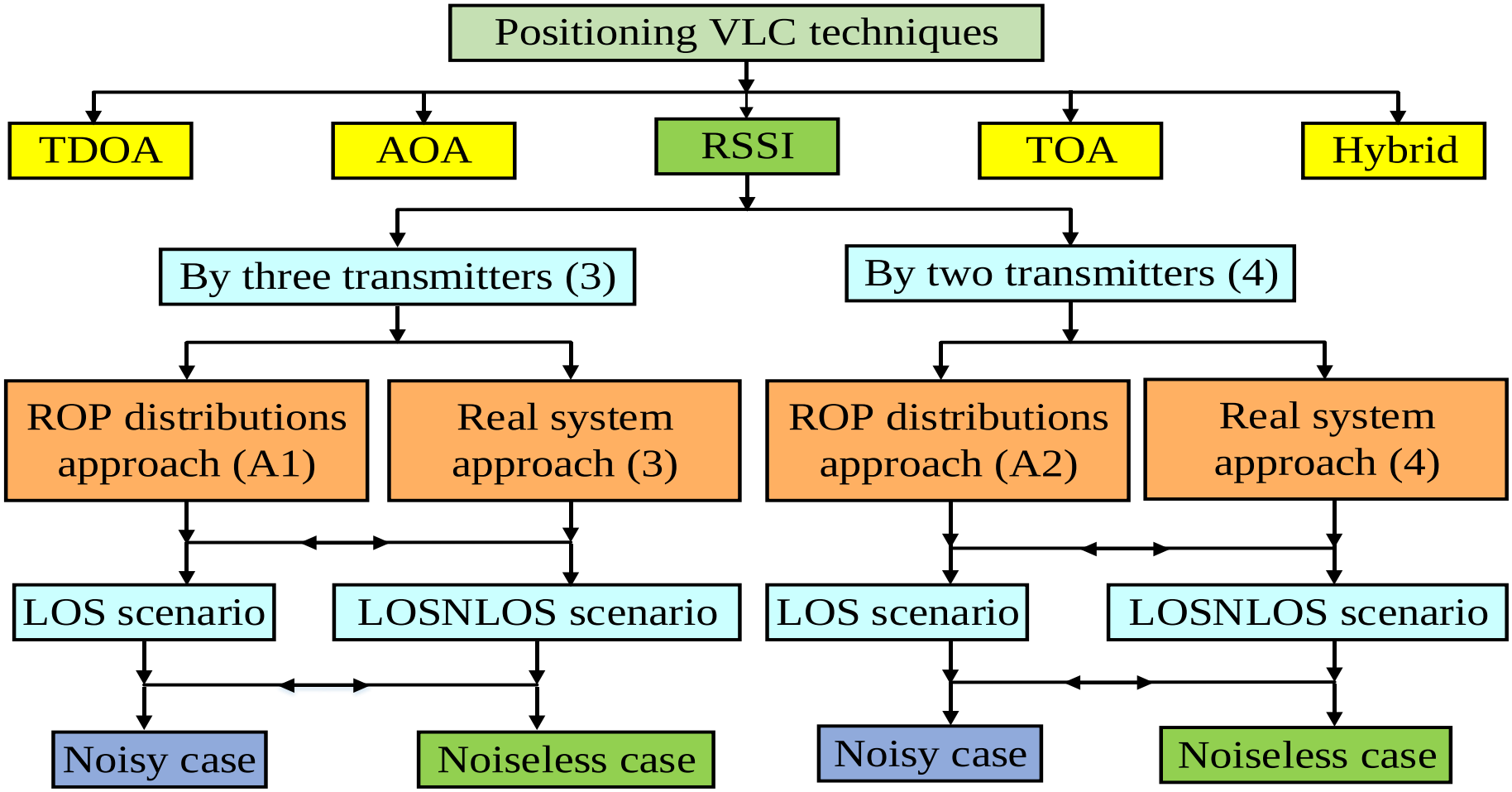


Fig. 1. 5 Summary of contributions in VLC positioning system  where the chapter numbers and appendices are provided in brackets.

- We have shown the ability to control the size of the encrypted VLC cells based on the user environment.
- We have investigated the BER of MIMO VLC using MMSE equalizer and positioning error distributions for ideal and real scenarios against a wide range of SNR levels. This work in this chapter has published in [50]

# 1.4. List of Publication

This work has generated the following journal and conference papers:

## 1.4.1. Journal Papers

1. **F. Mousa**; H. Le-Minh; Z. Ghassemlooy; X. Dai; T. T. Son; A. C. Boucouvalas; and S. K. Liaw; "*Indoor Localization System Utilizing Two Visible Light Emitting Diodes*", Opt. Eng. 55(11) 116114, (2016), doi: 10.1117/1.OE.55.11.116114.
2. **F. Mousa**, N. Almaadeed, K. Busawon, A. Bouridane and R. Binns, "*Secure MIMO Visible Light Communication System Based on User's Location and Encryption",* Journal of Lightwave Technology, vol. 35, pp. 5324-5334, 2017.
3. **F. Mousa**, N. Almaadeed, K. Busawon, A. Bouridane, R. Binns, and I. Elliot, "*Indoor Visible Light Communication Localization System Utilizing Received Signal Strength Indication Technique and Trilateration Method"*, Opt. Eng. 57(1), 016107, (2018), doi:10.1117/1.OE.57.1.016107.

## 1.4.2. Conference Papers

4. **F. Mousa**, T. T. Son, A. Burton, H. Le-Minh, Z. Ghassemlooy, T. Q. Duong, A. C. Boucouvalas, J. Perez and X. Dai., "*Investigation of Data Encryption Impact on Broadcasting Visible Light Communications*", 9th International Symposium on

Communication Systems, Networks & Digital Signal Processing (CSNDSP), pp. 390-394, 2014.

5. H. Le-Minh; Z. Ghassemlooy, A. Burton, **F. Mousa**, S. Biswas, P. A. Tuan, et al., "*Self-Correcting MIMO Visible Light Communications System Using Localization*", IEEE International Conference on Communication Workshop (ICCW), pp. 1362-1367, 2015.
6. T. T. Son, H. Le-Minh, **F. Mousa**, Z. Ghassemlooy, N. V. Tuan, "*Adaptive Correction Model for Indoor MIMO VLC using Positioning Technique with Node Knowledge*", International Conference Computing, Management & Telecommunication (ComManTel2015), DaNang, Vietman, 2015.

# 1.5. Organization of Thesis

This thesis is divided into seven chapters as outlined in the following:

**Chapter 1*: Introduction*.** Provides the research fundamentals and motivation and the summary of aims and objectives as well as the outline of the thesis.

**Chapter 2*: Optical wireless communication system overview.*** Gives an overview of OWC systems versus RF systems and the challenges for OWCs and the issues, drawback and challenges in a VLC system and multiple-input-multiple-output (MIMO). The Chapter also focuses on indoor VLC positioning techniques with related works.

**Chapter 3*: Indoor VLC positioning system using three transmitters*.** Presents the received optical power (ROP) distributions with and without optimum Lambertian order as well as some new ROP relationships. The Chapter also proposes a positioning VLC system based on three transmitters and RSSI for two scenarios (LOS and LOSNLOS) and a comparison with previous research work. Additionally, an overview of applications for VLC positioning in MIMO VLC system is given.

**Chapter 4*: Indoor VLC positioning system using two transmitters.*** Proposes a novel indoor VLC positioning system based on only two transmitters and the RSSI technique. The Chapter introduces the mathematical noise modelling and channel modelling for the LOS and the LOSNLOS scenarios. The results show that the localization error is decreased compared with other VLC positioning systems.

**Chapter 5*: Protection of VLC system*.** Presents the concept of information security, the requirements of information protection and cryptography, particularly the RSA technique, to encrypt data. It also proposes a new secured VLC system using the RSA technique and investigates the impact of protection of SISO VLC system for the LOS and the LOSNLOS scenarios and calculates the power penalty as well.

**Chapter 6*: Secure MIMO-VLC system.*** Proposes and designs a novel secure MIMO VLC system based on the user's location with the ability to control the size of the encrypted VLC cells and encryption as well as the deployment of the RSA method at the MAC layer with no overhead data.

**Chapter 7: *Conclusions and future work*.** Presents and reviews the main summaries of this research. The Chapter also proposes new ideas and research directions for further developments of this work.

# 1.6 Summary

This chapter has been outlined the main milestones in the OWC and VLC systems. This chapter also has been highlighted an VLC systems and its huge bandwidth which is 10,000 times larger than the RF bandwidth. In addition, Chapter 1 has is reviewed the motivation on positioning and on the security in OWC system. Secondly, this chapter has been introduced aims, objectives, and original contributions for the whole thesis and a number of publications that have generated from this thesis. Finally, the organization of thesis has been clarified in this chapter.

The next chapter will introduce the fundamentals of an indoor VLC system, an indoor MIMO VLC system and the common techniques in an indoor VLC positioning system.

# Chapter Two

# Optical Wireless Communication System Overview

## 2.1. Introduction

There is a significant demand for wireless communication technologies due to the rise of smartphone technology, video streaming, digital radio and cloud services in recent years. Among wireless communications, an OWC system is one of the candidates that has been strongly emerging in the last few decades [51]. There are two optical domains of the electromagnetic spectrum, which are the infrared spectrum and the visible light spectrum, that are used as the transmission medium [52]. OWC is a promising technology that provides an increased high data rate and to offer higher channel capacity for the existing indoor wireless communications [53],[54]. For instance, Gfeller and Bapst have proposed an OWC system utilising the IR domain. A large amount of research on optical wireless systems using IR domain of the optical spectrum (typically between 800 and 1500 nm in wavelength), started since the late 1970s for indoor local area network (LAN) applications. Most recently, the research on FSO communication in outdoor environment has seen a sharp increase as well [52]. On the other hand, the research on VLC, which is an alternative to the RF technology, in an indoor environment with a visible wavelength range from about 380 to 780 nm has begun since the early 2000s [55]. This range is appropriate for the light being detected by a photodiode. Future optical networks should tolerate the interoperability of RF, fiber-optic and FSO technologies. However, the incompatibility of RF/microwave and fiber optics technologies is the major limiting factor that affects further development of future transport capabilities of such hybrid networks [56].

### 2.1.1. OWC Systems Versus RF Systems

There are several advantages of OWC systems compared to RF systems, where, for instance, an OWC system has license-free wavelengths in the optical domain of the electromagnetic spectrum from 380 nm to 10,000 nm. Therefore, the bandwidth of an OWC system is more than 670 THz; meaning it is 10,000 times larger than that of an RF spectrum, which is 60 GHz. Furthermore, RF signals are strongly attenuated in water, therefore, the underwater RF transmission is not allowed [52, 55]. In addition, the effect of multipath fading, which is prominent in RF systems, does not exist in OWC systems. Moreover, the requirement of achieving large capacity for future 4G/5G communication is still present, and as such, higher data rates have to be utilised to achieve this target. While, the spectrum of RF is limited and expensive, RF communication systems have some key advantages such as mobility, outdoor and indoor coverage and high sensitivity of RF receivers. However, RF components are expensive and consume more electrical power than their OWC counterparts. For more details, Table 2.1 shows the comparison between the VLC system and RF system.

Table 2.1 Comparison of the VLC system and RF system [55]

| Property | RF system | VLC system |
|---|---|---|
| Bandwidth | Regulated and limited | Unlimited, 400-700 nm |
| EM interference | Yes | No |
| Line of sight | No | Yes |
| Distance | Short to long | Short |
| Security | Poor | Good |
| Standards | Matured | In progress |
| Services | Communications | Illumination & Communication |
| Noise sources | All electrical/electronic appliances | Sun light and other ambient lights |
| Power consumption | Medium | Relatively low |
| Mobility | Good | Limited |
| Coverage | Mostly wide | Narrow and wide |

### 2.1.2. Challenges facing OWC Systems

Over the past two decades, most of the research on OWC has focused on increasing data rates. However, there are still other challenges facing the wide deployment of OWC systems. Firstly, the presence of strong non-linear transfer of the optical transmitter front-end as well as the limited dynamic range of the optical transmitter. Secondly, the electrical modulation bandwidth is small compared to the optical bandwidth. Thirdly, optical multiple-input multiple-output (OMIMO) techniques to enhance the capacity is still an open issue. Fourthly, challenges associated with mobility, multi-user access, light dimming and shadowing. Last but not the least, indoor localisation and the security of OWC systems still present significant challenges and will be addressed in this thesis [57].

## 2.2. Visible Light Communications

In 2004, Toshihiko Komine proposed VLC as a newly emerging area in OWC using white LEDs [58].The VLC system provides two functions: one is lighting in indoor environments and the other is wireless data communications [51]. In addition, it provides high security, high data rates and precise positioning detection compared to other wireless communication technologies [53]. Wireless radio frequency communications work for indoor and short distance links without the need for any physical connection [54]. Therefore, optical wireless technology would be an attractive supplement or even alternative to a current wireless communication network, for example, Wi-Fi and Wi-Max. The technology can achieve very high data rates though there is one crucial limiting factor to achieve such high data rates which is the limited modulation bandwidth of white LEDs [58-60]. A feasible method of communication is intensity modulation with direct detection (IM/DD) to obtain low-cost OWC systems. A block diagram of a typical VLC is shown in Fig. 2.1 [61, 62].

The optical path depends on numerous factors, including room dimensions, the reflectivity of the ceiling, walls and objects within the chamber. In addition, the position and

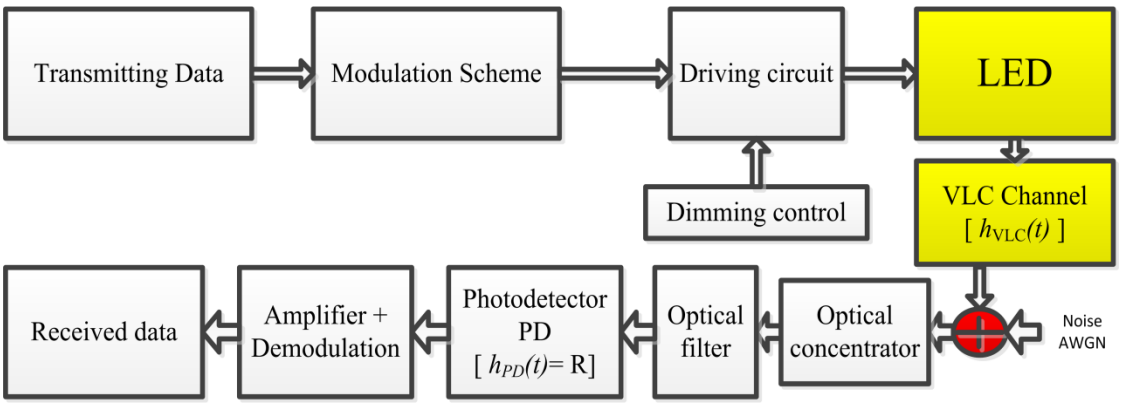


Fig. 2. 1 Block diagram of a typical VLC system.

orientation of the transmitter and receiver, also affect the optical path and as a result, it is more complex to predict and determine this loss. There are two optical components, namely, LEDs and Laser Diodes (LDs) that are used in OWC as they coincide with the peak responsivity of inexpensive silicon photodetector. On the other hand, photodetectors are divided into two types: the positive–intrinsic negative (PIN) and the avalanche photodiode (APD).

Light Fidelity (Li-Fi) is a high-speed communication variant of VLC. By using multi-carrier modulation techniques such as orthogonal frequency division multiplexing (OFDM) for a single point-to-point transmission, data rates of more than 500 Mbps can be achieved [63, 64]. Wu et al. [65] achieved 3.22 and 2.93 Gb/s for carrier amplitude power (CAP) and OFDM, respectively, as the maximum aggregate data rates after individually optimizing red-green-blue (RGB) chips. Helmi et al. [66] reported indoor wireless VLC transmission at 1 Gb/s and an average bit error rate of $10^{-3}$ by designing and developing a high-speed MIMO-OFDM VLC transmission system where they utilised wavelength division multiplexing (WDM) to achieve this performance. Furthermore, a fixed-length digital pulse interval modulation was proposed by Lei and Dianren achieving 1080 Mbps data rate with eight channels [63, 67, 68].

Link configurations are divided into four categories as illustrated in Fig. 2.2. Firstly, the directed line-of-sight (LOS) is mainly used outdoor, and it can be considered in the indoor

domain too, as shown in Fig. 2.2 (a). LOS links have a narrow field of view (FOV), and as such, they have a minimum optical path loss. Therefore, they provide high SNR and the lowest transmission power and hence offer the highest data rates. For instance, data rates of 1.25 Gbps and 12.5 Gbps were reported in [69] and [70], using directed LOS OWC links. Furthermore, there is no multipath-induced ISI in this structure. Secondly, the non-directed LOS achieves a wide coverage area and is suitable for single-input multi-output (SIMO) applications with more user mobility as shown in Fig. 2.2 (b). Thirdly, non-line-of-sight (NLOS) has sub configurations based on the number of reflection points. For instance, if it has one it is referred to as a directed NLOS or first reflection and so on as shown in Fig. 2.2 (c). It is also known as a diffuse system and is used to overcome the blocking or shadowing problem . This link is suitable for SIMO system applications as well. However, in this link,

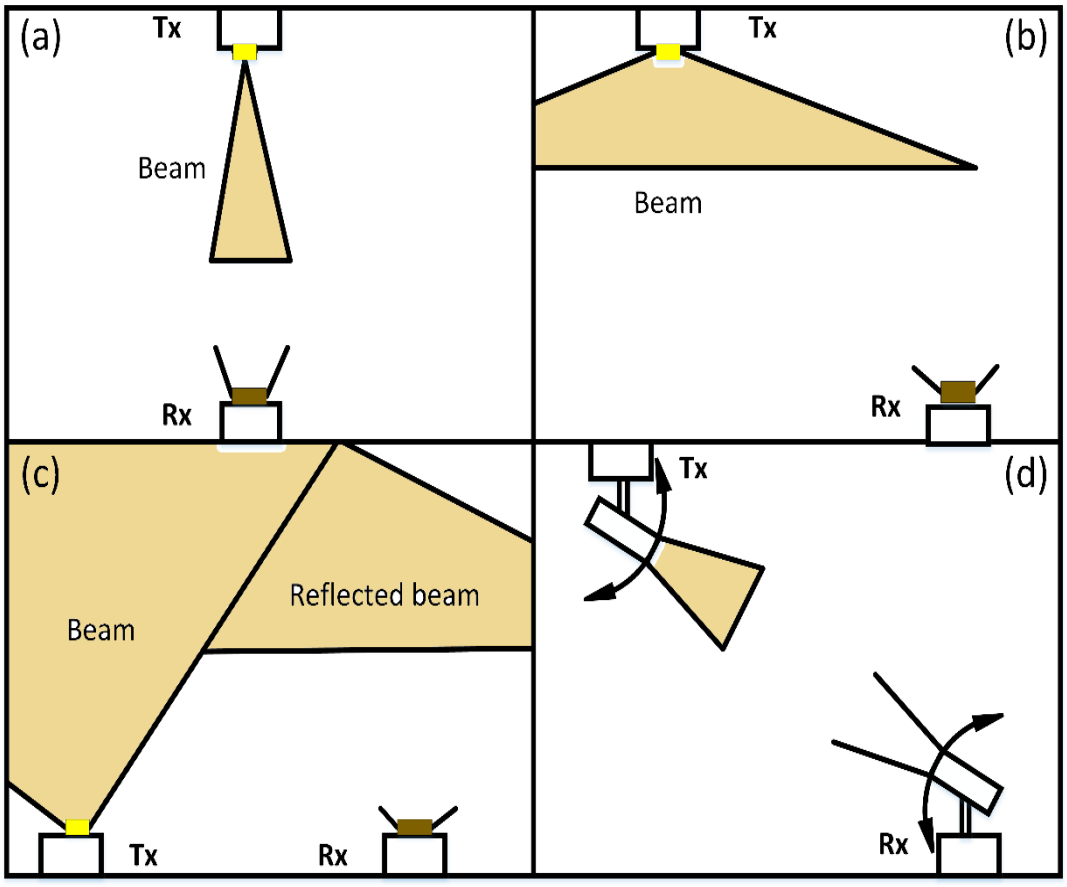


Fig. 2. 2 Link configurations (a) Directed line-of-sight (b) Non-directed line-of-sight (c) Non-line-of-sight by first reflection and (d) Tracked link.

data rate is restricted to approximately 260 Mbps [71, 72] as the presence of intersymbol interference (ISI) and the resulting loss of pulse amplitude lead to restrictions on the maximum transmission speed based on the room size. The last configuration is the tracked link which takes place when the transmitter and receiver are mechanically steerable optics as shown in Fig. 2.2 (d). However, this link is expensive and complex. In this study, only the directed and non-directed LOS, and directed NLOS will be considered [55, 73].

## 2.2.1. Light Emitting Diodes

LEDs and LDs are the incoherent and coherent OWC sources respectively. There are a number of advantages that an OWC transmitter offers including power reservation, high brightness in the visible spectrum for single wavelength or range of wavelengths, a long life, mercury absence and relatively small size display. Further advantages include the radiation pattern, the optical impulse response, E/O transfer, the electrical modulation bandwidth and the low drive current and forward voltage, all of which are key characteristics of optical transmitters. A high-directionality spectrum is required for OWC transmitters to achieve two targets: one is to accumulate as much transmission power as possible, and the other is to reduce the background ambient light. Light is generated due to the transition of an electron from an excited to a lower energy state. Therefore, there will be a difference of energy that leads to a radiative or non-radiative processes to create light or heat, respectively. This difference is related to the frequency and the wavelength by the following equation [8, 52, 55, 74]:

$$E = E_2 - E_1 = hf = \frac{hc}{\lambda} \quad (2.1)$$

where $E_2$ and $E_1$ are the energies before and after the transition, $h$ =6.626×10$^{-34}$ J.s is Planck's constant. $f$ , $c$ and $\lambda$ are the frequency, speed of light and wavelength of light waves,

respectively. There are a number of types of *p-n* junction devices, one of which is the LED which gives off spontaneous optical radiation to generate light [62].

White LEDs are currently made by using two different techniques (i) combining GaN (Gallium Nitride) LED and YAG (Yittrium Aluminum Garnet) phosphor in the blue range (i.e.; 450nm-470nm) to glare white (ii) combining three types of LEDs (red, green and blue) to realise a white colour. Luminous intensity and transmitted optical power are important characteristics of LED light. Luminous intensity describes the brightness of an LED and it is the first derivative of energy flux with respect to a solid angle, Ω. It is expressed as [35]:

$$I = \frac{d\Phi}{d\Omega} \tag{2. 2}$$

where $\Phi$ is the luminous flux. We can rewrite the formula above using the energy flux $\Phi_e$ as [55]:

$$\Phi = k_m \int_{380}^{780} V(\lambda)\, \Phi_e(\lambda) d\lambda, \tag{2. 3}$$

where $V(\lambda)$ is the spectral luminous efficiency and $k_m$ is the maximum visibility which can be estimated to be approximately 683 lm/W when $\lambda$ =555 nm.

The transmitted optical power point to the total energy that is emitted by the LED and it is given by [68]:

$$P_t = \iint_{\Lambda_{min}}^{\Lambda_{max}} \Phi_e \, d\theta d\lambda, \tag{2. 4}$$

where Λ is the photodetector sensitivity and $\theta$ is the irradiance angle.

## 2.2.2. Channel Modelling

The channel impulse response gives an important information about the characteristics of the communication channel such as channel distortion, optical path loss and multipath dispersion. The study of an indoor optical wireless communication channel is made according to the directionality and the configuration link between the transmitter and

receiver. There is a directly proportional relationship between the generated photocurrent at the receiver and the instantaneous optical power that is incident upon the photodetector surface. Intensity modulation with direct detection (IM/DD) is simple and thus can be used in the optical channel. The mathematical model for the optical channel can be defined by [55]:

$$y(t) = \Re x(t) \otimes h(t) + n(t)$$
$$= \int_{-\infty}^{\infty} \Re x(\tau) h(t-\tau) d\tau + n(t) \quad (2.5)$$

where $\Re$ is the responsivity of photodetector, $y(t)$ is the photocurrent, $x(t)$ is the transmitted optical power, $n(t)$ is channel noise such as shot noise or thermal noise and it is modelled as additive white Gaussian noise (AWGN), $\otimes$ symbolises the convolution process and $h(t)$ is the impulse response of optical channel in baseband and it is modelled by Gfeller and Bapst as follows [71]:

$$h(t) = \begin{cases} \frac{2\, t_0}{t^3 sin^2(FOV)} ; & t_0 \le t \le \frac{t_0}{\cos(FOV)} \\ 0 ; & elsewhere \end{cases} \quad (2.6)$$

where $t_0$ is the minimum delay and $FOV$ is the field of view of the receiver. This model can be illustrated as shown in Fig. 2.3.

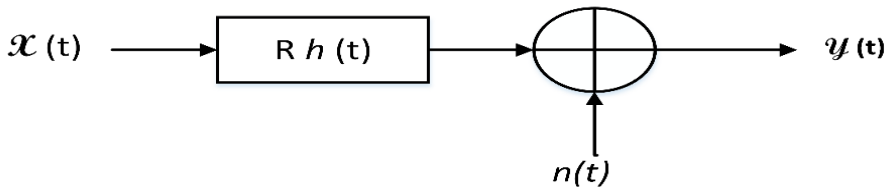


Fig. 2. 3 An optical wireless communication system utilising baseband IM/DD.

Two constraints on the instantaneous transmitted optical signal are required. Firstly, $x(t)$ must be always non-negative, which means:

$$x(t) \ge 0. \quad (2.7)$$

Secondly, the average of $x(t)$ must not exceed the average power requirement for eye safety requirements, which means [55]:

$$P_{max} \leq \lim_{T\to\infty} \frac{1}{2T} \int_{-T}^{T} x(t)\ dt \tag{2. 8}$$

where, $T$ is the period of signal $x(t)$. Generally, an indoor OWC channel is modelled based on the angular distribution utilising the Lambertian radiant intensity as shown in the following equation [55]:

$$R_0(\theta) = \begin{cases} \frac{(m_l+1)}{2\pi}\ cos^{m_l}(\theta); & -\pi/2 \leq \theta \leq \pi/2 \\ 0 \quad ; & \theta \geq \pi/2 \end{cases} \tag{2. 9}$$

where $m_l$ is the Lambertian emission which is given by [55]:

$$m_l = \frac{-\ln(2)}{\ln(\cos(\theta_{1/2}))} \tag{2. 10}$$

where $\theta_{1/2}$ is semi-angle at half luminance of the LED Fig. 2.4 (a). We can now express the radiant intensity $S(\theta)$ by [55]:

$$S(\theta) = P_t \frac{(m_l+1)}{2\pi}\ cos^{m_l}(\theta). \tag{2. 11}$$

The photodetector has an active area $A_r$ which collects the incident light at the incident angle $\psi$, which must be less than that of the FOV of the photodetector as shown in Fig. 2.4 (b). We can then define the effective collection area $A_{\text{eff}}$ by:

$$A_{\text{eff}}(\psi) = \begin{cases} A_r \cos\psi\,; & 0 \leq \psi \leq FOV \\ 0\,; & \psi > FOV. \end{cases} \tag{2. 12}$$

If the concentrator is an ideal non-imaging with refractive index $n$, the optical gain can then be expressed as [55]:

$$g(\psi) = \begin{cases} \frac{n^2}{\sin^2 FOV}; & 0 \leq \psi \leq FOV \\ 0\,; & \psi > FOV \end{cases} \tag{2. 13}$$

In Chapter 3, we will discuss the impulse response for two scenarios that LOS and LOSNLOS scenarios in the VLC environment.

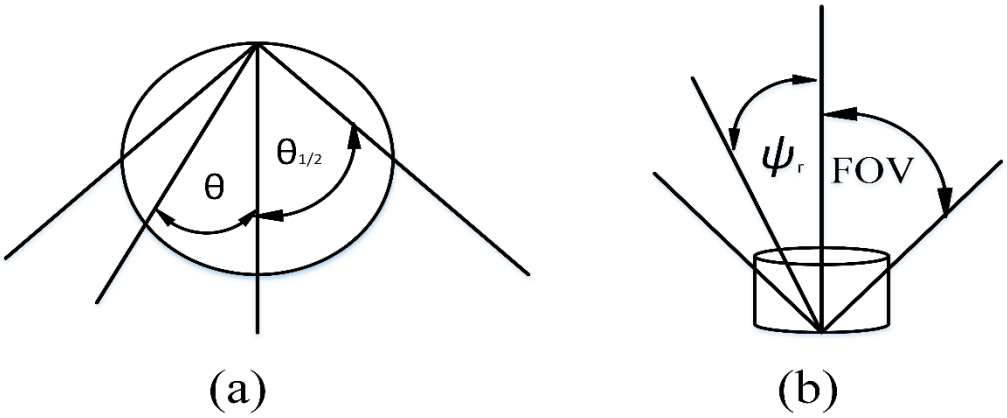


Fig. 2. 4 (a) The semi-angle at half luminance $\theta_{1/2}$ of the transmitter (LED) and the irradiance light angle $\theta$, (b) The field of view of receiver (FOV) and the incident angle $\psi$

## 2.2.3. Photodetector

A photodetector is a unique solid-state device used as an optical receiver. It generates an electrical current from the incident bright light on its surface based on the photoelectric effect in the depletion layer. The absorption process of photons creates electron-hole pairs as a result of electrons going to the *N* side and holes to the *P* side of the junction as shown in Fig 2.5. There is a proportional square relationship between the generated photocurrent by photodetectors and the instantaneous received optical power over a greatly superior dynamic range.

There are two types of photodetectors, namely, photodiodes and phototransistors. Photodiodes can be semiconductor pn junction, PIN photodiode or APDs. These types differ in the depletion layer size and gain. For instance, APDs provide gain whereas PINs do not and each have different bandwidth. Phototransistors are like photodiodes, except that there is an additional n-type region added to the photodiode and the response time of phototransistor is slower compared with a photodiode. The relation between the average photocurrent $I_p$ and the incident optical power $P_p$ or radiant flux in the basic steady-state operation can be modelled by the following expression [55]:

$$I_p = q\eta_i \frac{P_p}{hv}. \tag{2. 14}$$

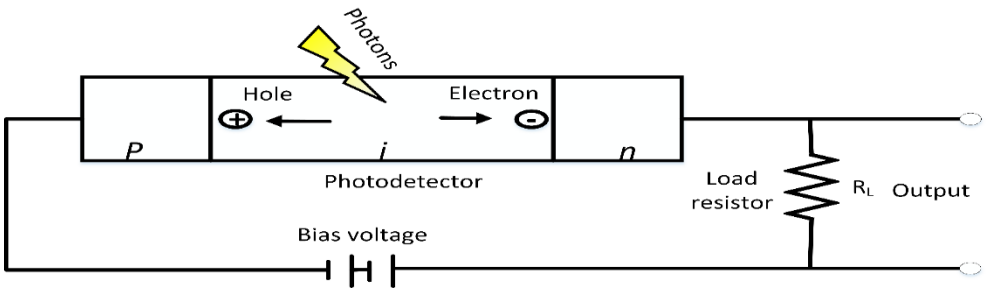


Fig. 2. 5 PIN Photodiode diagram.

where q is the electronic charge, $\eta_i$ is the quantum efficiency of the device in electrons per photon, $hv$ is the photon energy, $h$ is the Planck constant (eVs) and $v$ is the photon frequency (m/s). The flux responsivity ($\mathcal{R}$) in amps per watt is the ratio of photocurrent to the received optical power and can be derived from (2.6) as follows [55]:

$$\mathcal{R} = \frac{No.\ of\ electron{-}hole\ pairs\ generated/sec}{No.\ of\ incident\ photons/sec} = \frac{I_p}{P_i} = \frac{q\eta_i}{hv}. \quad (2.\ 15)$$

The responsivity can be rewritten based on the relation between the power and the length $x$ of semiconductor (i.e. $\exp(-\alpha x)$) as shown in the following equation [55]:

$$\mathcal{R} = \frac{q\lambda}{hv}(1 - R_f)\big(exp(-\alpha x_1) - exp(-\alpha x_2)\big) \quad (2.\ 16)$$

where $\lambda$ is the wavelength of light, $R_f$ is the reflectivity at the entrance of the photodiode and $\alpha$ is the absorption coefficient. The quantum efficiency is the probability of generating an electron-hole pair when a photon hits the active area of the photodiode and its typical values range between 0.7 to 0.9. The responsivity of APD can be greater than unity due to the fact that the gain can reach high values up to 300 [55].

## 2.2.4. Modulation Schemes

Previous studies have proposed a number of modulation techniques and have thoroughly analysed a number of the constraints imposed such as the maximum average radiation, power efficiency and transmitted power [42]. The majority of practical OWC systems employ the IM/DD scheme for indoor and outdoor applications. In RF systems, the amplitude, frequency

and phase of the carrier signal are modulated by the information signal. Whilst they cannot be applied in optical system, the intensity of the optical carrier is modulated when data rate is small than 2.5 Gbps. There are a number of modulation schemes that have been deployed in optical systems such as quadrature amplitude modulation (QAM) utilizing discrete multitones (DMT), binary and multi-level modulation schemes, for instance, on-off keying (OOK) modulation and multi-level pulse amplitude modulation [5, 8, 75]. These are suitable for VLC systems and are based on LEDs. The main metrics to select the modulation scheme are:

1. **Bandwidth efficiency**: theoretically the bandwidth is unlimited. However, the receiver bandwidth is limited by the photodetector area whereas multipath propagation confines the bandwidth of channel. Modulation schemes also affect the intersymbol interference (ISI). The efficiency of bandwidth $\eta_B$ is the ratio between achievable bit rate $R_B$ and bandwidth of the IR transceiver $B$ [55]:

$$\eta_B = {}^{R_b}/_{B}. \tag{2. 17}$$

   The second parameter is known by the power efficiency which is the relationship between the bandwidth efficiency and the average duty cycle $\gamma$ [55]:

$$\eta_p = {}^{\eta_B}/_{\gamma}. \tag{2. 18}$$

2. **Transmission reliability**: reliability requires a minimum acceptable error rate. Modulation schemes should overcome a number of problems such as phase jitter due to signal power variations, pulse extensions and pulse distortion.
3. **Power efficiency**: the average transmitted optical power for each modulation technique is limited because of safety regulations and illumination design. The power efficiency is the ratio between the pulse energy $E_{pulse}$ and the average energy per bit $E_B$:

$$\eta_p = \frac{E_{pulse}}{E_b}. \tag{2. 19}$$

These metrics must be taken into consideration in the selection of the modulation scheme based on bandwidth and power requirements. There are two common modulation schemes which are M-ary Pulse amplitude modulation (M-PAM) and L-pulse position modulation (L-PPM) [76]. The simplest modulation technique is OOK which is the lowest order of M-PAM and has the lowest bandwidth efficiency and is easy to implement. In this technique, the amplitude of the electrical current is proportional to the optical power intensity. OOK is based on two levels where the pulse energy is used to transmit a binary one (L-level) whilst the bit zero is represented by an absence of energy (0-level) as shown in following relation:

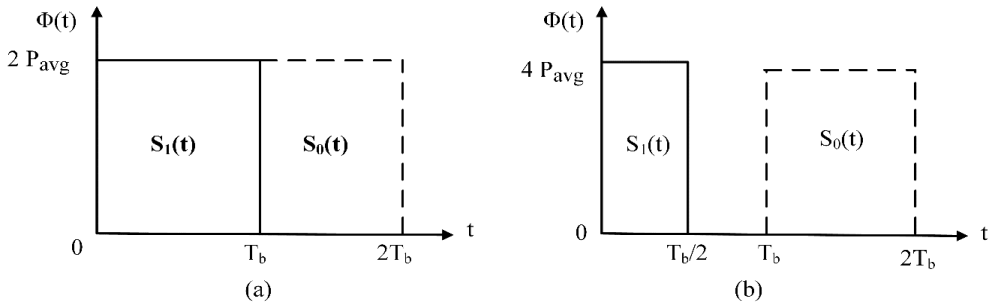


Fig. 2. 6 The OOK signal where $S_1(t)$ represents binary one and $S_0(t)$ represents binary zero. (a) NRZ scheme (b) RZ scheme ($\gamma = 0.5$)

$$P(t) = \begin{cases} P_0; & \text{if } 0 \leq t < T_b \\ 0; & elsewhere \end{cases} \tag{2. 20}$$

where $P_0 = 2\,P_{avg}$, $P_{avg}$ is over the symbol interval and $T_b$ is the bit duration. The OOK technique has two sub-techniques which are return-to-zero (RZ) and non-return-to-zero (NRZ) as illustrated in Fig. 2.6. The data rate achieved by OOK modulation is below 4 Mbps using IrDA and Fast IR links [77]. The OOK signal can be given by [55]:

$$\emptyset_{OOK}(t) = \frac{1}{\sqrt{T}}\, rect(\frac{t}{T}) \tag{2. 21}$$

where

$$rect\,(t) = \begin{cases} 1; & 0 \leq t < \mathrm{T} \\ 0; & otherwise \end{cases} \tag{2. 22}$$

The time varying optical intensity can be represented by the basis function as:

$$x(t)\ \sum_{k=-\infty}^{\infty} 2P\sqrt{T}\, A[k]\emptyset_{OOK}(t - kT) \tag{2. 23}$$

where $A[k] \in [0, 1]$ and it must be uniform. OOK-NRZ has electrical power spectral density (PSD) that is different to the PSD of OOK-RZ. They are given by [55]:

$$PSD_{OOKNRZ}(f) = (P_r\mathcal{R})^2 T_b sinc^2(\pi f T_b)(1 + R_b\delta(f)) \quad (2.\ 24)$$

$$PSD_{OOKNRZ(\gamma=0.5)}(f) = (P_r\mathcal{R})^2 T_b sinc^2(\pi f T_b)[1 + R_b \sum_{n=-\infty}^{\infty} \delta\left(f - \frac{n}{T_b}\right)] \quad (2.\ 25)$$

where $\delta()$ is the Dirac delta function. The power spectral density are plotted in Fig. 2.7. The average optical power is the same for NRZ and RZ schemes. The power efficiency $\eta_P$ is 2 for both but the bandwidth efficiency of NRZ ($\eta_B$) is 1, whereas for the RZ scheme, it depends on the duty cycle such as if $\gamma$=0.25, the bandwidth efficiency is 0.25 [7, 57, 78].

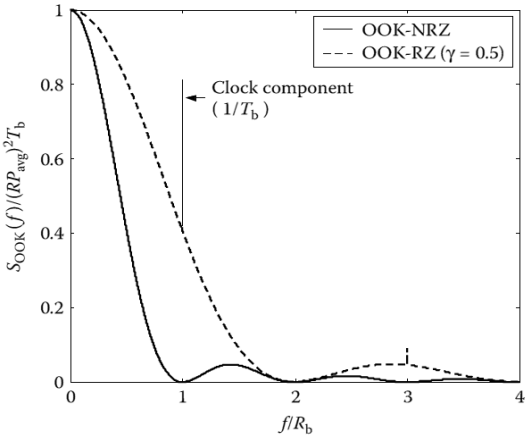


Fig. 2. 7 The power spectral density (PSD) of the OOK-NRZ scheme and the OOK-RZ scheme.

## 2.2.5. Noise in VLC Systems

All communication channels inherently contain noise. The received signal at the receiver side has the least power while the noise is at its highest at the end of propagation. The noise is typically generated from three types of sources, except in the case of APD where the noise can be generated from another noise type.

### 2.2.5.1. Dark Current Noise

The dark current noise is generated as a result of dark current generated in a circuit when there is no light incident on photodetector surface. Due to the reverse bias operation, a small

reverse saturation current flow through the device. The current magnitude is dependent on factors such as temperature, the bias voltage and the material type. Typically, the amplitude of dark current is 100 pA and 10 pA for Si PIN photodiode and Si APD, respectively.

### 2.2.5.2. Shot Noise

The shot noise is generated by the dark current which is a combination of the two currents from bulk and surface leakage. It exists in all optical receivers and is the major source of noise in photodetectors. Variances for bulk current and surface leakage current are given by [55]:

$$\sigma_{db}^2 = 2qI_d M^2 FB. \tag{2. 26}$$

$$\sigma_{ds}^2 = 2qI_l B. \tag{2. 27}$$

where $I_d$ and $I_l$ are the dark and the surface leakage currents, respectively, $F = \langle g^2 \rangle / g$ and $\langle g^2 \rangle$ is the mean-square current gain of the photodiode, $q$ is the electronic charge, B is the equivalent noise bandwidth and $M$ is the gain factor which is given by:

$$M = I_T / I_P. \tag{2. 28}$$

where $I_T$ is the average of the total output current and $I_P$ is the principal photocurrent without gain. The total variance of shot noise can be written as [79]:

$$\sigma_{shot}^2 = \sigma_{db}^2 + \sigma_{ds}^2 = 2q\mathcal{R}\left(P_{r-signal} + P_{rISI}\right)B + 2qI_{bg}I_2 B \tag{2. 29}$$

where $I_{bg}$ is the photocurrent due to background radiation, $P_{r-signal}$ is the received optical power from the signal and $P_{rISI}$ is the desired received power from multipath [80].

### 2.2.5.3. Thermal Noise

In general, all electronic devices (active or passive) have a load resistance $R_L$. Therefore, the thermal fluctuation of electrons with a random motion produce thermal energy even when there is no optical power or voltage applied to the photodetector. This noise source is

also referred to as the Johnson noise. Furthermore, it is white noise and its distribution is Gaussian with zero mean and its variance can be defined as [79]:

$$\sigma_{th}^2 = \frac{8\,\kappa T_e}{G_{oL}} C_{\mathrm{pd}} A I_2 B^2 + \frac{16\pi^2 \kappa T_e \Gamma}{\mathrm{g}_m} C_{\mathrm{pd}}^2 A^2 I_3 B^3. \quad (2.\ 30)$$

where $B$ is the bandwidth of the electrical filter, $\mathrm{g}_m$is the FET transconductance, $\kappa$ is the Boltzmann's constant, $C_{\mathrm{pd}}$ is the fixed capacitance of the photodetector per unit area, $T_e$ is absolute temperature, $G_{oL}$ is the open-loop voltage gain, Γ is the FET channel noise factor, $A$ is the photodetector area and $I_2$ =0.562 and $I_3$= 0.0868 are the noise-bandwidth factors [7, 80-82].

# 2.3. Multiple-Input Multiple-Output (MIMO)

In recent years, indoor VLC systems have been demonstrated to provide good illuminations and at the same time realise reliable high data rate transmission. Such systems are typically equipped with multiple LEDs [83]. This fact results in an increasing throughput which is a requirement of the next generation of communication networks (i.e. fifth Generation (5G)) [8]. The large bandwidth of the visible range of the electromagnetic spectrum can be readily exploited to create optical multiple-input-multiple-output (MIMO) communication systems. MIMO techniques have been applied in many RF systems to achieve high data rates by increasing the spectral efficiency and to make the transmission more robust without increasing the data rate. MIMO-VLC based systems have become an attractive approach for naturally increasing the channel capacity, particularly in indoor environments. These systems can achieve Gbit/s data rates and have already been reported in [66, 84-86].

It is still unclear whether MIMO techniques for indoor OWC can provide gains because there is no fading effect indoor, especially if we only have LOS scenarios. However, there is a high correlation between indoor optical wireless links, to achieve minor diversity gains.

i.e. MIMO techniques mostly depend on spatially uncorrelated channels. The benefits from OWC MIMO include increasing the throughput [87]. There are two main categories for MIMO-VLC: (a) Imaging MIMO, which is similar to a camera communication technique and needs an optical subsystem. (b) Non-imaging MIMO, which is simpler and robust against the mobility conditions as well as it employs multiple transmitters and multiple receivers to send and receive parallel data transmission. The receiver can receive data separately if it has full knowledge about the channel-state information (CSI) from the transmitted pilot signals (PS). Indoor VLC applications in homes and offices need to deal with more mobility and consider shadowing to make sure the link is available at all times. Therefore, if any shadowing takes place in any of the MIMO links, this will hinder the full knowledge of the CSI and as a result, cause a significant increase in the bit error rate (BER) [55, 57, 88].

### 2.3.1. The MIMO VLC Model

An optical wireless MIMO-VLC transmission system employs four transmitters (4-LED array) utilising intensity modulation and direct detection (IM/DD) with four independent and simultaneously transmitted data stream by means of multiple incoherent light sources and multiple photodetectors is shown in Fig. 2.8 (a). The number of transmitters and receivers can be increased or decreased depending on the place size and the illumination footprint requirement without affecting the MIMO principle.

The receiver array consists of four photodetectors (PD) elements (with optional non-imaging concentrators). The receivers collect the light from transmitters, estimate the channel matrix and recover the original data using MIMO signal processing. Fig. 2.8 (b) describes the 4×4 VLC MIMO system. The conventional model for VLC MIMO system can be expressed by [85, 89]:

$$y = Hx + n \tag{2. 31}$$

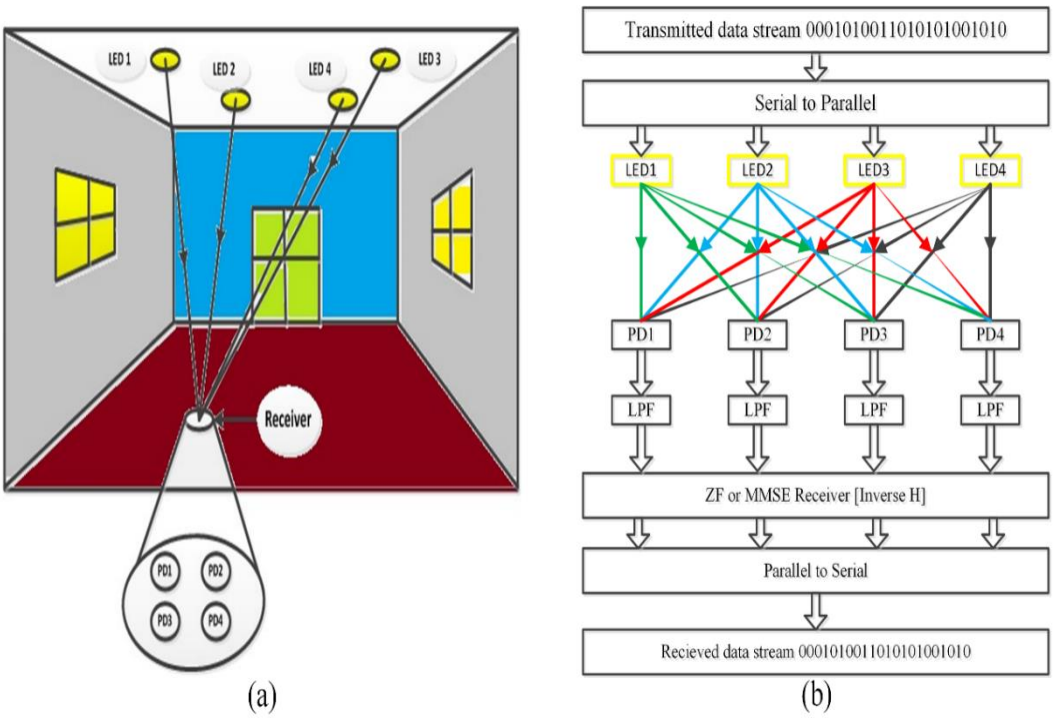


Fig. 2.8 (a) A 4×4 VLC MIMO system (b) Block diagram of the 4×4 VLC MIMO system.

where, y is the received signal vector, $H$ is the channel matrix, $x$ is the transmitted signal vector and $n$ is the AWGN vector. Equation (2.31) can be expanded further as follows:

$$\begin{bmatrix} y_1 \\ y_2 \\ y_3 \\ y_4 \end{bmatrix} = \begin{bmatrix} h_{11} & h_{12} & h_{13} & h_{14} \\ h_{21} & h_{22} & h_{23} & h_{24} \\ h_{31} & h_{32} & h_{33} & h_{34} \\ h_{41} & h_{42} & h_{43} & h_{44} \end{bmatrix} \cdot \begin{bmatrix} x_1 \\ x_2 \\ x_3 \\ x_4 \end{bmatrix} + \begin{bmatrix} n_1 \\ n_2 \\ n_3 \\ n_4 \end{bmatrix} \quad (2.\ 32)$$

The input data $S_d \in \{1,0\}$ is sent to the serial to parallel converter. This converter gives outputs which are a parallel data streams and subsequently, these outputs are DC-level shifted to apply to the IM LED transmitter $T_{xj}$. The transmitted signals are $x_j$ where $j = 1,2,\ldots M$ and $M$ is the number of LEDs at the transmitter side [8, 87, 90].

All data streams are transmitted at the same time. Every receiver will receive a signal which is a linear combination of all $x_j$. The retrieval process of the transmitted data from multiplex signal is based on estimating the channel coefficients between each transmitter $T_{xj}$ and receiver $R_{xi}$. These channel coefficients are called the CSI matrix (H matrix). In other

words, the channel gain $h_{ij}$ denotes the gain for the channel between $T_{xj}$ and $R_{xi}$, where $i$ is the number of PDs at the receiver side, (i.e.; the channel coefficient is $h_{ij}$, which is the gain between $j^{th}$ transmitter and the $i^{th}$ receiver ($1 \leq i, j \leq M$)).

## 2.3.2. MIMO Receivers

To cancel the effect of the channel matrix (H) at the receiver side, the received signal vector (y) is transformed using a matrix equaliser to obtain an estimation of the transmitted signal vector (x). There exist a number of criteria that can be used to estimate the channel coefficients which can be divided into two types of equalisers: Linear equalisers such as Zero-Forcing (ZF) and Minimum Mean Squared Error (MMSE). Whilst nonlinear equalisers such as decision feedback equaliser (DFE), maximum likelihood (ML) equaliser and sphere decoding. In this study, we present and used the linear equalisers as follows [89, 91]:

### 2.3.2.1. Zero-Forcing (ZF) Equaliser

Zero Forcing equaliser is a low complexity linear equaliser that owes its name due to the fact that it minimises the ISI to zero and gives a flat frequency response and a linear phase from the combination of the channel characteristics and the equaliser [92]. However, this equaliser has its disadvantages such as noise amplification and the need for accurate estimation of the channel state information (CSI) to achieve proper operation. The estimated signal vector, $\hat{x}$, using the ZF equaliser which chooses the minimum error vector (least squares solution) and is given by:

$$\hat{x} = \arg\min \|y - Hx\|^2, \tag{2. 33}$$

$$\frac{d\|y-Hx\|^2}{dx} = \frac{d(y-Hx)^T(y-Hx)}{dx}, \tag{2. 34}$$

$$-2H^T\bar{y} + 2HH^T\hat{x} = 0, \tag{2. 35}$$

$$\hat{x} = (H^TH)^{-1}H^T\bar{y}. \tag{2. 36}$$

$$\hat{x} = (H^HH)^{-1}H^H\bar{y}. \tag{2. 37}$$

where the equation (2.41) is used for the real channel matrix, whereas equation (2.42) is for the complex channel matrix and $(H^H H)^{-1} H^H = H^\dagger$ is the pseudo inverse of channel matrix H. We should also note that the existence of an inverse cannot always be guaranteed as is the case where the matrix does not have full rank and is thus not invertible.

## 2.3.2.2. Minimum Mean Squared Error (MMSE) Equaliser

In this technique, the squared error of a random variable is first computed and its mean taken. The mean value represents a very critical difference in statistics. This MMSE equaliser is a linear equaliser, and it works to alleviate ISI and reduce the noise as well. The mathematical model of MMSE equaliser is given as:

$$\hat{x} = \arg\min E\|\hat{x} - x\|^2, \tag{2. 38}$$

$$= \arg\min E\{\|\bar{C}^T \bar{y} - x\|^2\}, \tag{2. 39}$$

Then, the equaliser matrix is given as:

$$\bar{c} = P_d \, (P_d H H^T + \sigma_n^2 \, I)^{-1} \, H \tag{2. 40}$$

where $P_d$ and $\sigma_n^2$ are the powers of the transmitted signal and the noise at the receiver respectively. Finally, the LMMSE equalizer for the MIMO system is given as:

$$\hat{x} = P_d \, (P_d H H^T + \sigma_n^2 \, I)^{-1} \, H \, \bar{y} \tag{2. 41}$$

$$\hat{x} = P_d \, (P_d H H^H + \sigma_n^2 \, I)^{-1} \, H \, \bar{y} \tag{2. 42}$$

where (2.46) is used for a real channel matrix whereas equation (2.47) is used for a complex channel matrix. The above equation can be rewritten as [89]:

$$\hat{x} = \left(H H^H + \frac{1}{SNR} \, I\right)^{-1} \, H \, \bar{y} \tag{2. 43}$$

where $SNR = \frac{P_d}{\sigma_n^2}$. Here, at high SNR, the MMSE equalizer approaches the ZF equalizer [93].

# 2.4. Indoor VLC Positioning Techniques

In general, radio-band satellite-based positioning technologies (i.e. GPS) have been widely used for a number of years mostly for outdoor applications. However, GPS cannot be used in indoor environments (homes, factories, offices, tunnels, etc.) due to the significant signal attenuation by walls and enclosed objects [16, 94]. In addition, the location error in commercial GPS systems is in the order of a few meters, thus making them less attractive for indoor applications where a more accurate (i.e. a few centimetres e.g. in manufacturing and shopping environments) localisation is required. In indoor environments, there are a number of positioning schemes based on radio frequency wireless technologies such as wireless local area network (WLAN), Wi-Fi and Bluetooth which offer a range of accuracy, coverage and installation cost [17, 95, 96].

There are many techniques for positioning in indoor environment that can be used based on the user output including techniques utilising LEDs and are free of interferences from others working in different rooms. In other words, these are the same techniques that have been employed in Wi-Fi networks [97]. Indoor positioning algorithms in Wi-Fi networks can be categorized as:

- Proximity algorithm: Range-free algorithm which is based on the transmission range for a fixed node and a mobile node. In this case, if the power level is weak, this means that the mobile node might be out of the transmission range.
- Fingerprinting localisation algorithm estimate the user's position using two stages. The first stage is an offline learning or training stage to find the channel characteristics using received signal strength indication (RSSI), SNR and probability distribution of the estimated signal. Secondly, the online or runtime stage, where the user compares the data gathered from runtime and the training dataset from training stage to obtain the location[98].

- Trilateration/triangulation algorithm uses the geometrical dependencies between the user and transmitters whereas the trilateration method uses the distances and the angulation method uses the angles between the mobile node and transmitters [99]. The following subsections will explained some of the previous research on sub-techniques that utilise the trilateration and angulation methods in VLC environments [18, 100-102]

## 2.4.1. Time of Arrival (TOA)

The TOA technique uses the signal propagation time to determine the user's position, i.e. it is based on the time for the signal to travel from the transmitter to the receiver [18]. This method is sometimes referred to as Time of Flight and is utilised in GPS systems as well. The majority of current research points that the speed of light $c$ is 3/2 of the propagation speed $v$. Therefore [99]:

$$d = v.t_{propagation} = \frac{2}{3}.c.t_{propagation} \quad (2.44)$$

where $t_{propagation}$ is the propagation time and $d$ is the distance between the mobile node and the transmitters. The first step is to measure the propagation time and the subsequent step is based on the estimation process for the distances between the mobile node and the transmitters using equation (2.34) and utilising trilateration method to estimate the location of the user (mobile node). This technique requires an accurate synchronization between the transmitters and the receiver [99]. In [20, 103], the Cramer-Rao bound (RCB) of TOA-based ranging for an indoor positioning system achieved very accurate distance estimates with perfect synchronization based on the room's geometry, the frequency, the transmitted signal power and the LED and PD characteristics. The average positioning error ranged between 2 and 6 cm [33, 104].

## 2.4.2. Time Difference of Arrival (TDOA)

The study of the difference in arrival times between signals at multiple transmitters is used to determine the relative position of the user and is the main idea behind the TDOA method [18] and it is similar to Time-of-Arrival technique (TOA). The positioning system generates two simultaneously transmitted signals with different propagation speeds ($v_1$and $v_2$) through additional hardware. The difference in time ($t_{dif}$) between the two signals arrival can be given by [99]:

$$t_{dif} = t_2 - t_1 = \frac{d}{v_2} - \frac{d}{v_1}, \tag{2. 45}$$

$$d = \frac{v_1 v_2}{v_1 - v_2} t_{dif} \tag{2. 46}$$

where, $d$ is the distance between the transmitter and the receiver.

In [105], Nah et al. reported a VLC positioning model based on coherent heterodyne detection and simulated the system using MATLAB, achieving accuracies of less than 2 cm in positioning the target receiver. In [32], S-Y Jung et al. proposed a localization algorithm by using the phase difference and TDOA and evaluated it using computer simulations and obtained an average location error of 1.8 mm. In [106], Kim et al.; proposed and analysed a VLC-based location based service (LBS) and the mean of positioning error was around 0.14 meter.

## 2.4.3. Angle of Arrival (AOA)

The AOA technique is based on the intersection of several pairs of angle direction lines, each formed by the circular radius between the transmitter and the device's user [18, 107]. We assume that the position of the user is $(x_u, y_u)$, the transmitter's position is $(x_{\mathrm{Txi}}, y_{\mathrm{Txi}})$

and the angle between the transmitter and the user is $\phi_i$ as shown in Fig. 2.9. Thus, the position of user is given by:

$$x_u = x_{\mathrm{Tx}i} + d_{\mathrm{Tx}i,u}.\cos\phi_i \tag{2. 47}$$

$$y_u = y_{\mathrm{Tx}i} + d_{\mathrm{Tx}i,u}.\sin\phi_i \tag{2. 48}$$

where $i$ = 1, 2, 3…$N$, $N$ is the number of transmitters and $d_{\mathrm{Tx}i,u}$ is the distance between the user and the transmitter and it can be estimated via:

$$\hat{d} = \widehat{H_\alpha}^{\dagger} u_{xy} \tag{2. 49}$$

We can rewrite (2.54) using the matrix form as follows [99]:

$$\begin{bmatrix} -\cos\phi_1 & \cos\phi_2 & 0 & \cdots & 0 \\ 0 & -\cos\phi_2 & \cos\phi_3 & \cdots & 0 \\ \vdots & \vdots & \ddots & \ddots & \vdots \\ 0 & 0 & 0 & \ddots & \cos\phi_N \\ \cos\phi_1 & 0 & 0 & \cdots & -\cos\phi_N \end{bmatrix} . \begin{bmatrix} d_{1,u} \\ \vdots \\ d_{N,u} \end{bmatrix} = \begin{bmatrix} x_1 - x_2 \\ \vdots \\ x_{N-1} - x_N \end{bmatrix} \tag{2. 50}$$

$$\begin{bmatrix} -\sin\phi_1 & \sin\phi_2 & 0 & \cdots & 0 \\ 0 & -\sin\phi_2 & \sin\phi_3 & \cdots & 0 \\ \vdots & \vdots & \ddots & \ddots & \vdots \\ 0 & 0 & 0 & \ddots & \sin\phi_N \\ \sin\phi_1 & 0 & 0 & \cdots & -\sin\phi_N \end{bmatrix} . \begin{bmatrix} d_{1,u} \\ \vdots \\ d_{N,u} \end{bmatrix} = \begin{bmatrix} y_1 - y_2 \\ \vdots \\ y_{N-1} - y_N \end{bmatrix} \tag{2. 51}$$

Islam and Klukas [108] proposed an inertial navigation system (INS) with loosely coupled AOA and INS with tightly coupled AOA to achieve average errors of 2.34 cm and 1.67 cm, respectively, while using the AOA technique only achieved an average error of 4.21 cm. In [79], an AOA estimation algorithm using circular-PD array and truncated-weighting method to improve the accuracy was proposed by S. Lee and S. Jung.

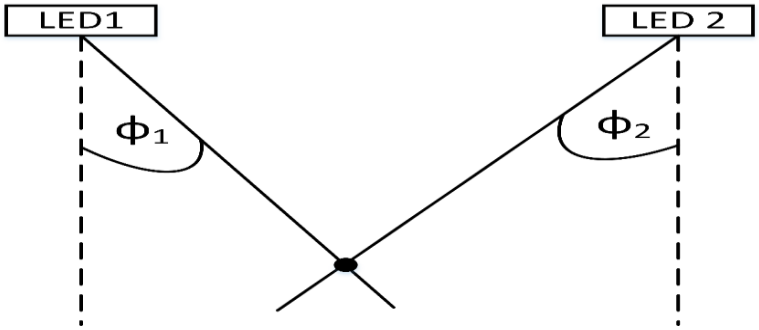


Fig. 2.9 VLC positioning using the AOA technique.

## 2.4.4. Received Signal Strength Indication (RSSI)

An RSSI trilateration method is widely employed in VLC-based localization, which requires at least three lighting sources installed on the ceiling to achieve positioning. This method uses the received power (the received signal strength) levels that are determined at the receiver to estimate the distances between the transmitters and the receiver. Assume that the transmitters' positions are $(x_i, y_i)$ and that they are known, where $i$ = 1, 2, 3 … $N$ ($N$ is the number of transmitters). The position of the user $(x_u, y_u)$ can then be calculated by [99]:

$$(x_i - x_u)^2 + (y_i - y_u)^2 = d_i^2. \quad (2.52)$$

Equation (2.57) can be rewritten in a matrix form as follows [99]:

$$2.\begin{bmatrix} (x_n - x_1) & (y_n - y_1) \\ \vdots & \vdots \\ (x_n - x_{n-1}) & (y_n - y_{n-1}) \end{bmatrix}.\begin{bmatrix} x_u \\ y_u \end{bmatrix} = \begin{bmatrix} (d_1^2 - d_n^2) - (x_1^2 - x_n^2) - (y_1^2 - y_n^2) \\ \vdots \\ (d_{n-1}^2 - d_n^2) - (x_{n-1}^2 - x_n^2) - (y_{n-1}^2 - y_n^2) \end{bmatrix} \quad (2.53)$$

where $d_i$ is the distance between transmitter $i$ and the receiver, which is estimated by the Friis transmission equation as [6]:

$$P_{\mathrm{rx}} = P_{\mathrm{tx}} * H(d) * G_{\mathrm{rx}}, \quad (2.54)$$

where $P_{\mathrm{rx}}$ and $P_{\mathrm{tx}}$ are the received and transmitted signal power respectively, $G_{\mathrm{rx}}$ is the receiver gain and $H(d)$ is the channel gain which is a function of the distance $d$ [12, 20-22, 109-114]. We can be able to compare the positioning techniques as presented in Table 2.2. From the comparison as shown in Table 2.2. we have selected RSSI technique to use in this work because of this method does not require synchronization.

Table 2.2. The comparison between the VLC positioning techniques [18]

| | TOA | TDOA | AOA | RSSI |
|---|---|---|---|---|
| Accuracy | Moderate-to-high | Moderate-to-high | Low-to-Moderate | Moderate |
| Synchronization | Yes (precisely) | Yes (precisely) | No | No |
| Position calculation | Network | Network | Network | Network |
| Implementation in one-way way positioning | Yes | Yes | Yes | Yes |
| Complexity | Complex | Most Complex | More complex than RSSI | Simplest |

# 2.5. Related Work for RSSI Technique in VLC System

The RSSI trilateration method is widely employed in VLC-based localizations and requires at least three lighting sources installed on the ceiling to achieve positioning. There are a number of previous researches on the RSSI technique in VLC positioning. However, these works made different assumptions and had different accuracies. For instance, the first assumption is a LOS and did not consider the effect of noise. As an example, the Epsilon system was implemented and evaluated by Liqun et al., in [115] and is based on the measured received signal strength (RSS) at a receiver using the following equation:

$$P_r = C.\sin(\tau\pi/T).\frac{\cos\theta\cos\phi}{d^2} \quad (2.55)$$

where $C$ and $\frac{\tau}{T}$ are the per-LED constant related to the maximum emission power and the current duty cycle of the LED, both included in its beacon. The positioning accuracies are 0.4 m, 0.7 m and 0.8 m for three typical environments. Yiqing et al. [116] have proposed an indoor localization scheme. This is known as Lightitude based on visible received light strength (RLS) and COST devices using this equation [116]:

$$L_s = \frac{L_0}{d^2}\cos(\phi)e^{-((\theta-\theta_0)/\delta)^2} \quad (2.56)$$

where $L_0$ is the maximum RLS while $\theta_0$ and $\delta$ are constant, $d$ is the distance between the transmitter and the receiver and can be obtained by a one-for-good calibration to achieve a mean accuracy of 1.93 m and 2.24 m in two different environments. In [117], [118] and [119], a positioning algorithm based on the extinction ratio (ER) distributions was reported by Yang et al. which can be expressed as [117]:

$$ER = 10\log_{10}(P_1/P_0) = 20\log_{10}(V_1/V_0) \quad (2.57)$$

where $V_1$ and $V_0$ are the high and low voltage values respectively using the trilateration method. That algorithm achieved extremely low average distance errors of 1.5787 cm, < 3

cm and 1.689 cm for references [117], [118] and [119] respectively. Jia Ziyan proposed in [16] an indoor VLC positioning system for indoor WSN based on hybrid method of the RSSI technique and the range-free VLC method in Rician fading environments. The accuracy was good with lower power consumption and with very small numbers of packets. In [120] and [121], Sertthin et al. proposed a switching estimated receiver position (SwERP) scheme using root mean square error distance (RMSED) which is given by [122]:

$$RMSED = \sqrt{\frac{1}{n}\sum_{i=1}^{n} E_{rr}D_i^2} \quad (2.58)$$

where $E_{rr}D_i$ is the error distance of each experimental result and $n$ is the number of experiments. This work is based on embedding 6-axis sensor and resulting in an accuracy of 298 mm under different field of view (FOV) configuration. Indoor three and two dimensional (3D and 2D) positioning systems were reported by Tuan and Jang in [18, 123] and are based on the following equation to calculate the distance between a user and a transmitter $i$:

$$\mathrm{d_{r,i}} = \sqrt{\mathrm{C_{otp}}/\mathrm{P_{r,i}}} \quad (2.59)$$

where $\mathrm{C_{otp}}$ is the optical constant related to the parameters of the VLC environment. The proposed system aims to improve the accuracy of VLC indoor positioning but the number of localization packets is quite large. In [35], Yong et al. proposed a new indoor 3D and 2D positioning system using a location code and a spatial distribution map based on the extinction ratio (ER) of location code which is the ratio of electrical power level of the location code. The positioning errors were found to be smaller than 3 cm and 12.3 cm for 2D and 3D positioning systems, respectively. The indoor VLC localization based on the received signal strength ratio (RSSR) and three equations was proposed by Jung et al. [124]. They presented the received power as:

$$P_r = k\frac{1}{d^{n+3}} \quad (2.60)$$

where $k = \frac{m+1}{2\pi} A_R h^{m+1} P_T$, $P_T$ is the source power and $h$ is the height of the room. The average and maximum of positioning error were 1.12 cm and 3.65 cm, respectively. An indoor positioning was demonstrated by Hann et al. in [125] using the correlation values between the received data and each address vector as a result to get correlation sum ratio (CSR). The distance error has maximum and average values of 1.495 cm and 0.651 cm respectively. Indoor location estimation was proposed using RSSI and the relative position between multiple optical receivers by Yang in [126]. The maximum estimated position obtained was smaller than 1.5 cm of error and the average was 0.65 cm in symmetric and asymmetric circular pattern. In [110], Yamaguchi et al. designed and evaluated an indoor positioning system using optical orthogonal codes (OOC) theory, code mapping table and trilateration method based on [110]:

$$d = \sqrt{\frac{(m+1)A_{PD}T_s(\psi)g(\psi)\cos^{m+1}(\phi)P_t}{2\pi P_r}} \quad (2.\ 61)$$

The maximum and mean of location errors are 0.403 m and 0.08 m respectively. Three dimensional indoor VLC positioning algorithm based on nonlinear estimation and RSSI technique was proposed by Wenjun, et al. in [127]. They used the following RSSI equation:

$$d_i = \sqrt[4]{\frac{(m+1)A\,T_s(\psi)g(\psi)P_t h^2}{2\pi P_{ri}}} \quad (2.\ 62)$$

and non-linear estimation to minimize the error defined as:

$$\bar{S} = \sum_{i=1}^{4}(\sqrt{(\tilde{x}-x_i)^2+(\tilde{y}-y_i)^2+(\tilde{z}-z_i)^2}-d_i)^2. \quad (2.\ 63)$$

The RMS error was 0.0464 m of the 3D positioning system. In [128], Iturralde et al. have proposed a novel location system using VLC and location identification based on dynamic active radio frequency identification (RFID) calibration (LANDMARC) algorithm with adoption of a mathematical formulation using quadratic equations and the trilateration method to minimize the location estimation error compared to the LANDMARK algorithm [123]. In [31], Cossu et al. reported LOS localization OWC algorithm in a 1-D indoor positioning system. However, there were not any values on location error average. In [34,

53], Hyun-Seung et al. proposed an indoor VLC positioning using RF carriers allocation based on the following equations [34]:

$$d_{ei} = \sqrt{C_{opt}/P_{ri}} = \sqrt[4]{C_{RF}/P_{RFi}}. \quad (2.64)$$

where $P_{ri}$ and $P_{RFi}$ are the received optical power and the RF received power respectively. The adjusted distance $P_{ri}$ can be expressed as [34]:

$$d_{ci} = W_i d_{ei} = (C_n/d_{ei})^n d_{ei}, \qquad 0 \leq n \leq 1 \quad (2.65)$$

where $W_i$ is a weighting factor, $n$ and $C_n$ are the normalizing factor and the normalizing constant, respectively, $d_{ei}$ is the estimated distance and $d_{ci}$ is the adjusted distance. This technique has an average positioning error of 141.1 cm and 2.4 cm with and without using the adjustment process for different values of semi-angle respectively. A novel indoor localization by Wang et al. in [129-131]. It is dependent on the RSSI technique using the following equation:

$$\frac{P_r}{S_r} = \frac{2P_r}{\pi\omega^2}\exp(\frac{-2r^2}{\omega^2}). \quad (2.66)$$

where, $S_r$ is the receiver's area and $\omega$ is the beam footprint of the localization beam. The results in this demonstration show that an average positioning precision of ≈ 15 cm with the ability to reduce the positioning time by 80% [129], while it was ≈ 5.26 cm for work [130]. However, in [131], the authors used the signal incident angle ($\alpha_{in,x}, \alpha_{in,y}$) to estimate the distance and the results show that an average localization accuracy of 3.81 cm. In [132], Saadi et al. presented an indoor positioning system based on RSS of LED, and TDM was used to incorporate angle information at the receiver and different frequencies for $LED_1$ and $LED_2$. The precision of the proposed algorithm is ≈13 cm even in the presence of moderate noise.

The second assumption is a LOS scenario in the presence of noise while the SNR is very high, meaning that the noise has little effect. For instance, in [133], Zhang and Kavehrad

proposed a 2D indoor localization based on LED and the difference in transmitted power between 0s and 1s at the transmitter side $P_{diff,t}$ and at the receiver side $P_{diff,r}$:

$$d_{est} = \sqrt{\frac{(m+1)A\cos^m(\phi)T_s(\psi)g(\psi)\cos(\psi)P_{diff,t}}{2\pi P_{diff,r}}}. \quad (2.67)$$

From the results, the localization error was higher than 5 cm when the average SNR is 30 dB only. An asynchronous indoor positioning system was introduced by Zhang et al. in [134] using VLC technology and least square estimation for two scenarios (direct and sunlight exposure) and with accuracy of 17.25 cm and 11.2 cm, respectively. In [135], Luo et al. proposed an indoor VLC positioning system using dual tone multi-frequency (DTMF) technique without the need for clock synchronization and the system was analysed both in time and frequency domains. The average positioning error from this technique was 18 millimeters when the SNR = 10 dB. In [136], Jaechan Lim published a paper in which the author described an indoor positioning system based on RSS measurement and trilateration using the least square (LS) method and the maximum likelihood (ML) estimator. The results show that the ML method is better than the LS method by approximately 10 dB gain for 10 cm error. In [137], Bangjiang Lin et al. proposed an indoor VLC positioning system using orthogonal frequency division multiplexing access (OFDMA) scheme with a mean positioning error of 1.32 cm and error vector magnitude (EVM) of 12 cm when the SNR > 10 dB.

The third assumption is an LOSNLOS scenario in the absence of noise as described in [138] where Wenjun et al investigated the impact of multipath reflections on the positioning accuracy of indoor VLC positioning system using the RSS technique with a linear LS estimation approach and combined deterministic and modified Monte Carlo (CDMMC). The root mean square (RMS) error was 0.0423 m when the reflections were neglected and it was 0.8064m when the reflections were considered. However, the authors calculated the RMS error for two types of estimations: linear and non-linear [139]. The RMS error was 0.5589 m and 0.4642 m for linear and non-linear estimations respectively for the whole room. In

[140], Abd Elkarim et al. presented two lighting systems that are distinct and provide a uniform lighting system based on the RSSI technique as defined in:

$$d_0 = \sqrt[2m+6]{\frac{(RP_t(m+1)AT_s(\psi)g(\psi)h^{m+1})^2}{4\pi^2 P_{ele.}}} \quad (2.\ 68)$$

where, $P_{ele}$ is the output electrical power from the PD. The mean localization errors were 0.0462 mm and 4.3 mm for distinct and uniform lighting respectively when assuming only a LOS. However, the mean localization errors were 14.98 cm and 9.61 cm for distinct and uniform lighting respectively when considering the effect of diffuse reflections. In [141], Keon et al. developed an indoor localization device based on TDM using bit stuffing method (to avoid light flickering and to prevent inter-pulse interference) as well as the RSSI technique which is presented as:

$$l = a_1 e^{-b_1 S} + a_2 e^{-b_2 S} \quad (2.\ 69)$$

where $l$ is the distance between the light source and receiver, S is the signal strength measure and $a_1, a_2, b_1$ and $b_2$ are values from experimental setup. The maximum and mean of location errors were 3.89 cm and 1.68 cm in simulation whereas 10.29 cm and 3.24 cm in experiment respectively.

The fourth assumption is a LOSNLOS scenario in the presence of noise and was studied in a small number of work such as in [142] by Zhuo et al. where the authors proposed the novel indoor positioning algorithm using VLC environment based on the signal received at the mobile terminal (ML), which is expressed by:

$$r_{MT}(t) = P_0 \sum_{i=1}^{4} S_i(t) \circledast h_i(t) + n(t) \quad (2.\ 70)$$

where, $P_0$ is the emitted power from each LED. This provides a positioning resolution higher than 0.5 mm but the noise level was minuscule (i.e. the noise power level is -140 dBm to -180 dBm). In [143, 144], Aminikashani et al. reported a positioning algorithm based on the RSSI technique which can be presented by:

$$d^{m+3} = \frac{(m+1)AT_s(\psi)g(\psi)(\mathrm{H}-\mathrm{h})^{m+1}}{2\pi P} \quad (2.\ 71)$$

Table 2.3. The classification of the RSSI techniques in the VLC positioning systems.

| No. | author's name | reference | VLC environment | Modulation scheme | Noise | Accuracy |
|---|---|---|---|---|---|---|
| Noiseless LOS scenario | | | | | | |
| 1 | Liqun, et al. | [115] | 20×20×3 $m^3$ | BFSK | No | 0.4 & 0.7 &0.8 m |
| 2 | Yiqing, et al. | [116] | 720$m^2$, 960$m^2$ | not specified | No | 1.93 & 2.24 m |
| 3 | Yang, et al. | [117] | 90×90×150 $cm^3$ | NRZ-OOK | No | 1.57587 cm |
| 4 | Yang, et al. | [118] | 1.5×1.5×2.0 $m^3$ | FDM | No | < 3 |
| 5 | Yang, et al. | [119] | 80×80×150 $cm^3$ | TDM | No | 1.689 cm |
| 6 | Jia Ziyan | [16] | 8×8×3 $m^3$ | not specified | No | not specified |
| 7 | Sertthin, et al. | [120] | 1.2×5×2.05 $m^3$ | SC-4PPM | No | 331.5 &672.5 mm |
| 8 | Sertthin, et al. | [121] | not specified | not specified | No | 298 & 463 mm |
| 9 | Tuan & Jang | [18] | not specified | not specified | No | not specified |
| 10 | Yong, et al. | [35] | 1.5m×1.5m×2.35m | not specified | No | 3 & 12cm |
| 11 | Jung, et al. | [124] | 5×5×3 $m^3$ | TDM | No | 1.12 cm |
| 12 | Hann, et al. | [125] | 30×30×50 $cm^3$ | RZ-OOK | No | 0.651 cm |
| 13 | Yang, et al. | [126] | 2×2×2 $m^3$ | QPSK | No | 0.65 cm |
| 14 | Yamaguchi, et al. | [110] | 36×12×3 $m^3$ | not specified | No | 0.08 m |
| 15 | Wenjun, et al. | [127] | 6×6×3.5 $m^3$ | OOK-TDM | No | 0.0464 m |
| 16 | Iturralde, et al. | [123, 128] | 10×10×20 $m^3$ | not specified | No | not specified |
| 17 | Cossu, et al. | [31] | not specified | OFDM | No | not specified |
| 18 | Hyun-Seung, et al. | [34] | 60×60×60 $cm^3$ | QPSK | No | 141.1 & 2.4 cm |
| 19 | Hyun-Seung, et al. | [53] | 60×60×60 $cm^3$ | QPSK | No | 6 cm |
| 20 | Wang, et al. | [129] | 5×4×3 $m^3$ | not specified | No | < 15 cm |
| 21 | Wang, et al. | [130] | not specified | OOK | No | ≈ 5.26 cm |
| 22 | Wang, et al. | [131] | not specified | OOK | No | ≈ 3.81 cm |
| 23 | Saadi, et al. | [132] | 3×3×2 $m^3$ | TDM | No | ≈ 13 cm |
| Noisy LOS scenario | | | | | | |
| 24 | Zhang, et al. | [133] | 6×6×4 $m^3$ | OOK | 30dB | ≈ 5 cm |
| 25 | Zhang, et al. | [134] | 6×6×4 $m^3$ | OOK | 30dB | 17.25 &11.2cm |
| 26 | Luo, et al. | [135] | 2×2×2 $m^3$ | not specified | 10dB | 18 mm |
| 27 | Jaechan Lim | [136] | 6×6×4 $m^3$ | OOK | 15dB | 10 cm |
| 29 | Bangjiang, et al. | [137] | 10×10×9 $cm^3$ | QPSK -OFDMA | 10dB | 1.32 cm |
| Noiseless LOSNLOS scenario | | | | | | |
| 30 | Wenjum, et al. | [138] | 6×6×3.5 $m^3$ | OOK | No | 0.0423 &0.8064m |
| 31 | Wenjum, et al. | [139] | 8×8×3.5 $m^3$ | OOK | No | 0.5589 &0.4642m |
| 32 | Abd Elkarim, et al. | [140] | 5×5×4 $m^3$ | not specified | No | 0.0462 &4.3 mm<br>14.98 &9.61 cm |
| 33 | Keon, et al. | [141] | 120×120×170 $cm^3$ | not specified | No | 3.89 &1.68 cm<br>10.29 & 3.24cm |
| Noisy LOSNLOS scenario | | | | | | |
| 34 | Zhuo, et al. | [142] | 3×3×3 $m^3$ | RZ-OOK | -140 dBm, -180 dBm | 0.5 mm |
| 35 | Aminikashani, et al. | [143, 144] | 6×6×3.5 $m^3$ | OFDM, OOK | 15dB, 25dB | 0.2609 & 1.01m |
| 36 | Wei Xu, et al. | [145] | 6×6×3 $m^3$ | not specified | 10 dB | 6 & 4 cm |

where, H is the height of the transmitter, $h$ is the height of the receiver and $P$ is the power attenuation. The mean of positioning errors was 0.2609 m and 1.01 m for OFDM and OOK modulation schemes respectively when the SNR is 15 dB and 25 dB with different number of subcarriers. In [145], Wei Xu et al. presented an indoor positioning scheme for VLC system using multi-PDs and the RSSI technique based on the following equation:

$$d = \sqrt[m+3]{\frac{m+1}{2\pi} A h^{m+1} \frac{P_t}{P_r}} \quad (2.72)$$

where, $A$ is the PD area, and $h$ is the vertical distance between the LED and PD. The mean positioning error was 6 cm and its maximum error was around 14 cm under M =1 (number of LEDs) and N=3 (number of PDs), whereas under M=2 and N=2 the mean positioning error was 4 cm and its maximum was 13 cm under the real VLC channel when SNR=10 dB.

Finally, the Table 2.2 shows the summary of the classification of the RSSI techniques in the VLC positioning systems for four different scenarios as well as different modulation schemes and different VLC environments.

# 2.6. Summary

The main goal of Chapter 2 was to review the indoor visible light communications and its fundamentals as well as an indoor MIMO VLC system. This chapter has highlighted a number of features of VLC systems, compared it to RF communications systems counterpart and some of the challenges were also mentioned. In addition, Chapter 2 has comprehensively reviewed a VLC system. For instance, LEDs, PDs and the VLC channel with mathematical model of transmitted optical power and the impulse response for LOS and NLOS scenarios were discussed. Furthermore, the optical receiver (i.e.; photodetectors) and OOK modulation scheme were studied with different types of noises that are common in a VLC system. This chapter also introduced the MIMO VLC system with the ZF and MMSE equalizers that were

used. Finally, there are four common techniques in indoor VLC positioning system that have been discussed as well. In addition, the chapter summarises all results from related works on indoor VLC positioning systems which use the RSSI technique under different assumption.

The next chapter will introduce a new algorithm for an indoor VLC positioning system based on the received power levels of LEDs and the trilateration method with comprehensive investigation of the impact of noise for both LOS and LOSNLOS scenarios and applied that in MIMO VLC application to recover the data with a partial CSI knowledge.

# Chapter Three

# Indoor VLC Positioning System Using Three Transmitters

## 3.1. Introduction

VLC systems based on LEDs technology not only provide higher data rates for indoor wireless communications and offer room illumination, but also have the potential for indoor localization. We begin with an investigation on the received optical power (ROP) distributions with and without optimum Lambertian order which are evaluated and simulated by MATLAB for indoor cellular VLC system considering two types of illuminations. A further analysis of the results are also presented as well as an analysis into the ROP relationship.

In addition, we propose a new algorithm for indoor VLC positioning using the RSSI technique and the trilateration method. The end of chapter, we report an application based on indoor VLC positioning in a MIMO-VLC system by simulation as well.

## 3.2. Received Optical Power (ROP) Distributions

### 3.2.1. Optimum Lambertian Order

There are a number of studies on cellular VLC systems which focus mainly on the uniform received power distribution and the reduction of distortion that is generated from multi-reflections. A new genetic algorithm has been reported obtaining a uniform ROP distribution for cellular VLC systems without increasing the distortion from multipath [146, 147]. In [148, 149], a spotlight scheme provides low channel distortion when using small divergence angles of LEDs. Subsequently, the cellular configuration is the best solution to

achieve a higher data rate and obtain a uniform optical power distribution. The conclusion from these studies is that the divergence angle (i.e., semi-angle at half power) of the LED is an essential parameter as it affects both ROP distributions and the channel distortion for indoor VLC system [150, 151].

From equation (2.10), it can be noted that the Lambertian emission order only depends on the semi-angle at half luminance (divergence angle) of the LED. Subsequently, an optimum Lambertian order (OLO) is dependent on the optimum divergence angle of the LED. The OLO is used to minimize the channel path loss and to obtain uniform ROP based on the number of cells in a standard room. The OLO can be derived from the conventional Lambertian model as follows.

From (2.9), we can derive the output power of Lambertian radiance depending on the irradiance angle, $\theta$, as [149, 152]:

$$dP_i = \frac{(m+1)}{2\pi} P_i cos^m(\theta) d\Omega \quad (3.1)$$

Where $dP_i$ is the optical power radiated into the solid angle $d\Omega$. Therefore, the total transmitted optical power can be written as [149]:

$$P = \int_{Hemisphere} dP_i \quad (3.2)$$

In this derivation, we assume only a LOS path. By using (2.14), for each cell, the maximum ROP occurs at $\theta = 0$ and the minimum ROP at $\theta = \theta_{max}$. Those are presented as [149]:

$$P_{Rx\_max} = P_{Tx} \frac{(m+1)A_r}{2\pi V^2} \cos(\psi)\, T_s(\psi) g(\psi), \qquad 0 \le \psi \le \text{FOV}. \quad (3.3)$$

$$P_{Rx\_min} = P_{Tx} \frac{(m+1)A_r}{2\pi {d_{max}}^2} cos^m(\theta_{max}) \cos(\psi)\, T_s(\psi) g(\psi), \qquad 0 \le \psi \le \text{FOV}. \quad (3.4)$$

where $\theta_{max}$ and $d_{max}$ are the maximum irradiance angle and the maximum distance between the transmitter and the receiver inside every single cell (Radius of VLC cell), respectively,

$V$ is the perpendicular distance between the transmitter and the receiver. The maximum value of minimum ROP ($P_{Rx\_min}$) occurs when $\frac{\partial P_{Rx\_min}}{\partial m} = 0$, where [151]:

$$\frac{\partial P_{Rx\_min}}{\partial m} = kcos^{m}(\theta_{max})(1 + (m+1)\ln(\cos(\theta_{max})), \quad (3.5)$$

where,

$$k = P_{Tx}T_s(\psi)g(\psi)\cos(\psi)\frac{A_R}{2\pi d_{max}^2}. \quad (3.6)$$

We can express the OLO ($m_{\text{opt}}$) as:

$$m_{\text{opt}} = \frac{-1}{\ln(\cos(\theta_{max}))} - 1, \quad (3.7)$$

where $\theta_{max} = \cos^{-1}(\frac{V}{d_{max}})$ and the optimum semi-angle at half power $\theta_{1/2\_\text{opt}}$ can be given as [149]:

$$\theta_{1/2\_\text{opt}} = \cos^{-1}\left(\exp\left(\frac{-\ln(2)}{m_{\text{opt}}}\right)\right). \quad (3.8)$$

## 3.2.2. VLC System Configurations

The illumination of the proposed indoor VLC system has been divided into two types in this chapter. The first proposal is a single cell for the whole room, and the transmitter constitutes of LEDs array that is in the middle of the ceiling where that the dimension of the room is 5m×5m×3m (width, length, height) as shown in Fig. 3.1 (a). The second proposal uses four cells, where each single cell has a transmitter in the middle. The typical room has a dimension of 5m×5m×3m as shown in Fig. 3.1 (b). Here, the assumption is that all transmitted optical power from transmitters and the semi-angle at half power of each LED are the same. The next investigation will be on the ROP by a photodetector (PD) with and without the optimum Lambertian order from a LOS path, a NLOS path and both LOS and NLOS paths from the first reflection.

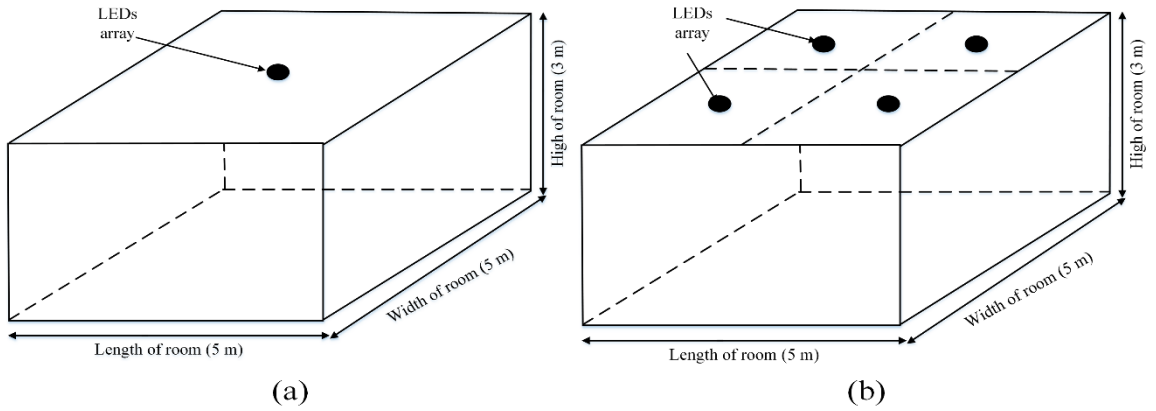


Fig. 3.1 An indoor VLC system with two types of illumination using (a) one transmitter (b) four transmitters.

## 3.2.3. The ROP Distributions

LEDs are used for illumination and data communication in future applications and have a number of advantages including luminous intensity and transmitted optical power at visible light spectrums. In this chapter, the ROP distributions are analysed and discussed. The simulations are carried out using the parameters which presented in Table 3.1. The illumination and data communication for standard room is implemented using two different types of illumination, namely, single and four transmitters configurations as follow:

### 3.2.3.1. Single Transmitter Configuration

For office environment, there is a requirement for room illumination which is defined by the international organization for standardization (ISO) to be between 300 lx to 1500 lx [149, 153, 154]. In these simulations, the maximum illuminance is ≈ 1200 lx, whereas the minimum illuminance is ≈ 400 lx at the centre and the corners of the room respectively [149]. The ROP distributions were investigated for LOS and NLOS using (3.9) and (3.10), respectively, based on (2.14), (2.15) and (2.16). While, for LOSNLOS, using both equations to calculate the total ROP [6].

$$P_{Rx} = P_{Tx}.\frac{(m+1)}{2\pi d^2}\, cos^m(\theta)\,.\cos(\psi).T_s(\psi).g(\psi), \quad 0 \leq \psi \leq FOV \tag{3.9}$$

$$P_{Rx} = P_{Tx}.\frac{(m+1)}{2\pi^2 L_1^2 L_2^2}.\rho A_R dA_{wall}\cos^m(\theta_r)\cos(\psi_r)\cos(\alpha_r)\cos(\beta_r)\ T_s(\psi).g(\psi),$$
$$0 \leq \psi_r \leq FOV \quad (3.10)$$

Fig. 3.2 (a) and (b) show the ROP distributions in absolute value (watt) and dBm when the semi-angle at half power is equal to 70° from LOS path. Note that the maximum received power is ≈ -17 dBm and the minimum value is ≈ -26 dBm. The communication system is able to detect a received optical sensitivity (used with the AD8015 trans-impedance amplifier) equal to -36 dBm at 155.52 Mbps [155]. The ROP distribution in dBm units from NLOS path is shown in Fig. 3.2 (c). Note that the maximum is ≈ -29 dBm and the minimum is ≈ -37 dBm at the corner and the centre respectively whereas Fig. 3.2 (d) shows the total ROP from both LOS and NLOS paths. Some statistical standards are presented in Table 3.2 which shows that there is a very small difference between the ROP with and without optimum Lambertian order (i.e.; optimum semi-angle at half power). This means that the optimum order does not have an effect on the ROP for an indoor VLC system using single cell [156].

Table 3. 1 Parameters of an indoor VLC system

| Parameters | Values |
|---|---|
| Transmitted optical power ($P_{Tx}$) (watt) | 10 |
| Semi-angle at half power ($\theta_{1/2}$) | Optimum, 70° |
| The height from floor to receiving plane (m) | 0.75 |
| FOV of a receiver | 60° |
| Refractive index of a lens at a PD ($n$) | 1 |
| Effective collection area ($A_{\text{eff}}$) ($m^2$) | $16\times10^{-6}$ |
| Gain of an optical filter ($T_s(\psi)$) | 1.0 |
| Received optical sensitivity (used with the AD8015 trans-impedance amplifier) | -36 dBm at 155.52 Mbps |
| Reflectance factor (ρ) | 0.7 |
| The size of room | See Fig. 3.1 |
| The maximum horizontal distance ($d_{max}$) (m) | 3.5, 1.77 |
| Transmitter's position for one cell (m) | (2.5, 2.5) |
| Transmitters' positions for four cell (m) | (1.25,1.25),(1.25,3.75), (3.75,1.25), (3.75, 3.75) |

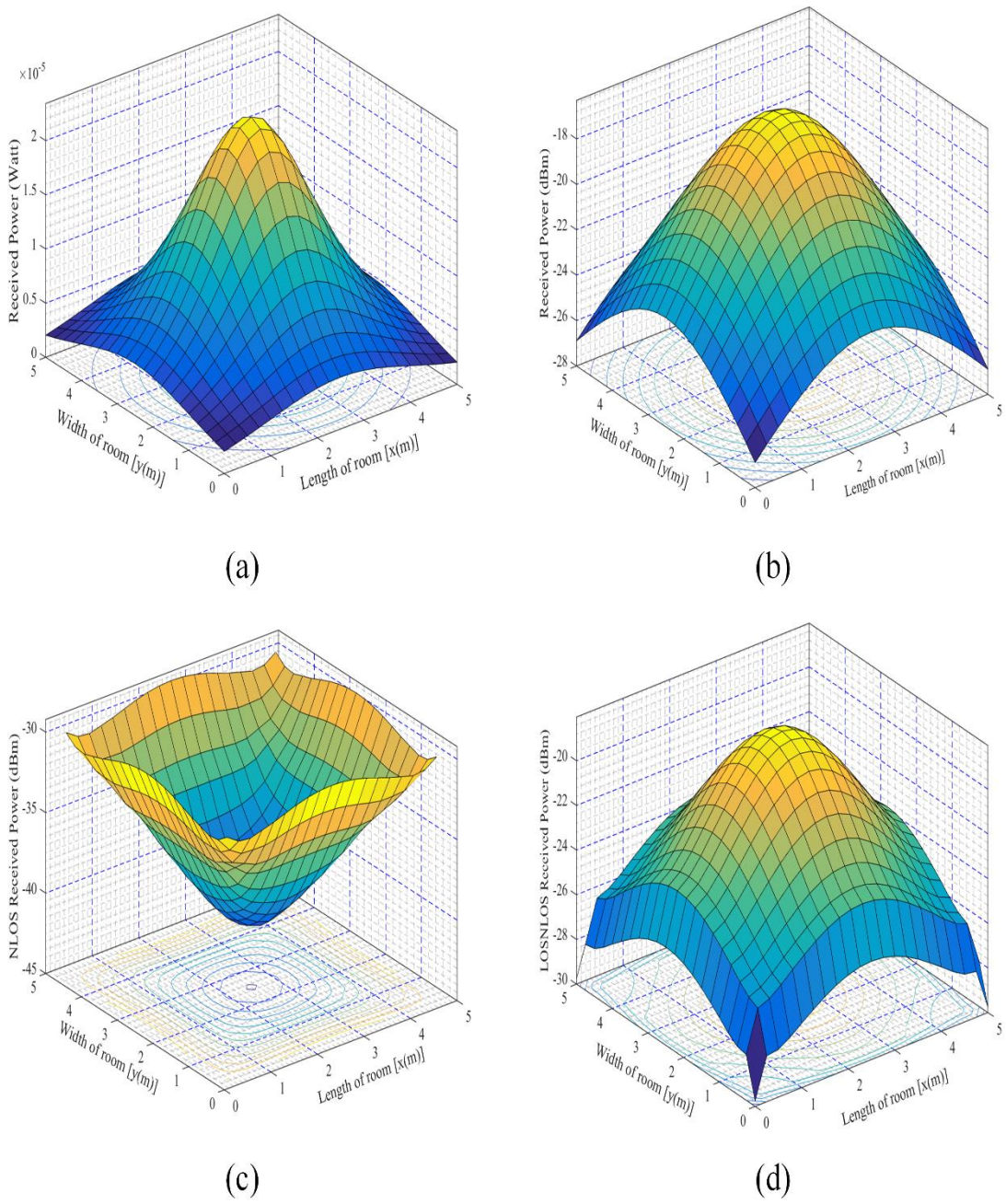


Fig. 3.2 The ROP distributions from LOS, NLOS and LOSNLOS for one transmitter (a) the ROP by watt from LOS only (b) the ROP by dBm from LOS only (c) the ROP by dBm from NLOS only (d) the ROP by dBm from LOSNLOS.

Table 3. 2 Some statistical standards for ROP from one transmitter

| Received optical power (ROP) | | LOS | NLOS | LOSNLOS |
|---|---|---|---|---|
| Optimum semi-angle at half power and $d_{max}$ =3.5 m | Max. | -18.065 dBm | -29.212 dBm | -18.044 dBm |
| | Min. | -29.755 dBm | -41.137 dBm | -26.085 dBm |
| | mean | -23.697 dBm | -35.130 dBm | -21.668 dBm |
| Semi-angle at half power = 70° | Max. | -19.750 dBm | -29.111 dBm | -19.499 dBm |
| | Min. | -29.419 dBm | -37.376 dBm | -29.419 dBm |
| | mean | -24.315 dBm | -33.355 dBm | -22.393 dBm |

### 3.2.3.2. Four Transmitters Configuration

The positions of transmitters are selected as mentioned in Table 3.1 to obtain an illumination profile as flat as possible. The comparison may be divided into three main categories. Firstly, the ROP from LOS path as shown in Fig. 3.3 (a) and (b), has ≈ 4 dBm difference between the maximum ROP with a semi-angle at half power of 70° and the maximum of ROP with optimum semi-angle at half power. On the other hand, the difference of the minimum ROP is quite low (i.e. less than 1 dBm) when using semi-angle at half power equal to 70° and optimum semi-angle at half power. Secondly, the ROP from NLOS path as shown in Fig. 3.3 (c) and (d), where we use semi-angle at half power of 70° and optimum angle respectively. The statistical data in Table 3.3 indicate that the difference between the maximum of the ROP with and without optimum Lambertian order is very small. However, the difference is quite high (i.e. ≈ 18 dBm) between the minimum of ROP with optimum Lambertian order and with semi-angle at half power of 70°. As a result, this causes very high multipath-induced ISI but it provides a good flat illumination as shown in Fig. 3.3 (e) compared to a four transmitter configuration with optimum Lambertian order which is shown in Fig. 3.3 (f).

Table 3. 3 Some statistical standards for ROP from four transmitter

| Received optical power (ROP) | | LOS | NLOS | LOSNLOS |
|---|---|---|---|---|
| Optimum semi-angle at half power and $d_{max}$ =1.77 m | Max. | -13.203 dBm | -24.914 dBm | -13.154 dBm |
| | Min. | -22.555 dBm | -47.939 dBm | -22.555 dBm |
| | Mean | -16.210 dBm | -33.686 dBm | -16.007 dBm |
| Semi-angle at half power = 70° | Max. | -17.322 dBm | -23.171 dBm | -16.954 dBm |
| | Min. | -23.377 dBm | -29.602 dBm | -23.377 dBm |
| | Mean | -18.600 dBm | -26.434 dBm | -17.984 dBm |

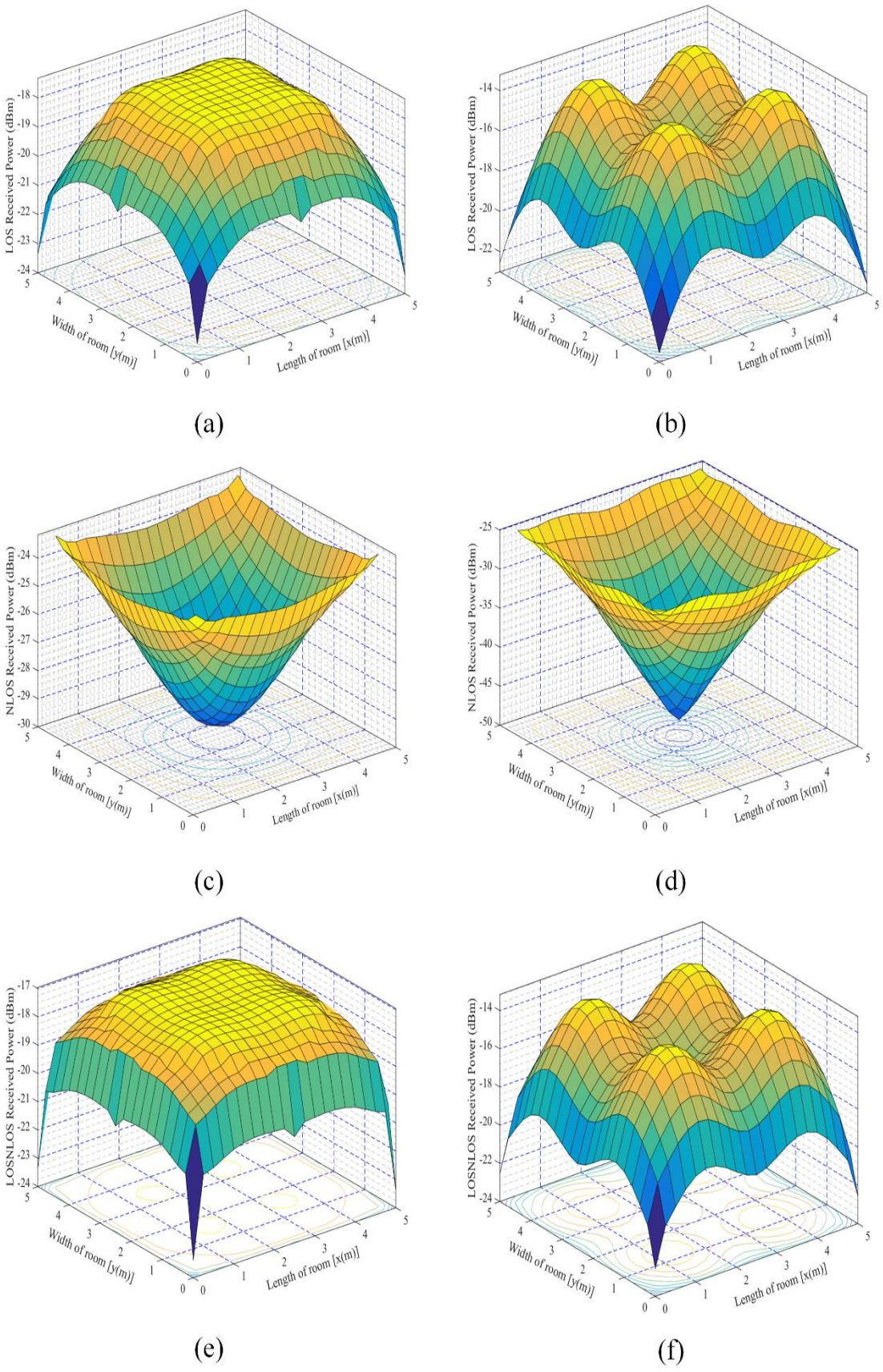


Fig. 3.3. The ROP distributions for four transmitters configuration where

(a) the ROP from LOS when $\theta_{1/2}$=70° (b) the ROP from LOS when $\theta_{1/2}$ is optimum,

(c) the ROP from NLOS when $\theta_{1/2}$=70°, (d) the ROP from NLOS when $\theta_{1/2}$ is optimum,

(e) the ROP from LOSNLOS when $\theta_{\frac{1}{2}}$ =70°, (f) the ROP from LOSNLOS when $\theta_{\frac{1}{2}}$ is optimum.

## 3.2.4. The ROP Relationships

Fig. 3.4 shows the relationship between the semi angle at half illuminance of an LED and the ROP. The curves explain how the maximum power underneath of transmitter changes with different semi-angles at half power. We note that there is an intelligible exponential relationship between the maximum received optical power levels and semi-angle at half power ($\theta_{1/2}$) less than 40 degrees but it is linear between 40° and 80°. However, there is a clear difference in the maximum received optical power levels when using a transmitted power level of less than 10 watts. However, the difference is significantly decreased when the transmitted power level is more than 15 watts. On the other hand, Table 3.2, Table 3.3. and Fig. 3.4 provide some information for ROP from one and four transmitters to design indoor VLC positioning system based on ROP distributions and RSSI techniques.

As shown in Fig. 3.5, bar charts explain the relationship between the transmitted power and the maximum horizontal distance for a VLC cell for different values of half-angle ( i.e., $\theta_{1/2}$ equal to 5°, 10°, 15°, 20°, 25°, and 30° ) and different transmitted LEDs power

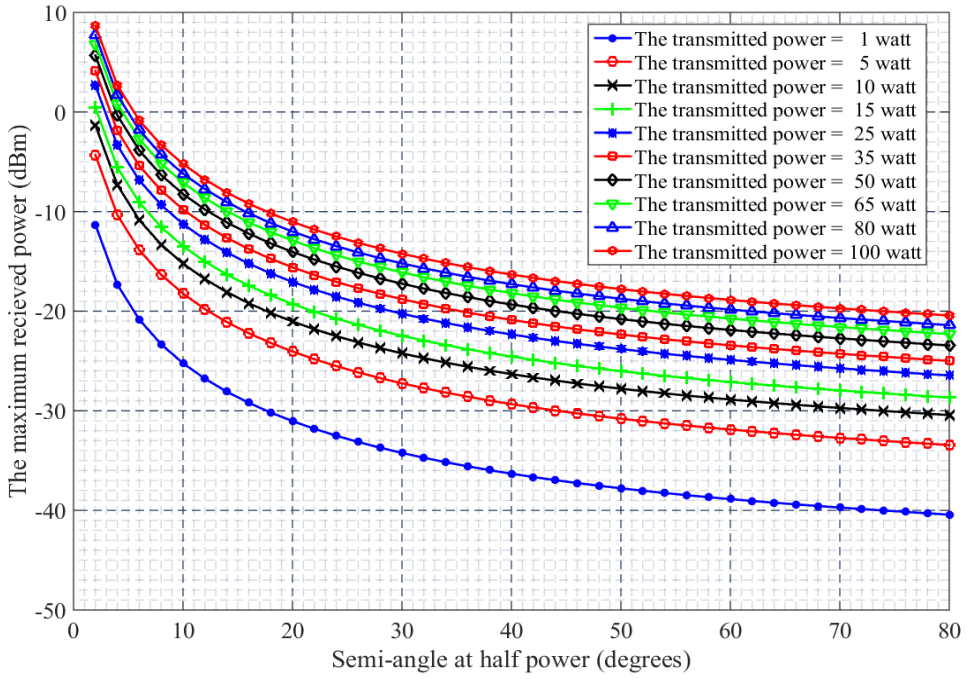


Fig. 3.4. The relationship between the maximum ROP and semi-angle at half power for different transmitted power levels.

( i.e., $P_{Tx}$ = 1, 5, 10, 15, 25, 35, 50, 65, 80 and 100 watts). Fig. 3.5 (a) shows the previous relationship when the receiver sensitivity is -36 dBm whereas Fig. 3.5 (b) shows the relationship when the receiver sensitivity is -30 dBm. These are based on the received optical

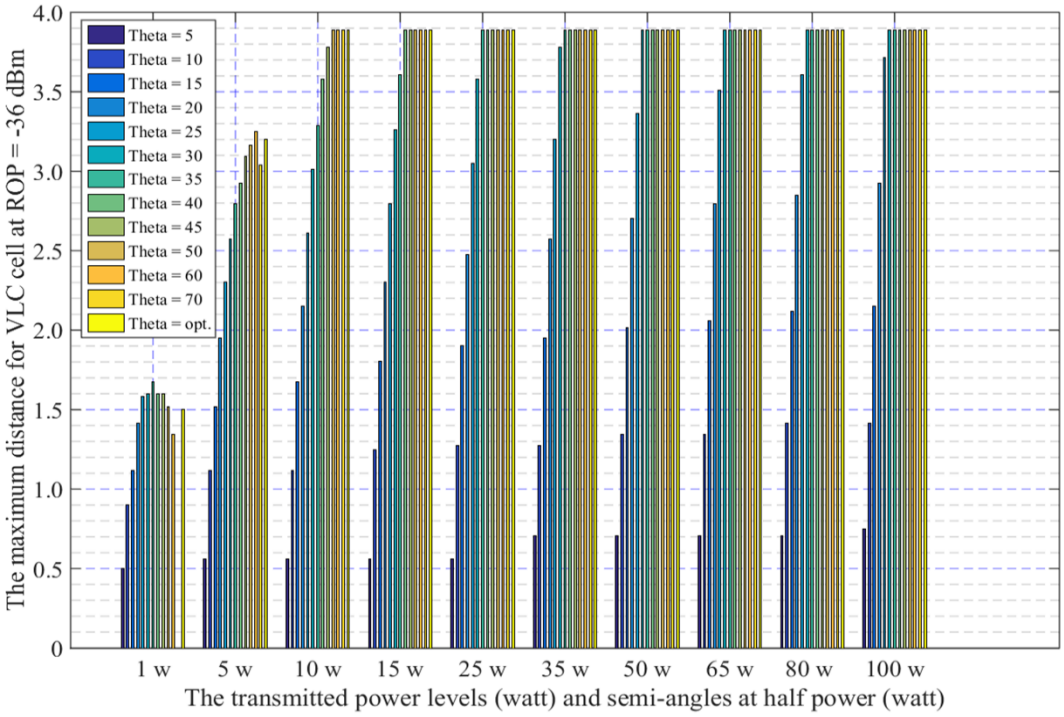


(a)

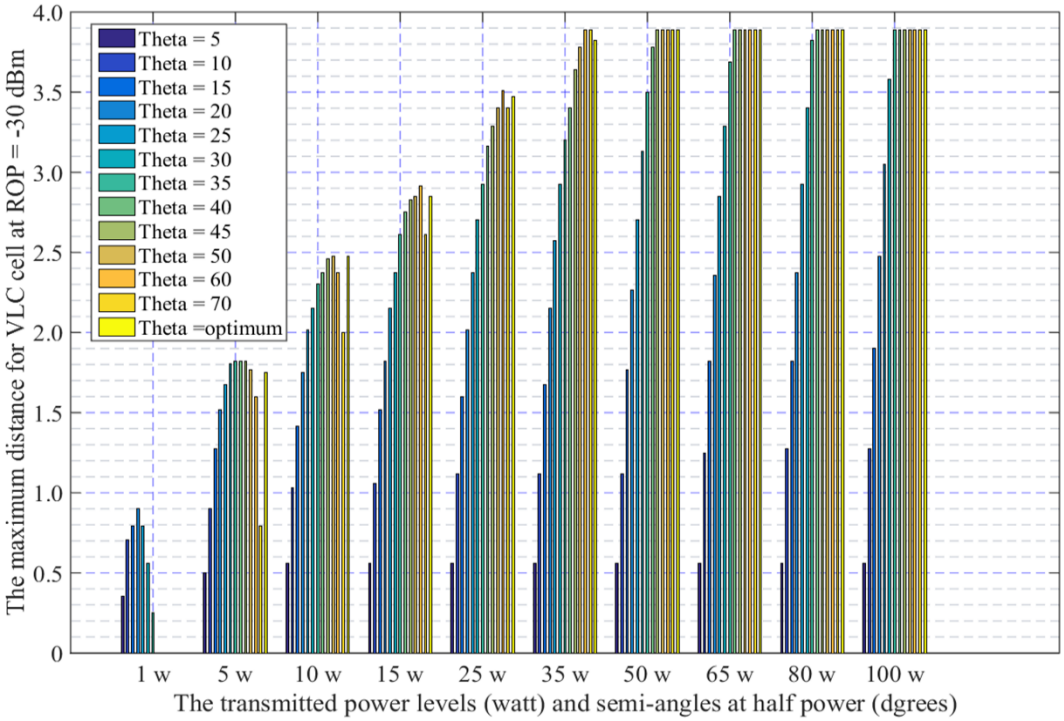


(b)

Fig. 3.5. The maximum horizontal distance against the transmitted power level and semi-angle at half power when (a) receiver sensitivity = -30 dBm (b) receiver sensitivity = -36 dBm.

sensitivity of PD but the second case was plotted to compare the effect of the sensitivity on the maximum horizontal distance. From the chart, it can be seen that there was no difference between the maximum horizontal distances when the transmitted power is more than 10 watts and the semi-angle at half power is more than 50 degrees or the optimum semi-angle when the sensitivity of PD is -36 dBm.

# 3.3. Proposed Indoor VLC Positioning System

## 3.3.1. The System Description

Throughout this work, we consider an indoor VLC environment as illustrated in Fig. 3.6 (a). The coordinator, the visible LED and the smart device as a mobile user are the three main parts as required by the IEEE 802.15.7 protocol [3, 18]. The standard room size is 5 × 5 $m^2$ with a height of 3 m and the receiver plane is 0.75m above floor as illustrated in Fig. 3.6 (a) and Fig. 3.7. The room is assumed to be empty. The coordinator generates different location codes for four transmitters based on the transmitters' positions and use the locations and combines them to the transmitted data (i.e. is to frame). The transmitted data is modulated using on-off keying-time division multiplexing (OOK-TDM) modulation scheme. The intensity modulation/direct detection (IM/DD) technique is employed to generate the transmitted signal, $x(t)$, as shown in Fig. 3.6 (b). These transmitted signals are up-sampled by 10 times.

**Notations:** In what follows, we shall use the following notations:

- $h_{LED}(t)$: The impulse response of LED.
- $h_{Ch}(t)$: The impulse response of VLC channel.
- $h_{Ch,LOS_i}(t)$: The impulse response of VLC channel in LOS scenario.
- $h_{Ch,NLOS_i}(t)$: The impulse response of VLC channel in NLOS scenario.
- $h_{Ch,LOSNLOS_i}(t)$: The impulse response of VLC channel in LOS and NLOS scenarios.

- $h_{\mathrm{PD}}(t)$: The impulse response of the PD.
- $n(t)$: An additive white Gaussian noise (AWGN).

The impulse response of LED, $h_{LED}(t)$, was derived by applying a pulse function to the LEDs in the lab as shown in Fig. 3.8 (a). As a result, the output signal, $y(t)$, of the LED is given by [142]:

$$y(t) = x(t) \circledast h_{\mathrm{LED}}(t) = \int_0^{\infty} x(t-\tau) h_{\mathrm{LED}}(\tau)\, d\tau, \tag{3. 11}$$

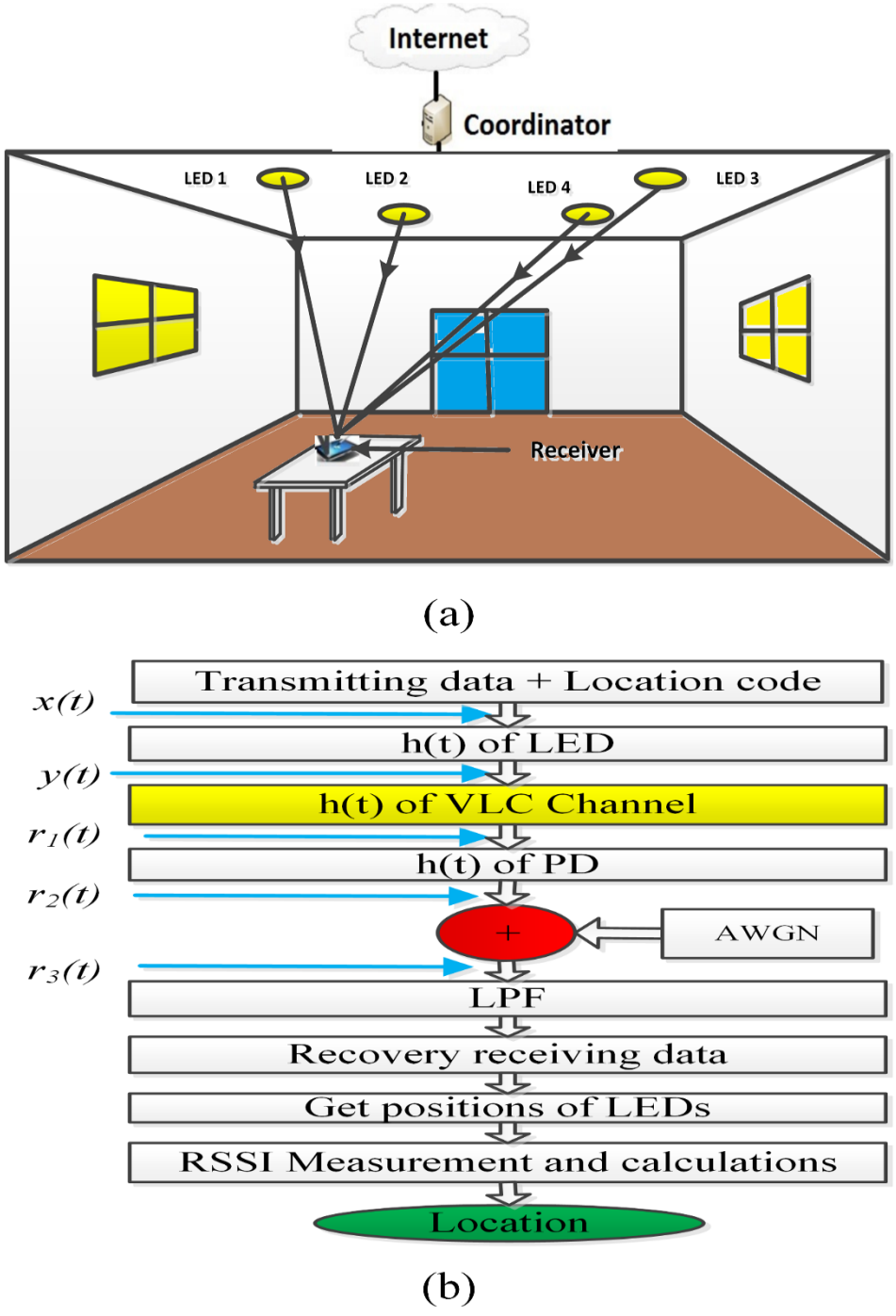


Fig. 3.6. (a) Indoor VLC positioning system (b) Block diagram of indoor VLC positioning system.

where, $\circledast$ denotes the convolution operation. Then, the output signal, $y(t)$, is sent to the VLC channel with the impulse response, $h_{Ch}(t)$, as shown in Fig. 3.8 (b) and (c). Fig. 3.8 (b) shows the impulse response of the VLC channel in LOS scenario, $h_{Ch,LOS_i}(t)$, whereas, Fig. 3.8 (c) shows the impulse response of the VLC channel in a NLOS scenario, $h_{Ch,NLOS_i}(t)$, where we have considered only the first reflection. The signal $r_1(\mathrm{t})$ in front of the PD is:

$$r_1(\mathrm{t}) = y(t) \circledast\ h_{Ch}(t) = \begin{cases} y(t) \circledast h_{Ch,LOS_i}(t) & \text{for LOS case} \\ y(t) \circledast h_{Ch,LOSNLOS_i}(t) & \text{for LOSNLOS case} \end{cases} \quad (3.\ 12)$$

at the receiver side, we receive four signals from four transmitters (i.e., four LEDs) using one PD based on OOK-TDM scheme and the output of the PD is given by:

$$r_2(t) = r_1(t) \circledast h_{\mathrm{PD}}(t) \quad (3.\ 13)$$

where $h_{\mathrm{PD}} = constant$. In this work, we assume $h_{\mathrm{PD}}(\mathrm{t}) = 0.6$. Ultimately, the received signal of the overall system can be expressed as:

$$r_3(t) = r_2(t) + n(t), \quad (3.\ 14)$$

where $n(t)$ is the background noise which is the combination of thermal, shot and dark noise and can be modeled as AWGN. A low pass filter (LPF) was used to reduce the impact of noise. The RSSI technique was implemented to obtain the user's location. Using this technique, the receiver separates the received data from each transmitter by slot time and recover the original data with location codes. These location codes are then used to detect the locations of the transmitters and simultaneously measure the power level for every LED, $P_{\mathrm{Rx},L_i}(\theta_{L_i})$. Consequently, we can obtain the received power level, $P_{\mathrm{Rx},h}(0)$, at distance $h$, from the typical room measurements. Finally, by applying the RSSI algorithm and the trilateration method, we obtain the user's location. In the next section, the user's location methodology will be explained. The flow of the mathematical and signal process is illustrated in Fig. 3.6 (b).

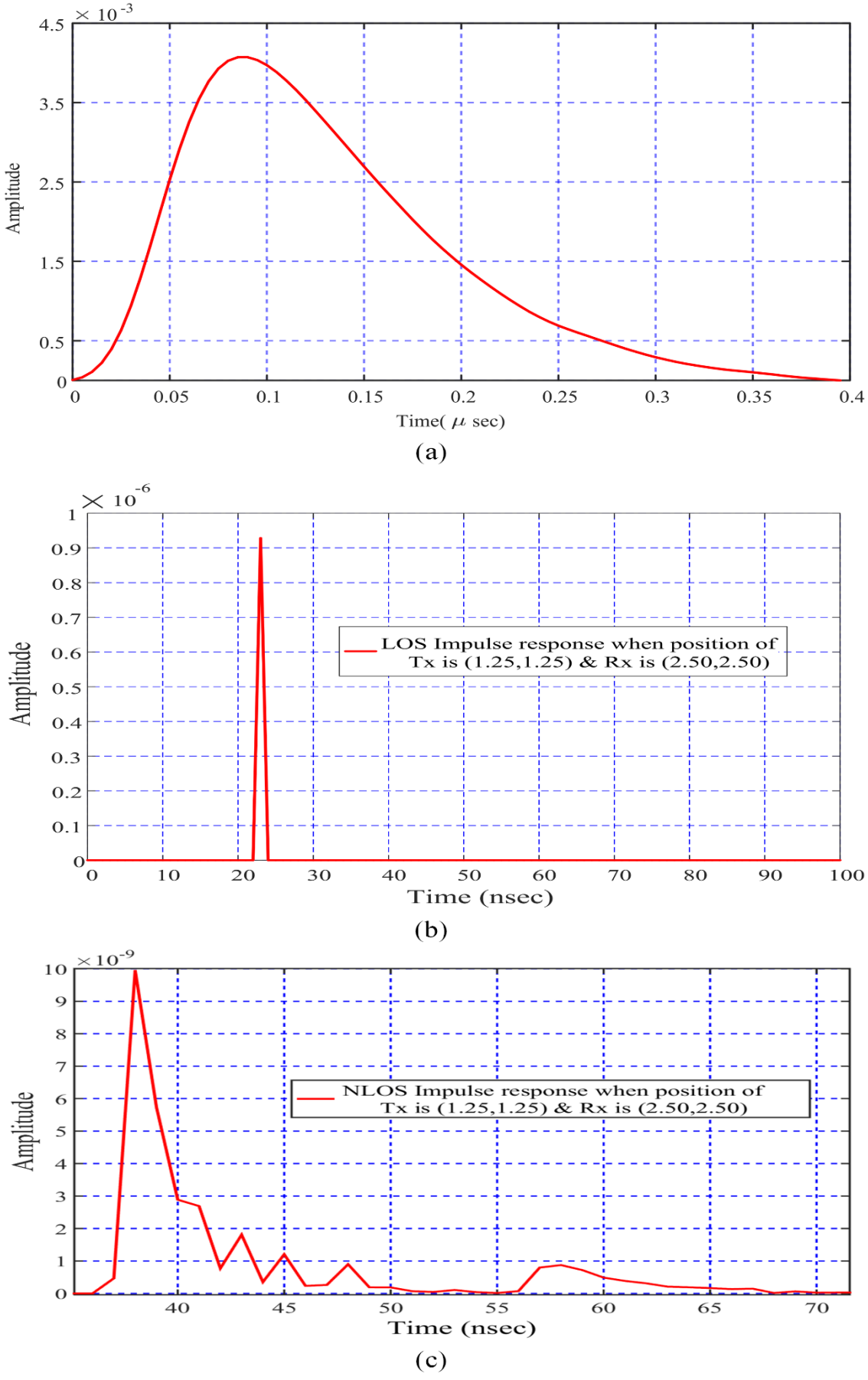


Fig. 3.7. Impulse responses of VLC positioning system (a) the LED impulse response (b) impulse response of VLC channel for the LOS scenario (c) impulse response of VLC channel for NLOS.

Fig. 3.9 shows the flowchart of the proposed VLC positioning system which is an end to end positioning system from the coordinator to the receiver. The coordinator generates different location codes for the four transmitters based on the transmitters' positions and it combines them with the transmitted data as shown in Fig. 3.6. The receiver on the other side recovers the data based on the OOK-TDM scheme and hence it obtains the locations of transmitters from the transmitted location codes. During the location code transmission, only one LED is active at a time to ensure the receiver gets the correct code from a dedicated LED. Because we have been used the RSSI technique, therefore, the best way to select three transmitters is to measure the three strongest signals to reduce the impact of the noise on these signals and to reduce the positioning error. The positioning algorithm then uses the transmitters' positions and the received power levels.

## 3.3.2. Channel Modelling

In this subsection, we recall some of the basic methodologies for VLC channel modelling that exist in the literature. The general form of Friis transmission equation gives the relationship between transmitted and received power for any communication system [115, 157]:

$$P_{\mathrm{Rx}} = P_{\mathrm{Tx}}.H(L).G_{\mathrm{Rx}}, \tag{3. 15}$$

where $P_{\mathrm{Rx}}$ and $P_{\mathrm{Tx}}$ are received and transmitted signal power respectively, $G_{\mathrm{Rx}}$ is the receiver gain and $H(L)$ is the channel gain which is function of distance $L$. The relationship between transmitted and received optical power can be written as follows [90, 158, 159]:

$$\mathrm{P_{Rx}} = \sum_i (P_{\mathrm{Tx}_i}\, h_{\mathrm{ch,LOS}_i}(0)) + \int_{\mathrm{walls}} P_{\mathrm{Tx}_i}\, dh_{\mathrm{ch,NLOS}_i}(0) \tag{3. 16}$$

where $i$ is the index of the $i^{\mathrm{th}}$ transmitter and LOS stands for line-of-sight and $N$LOS refers to the non-line-of-sight (NLOS) paths (also referred to as the diffused configurations). In this work, we distinguish two cases: (*i*) LOS only and (*ii*) LOSNLOS.

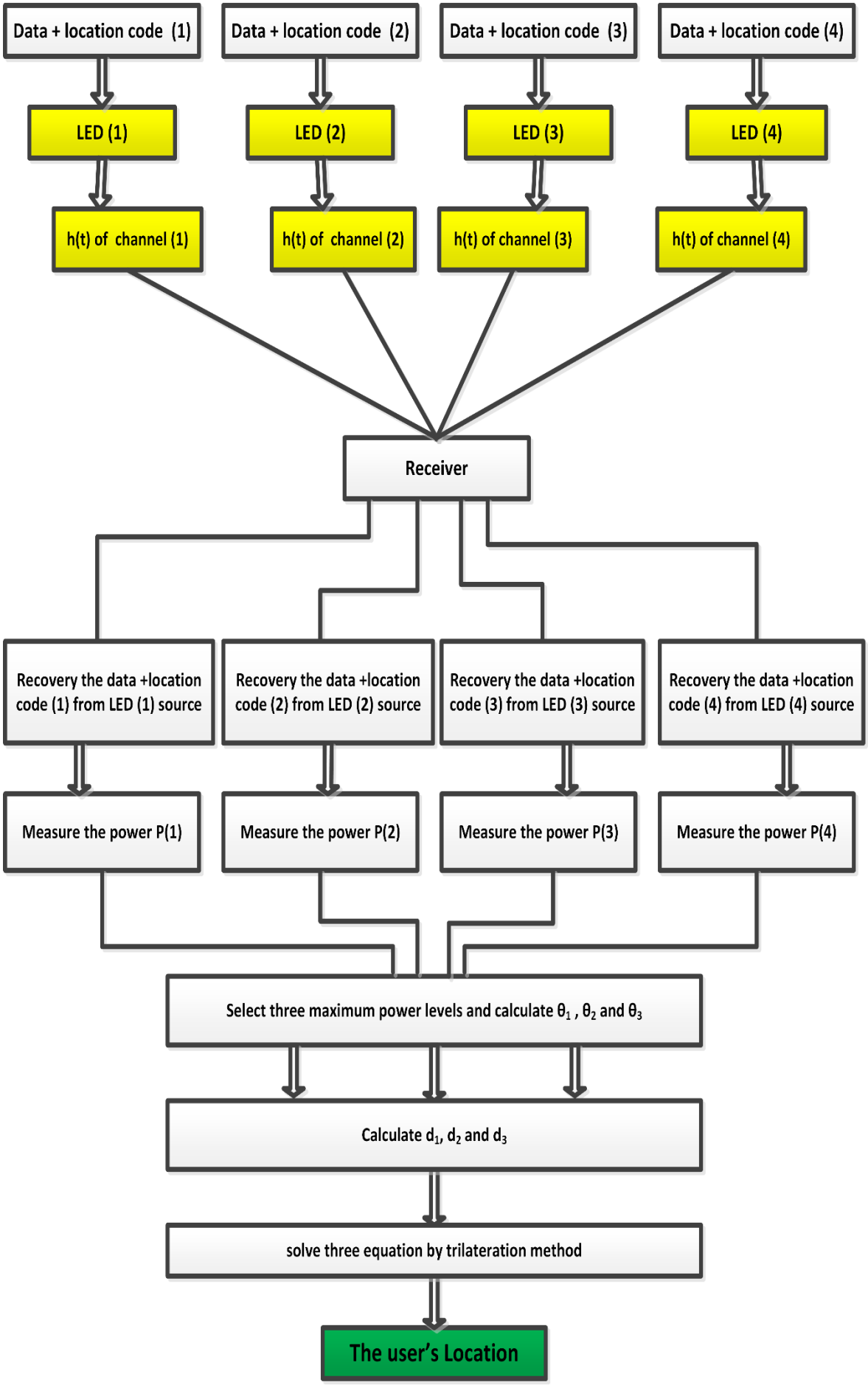


Fig. 3.8. Flowchart of the proposed VLC positioning system using three transmitters.

### 3.3.2.1. Mathematical Model of LOS Path

For the first LOS case, the impulse response of VLC channel based on Subsection 2.2.2. when the distance between the transmitter and receiver is $L$ and the irradiance angle $\theta$ can0 expressed as [142, 160]:

$$h_{\mathrm{ch,LOS}_i}(t) = \begin{cases} R_{0,LOS}(\phi) A_{eff,LOS}(\psi) \delta(\mathrm{t} - \frac{Li}{c}) / {L_i}^2 & ; 0 \leq \Psi \leq FOV \\ 0 & ; \text{otherwise} \end{cases}, \quad (3.\ 17)$$

with

$$R_{0,LOS}(\phi) = \frac{m+1}{2\pi} \cos^m(\theta) \quad \text{and} \quad A_{eff,LOS}(\psi) = A_{\mathrm{R}} \cos(\psi)\, T_s(\psi) \mathrm{g}(\psi)$$

where:

- $R_{0,LOS}(\phi)$ is the transmitter radiant intensity for the LOS scenario,
- $A_{eff,LOS}(\psi)$ is the effective signal collection for the LOS scenario,
- $\theta$ is the irradiance angle,
- $\Psi$ is the incidence angle,
- $T_s(\psi)$ is the gain of an optical filter,
- $g(\psi)$ is the gain of an optical concentrator,
- $A_R$ is the detector effective area,
- $L = d(Tx_i, Rx)$ is the distance between $i^{th}$ transmitter-to-receiver $Rx$,
- *FOV* is the field of view of the receiver,
- $m$ is the Lambertian emission which is given in equation (2.10).

### 3.3.2.2. Mathematical Model of non-LOS Path

In this study, the non-LOS configuration is considered depending on a number of factors such as the size of the room and the reflection factor of walls, ceiling and objects inside the room as well as the site and coordination of the receiver and the transmitter. There are a number of factors affecting the reflection by objects, walls and ceiling such as wavelength, surface material and its roughness and the incident angle. In the second NLOS case, the impulse response of VLC channel is given by [55, 142]:

$$h_{\mathrm{ch,ref}_i}(t) = \begin{cases} \frac{\rho dA_{wall}}{L_{1j}^2 L_{2j}^2} R_{0,NLOS}(\phi) A_{eff,NLOS}(\psi) \cos(\alpha_{rij}) \cos(\beta_{rij}) \, \delta\left(\mathrm{t} - \frac{L_{1ij}+L_{2ij}}{c}\right); & 0 \le \Psi_{rij} \le FOV \\ 0; & \text{otherwise} \end{cases} \quad (3.\ 18)$$

With

$$R_{0,NLOS}(\phi) = \frac{m+1}{2\pi^2} \cos^m(\theta_{rij}) \text{ and } A_{eff,NLOS}(\psi) = A_{\mathrm{R}} \cos(\psi_{rij}) \, T_s(\psi_{rij}) g(\psi_{rij})$$

where:

- $R_{0,NLOS}(\phi)$ is the transmitter radiant intensity for the NLOS scenario,
- $A_{eff,NLOS}(\psi)$ is the effective signal collection for the NLOS scenario,
- $j$ is the index of the $j^{\mathrm{th}}$ of multipath,
- $\rho$ is the reflectance factor,
- $dA_{wall}$ is a reflective area of small region,
- $L_1$ is the distance between LED and a reflective point,
- $L_2$ is the distance between a reflective point and a receiver,
- $\alpha_r$ is the angle of irradiance to a reflective point,
- $\beta_r$ is the angle of irradiance to the receiver from multipath as depicted in Fig. 3.7.

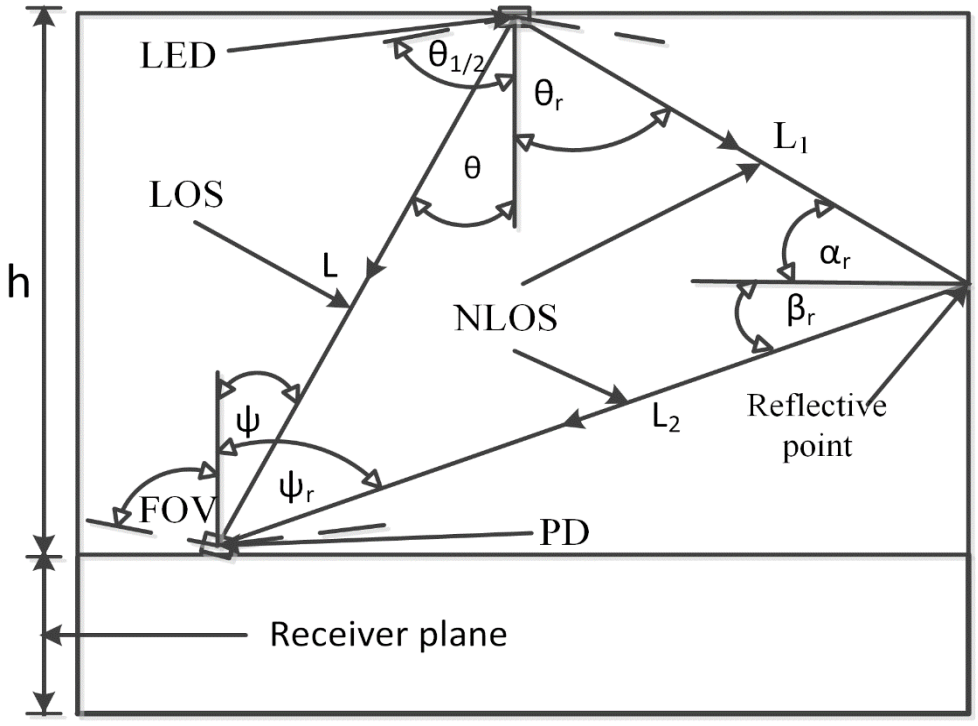


Fig. 3.9. the VLC channel modelling for direct and diffused links.

# 3.4. User Location Methodology Using RSSI Technique

This section discusses the RSSI technique of indoor positioning using three transmitters with the trilateration method. This approach recovers the channel characteristics from the incident light and estimates the receiver location by analytically solving a Lambertian equation group. In what follows, we describe the algorithm that allows the calculation of the path loss as a result of attenuation. From equation (2.15), which is a basic equation that can calculate the received power in VLC environment for any location inside a room, the received power at distance $L_i$ utilizing (2.14) and (2.16) can be expressed as:

$$P_{\mathrm{Rx},L_i}(\theta_{L_i}\,\psi_{L_i}) = P_{\mathrm{Tx}}.\frac{(m+1)}{2\pi {L_i}^2}\,.\cos^m\theta_{L_i}\,.T_s(\psi_{L_i}).g_s(\psi_{L_i}).\cos(\psi_{L_i}), \tag{3. 19}$$

The received power underneath the transmitter, i.e. at distance $h$ and $\psi_{L_i} = \theta_{L_i} = 0$, is given as:

$$P_{\mathrm{Rx,h}}(0,0) = P_{\mathrm{Tx}}\frac{(m+1)}{2\pi h^2}. \tag{3. 20}$$

as shown in Fig. 3.10.

From (3.37) and (3.38), assuming $T_s(\psi).g_s(\psi) = 1$ (This means that we do not have any attenuation or amplification for the received optical signal from these stages because of the employed positioning VLC technique here is RSSI technique which is depend on the received power level), and $\psi_{L_i} = \theta_{L_i}$, therefore, the mathematical equation of the RSSI technique can be written as:

$$P_{\mathrm{Rx},L}(\theta_{L_i},\theta_{L_i}) = P_{\mathrm{Rx,h}}(0,0).\cos^{(m+\gamma+1)}(\theta_{L_i}) \tag{3. 21}$$

where $i = 1,2,3$ or 4 represents the number of transmitters in the room and $\gamma = 2$ is a path-loss exponent correction factor [31]. Subsequently, for the sake of simplicity, we shall rewrite the above equation (3.39) as:

$$P_{\mathrm{Rx},L}(\theta_{L_i}) = P_{\mathrm{Rx,h}}(0).\cos^{(m+\gamma+1)}(\theta_{L_i}) \tag{3. 22}$$

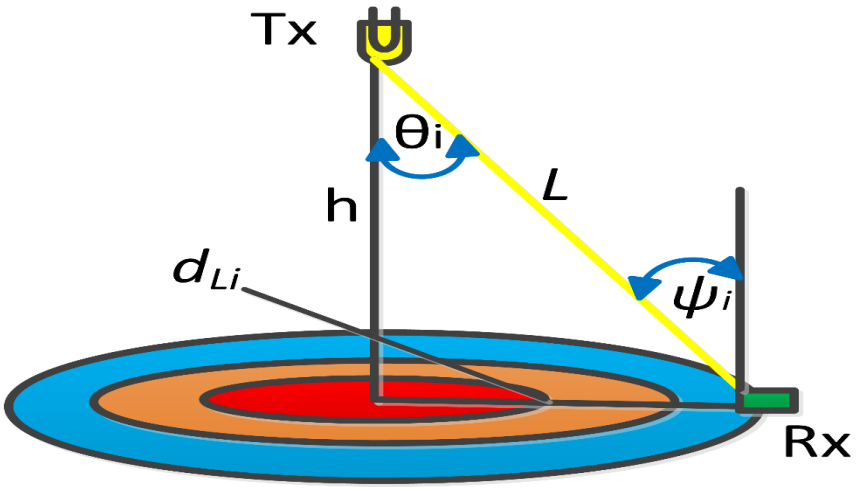


Fig. 3.10. Side view of 1-D indoor VLC system.

## 3.4.1. Horizontal Distance Estimation

From (3.40), we can calculate the angle of irradiance ($\theta_{L_i}$) using measurements of the received power at distance *h* and at distance $L_i$. We can now calculate the horizontal distance estimation, $d_{L_i}$, as:

$$d_{L_i} = h.tan\,\theta_{L_i}. \tag{3. 23}$$

## 3.4.2. Trilateration Method

The process of determining absolute or relative locations of targets by measuring the distances using the geometry of circles is shown in Fig. 3.11. There are four power levels to be determined at the receiver. However, the receiver will select only the three maximum power levels that will be used in the positioning algorithm in order to determine the location of the user. So, we can use the RSSI algorithm to calculate $\theta_{L_i}$ (i.e., $\theta_{L_1}$, $\theta_{L_2}$ and $\theta_{L_3}$). We then calculate $d_{L_1}, d_{L_2}$ and $d_{L_3}$using equations (3.40) and (3.41) respectively. Now, the trilateration method can be used to determine the position of the user by obtaining the intersection point from the three following equations:

$$\begin{cases} (x_{Rx} - x_{Tx_1})^2 + (y_{Rx} - y_{Tx_1})^2 = d_{L_1}^2 \\ (x_{Rx} - x_{Tx_2})^2 + (y_{Rx} - y_{Tx_2})^2 = d_{L_2}^2 \\ (x_{Rx} - x_{Tx_3})^2 + (y_{Rx} - y_{Tx_3})^2 = d_{L_3}^2 \end{cases} \tag{3. 24}$$

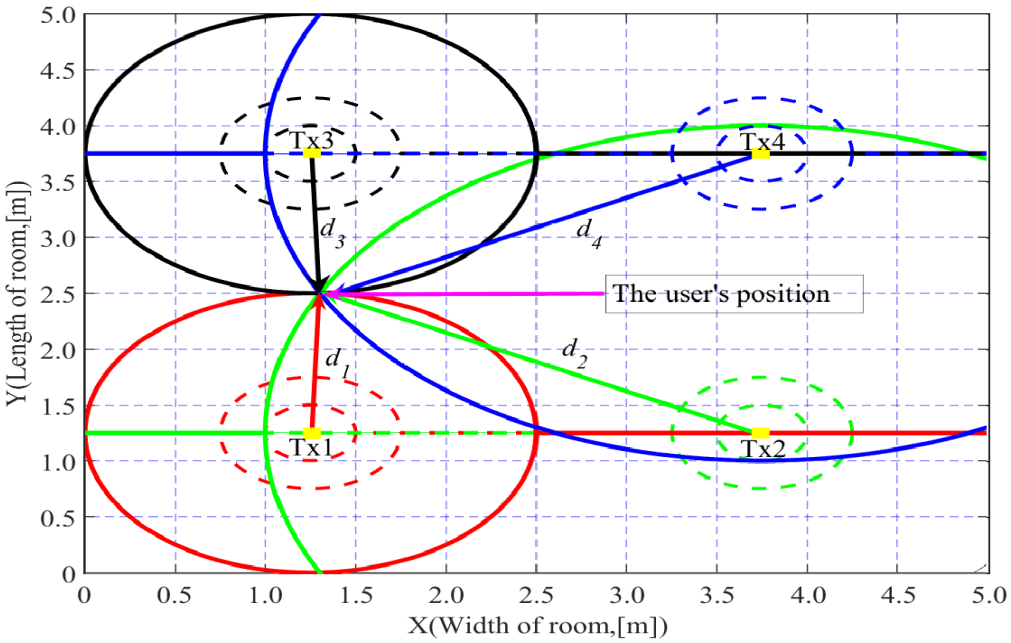


Fig. 3.11. Top view of 2-D positioning system.

where $d_{L_1}, d_{L_2}$ and $d_{L_3}$ are the horizontal distances between the transmitters and the receiver and $(x_{Tx_1}, y_{Tx_1})$ , $(x_{Tx_2}, y_{Tx_2})$ and $(x_{Tx_3}, y_{Tx_3})$ are the position coordinates of the transmitters, whereas $(x_{Rx}, y_{Rx})$ is the position of the receiver.

## 3.4.3. Mathematical Analysis of Noise

In this subsection, we conduct a noise analysis for the proposed positioning system. By setting $k = m + \gamma + 1$, (3.40) can then be written as:

$$P_{\mathrm{Rx},L_i}(\theta_{L_i}) = P_{\mathrm{Rx,h}}(0).\cos^k(\theta_{L_i}) \tag{3. 25}$$

Equation (3.43) expresses the ideal system case which means there is no noise affecting the system. From this, we can derive:

$$\theta_{L_i} = \cos^{-1}\left(\sqrt[k]{\frac{P_{\mathrm{Rx},L_i}(\theta_{L_i})}{P_{\mathrm{Rx,h}}(0)}}\right) \tag{3. 26}$$

On the other hand, in the presence of noise, we have:

$$P_{\mathrm{Rx},L_i}(\theta_{L_i}) + P_{n_i} = (P_{\mathrm{Rx,h}}(0) + P_{n_0})\cos^k(\theta_{L_i} + \Delta\theta_{L_i}) \tag{3. 27}$$

where $P_{n_i}$ and $P_{n_0}$ are the noise power levels at distance $L_i$, and $h$ respectively, both are white Gaussian noise, and $\Delta\theta_{L_i}$ is the angular error at distance $L_i$, Consequently:

$$\theta_{L_i} + \Delta\theta_{L_i} = \cos^{-1}\left(\sqrt[k]{\frac{(P_{\mathrm{Rx},L_i}(\theta_{L_i}) + P_{n_i})}{(P_{\mathrm{Rx,h}}(0) + P_{n_0})}}\right) \quad (3.\ 28)$$

that is,

$$\Delta\theta_{L_i} = \cos^{-1}\left(\sqrt[k]{\frac{\left(P_{\mathrm{Rx},L_i}(\theta_{L_i}) + P_{n_i}\right)}{(P_{\mathrm{Rx,h}}(0) + P_{n_0})}}\right) - \cos^{-1}\left(\sqrt[k]{\frac{P_{\mathrm{Rx},L_i}(\theta_{L_i})}{P_{\mathrm{Rx,h}}(0)}}\right). \quad (3.\ 29)$$

From (3.41), we can calculate the horizontal distance in the ideal and the real cases as shown in (3.41) and (3.48):

$$d_i + \Delta d_i = \mathrm{h} * \tan(\theta_{L_i} + \Delta\theta_{L_i}). \quad (3.\ 30)$$

$$\Delta d_i = \mathrm{h} * (\tan(\theta_{L_i} + \Delta\theta_{L_i}) - \tan(\theta_{L_i})) \quad (3.\ 31)$$

Finally, from (3.47) and (3.49), we can obtain the relationship between the angular error ($\Delta\theta_{L_i}$) or the horizontal distance error ($\Delta d_i$) for wide range of SNR at any point in the VLC room.

# 3.5. Results and Discussion

The indoor positioning system is simulated using MATLAB to pinpoint the user's position. The system parameters are shown in Table 3.5. First of all, the location algorithm which is shown in Fig. 3.6 (b) was applied in order to obtain the performance of the location error at 441 points on the floor in a typical room (5m × 5m × 3m) by the two scenarios mentioned before (i.e. LOS and LOSNLOS). According to [6], the required SNR to achieve a target BER of $10^{-6}$ is 13.6 dB. Therefore, our simulations consider an SNR of more than 13.6 dB. From the mathematical analysis of noise, we have simulated two scenarios which are LOS and LOSNLOS scenarios as follow:

## 3.5.1. Line of Sight Scenario

we simulated and plotted the relationship between the angular error ($\Delta\theta$) and a wide range of SNR when the receiver is at different positions of the room for LOS scenario as shown in Fig. 3.12 (a), where we select three different positions. It is noted that the angular error is

different from one position to another when the SNR is less than 10 dB. However, it has approximately the same effect when the SNR is high. Moreover, the relationship between the horizontal distance error ($\Delta d$) and the SNR is plotted in Fig. 3.12 (b) for three different positions of the receiver, where it becomes stable at high values of SNR. In addition, we note that the performance of angular error and horizontal error for the position of the receiver is (2.5,2.5) m do not have the same trend in terms of the position (0,2.5) m, and (0,0) m because of the distances between the transmitter and the receiver are not equal. Moreover, the errors are negative because the angle from the first term in (3.47) is less than the angle from the second term as well as the distance from the first term in (3.48) is less than the distance from the second term based on the negative angular error.

Now, we investigate the effect of different location codes on the angular error and the horizontal distance error for LOS scenario. We assume four different location codes which are [0000 0001], [1000 0000], [1010 1010] and [1111 1111]. This means that every signal has a different average normalized power level which are 0.125, 0.125, 0.50 and 1, respectively. Then, there is a difference between location codes when the SNR is less than 15 dB, because the VLC system is stable only.when SNR is more than 15 dB then we can use different location codes and there is not any impact on the positioning accuracy for an angular error or horizontal distance error when SNR is more than 15 dB as shown in Fig. 3.13 (a) and (b). Therefore, we can conclude that there is not any impact on the positioning accuracy when we use different location codes with OOK modulation.

The result in LOS scenario (i.e. in the absence of any reflections from walls) were generated under both noisy and noiseless cases. In the first case, the VLC positioning system is considered to be an ideal system meaning that noise does not affect any stage in the aforementioned VLC system. The spatial distribution of localization errors of the device are plotted in Fig. 3.14 for the ideal scenario.

Table 3. 4 Simulation Parameters for indoor VLC positioning using three transmitters.

| Parameters | Values |
|---|---|
| Size of room | |
| Length(m) × Width(m) × Height(m) | 5× 5 × 3 |
| Number of LED-based transmitters | 4 |
| Transmitters locations | See Fig. 3.11 |
| LED characteristics | |
| The LED's semi-angle at half power (FWHM) | $70^{o}$ |
| Transmitted power (per transmitter) (watt) | 10 |
| LED bandwidth (MHz) | 3 |
| Transmit data rate $R_B$ (Mbps) | 5 |
| Optical receiver (PD) | |
| Receiver plane above the floor (m) | 0.75 |
| Photodetector (PD) type | OSD-15T |
| Active area (AR) of receiver ($m^2$) | $50\times10^{-6}$ |
| PD responsivity | 0.6 |
| Half angle FOV of receiver | 80 |
| Detector orientation: tilt horizontal (elevation) | $0^{o}$ |
| Detector orientation: tilt vertical (azimuth) | $0^{o}$ |
| Refractive index of lens at PD | 1 |
| PD O/E conversion efficiency (A/W) | 0.6 |
| Receiver sensitivity (used with the AD8015 trans-impedance amplifier) (dBm). | -35 |
| LPF cut-off frequency (MHz) | $R_B$ |
| Test setup | |
| X-Y sweep resolution (m) | 0.25 × 0.25 |

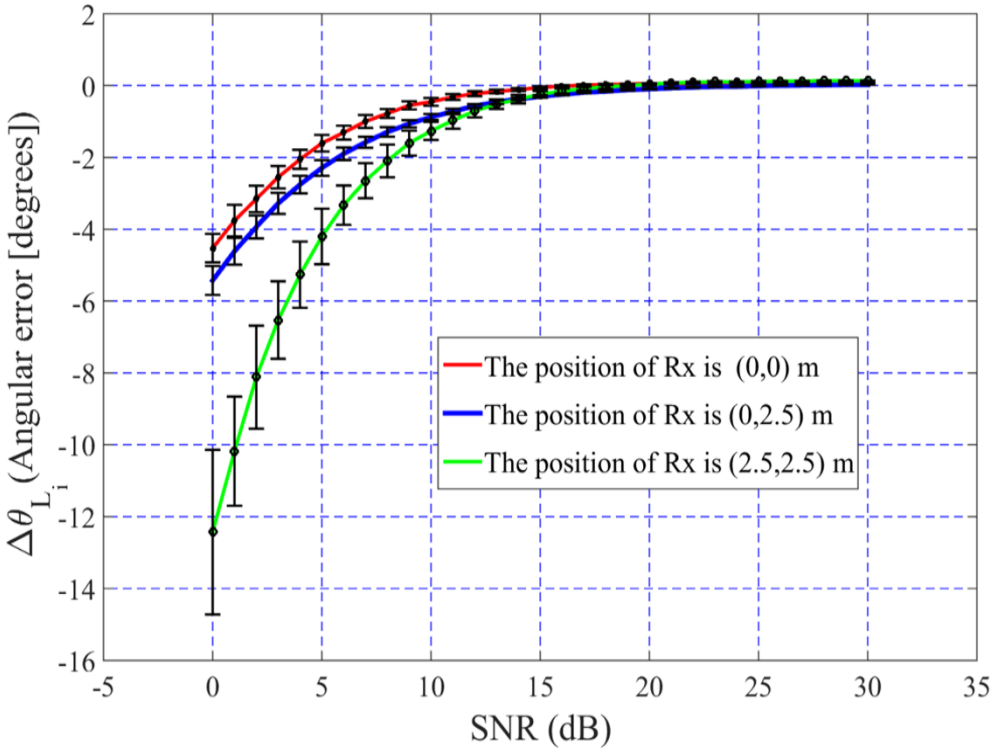


(a)

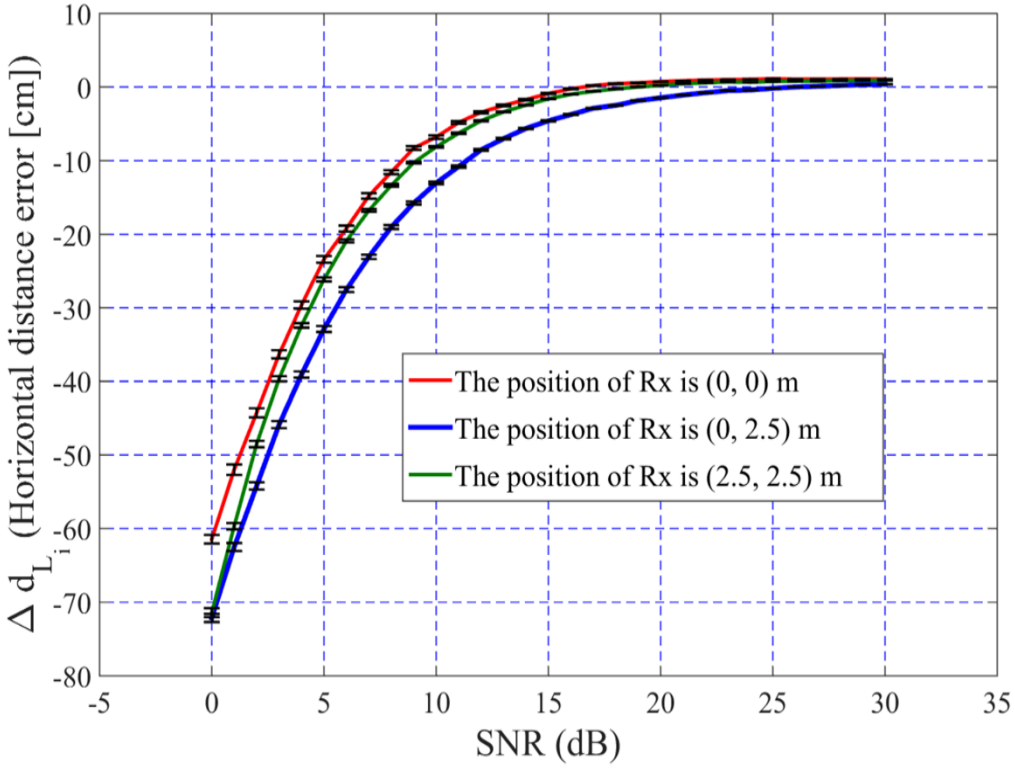


(b)

Fig. 3.12. The relationship between the SNR and the average and variance bar for (a) angular error ($\Delta\boldsymbol{\theta}_{\boldsymbol{L_i}}$) (b) horizontal distance error ($\Delta d_{L_i}$).

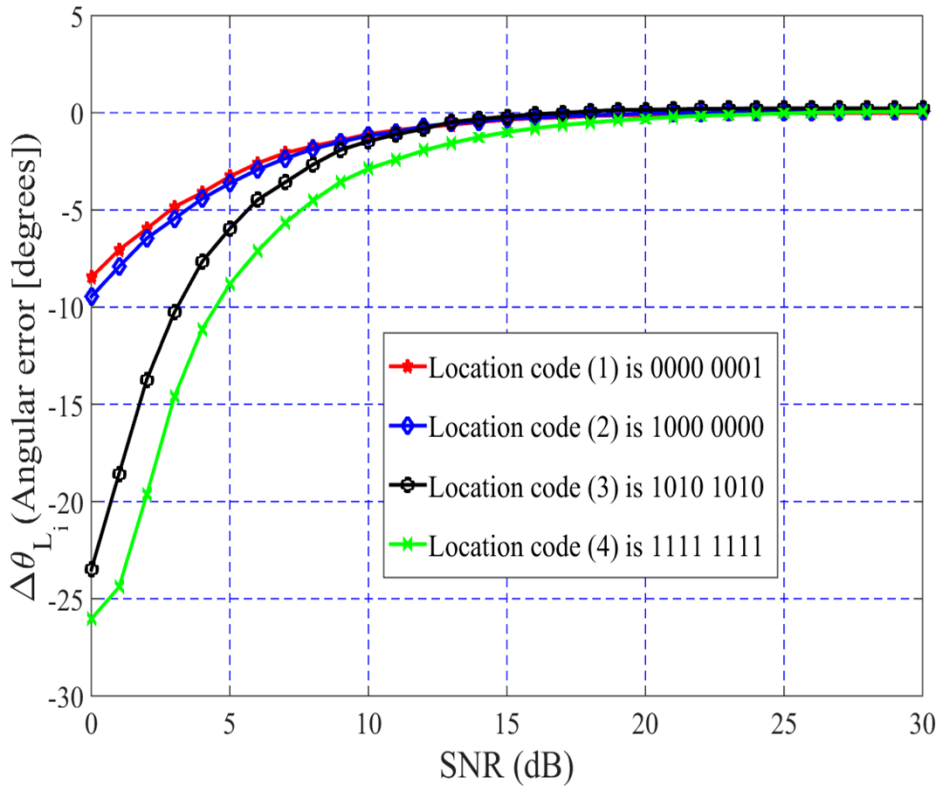


(a)

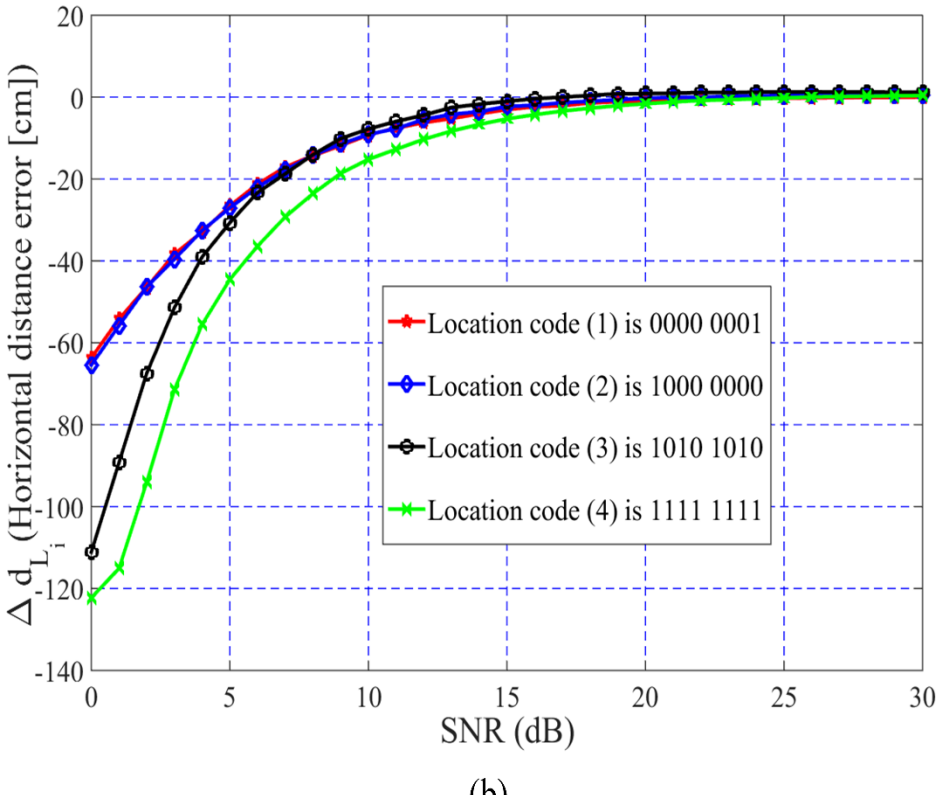


(b)

Fig. 3.13. The relationship between SNR and the average (a) angular error ($\Delta\theta_{L_i}$) (b) horizontal distance error ($\Delta d_{L_i}$) for different location codes when the position of receiver is (2.5, 2.5) m.

In the second case, we investigate the senario where noise is present in the system. Here, the same positioning algorithm is applied but with noise added to the received signal. The noise is modeled as normal AWGN over the SNR range of 0 dB to 30 dB. The selected localization error distribution is poltted at 20 dB in Fig. 3.15. Furthermore, the real and estimated positions of device poltted at 20 dB are depicted in Fig. 3.16. In addition, all statistical measures of central tendency (mean, standard deviation and maximum value) indicate that there is free error in the noiseless LOS scenario. However, in the noisy LOS scenrio, the localization error average decreases spectacularly when the SNR increases (as shown in Fig. 3.15) and from all statistical measures of central tendency that are illustrated in Table 3. 5. For instance, we obtained an average positioning error of less than 5.6 cm when the SNR was more than 15 dB, whereas, the average positioning error was less than 1 cm when SNR = 30 dB. There are extra results from ROP distributions approach for positioning using three transmiters that have presented in appendix A.

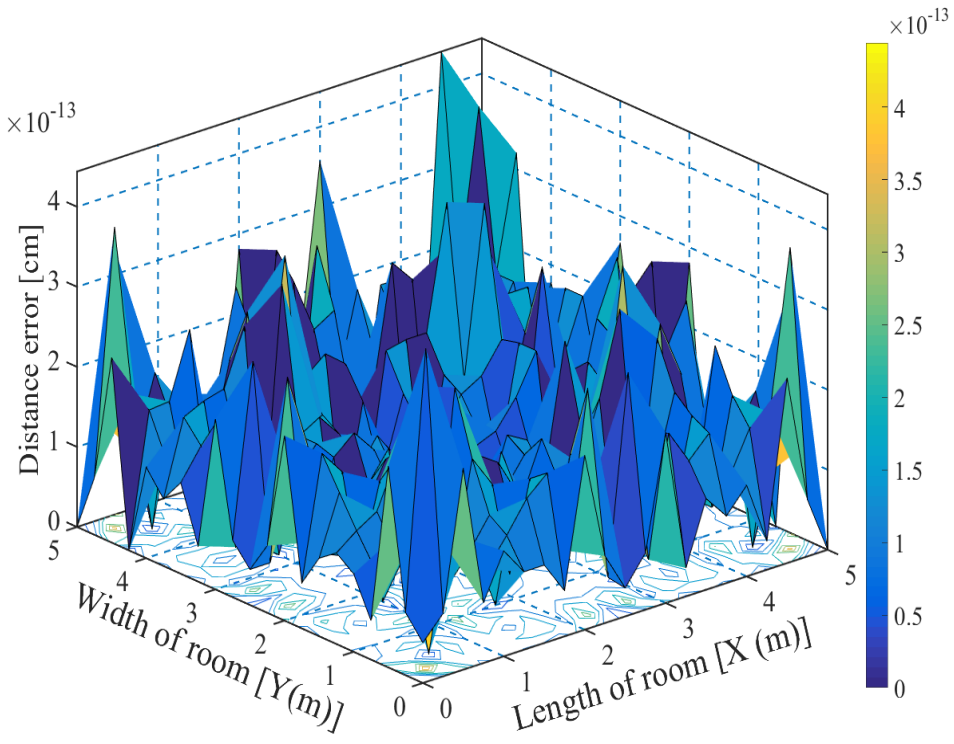


Fig. 3.14. Spatial distribution of the localization error of the positioning VLC system for noiseless LOS scenario.

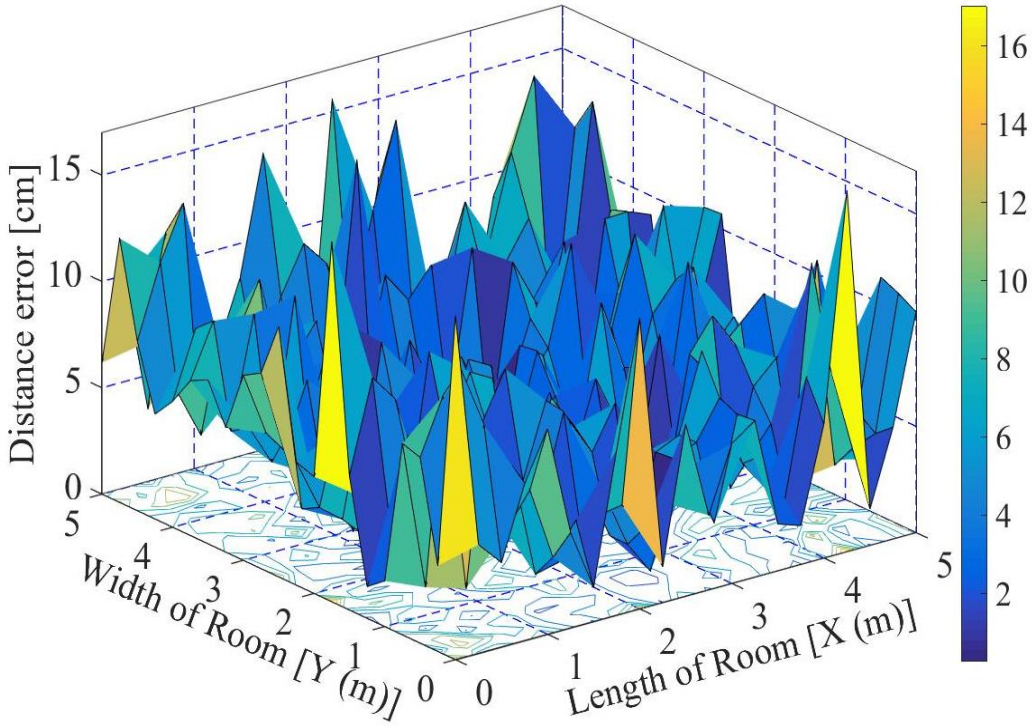


Fig. 3.15. Spatial distribution of the localization error of the positioning VLC system for the noisy LOS scenario when SNR = 20 dB.

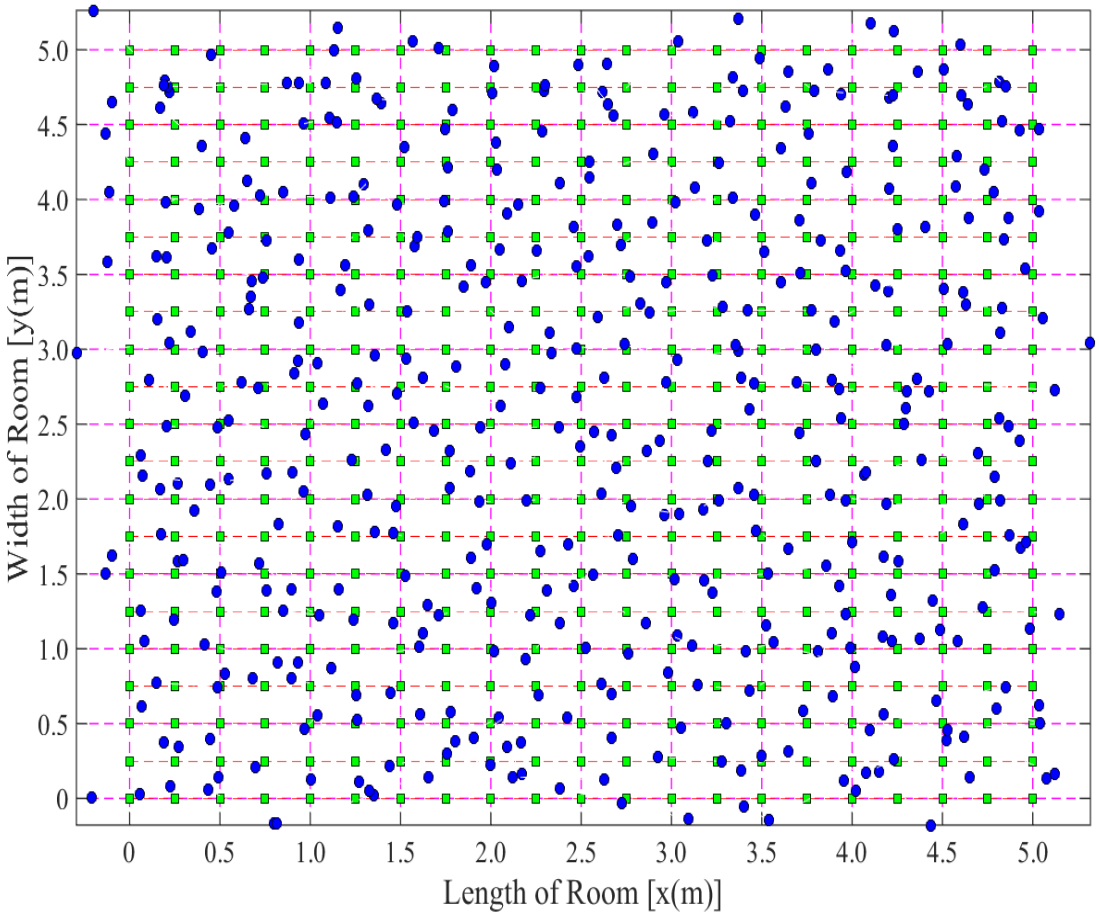


Fig. 3.16. Estimated (blue circles) and real positions (green squares) for the real system at SNR=20 dB

## 3.5.2. LOS and non-LOS (LOSNLOS) Scenario

In this scenario, we used the same positioning algorithm utlilised in the LOS scenario. To further investigate the LOSNLOS scenario we considered both the LOS paths and the NLOS (LOSNLOS) paths (i.e. the received optical power is calculated from LOS paths and from the first refection off the walls). This scenario is carried out for two cases. The first case is a noiseless LOSNLOS scenario which means that no noise is present at any stage in the aforementioned VLC system. The average error slightly increases in all locations in the typical room, especially nearby the walls where the maximum error here is < 20 cm due to the directionality of Lambertian as shown in Fig. 3.17.

On the other hand, in the noisy LOSNLOS scenario, the selected localization error distributions are poltted at 20 dB and depicted in Fig. 3.18. Furthermore, the real and estimated positions of the device are poltted at 20 dB and depicted in Fig. 3.19. It can be noted that, in Fig. 3.19 there is a clear difference between the positioning error in most positions in the room and positions near the walls. We note that the majority of the estimated positions are inside the room (useful feature), and that the effect of reflections are clear on the estimated positions that are close to walls. In addition, we have some statistical standards that are shown in Table 3. 5 which show that the localization error average decreases signifincantly when the SNR increases.

Furthermore, Fig. 3.20 illustrates the relationship between the average positioning error and the SNR for the LOS and the LOSNLOS scenarios. Indeed, both scenarios provide an average error of less than 7 cm when SNR = 15 dB. On the other hand, when the SNR is approximately 30 dB, the LOS scenario provides an average error that is close to zero whereas the average error in the LOSNLOS procedure is less than 5 cm, where reason behind that stems from the directionality of Lambertian as well as the impact of noise.

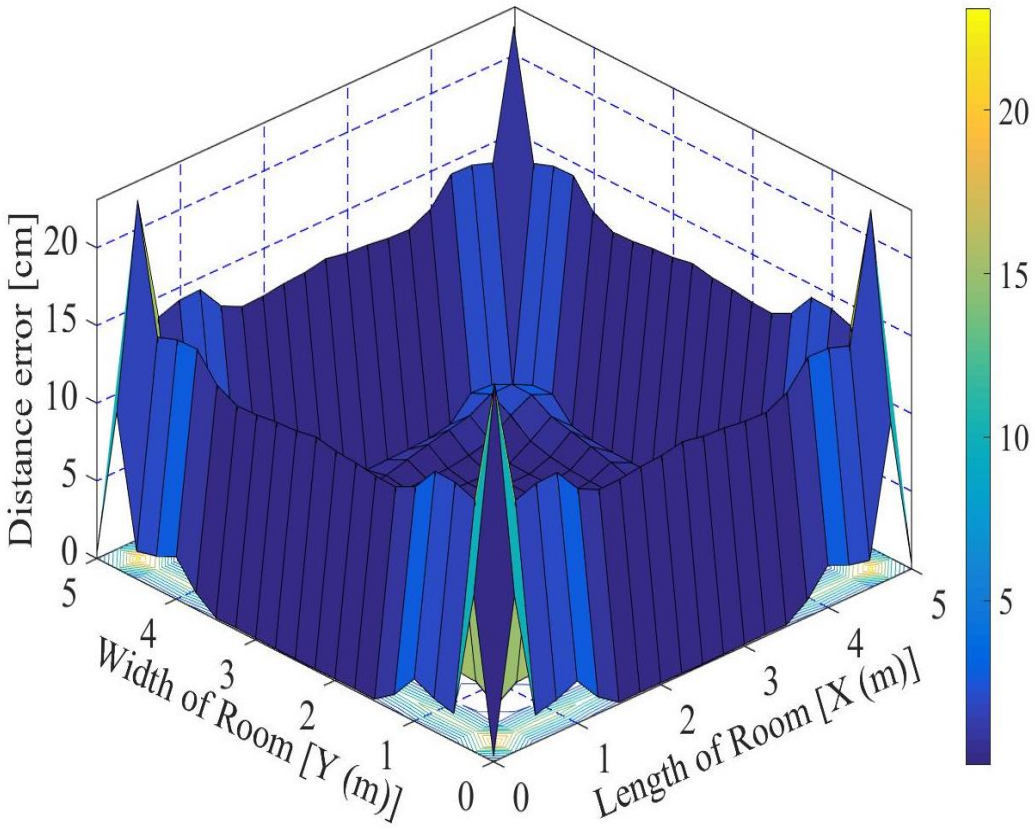


Fig. 3.17 Spatial distribution of the localization error for the noiseless LOSNLOS scenario.

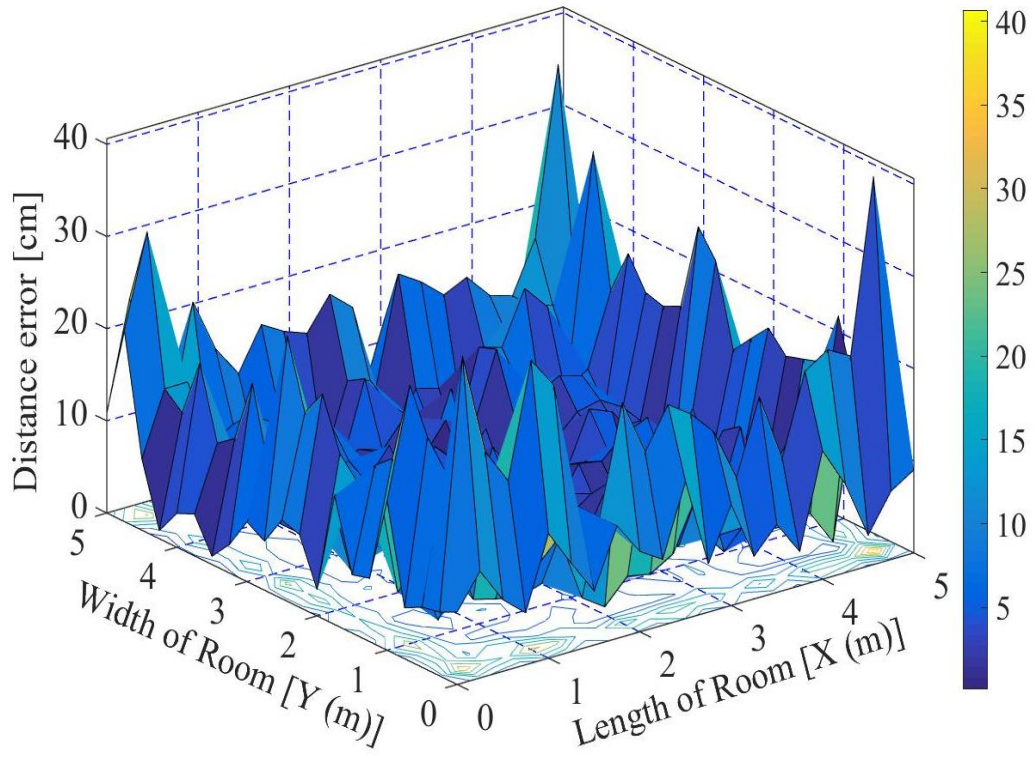


Fig. 3.18. Spatial distribution of the localization error for the noisy LOSNLOS scenario at SNR=20 dB.

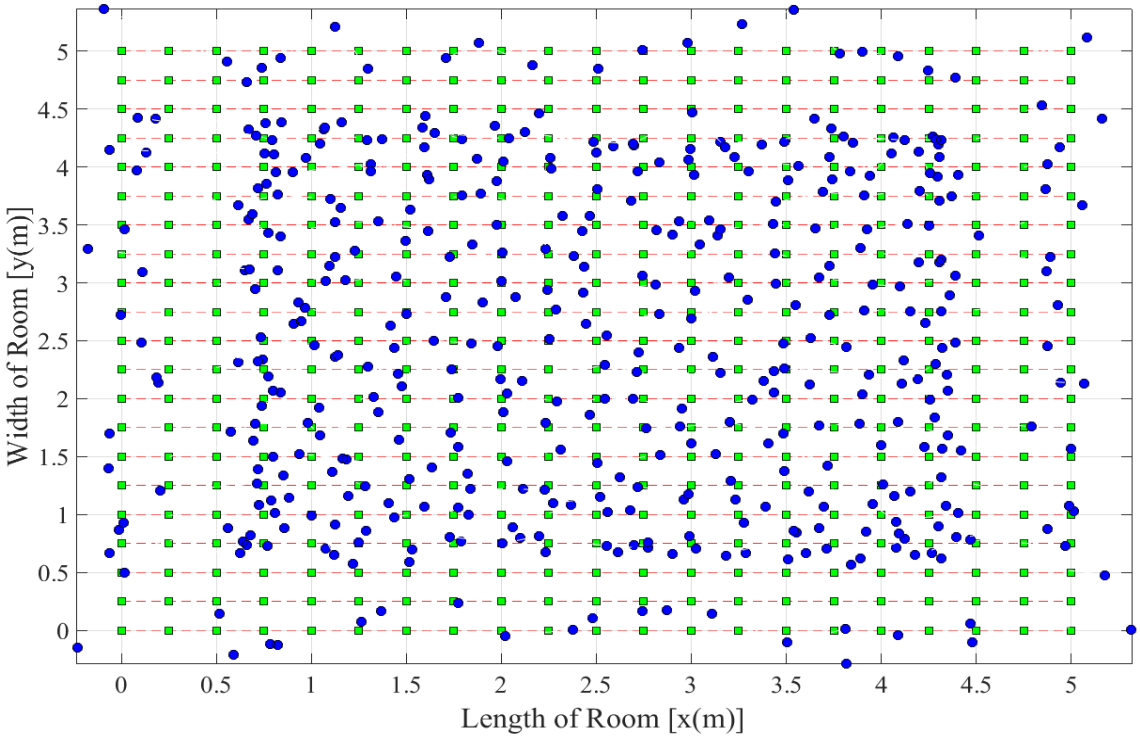


Fig.3.19. Estimated and real positions for the noisy LOSNLOS scenario at SNR=20 dB.

Table 3. 5 The statistical standards of positioning error for the LOS and LOSNLOS scenarios.

| LOS scenario | | | |
|---|---|---|---|
| SNR(dB) | Max. (cm) | Mean (cm) | Std. (cm) |
| 0 | 103.57 | 53.45 | 20.57 |
| 5 | 61.09 | 26.62 | 12.62 |
| 10 | 33.23 | 11.59 | 6.24 |
| 15 | 21.76 | 5.61 | 3.25 |
| 20 | 12.67 | 2.97 | 1.82 |
| 25 | 5.61 | 1.63 | 0.97 |
| 30 | 2.57 | 0.90 | 0.50 |
| LOSNLOS scenario | | | |
| SNR (dB) | Max. (cm) | Mean (cm) | Std. (cm) |
| 0 | 117.35 | 54.72 | 22.24 |
| 5 | 80.97 | 29.23 | 14.66 |
| 10 | 46.53 | 14.50 | 9.00 |
| 15 | 37.15 | 8.15 | 6.50 |
| 20 | 28.51 | 5.28 | 5.29 |
| 25 | 24.76 | 4.21 | 5.24 |
| 30 | 23.56 | 3.56 | 5.20 |

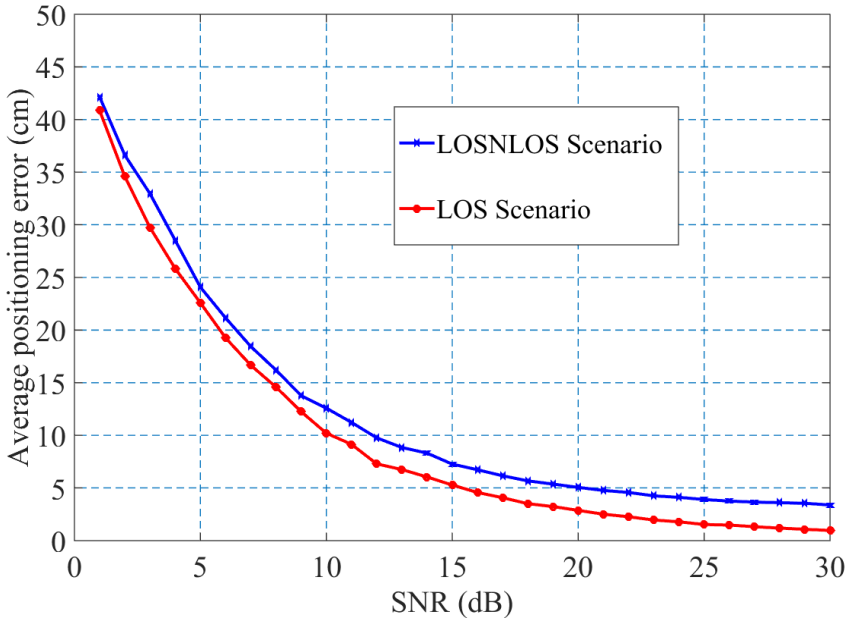


Fig. 3.20.The relationship between the positioning error average and the SNR for a real positioning system.

## 3.5.3. Comparative Analysis of the Results

In order to evaluate the proposed positioning system in which the same RSSI technique and trilateration method are used, a comparison of the results in literature is required. For the table of a fair comprising the some condition under which the results in the previous works were conducted were also used in the proposed study (for instance, the VLC environment and modulation scheme parameters are illustrated in Table 3.7). The summary in Table 3.7 is divided into two scenarios: a LOS scenario and a LOSNLOS scenario. Each scenario has two cases: noisy and noiseless. Notably, in this study there is free error in noiseless LOS scenario, whereas, there were errors in the previous studies. On the other hand, in the noisy LOS scenario, the results in the previous work show the positioning accuracy at specific values of SNR only such as in [133] and [136], and the accuracies are 5 cm and 10 cm when SNR are 30 dB and 15 dB respectively.

In the noiseless LOSNLOS scenario, the previous results show that the average positioning error is high (for example, 0.8064 m and 14.98 cm in [138] and [140] respectively). Whereas in the positioning system, the average distance error is less than 3.5

cm. On the other hand, in the noisy LOSNLOS scenario, the average positioning error was 0.5 mm in [142] but the noise power was very low (i.e. the range of noise power was from -140 dBm to -180dBm). In addition, in [144] the RMS error was 1.01 m when SNR =25 dB. However, in our work, the average distance error is 4.21 cm when the SNR is 25 dB. At the end of this comparison, we can conclude that the proposed positioning system is investigated in LOS and LOSNLOS scenarios under both noisy and noiseless cases. In other words, this study is more comprehensive with the highest accuracy reported so far.

Table 3. 6 The comparison of the RSSI techniques in the VLC positioning system.

| Author's name | Ref | Typical room | Modulation | Noise | Average error |
|---|---|---|---|---|---|
| LOS scenario | | | | | |
| Yang, et al | [117] | 90×90×150 m³ | NRZ-OOK | No | 1.575 cm |
| Wenjun, et al. | [127] | 6×6×3.5 m³ | OOK | No | 0.0464 m |
| Zhang, et al. | [133] | 6×6×4 m³ | OOK | 30 dB | ≈ 5 cm |
| Jaechan Lim | [136] | 6×6×4 m³ | OOK | 15 dB | 10 cm |
| LOSNLOS scenario | | | | | |
| Wenjum, et al. | [138] | 6×6×3.5 m³ | OOK | No | 0.8064 m |
| Abd Elkarim, et al. | [140] | 5×5×4 m³ | not specified | No | 14.98 cm |
| Zhuo, et al. | [142] | 3×3×3 m³ | RZ-OOK | -140dBm to -180 dBm | 0.5 mm |
| Aminikashani, et al. | [143, 144] | 6×6×3.5 m³ | OOK | 25 dB | 1.01 m |

# 3.6. Application of the VLC Positioning in MIMO-VLC Systems

## 3.6.1. Shadowing Issue

Generally, a uniform illumination within a room is required in a VLC environment. This can be achieved by using the irradiance of light with a wide semi-angle at half power as lighting equipment, where at the same time, it can be used to minimize a shadowing effect [68]. There is an optimal number of lighting sources based on the data rate, mean density of pedestrians and room model, etc. to make the VLC system robust against shadowing. Overall, this study highlights the need for the optimal number of the four lighting sources as transmitters as mentioned, which can achieve better blocking rate performance. Note that the previous VLC model was MISO system based on TDMA in Section 3.1[161].

The lighting distribution is not only used to achieve a uniform illumination but to also increase the channel capacity. This is done using multiple lighting sources (i.e. LEDs) as multiple transmitters (with each of them sending independent data streams) and multiple photodetectors at the receiver side. Resulting in a MIMO VLC system (which is explained in Section 2.3 of Chapter 2). We propose a 4 × 4 MIMO VLC system which is shown in Fig. 2.8. Here, we use a ZF equalizer at the receiver side to separate and recover the transmitted signals. In this equalizer, we need to obtain an inverse of $H$ (i.e. $H^{-1}$) and multiply it with the received signal $Y$ to estimate the original signal $\hat{X}_{est}$ as follows:

$$\hat{X}_{est} = H^{-1}Y. \tag{3. 32}$$

This is valid when the $H$ matrix is square and full rank which means the inversion holds, in other words, the determinant of $H$ matrix is non-zero. This model suffers from the shadowing problem. The shadowing problem is defined as a blockage of one or two of the LOS paths during the process of gathering full channel state information (CSI). The CSI is required in a MIMO VLC system and can be estimated by sending a pilot signal (PS) at a specific time. Thus, if one transmitting signal from four transmitting signals (for example $Tx_4$) was blocked, the receiver cannot receive the PS from $Tx_4$ As such, the ZF equalizer cannot estimate the original data, not only from the shadowed transmitter but also from the other transmitters (i.e., the data from $Tx_1$, $Tx_2$, and $Tx_3$) due to the determinant of $H$ matrix being zero. In this case, the matrix inversion is not available.

There are two approaches to address this rank-reduced problem. The first and simplest approach is to reduce the MIMO order (i.e. from 4×4 (M = 4) to 3×3 (M = 3)). Therefore, it is possible to apply (3.50). This approach requires the knowledge of the Tx's link failure. In addition, it needs to ensure that $Tx_4$ is not active while data is being transmitted (e.g. $Tx_4$ might only be briefly shadowed during the piloting process but thereafter not shadowed during the data transmission which will create interference with other channels). The second solution possibility to deal with rank-reduction is to use pseudo-inversion (PI), which is

detailed in [162]. In contrast to the previous approach, PI does process the rank-reduced matrix and produce the inversion, and therefore does not require the knowledge of the $Tx_4$ link blocking. However, the data recovery process will still demand that $Tx_4$ is completely blocked during data transmission for two previous approaches, which is not practically feasible. In the next section, we propose new methods to solve this problem and to minimise the system complexity.

## 3.6.2. Self-correcting MIMO-VLC system using positioning

### 3.6.2.1. Mathematical Modelling

In this section, we model the proposed self-correction method. When PS from $Tx_4$ is blocked, the full-rank channel matrix $H$ in equation (2.35) with elements obtained by (2.36) can be represented as:

$$H = \begin{bmatrix} h_{11} & h_{12} & h_{13} & 0 \\ h_{21} & h_{22} & h_{23} & 0 \\ h_{31} & h_{32} & h_{33} & 0 \\ h_{41} & h_{42} & h_{43} & 0 \end{bmatrix} \quad (3.\ 33)$$

In (3.51), the last column (i.e. the fourth column) is zero as there is no PS from $Tx_4$. In a noisy channel (i.e. strong ambient light) the values in the fourth column might not be zeros but containing random noise values. For the proof of concept, we consider that the channel here has a high signal-to-noise ratio (SNR) level, and as such, noise can be assumed to be low and not included in (3.51). However, noise will be considered in the simulations. The inversion of $H$ matrix does not exist due to the matrix determinant being equal to zero, therefore, an estimate of the 4th column elements for data recovery is needed as in (3.50). Since $Rx$ receives the signals and $Tx$-locations from 3-$Txs$ ($Tx_1$, $Tx_2$ and $Tx_3$) during the piloting period, we can estimate the $Rx$ position and determine $h_{14}$, $h_{24}$, $h_{34}$ and $h_{44}$ Having

obtained the $Rx$ position, which will be discussed in the next subsection, the values of $\hat{\theta}_{i4-est}$, $\hat{d}_{i4-est}$ and $\hat{\psi}_{i4-est}$ are determined and we can thus estimate the CSI:

$$\hat{h}_{i4-est} = \frac{m+1}{2\pi}\left(\frac{A_{eff}}{d_{i4}^2}\right)\cos^m(\theta_{i4})\cos(\psi_{i4})\, g(\psi_{i4})T_s(\psi_{i4}) \tag{3. 34}$$

Hence, the estimated channel matrix ($\widehat{H}_{est}$) is:

$$H_{est} = \begin{bmatrix} h_{11} & h_{12} & h_{13} & \hat{h}_{14-est} \\ h_{21} & h_{22} & h_{23} & \hat{h}_{24-est} \\ h_{31} & h_{32} & h_{33} & \hat{h}_{34-est} \\ h_{41} & h_{42} & h_{43} & \hat{h}_{44-est} \end{bmatrix} \tag{3. 35}$$

Once $H_{est}$ is computed, $Rx$ can accept and successfully recover data for all four channels, which is a significant improvement over the PI approach. Note that the proposed method can be applied to any MIMO VLC system (i.e. with $M > 4$). Furthermore, it can also function even if the system loses all PSs from $Tx_4$, $Tx_5$,…., $Tx_M$.

## 3.6.2.2. Positioning Estimation Using Three Transmitters

In section 3.4, the positioning algorithm considered a SISO-VLC system based on the TDMA technique, the RSSI method and the trilateration method to get the position of the device in the VLC environment. We have applied this algorithm in MIMO-VLC system (note that, a MIMO -VLC receiver has four photodetectors and we have to use at least two of them to apply the positioning algorithm). The receiver already has knowledge of all the positions of photodetectors using the positioning algorithm (i.e.; from the RSSI technique that has explained in previous subsection). This is because when the positions of photodetectors are known and the transmitters' positions are already known from the typical VLC room, then, the distances between the transmitters and photodetectors are also known. In other words, we can calculate the distance between the transmitter which is blocked and the photodetectors ($d_{i4}$). Therefore, the uncompleted CSI matrix $H$ can be corrected from the fourth transmitter without having a pilot signal as indicated below:

1. We know the distance $d_{i4}$ from the positioning algorithm and the room dimensions.
2. We calculate the incidence angle $\theta_{i4}$ using the following equation:

$$\theta_{i4} = \cos^{-1}(h/d_{i4}) \quad (3.\ 36)$$

where $h$ is the vertical distance between the transmitters and the receiver.

3. We use the same assumption which is $\theta_{ij} = \psi_{ij}$ and $g(\psi_{ij}) = T_s(\psi_{ij}) = 1$.
4. Finally, we can calculate $\hat{h}_{i4-est}$ using (3.52).

## 3.6.3. Results and Discussions

The proposed self-correcting MIMO–VLC system is simulated and evaluated using MATLAB to validate the above concept. The simulation parameters used in this case are depicted in Table 3.7.

Table 3. 7 The simulation parameters for the self-correct MIMO-VLC system.

| Parameter | Value |
|---|---|
| Room and Transmitters | |
| Length (m) × Width (m) × Height (m) | 5 × 5 × 3 |
| Number of LED-based transmitters | 4 |
| Transmitters' positions | See Fig. 3.11 |
| Transmitted power (per transmitter) | 100 w |
| LED bandwidth (Luxeon Rebel cool white SR-01-WC310) | 3 MHz |
| Transmit data rate $R_B$ | 2 Mbps |
| Optical receivers | |
| Photodetector (PD) type | OSD-15T |
| PD active area | 15 $mm^3$ |
| PD responsivity (as average over visible band) | 0.6 |
| Receiver sensitivity (used with the AD8015 trans-impedance amplifier) | -30 dBm |
| Receiver field of view (FOV) | $70^o$ |
| Receiver pitch | 10 cm |
| LDF cut-off frequency | 0.75* $R_B$ MHz |

The proposed self-correcting MIMO VLC system works under the condition that the receiver does not receive CSI from $Tx_4$ due to the shadowing problem. However, in the data transmission period, all transmitters still transmit signals and the receiver collects signals as per the normal scenario. In this proposed model, we used data rate of 0.5 Mbps as it can be sent within the experimentally measured 3 dB bandwidth of the LEDs. However, it is possible to use higher data rates based on the 3 dB bandwidth, but the focus here is on the operation demonstration of the self-correcting method. The localization error distributions were plotted in two cases (noiseless and noisy cases) when SNR = 20 dB as shown in Fig. 3.21 (a) and (b), respectively.

We divided the results in this section into two parts: the first part is for the normal scenario and the second part is for the "blocking problem" scenario. In the normal scenario, we firstly examine the BER performance for 4–channels of 4×4 MIMO–VLC system (i.e. the data sent from $Tx_1$ , $Tx_2$, $Tx_3$, and $Tx_4$) without considering any noise. In Fig. 3.22, the results show that the MIMO–VLC system has free BER in an ideal case.

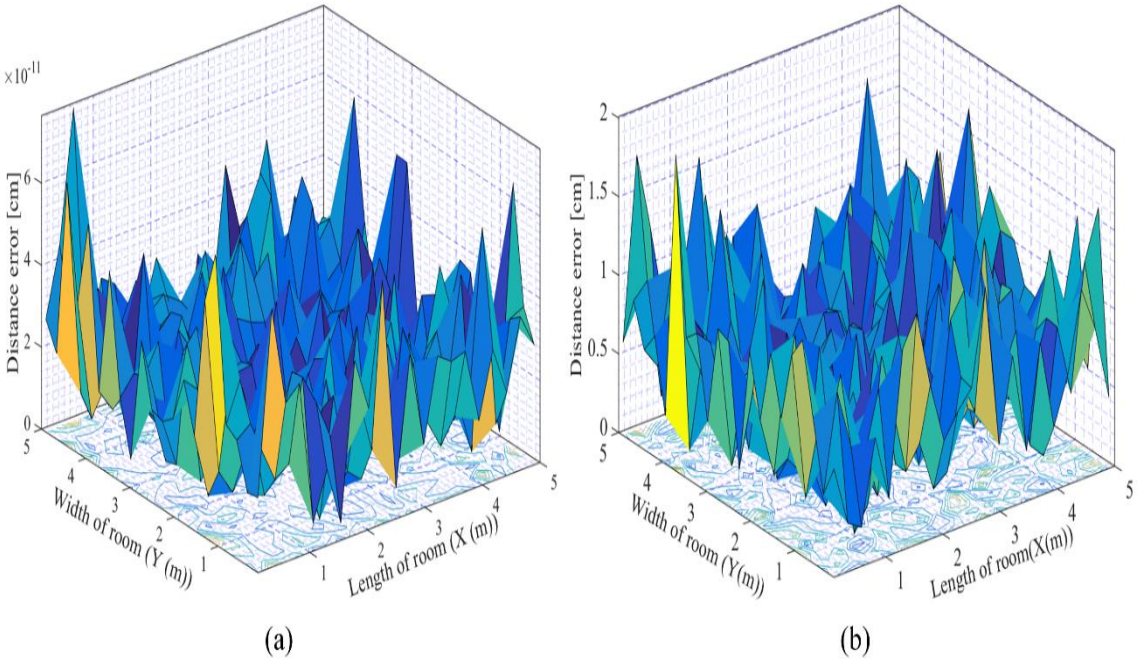


Fig. 3. 21. Spatial distribution of the localization error for MIMO VLC system (a) noiseless case (b) noisy case when SNR = 20 dB.

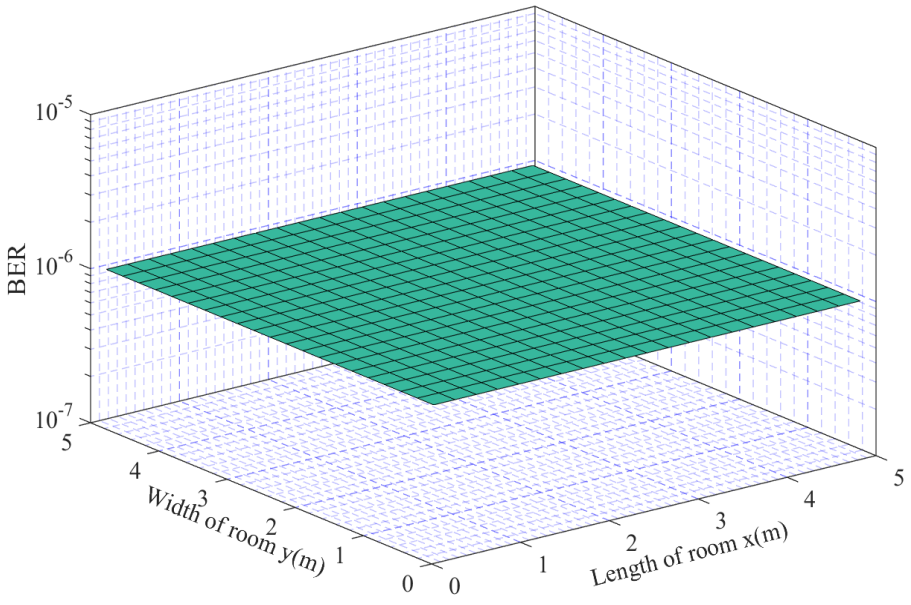


Fig. 3. 22. BER map of total received data from four channel including $Tx_1$ , $Tx_2$, $Tx_3$, and $Tx_4$ without noise.

Note that BER value below $10^{-6}$ is truncated to this level. Lower BER can be obtained with longer tests but there is no gain in doing so in this proof of concept study. Secondly, we examine the BER performance for 4–channels of 4×4 MIMO–VLC system with the presence of noise and when SNR = 20 dB. Fig. 3.23 shows the BER distribution maps in the receiving plane of the four channels. The BER of channel (1), which is evaluated by the receiving data from $Tx_1$, is very low underneath $Tx_1$ and in the nearby area. However, the combination effect of low received power (from $Tx_1$) at the opposite corner area and the noise amplification increases the BER at the corner due to large value of $H^{-1}$ (i.e. that means the $h_{i1}$ coefficients are very small). Due to the dependence on the room configuration, other interference light sources, and different noise power distribution might be able to help alleviate this effect. However, such consideration are not part of the scope of this work. The BER for channels (2), (3) and (4) are similar to the BER of channel (1) as shown in Fig. 3.23. Furthermore, the total BER performance of the MIMO-VLC system is shown in Fig. 3.24 when SNR = 20 dB. The results show that the proposed MIMO-VLC system does not work at corners as the BER is very low.

In the second scenario, which has the blocking issue, we assume that the MIMO–VLC system operates under the condition of interchangeably missing a pilot signal from one transmitter (in this work it will be from $Tx_4$). The results in Fig. 3.25 and Fig. 3.26 show that the self-correcting method (explained above) allows the MIMO-VLC system to recover the original data even in the absence of a pilot signal from a transmitter. By applying the self-correcting method, the receiver is able to adapt to the missing pilot signal from one transmitter to fulfil the $H$ matrix and recover data. Note that the BER performance for four channels in Fig. 3.25 obtained using self-correcting method is similar to the BER performance for 4-channels in Fig. 3.23. Furthermore, the total BER performance of the self-correcting MIMO-VLC system is similar to the total BER performance of MIMO-VLC system without missing any pilot signal as shown in Fig. 3.26 and Fig. 3.24 respectively. To

date, one can therefore see that this work has proposed a novel self-correcting model for recovering 4×4 MIMO–VLC data in the case of missing pilot signal from one transmitter. The indoor VLC positioning algorithm has been used to estimate the missing CSI thus fully restoring the full MIMO-VLC transmission.

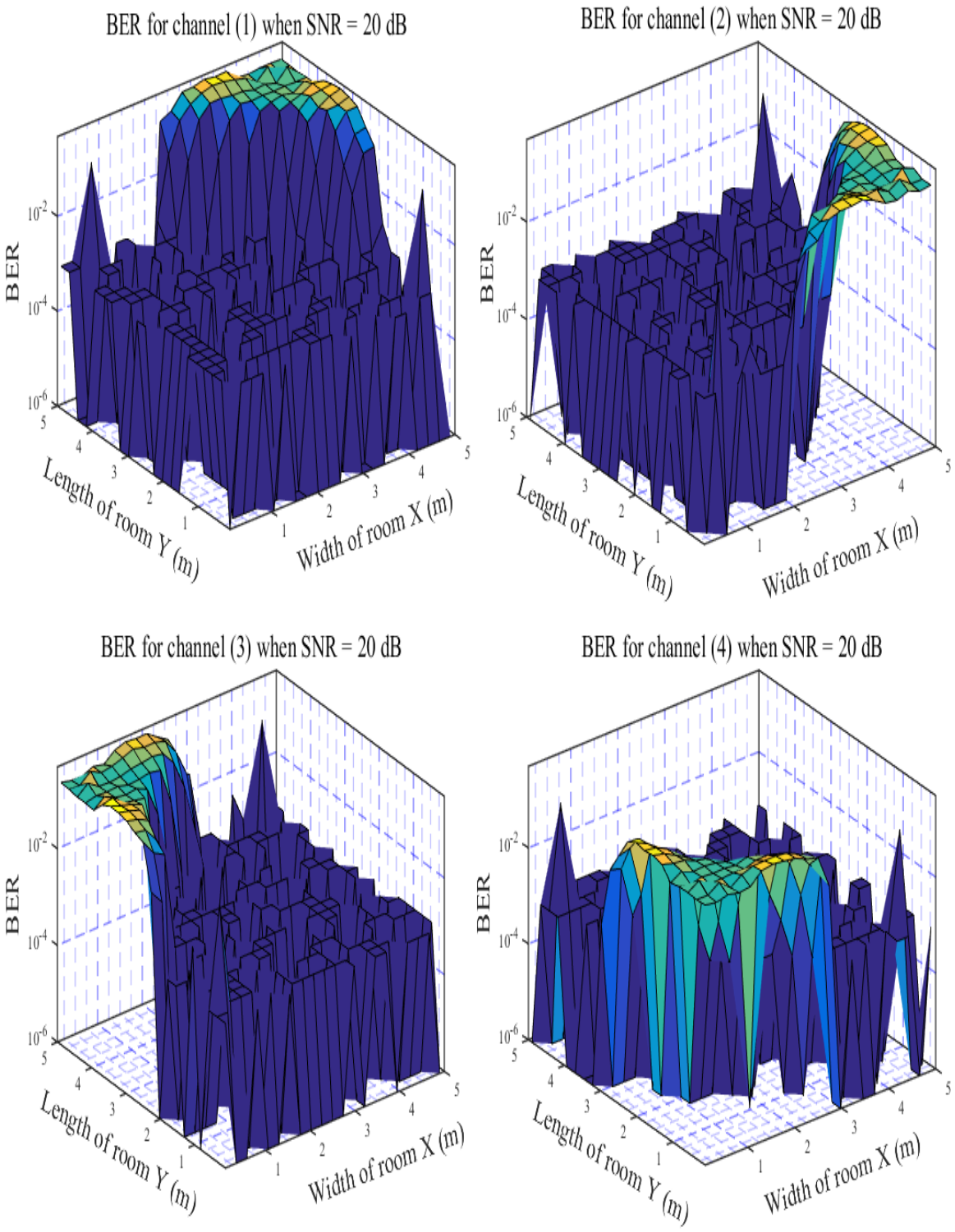


Fig. 3. 23. BER distribution maps in the receiving plane of the four channels, including from $Tx_1$(channel (1)) , $Tx_2$(channel (2)), $Tx_3$(channel (3)), and $Tx_4$(channel (4)) when SNR = 20 dB.

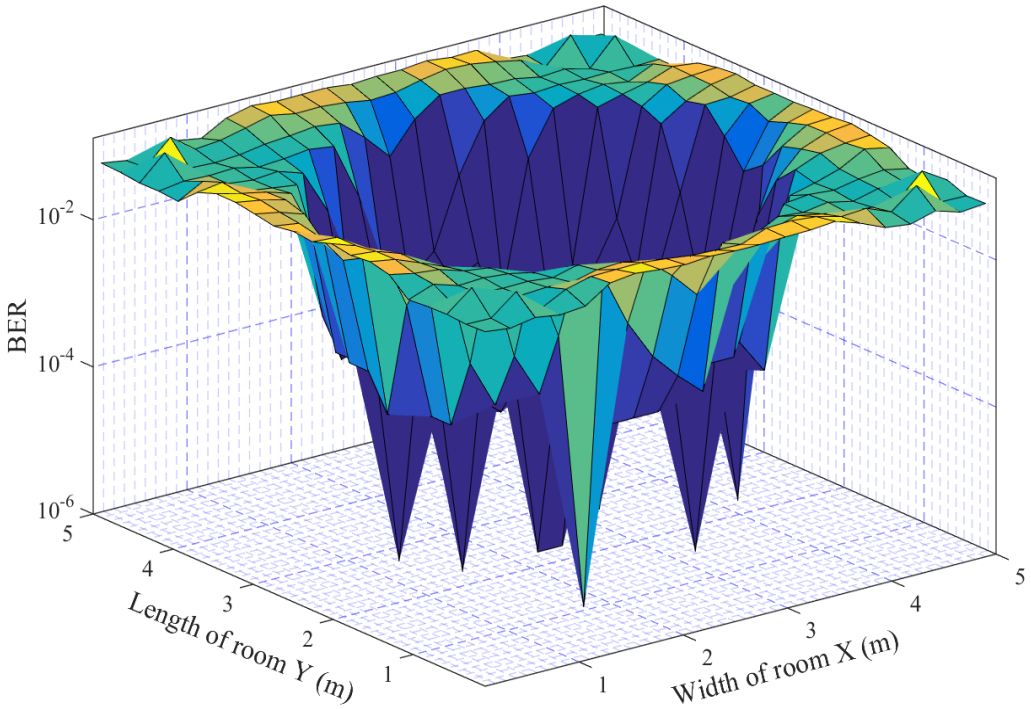


Fig. 3. 24. Total BER for the MIMO-VLC system when SNR = 20 dB.

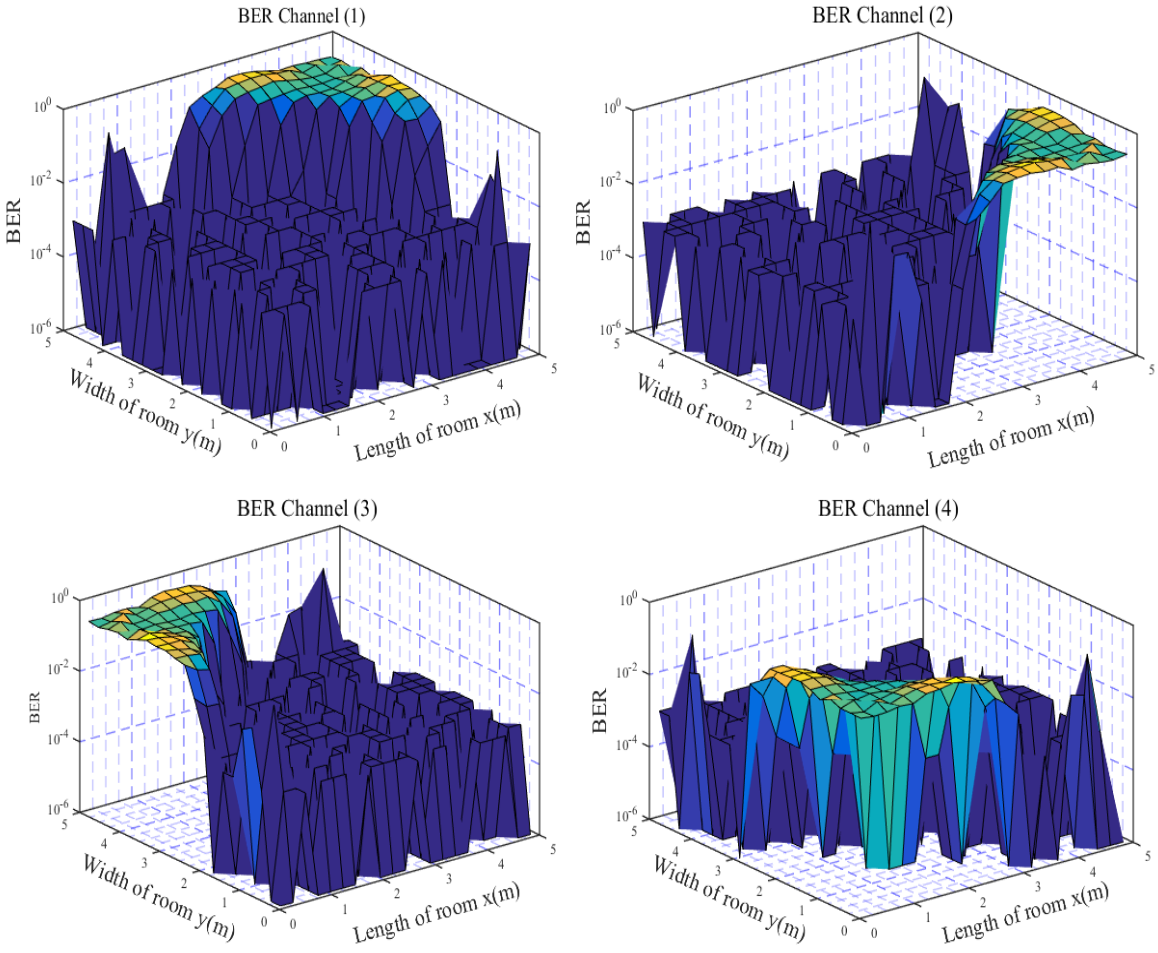


Fig. 3. 25. BER for four channels using the self-correcting method when channel (4) is blocked and the SNR = 20 dB.

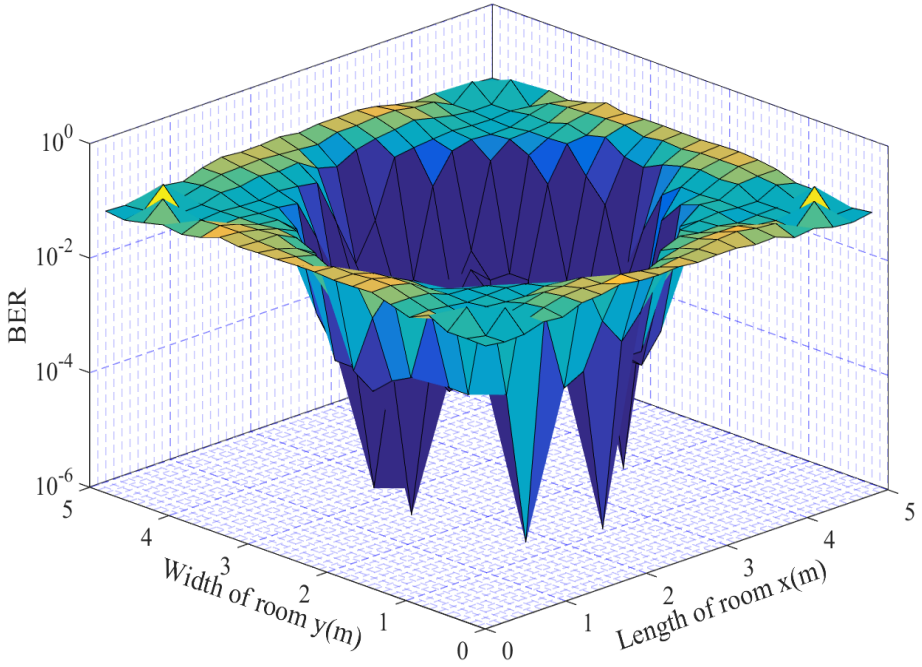


Fig. 3. 26. Total BER for the MIMO-VLC system using the self-correcting method when channel (4) is blocked and the SNR = 20 dB.

# 3.6. Summary

In this chapter, an indoor VLC system was investigated using two types of illumination: single and four cell configurations. The comparison has shown that the four cell configuration has a superior flat illuminance over the single cell configuration. In addition, a comprehensive investigation of the ROP distributions was conducted and a comparison between the ROP with and without optimum Lambertian order for single and four cell configurations was made. The spatial distribution of ROP and the numerical simulation results have shown a very small difference of ROP for single cell with and without optimum Lambertian order, whereas the difference is quite high for the four cell configuration. Moreover, the relationship between the semi-angle at half power of LED and the ROP has also been studied as well as the relationship between the maximum horizontal distance and the transmitted power level and semi-angle at half power with different levels of receiver sensitivity. We have also compared our work with the existing works on the indoor VLC positioning system which have the same modulation scheme and used the RSSI technique.

The chapter has also discussed a novel 2D indoor positioning system using LED ceiling lamps which are modelled mathematically using the RSSI technique. The simulations were carried out to calculate the effect of distortions on the received optical power from three transmitters using the trilateration method. We have found that there is no effect on the positioning accuracy when different location codes are used. The proposed positioning algorithm is able to determine the user's location with an average error of 5 cm when the SNR is 15 dB for a LOS system. However, the error average in LOSNLOS is around 8 cm when SNR is 15 dB. In general, the average error decreases dramatically when the SNR is increased above 15 dB. A comparison is made with previous works on the subject and we have demonstrated the good performance of the proposed positioning scheme.

Finally, we have introduced a novel approach based on the proposed positioning scheme for recovering 4×4 MIMO–VLC data with a partial CSI knowledge. Theoretical analysis and numerical evaluation have been outlined both in noisy and noiseless cases and have shown the capability of the self-correcting method using the RSSI positioning technique with the trilateration method.

The next chapter will introduce a new indoor VLC positioning system based on the received power levels of only two LEDs for different environments. The proposed model will use only two equations to estimate the user location (in a full 2D receiving plane).

# Chapter Four

# Indoor VLC Positioning System Using Two Transmitters

## 4.1. Introduction

Indoor positioning or localization based on VLC is an emerging technology with wide applications. In conventional localization schemes, the trilateration technique is widely used with at least three separate lighting sources to determine the user's location. In indoor environments, LED based lighting fixtures offer in addition to illumination and data communications, highly accurate positioning [110, 163]. There exist a number of techniques for indoor positioning systems (IPSs). However, in certain environments such as (i) small rooms, long rectangular rooms,…etc., where the number of lighting sources is less than three, (ii) long corridor, tunnels etc. where lighting sources are positioned in a single row; and (iii) rooms, halls etc. where a selected number of LEDs could be used for localisation, the trilateration method does not work accurately.

In this chapter, a new indoor VLC positioning scheme based on the received power distributions of only two LEDs, and offering to alleviate the dependence on trilateration, is reported for different environments. The proposed scheme considers both RSSIs and the lighting fixture layout within a room. This could help reduce the cost and complexity and offers similar performance to the trilateration based IPS. The chapter outlines a mathematical model for the VLC channel with Gaussian noise and will numerically evaluate the system performance over a large range of SNR. We also study the effect of noise on IPS. In addition, the results are compared with the exiting trilateration technique.

# 4.2. Indoor VLC Positioning System

## 4.2.1. System Description

In this section, we consider all stages of the proposed VLC positioning system as shown by the block diagram illustrated in Fig. 4.1. The coordinator, visible LED and smart device are the three main parts as mentioned in the IEEE 802.15.7 protocol [18]. These parts are considered as the three main stages of the proposed VLC positioning system using two transmitters. The typical room size is 3 × 3 $m^3$ with a 3 m height and the receiver plane is 0.75 m above floor as shown in Fig. 3.6 (a). We assume an empty room. The coordinator generates two location codes (Location code (A) and location code (B)) for the two transmitters depending on the transmitters' positions. These location codes are combined to the transmitting data (i.e. to the frame). The transmitted data is modulated using the OOK-TDM modulation scheme. The IM/DD technique is employed to generate the transmitted signal $x_1(t)$ and $x_2(t)$ as shown in Fig. 4.2. These signals ($x_1(t)$, $x_2(t)$) are up-sampled by 10 times. The impulse response of LED, $h_{LED}(t)$, is derived by applying a pulse function to the LED in the Lab. As shown in Fig. 3.8 (chapter three). As a result, the output signal, $y(t)$, of the LED is given by:

$$y(t) = \begin{cases} y_1(t) = x_1(t) \circledast h_{\mathrm{LEDA}}(t), & t_i \le \mathrm{t} \le t_{i+\Delta t} \\ y_2(t) = x_2(t) \circledast h_{\mathrm{LEDB}}(t), & t_{i+\Delta t} \le \mathrm{t} \le t_{i+2\Delta t} \end{cases} \quad (4.1)$$

where, $t$ is the time and $\Delta t$ is the duration time of $LED_i$ to send its data Then, the output signal, $y(t)$, is sent to the VLC channel with impulse response $h_{Ch}(t)$, as shown in Fig. 3.8 (b) and (c). The impulse response of the VLC channel is calculated for two scenarios: the LOS scenario ($h_{Ch,LOS_i}(t)$) that is generated based on (3.17) and the LOSNLOS scenario ($h_{Ch,LOSNLOS_i}(t)$) that is generated based on (3.18). The received signal, $r_1(\mathrm{t})$, at the input of the PD for the LOS scenario and is given by:

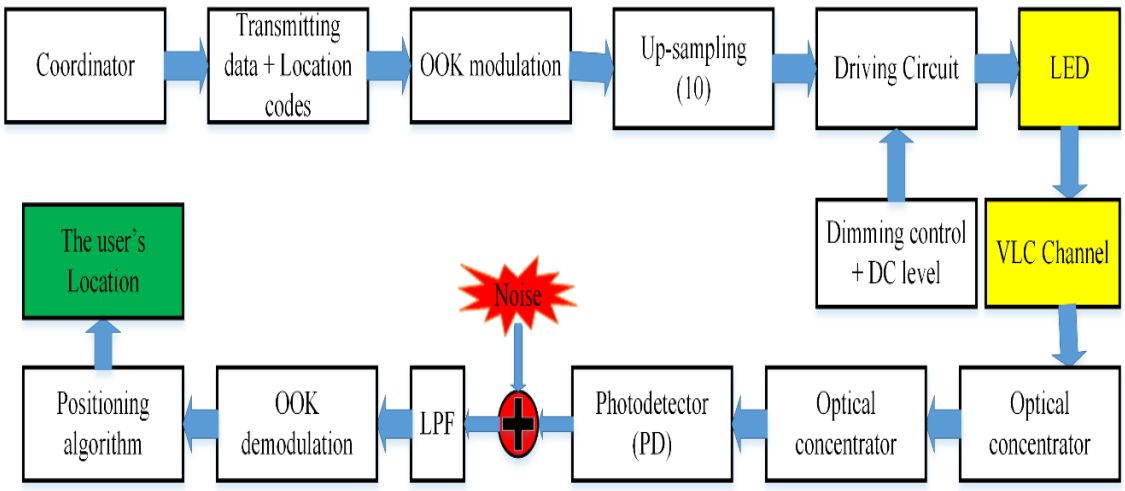


Fig. 4. 1 the block diagram of proposed VLC positioning system.

$$r_1(t) = \begin{cases} r_{11}(t) = y_1(t) \circledast h_{Ch,LOS_i}(t), & t_i \le t \le t_{i+\Delta t} \\ r_{12}(t) = y_2(t) \circledast h_{Ch,LOS_i}(t), & t_{i+\Delta t} \le t \le t_{i+2\Delta t} \end{cases} \quad (4.2)$$

whereas for LOSNLOS scenario, $r_1(t)$ is given by:

$$r_1(t) = \begin{cases} r_{11}(t) = y_1(t) \circledast h_{Ch,LOSNLOS_i}(t), & t_i \le t \le t_{i+\Delta t} \\ r_{12}(t) = y_2(t) \circledast h_{Ch,LOSNLOS_i}(t), & t_{i+\Delta t} \le t \le t_{i+2\Delta t} \end{cases} \quad (4.3)$$

at the receiver side, the output of the PD is given by:

$$r_2(t) = \begin{cases} r_{21}(t) = r_{11}(t) \circledast h_{\mathrm{PD}}(t), & t_i \le t \le t_{i+\Delta t} \\ r_{22}(t) = r_{12}(t) \circledast h_{\mathrm{PD}}(t), & t_{i+\Delta t} \le t \le t_{i+2\Delta t} \end{cases} \quad (4.4)$$

where $h_{\mathrm{PD}}(t)$ is constant. In this study, we assume $h_{\mathrm{PD}}(t) = 0.6$. In the following stage, the received signal of the overall system in the presence of noise can be expressed as:

$$r_3(t) = \begin{cases} r_{31}(t) = r_{21}(t) + n_1(t), & t_i \le t \le t_{i+\Delta t} \\ r_{32}(t) = r_{22}(t) + n_2(t), & t_{i+\Delta t} \le t \le t_{i+2\Delta t} \end{cases}. \quad (4.5)$$

where $n_1(t)$ and $n_2(t)$ are the background noise for the two VLC channels which exists between the two transmitters and the receiver. These noise sources are the combination of thermal, shot and dark noise and can be modelled as AWGN.

A LPF was used to reduce the impact of the noise. Finally, the RSSI technique is implemented to obtain the user's location. By using the positioning algorithm, the received signal is separated from each transmitter by slot time and is demodulated

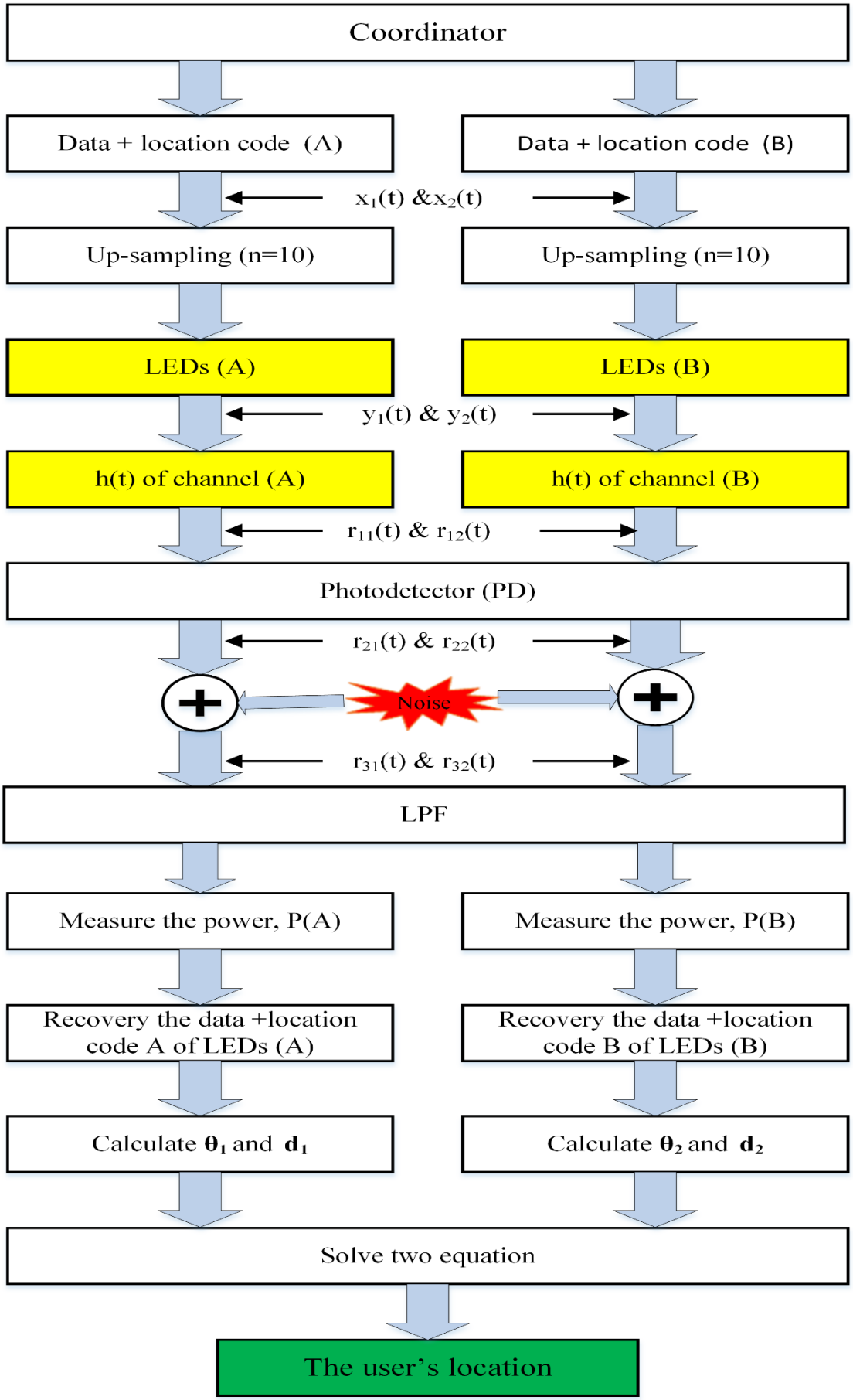


Fig. 4. 2 Flowchart of a real scenario for VLC positioning using two transmitters.

(i.e. OOK demodulation) to recover the original data which contains the location codes as well. From the two location codes, we can find the positions of the transmitters and at the same time, measure the power level for each transmitter ($P_{\mathrm{Rx},L_1}(\theta_{L_1})$ and $P_{\mathrm{Rx},L_2}(\theta_{L_2})$). Consequently, we can obtain the received power level, $P_{\mathrm{Rx},h}(0)$, at distance $h$, from the typical room measurements. After that, we can calculate $\theta_1$ and $\theta_2$ and then calculate $d_1$ and $d_2$. The final step in the proposed positioning algorithm is finding the solution for two equations only to get the user's location. The flow of signal process is illustrated in Fig. 4.2. In the next sub-sections, the proposed positioning algorithm will be explained.

## 4.2.2. Mathematical Model for Localization Using RSSI

A 1-D localization scheme based on the signal path losses from two Txs was reported in [31]. Here, we will use two Txs for the 2-D positioning system. From (4.7) and (4.8), we have the received power for the case when the Rx is just beneath the Tx at a height $h$ (i.e., $L = h$) (see Fig. 4.3), which is defined as:

$$P_{\mathrm{Rx},h}(0,0) = P_{\mathrm{Tx}}\frac{(m+1)}{2\pi h^2}\cos^m(0)\cos(0),$$

$$P_{\mathrm{Rx},h}(0,0) = P_{\mathrm{Tx}}\frac{(m+1)}{2\pi h^2}. \tag{4. 6}$$

Note that $P_{\mathrm{Rx},h}(0,0)$ is the received optical power determined at distance $h$, which is the vertical distance between the transmitter and receiver, (i.e., underneath the transmitter) as shown in Fig. 4.3. Here, $\psi_{Li} = \theta_{Li}$ as the transmitter and the receiver are assumed to be in the parallel planes. Underneath the Txs (i.e., at distance $h$), in this case, these angles ($\psi_{Li}, \theta_{Li}$) are zero. From (4.7) and (4.12), the relationship between the received optical powers at $h$ and $L$ distances ($P_{\mathrm{Rx},h}$ and $P_{\mathrm{Tx},L}$ respectively) is given by:

$$P_{\mathrm{Rx},Li}(\theta_{Li},\psi_{Li}) = P_{\mathrm{Rx},h}(0,0)\frac{h^2\cos^m(\theta_{Li}).\cos(\psi_{Li})}{L_i^2} \tag{4. 7}$$

where $\theta_{Li}$ and $\psi_{Li}$ are the angles at distance $L_i$. Note that, for $L_i = {}^{h}/_{\cos\theta_{Li}}$, we have:

$$P_{\mathrm{Rx},Li}(\theta_{Li}) = P_{\mathrm{Rx},h}(0)\cos^{m+\gamma+1}(\theta_{Li}), \quad i = 1,2 \tag{4. 8}$$

where $i^{\mathrm{th}}$ is the number of transmitters in the room ($i = 1, 2$ in this work), $L_i$ is the distance from $\mathrm{Tx}_i$ to the receiver and $\gamma = 2$ is a path-loss exponent correction factor [31]. From (4.14), and knowing $P_{\mathrm{Rx},Li}(\theta_{Li})$ and $P_{\mathrm{Rx},h}(0)$, we can determine the angle of irradiance $\theta_{Li}$ Therefore, the projected horizontal distance $d_i$ between the transmitter and the receiver can be determined as follows:

$$d_i = h * \tan\theta_{Li}. \tag{4. 9}$$

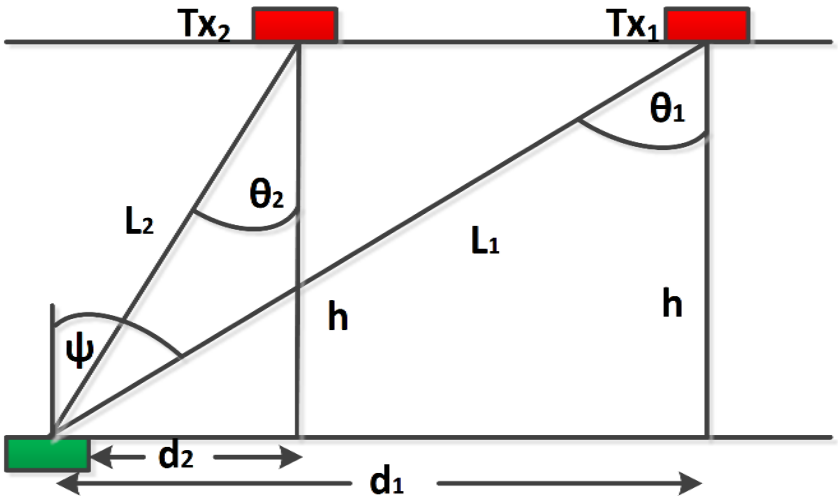


Fig. 4. 3 Side view of 1-D indoor VLC system

# 4.3. Novel Indoor Model for Positioning using RSSI Technique

Here, we propose an indoor localization system using only two transmitters as illustrated in Fig. 4.4. We will also investigate the accuracy of the localisation using the proposed approach in different scenarios. From (4.14), it is possible to calculate the irradiance angle $\theta_{Li}$. The receiver needs to determine the received optical powers at (i) beneath each Txi (i.e.; $P_{\mathrm{Rx,h}}$); and (ii) at the current user's location (i.e., $P_{\mathrm{Rx},Li}(\theta_{Li})$). Using equation (4.14), we can determine $\theta_{L1}$ and $\theta_{L2}$ for $\mathrm{Tx}_1$ and $\mathrm{Tx}_2$ respectively as shown in Fig. 4.4. Next, $d_1$ and $d_2$

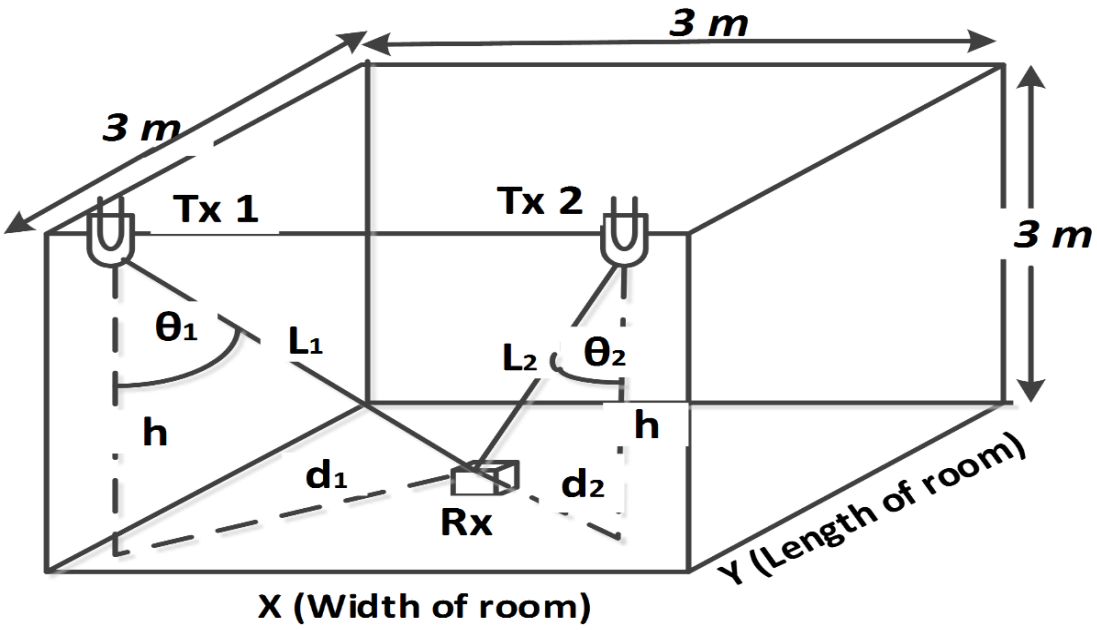


Fig. 4. 4 Two Txs indoor positioning system.

(horizontal distances between $Tx_1$, $Tx_2$ and the receiver) can be calculated from $\theta_{L1}$ and $\theta_{L2}$ using (4.15). Fig. 4.5 shows the top view of the 2-D system as well as the predicted power contours of the two transmitters at the positions (0.25m, 0m) and (2.75m, 0m). To determine the user's location, we need to find the intersection of the predicted power contours, which can be obtained by solving the following equations:

$$\begin{cases}(x_{\mathrm{Rx}} - x_{\mathrm{Tx1}})^2 + (y_{\mathrm{Rx}} - y_{\mathrm{Tx1}})^2 = d_{L1}^2 \\ (x_{\mathrm{Rx}} - x_{\mathrm{Tx2}})^2 + (y_{\mathrm{Rx}} - y_{\mathrm{Tx2}})^2 = d_{L2}^2\end{cases} \quad (4.\ 10)$$

where $(x_{\mathrm{Tx1}}, y_{\mathrm{Tx1}})$ and $(x_{\mathrm{Tx2}}, y_{\mathrm{Tx2}})$ are the position coordinates of the transmitters and $(x_{\mathrm{Rx}}, y_{\mathrm{Rx}})$ is the position of the receiver to be determined.

In previous works, there has been no analytical model for the impact of noise on the positioning accuracy in a standard size room as previously mentioned in Section 4.3.1. In this section, we will develop the noise analysis for the proposed system. Equation (4.14) can be rewritten by setting $k = m + \gamma + 1$:

$$P_{\mathrm{Rx},L_i}(\theta_{Li}) = P_{\mathrm{Rx},h}(0)\ \cos^k(\theta_{L_i}), \quad (4.\ 11)$$

In the case of a noise-free scenario, from (4.17), we also have:

$$\theta_{Li} = \cos^{-1}\left(\sqrt[k]{\frac{P_{\mathrm{Rx},Li}(\theta_{Li})}{P_{\mathrm{Rx},h}(0)}}\right). \quad (4.\ 12)$$

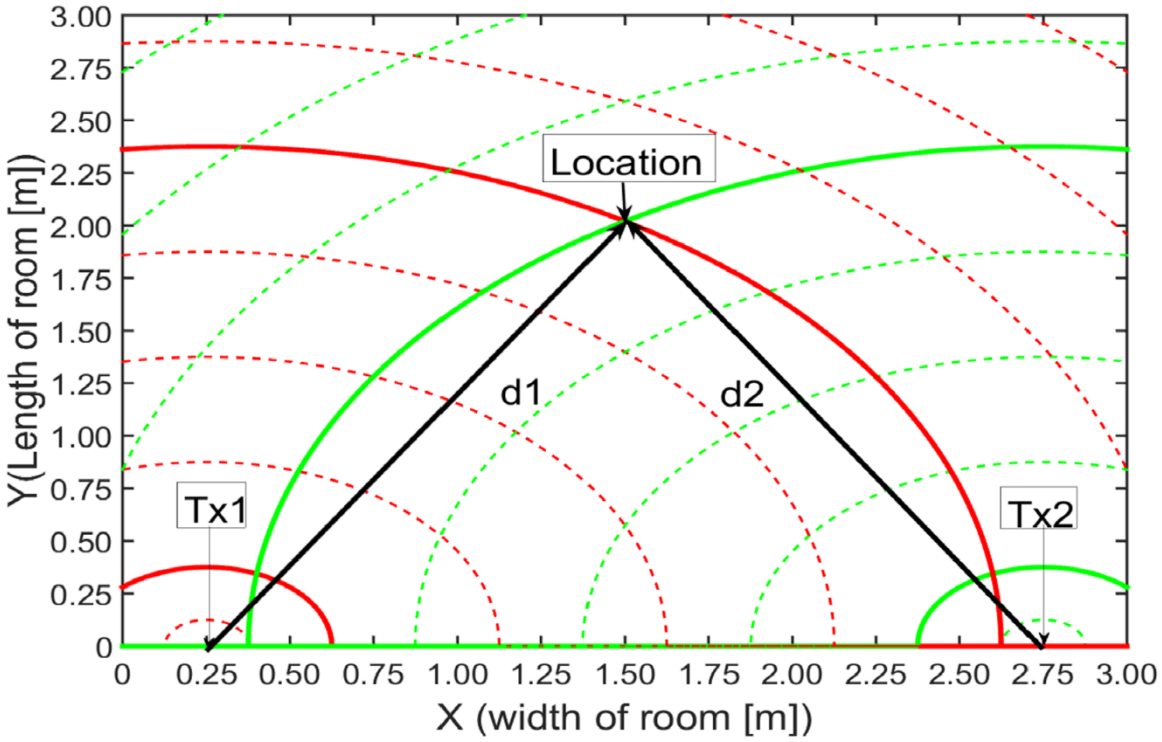


Fig. 4. 5 top view of the 2-D positioning system.

However, if there are noises with the powers of $P_{n_i}$ and $P_{n_o}$ that are present at the receiver position and underneath the transmitter, respectively, these noises will be added to the measured received optical powers $P_{\mathrm{Rx},Li}(\theta_{Li})$ and $P_{\mathrm{Rx},h}(0)$ at distances of $L_i$ and $h$ respectively and are given by:

$$P_{\mathrm{Rx},Li}(\theta_{Li}) + P_{n_i} = \left(P_{\mathrm{Rx},h}(0) + P_{n_o}\right)\cos^k(\theta_{Li} + \Delta\theta_{Li}), \tag{4. 13}$$

where

$$\theta_{Li} + \Delta\theta_{Li} = \cos^{-1}\left(\sqrt[k]{\frac{(P_{\mathrm{Rx},Li}(\theta_{Li}) + P_{n_i})}{(\mathrm{P}_{\mathrm{Rx},h}(0) + P_{n_o})}}\right), \tag{4. 14}$$

$$\Delta\theta_{Li} = \cos^{-1}\left(\sqrt[k]{\frac{\left(P_{\mathrm{Rx},Li}(\theta_{Li}) + P_{n_i}\right)}{(P_{\mathrm{Rx},h}(0) + P_{n_o})}}\right) - \cos^{-1}\left(\sqrt[k]{\frac{P_{\mathrm{Rx},Li}(\theta_{Li})}{\mathrm{P}_{\mathrm{Rx},h}(0)}}\right), \tag{4. 15}$$

Therefore, the link SNR is given by:

$$\mathrm{SNR} = 10\log\left(\frac{P_{\mathrm{Rx},Li}(\theta_{Li})}{<n_i^2>}\right) \quad \Leftrightarrow \quad \mathrm{snr} = \frac{P_{\mathrm{Rx},Li}(\theta_{Li})}{<n_i^2>}\,. \tag{4. 16}$$

where snr and SNR are the linear and logarithmic values of signal-to-noise ratio respectively. Note that the noises $n_i$ and $n_o$ have normal distributions (i.e. AWGN) and the average noise power can be written as:

$$P_{n_i} = \frac{f(n)_{\mathrm{i}}\, P_{\mathrm{Rx},Li}(\theta_{Li})}{\mathrm{snr}}, \tag{4. 17}$$

Where $f(n_i) = \mathrm{N}(\mu, \sigma)$ is AWGN ($\mu$ is mean and is equal to zero and $\sigma$ is the variance of noise and is equal to one). Substituting for the noise in (4.21), we have:

$$\Delta\theta_{Li} = \cos^{-1}\left(\sqrt[k]{\frac{\left(P_{\mathrm{Rx},Li}(\theta_{Li}) + f(n)_i\, P_{\mathrm{Rx},Li}(\theta_{Li})/\mathrm{snr}\right)}{\left(P_{\mathrm{Rx},h}(0) + f(n)_0\, P_{\mathrm{Rx},h}(0)/\mathrm{snr}\right)}}\right) - \cos^{-1}\left(\sqrt[k]{\frac{P_{\mathrm{Rx},Li}(\theta_{Li})}{P_{\mathrm{Rx},h}(0)}}\right),$$

$$= \cos^{-1}\left(\sqrt[k]{\frac{\left(P_{\mathrm{Rx},Li}(\theta_{Li})[snr + f(n)_i]\right)}{\left(P_{\mathrm{Rx},h}(0)[snr + f(n)_0]\right)}}\right) - \cos^{-1}\left(\sqrt[k]{\frac{P_{\mathrm{Rx},Li}(\theta_{Li})}{P_{\mathrm{Rx},h}(0)}}\right). \tag{4. 18}$$

Equation (4.24) shows the relationship between $\Delta\theta_{Li}$ and SNR. From (4.15), it is possible to calculate the horizontal distance under the condition of without and with noise as shown in (4.15) and (4.25), respectively.

$$d_i + \Delta d_i = h * \tan(\theta_{Li} + \Delta\theta_{Li}). \tag{4. 19}$$

Therefore, the distance difference due to noise is given by:

$$\Delta d_i = h * \tan(\theta_{Li} + \Delta\theta_{Li}) - h * \tan\theta_{Li},$$

$$= h * (\tan(\theta_{Li} + \Delta\theta_{Li}) - \tan(\theta_{Li})). \tag{4. 20}$$

From the above equations ((4.24) and (4.26)), the relationship between $\Delta\theta_{Li}$ or $\Delta\, d_i$ and SNR at any position in the room is determined.

# 4.4. Results and Discussions

## 4.4.1. System Setup

The proposed 2-Tx indoor positioning system as shown in Fig. 4.4 is simulated and evaluated using MATLAB. The coordinator generates different location codes [117, 142] for the two transmitters based on the transmitters' positions and combines them to the transmitted data as shown in Fig. 4.2. The receiver on the other side recovers the data based on OOK-TDM (time division multiplexing) scheme and hence obtains the locations of transmitters from the transmitted location codes. During the location code transmission, only

one LED is active at a time to ensure that the receiver receives the correct code from a dedicated LED. The positioning algorithm then uses the transmitters' positions and received power levels. The main simulation parameters adopted are presented in Table 4.1. Each Tx contains a number of LEDs whose parameters match those of commercially available LED devices.

## 4.4.2. The Transmitters' Positions

The proposed system is evaluated in four scenarios where the positions of the two transmitters mounted on ceiling are changed as shown in Fig. 4.6 (a). The positioning performance is evaluated at 169 points (i.e. on a 13×13 grid) on the floor of the room. These scenarios are summarised in Table 4.2. In each scenario, we test five different transmitter positions to evaluate the proposed approach.

Table 4. 1 Simulation parameters for the proposed VLC positioning system using two transmitters.

| Parameters | Values |
|---|---|
| Size of room | |
| Length(m) × Width(m) × Height(m) | 3 × 3 × 3 |
| Number of LED-based transmitters (using for localisation) | 2 |
| Transmitters locations | as in Fig. 4.6 (a) |
| The LED's semi-angle at half power (FWHM) | $70^{o}$ |
| Transmitted power per Tx | as in Table 4.3 |
| Receiver plane above the floor | 0.5 m |
| Active area ($A_R$) of receiver | 50 $mm^2$ |
| Half angle FOV of receiver | $60^{0}$ |
| Detector orientation: tilt horizontal (elevation) | $0^{o}$ |
| Detector orientation: tilt vertical (azimuth) | $0^{o}$ |
| Refractive index of lens at PD | 1.5 |
| Receiver sensitivity (used with the AD8015 trans-impedance amplifier)[23] | -36 dBm |
| X-Y sweep resolution (m) | 0.25 × 0.25 |

Table 4. 2 The simulated scenarios of the transmitters' positions.

| | |
|---|---|
| ○ | Scenario (1) when $Tx_i$ coordinate $x_{Txi} > 0$ and $y_{Txi} = 0$ |
| □ | Scenario (2) when $Tx_i$ coordinate $x_{Txi} > 0$ and $y_{Txi} = 25$ cm |
| ✡ | Scenario (3) when $Tx_i$ coordinate $x_{Txi} = y_{Txi}$ |
| △ | Scenario (4) when $Tx_i$ coordinate $x_{Txi} = 0$ and $y_{Txi} > 0$ |

In scenario (1), the two transmitters are located at the corners of the room and are then moved towards the middle of the wall by a 25 cm step. Five different positions were tested where Fig. 4.7 (a) shows the average position error against the SNR for all possible positions in a typical room. In all cases, all curves are close to each other, and the average positioning error (for the entire room) tends towards zero for SNR more than 25 dB (i.e. for high SNR values). In the second scenario (2), when the transmitters are away from the wall (i.e.; $y_{Txi}$ = 25 cm), the distance between the two transmitters is decreased by 50 cm in every step (i.e. $Tx_1$ and $Tx_2$ are moved towards each other by 25 cm in each step). The relationship between the SNR and the average error is plotted in Fig. 4.7 (b). The obtained average positioning errors is slightly higher than that of the first scenario because there are two solutions when solving equation (10) and equation (11). Each solution can be equally considered as the user's location. Therefore, we can consider that the receiver is in a bigger area whereas there is a

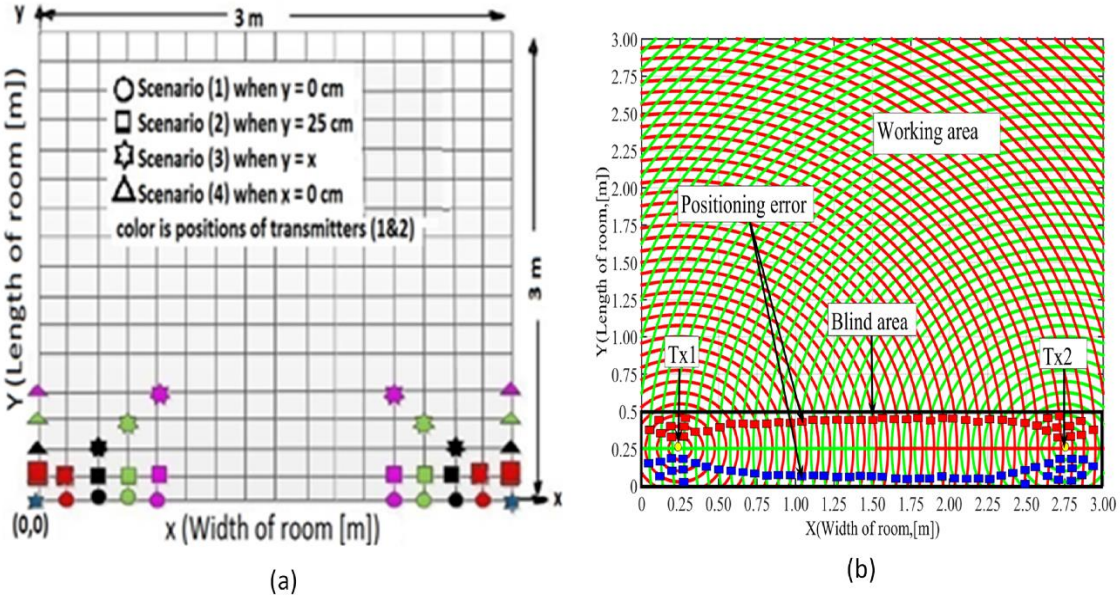


Fig. 4. 6 (a) Different positions of transmitters in the proposed VLC positioning system and (b) the blind spot and the working area.

blind zone for determining the receiver position if it moves to the small area between Txs and the wall as illustrated in Fig. 4.6 (b). Note that in Fig. 4.6 (b), there is two possible solutions due to the intersection of the power circles of $Tx_1$ and $Tx_2$. The blind zone is shown as the line drawn through the top intersection points (red points).Within the blind zone, we cannot determine the accurate position of the receiver. Outside this blind zone (i.e. working area), the system should operate normally.

We have also carried out the evaluation of scenarios (3) and (4) to explore the system performance under different transmitter configurations. The relationships between SNR and average errors are plotted in Fig. 4.7 (c) and (d) for scenarios (3) and (4) respectively. For the third scenario the average positioning error is higher than those of the first and second scenarios. For instance, for the transmitters' positions of (1.00, 1.00), (2.00, 1.00) m and (0.25, 0.25), (2.75, 0.25) m at an SNR of 15dB, the average position errors are 51.24 cm and 28.77 cm. This is due to the presence of the blind spot as was the case for the second scenario. As shown, Fig. 4.7 (c) and (d) are approximately similar and both show a significant average error compared to scenarios (1) and (2). The minimum positioning errors in a blind zone for scenarios (3) and (4) are 0.5, 1, 1.5, 2 meters when the y-coordinate is 25, 50, 75, 100 centimetres, respectively, for the four different positions.

Note that in scenario (1) there is no blind zone whereas the blind zone slowly emerges in scenario (2). In some suggested environments, there does not exist a blind zone problem when transmitters' positions are located at the corners (i.e.; scenario (1)). However, in the proposed environment, and other similar environments, the proposed environment, the second position of transmitters is optimal (i.e.; scenario (2)), and at the same time, the blind zone is small. Then, it does not affect the positioning error except in 16% of the total area. Therefore, we suggest that this area (i.e.; the blind zone) does not use for users but it can be used for furniture.

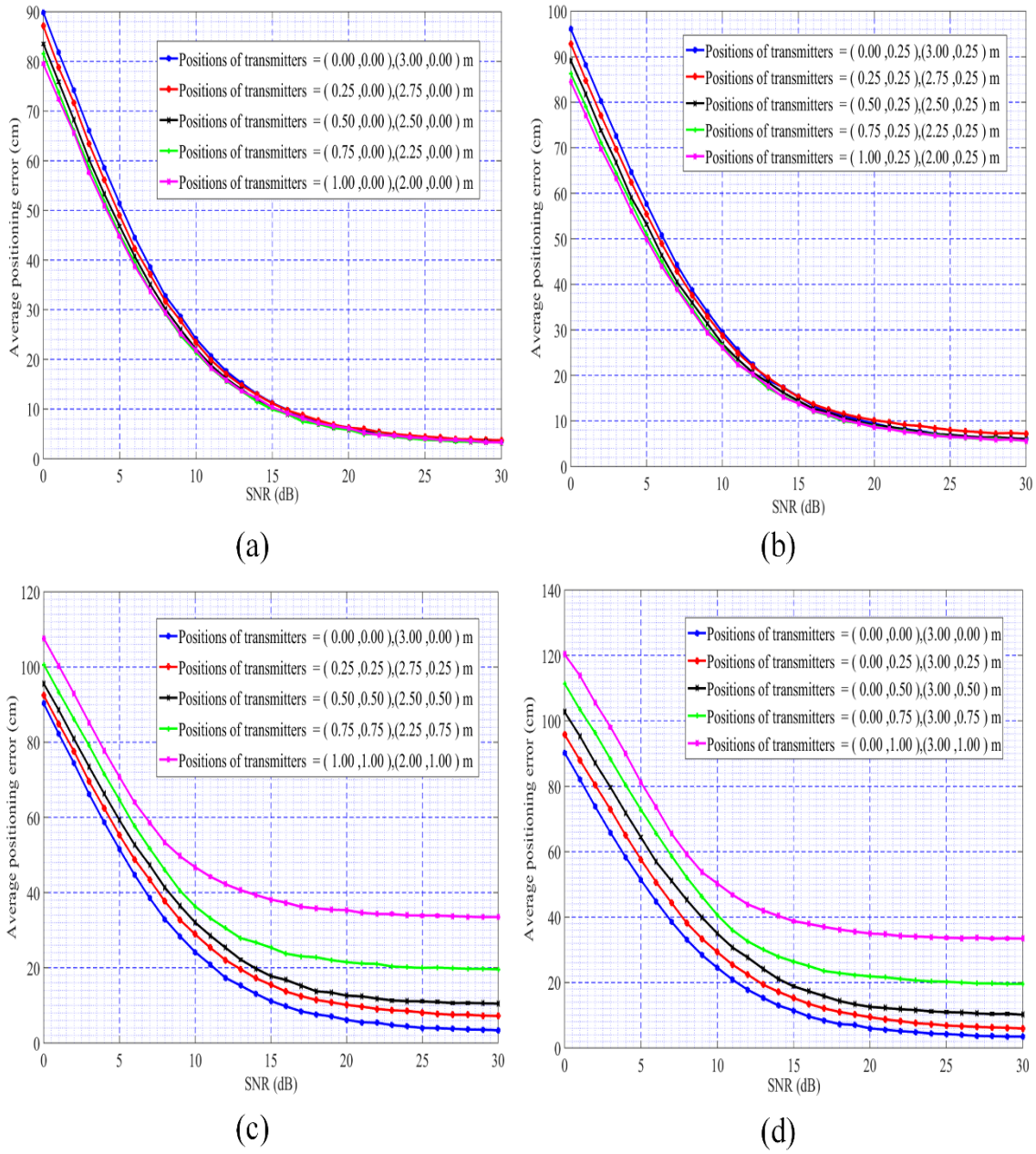


Fig. 4. 7 Average position errors against the SNR of LOSNLOS scenario for four scenarios and different transmitters' locations: (a) Scenario (1) with $y_{\mathrm{Tx}_i}$ = 0 cm, (b) Scenario (2) with $y_{\mathrm{Tx}_i}$= 25 cm, (c) Scenario (3) with $x_{\mathrm{Tx}_i}$= $y_{\mathrm{Tx}_i}$, and (d) Scenario (4) with $x_{\mathrm{Tx}_i}$= 0 (see Table 4.2 and Fig. 4.6 (a)) from the extending proposed positioning system (End-to-end proposed positioning system).

We have applied different SNR values to the process. At very high SNRs, the average error (across the room) in scenario (2) is a marginally higher than in scenario (1) (see the range of SNR above 22 dB in both Fig. 4.7 (a) and (b)). It is also shown that the performance obtained is similar for low SNRs. However in scenario (3) and (4), both poor SNR and the locations of transmitters contribute towards a worse performance (see Fig. 4.7 (c) and (d)). From the evaluation, it can be noted that the best locations for the transmitters are those

shown in Fig. 4.7 (a) (i.e.; from the first scenario). However, there are many possible positions of $Tx_1$ and $Tx_2$. Note that the locations of these transmitters will have an impact on the transmission power in VLC. Ideally, the power should be minimum whilst maintaining a proper operation. Next, we investigate the minimum transmission power required to achieve accurate positioning where the received power needs to meet the sensitivity given in Table 4.3. Table 4.3 depicts the transmission power obtained for scenarios (1) and (2). As

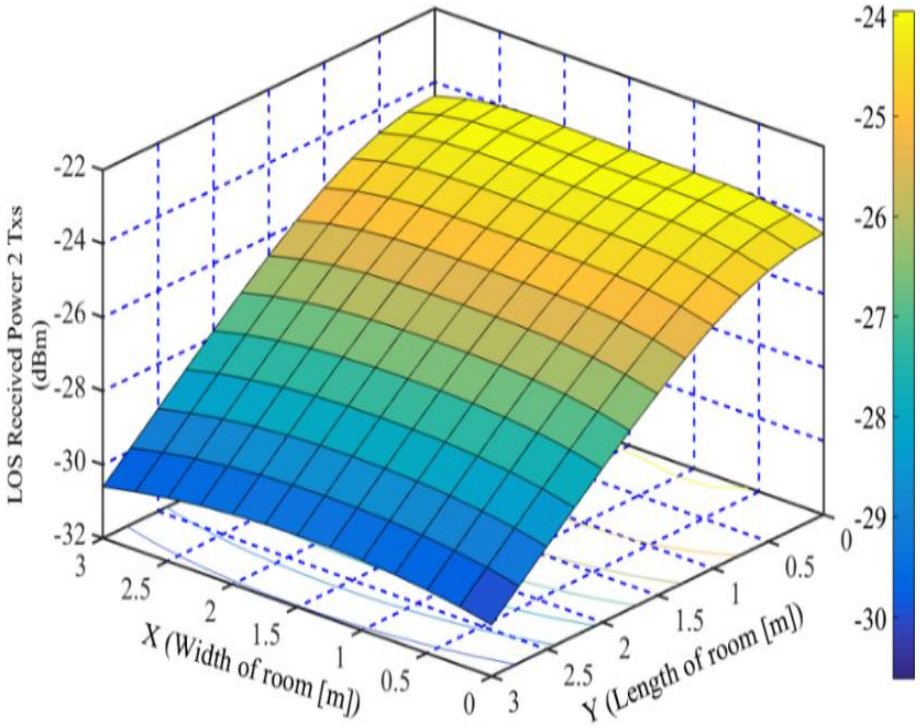


Fig. 4. 8 Received optical power distribution for two transmitters

Table 4. 3 The required transmission power as a function of the transmitters' positions.

| No. | Position of $Tx_1$ (m) | Position of $Tx_2$ (m) | Required transmitted power of $Tx_i$ (W) |
|---|---|---|---|
| Scenario (1) | | | |
| 1 | (0,0) | (3,0) | 10 |
| 2 | (0.25,0) | (2.75,0) | 9 |
| 3 | (0.50,0) | (2.50,0) | 8 |
| 4 | (0.75,0) | (2.25,0) | 7 |
| 5 | (1.00,0) | (2.00,0) | 6 |
| Scenario (2) | | | |
| 1 | (0,0.25) | (3,0.25) | 10 |
| 2 | (0.25,0.25) | (2.75,0.25) | 8 |
| 3 | (0.50,0.25) | (2.50,0.25) | 7 |
| 4 | (0.75,0.25) | (2.25,0.25) | 6 |
| 5 | (1.00,0.25) | (2.00,0.25) | 6 |

it can be seen, a reduction in transmission power levels is observed when two transmitters are close to one another. This result indicates that the optimum transmission power requires the lighting distribution to be as flat as possible. Fig. 4.8 shows that the received optical power distribution for position number (2) in Table 4.3 (i.e. the transmitters positions being (0.25 0) & (2.75, 0) m) has flatness.

Therefore, a compromise between the power and the lighting should be reached. Note that the minimum received power is above the receiver sensitivity meaning that the VLC positioning process reaches the best position for scenario (1). This proposed configuration (the transmitters positions) being (0.25, 0) & (2.75, 0) m) is practical for environments such as long corridors, tunnels and areas close to buildings etc. where the lighting units along small corridors are typically placed at the intersection line between the wall and ceiling. Another application could be in areas that are close to buildings such as gardens as shown in Fig. 4.9 (a) and (b). We have performed the same approach for scenario (2) by selecting the transmitters' positions (1&2) at (0.25, 0.25) & (2.75, 0.25) m which are the optimum positions for scenario (2). The layout of LEDs in the configurations in scenario (2) are

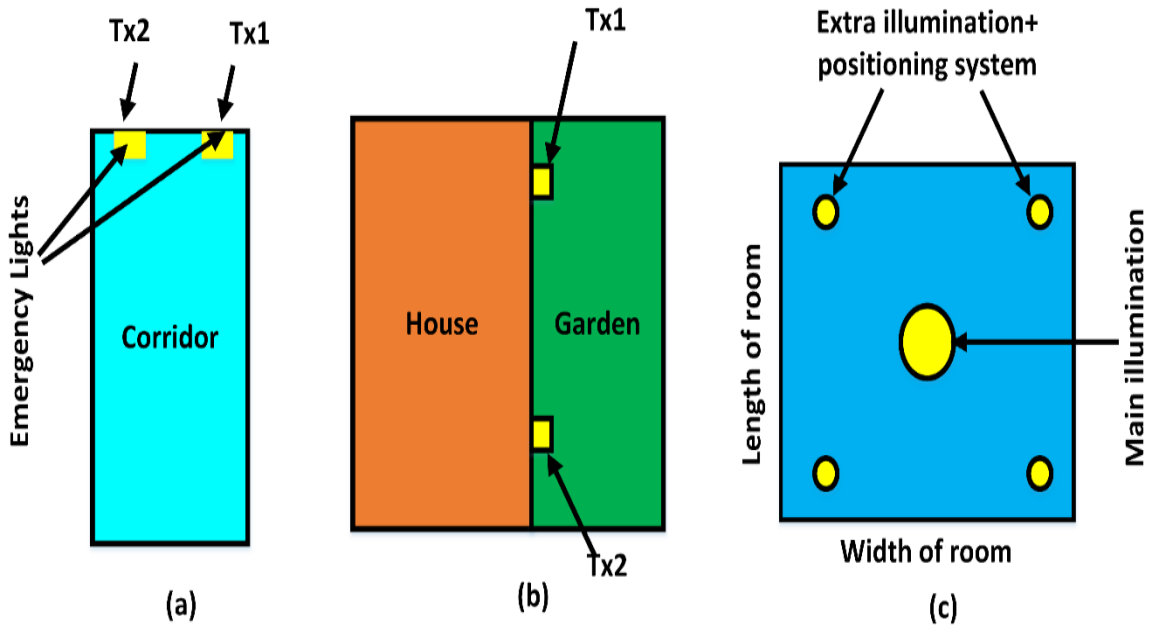


Fig. 4. 9 Different applications for the proposed system:(a) & (b) the best options for the scenario (1) and (c) the best case for scenario (2).

practically related such that one could use a line of LEDs for localization compared to more than two LEDs in the traditional IPSs. Similarly, this configuration (i.e. the transmitters positions (1&2) being (0.25, 0.25) & (2.75, 0.25) m) may also be adopted in a room or a hall using the extra illumination sources for positioning system when the main illumination source is used for lighting only as shown in Fig. 4.7 (c).

## 4.4.3. The Impact of Noise on Angular Error and Distance Error

In the subsequent investigation, using (4.15), we have determined and plotted the relationships between the angular error $\Delta\theta_{Li}$ (note that $\Delta\theta_{L1}$ is the angular error of $Tx_1$ and $\Delta\theta_{L2}$ is the angular error of $Tx_2$) for a range of SNR. Fig.4.10 (a) shows these relationships when the receiver is at the centre of the room. It is noted that the angular error is very sensitive to the signal quality; however, it is more stabilized at high SNR levels. In addition, the relationship between the horizontal distance error $\Delta d_i$ (where $\Delta d_1$ and $\Delta d_2$ are the horizontal distance errors for $Tx_1$, and $Tx_2$ respectively) and the SNR is determined using (4.26) and is plotted in Fig.4.10 (b). The results are shown for the optimum positions of the first and second scenarios.

## 4.4.4. Positioning Error and its Distributions

### 4.4.4.1. LOS Approach

We also investigate the positioning error (the difference between the estimated position and the actual position) in the noisy and noiseless cases for the LOS approach only (i.e.; the effect of reflections are ignored). This can be expressed as:

$$E = \sqrt{(x_{est} - x_{real})^2 + (y_{est} - y_{real})^2} \qquad (4.21)$$

For the investigation considering the noiseless care (i.e. ideal case), we present two optimum positions of the two transmitters as mentioned in the previous section. Fig. 4.11 (a) depicts the 2-D localization error distribution of this algorithm for the best position of scenario (1) when the transmitters' positions (1&2) are (0.25m, 0m) and (2.75m, 0m). Fig.4.11 (b) shows the distance error distribution for the best position of scenario (2) when the transmitters' positions (1&2) are (0.25m, 0.25m) and (2.75m, 0.25m). From these figures, an error of less than one cm is observed for the best position of scenario (1).

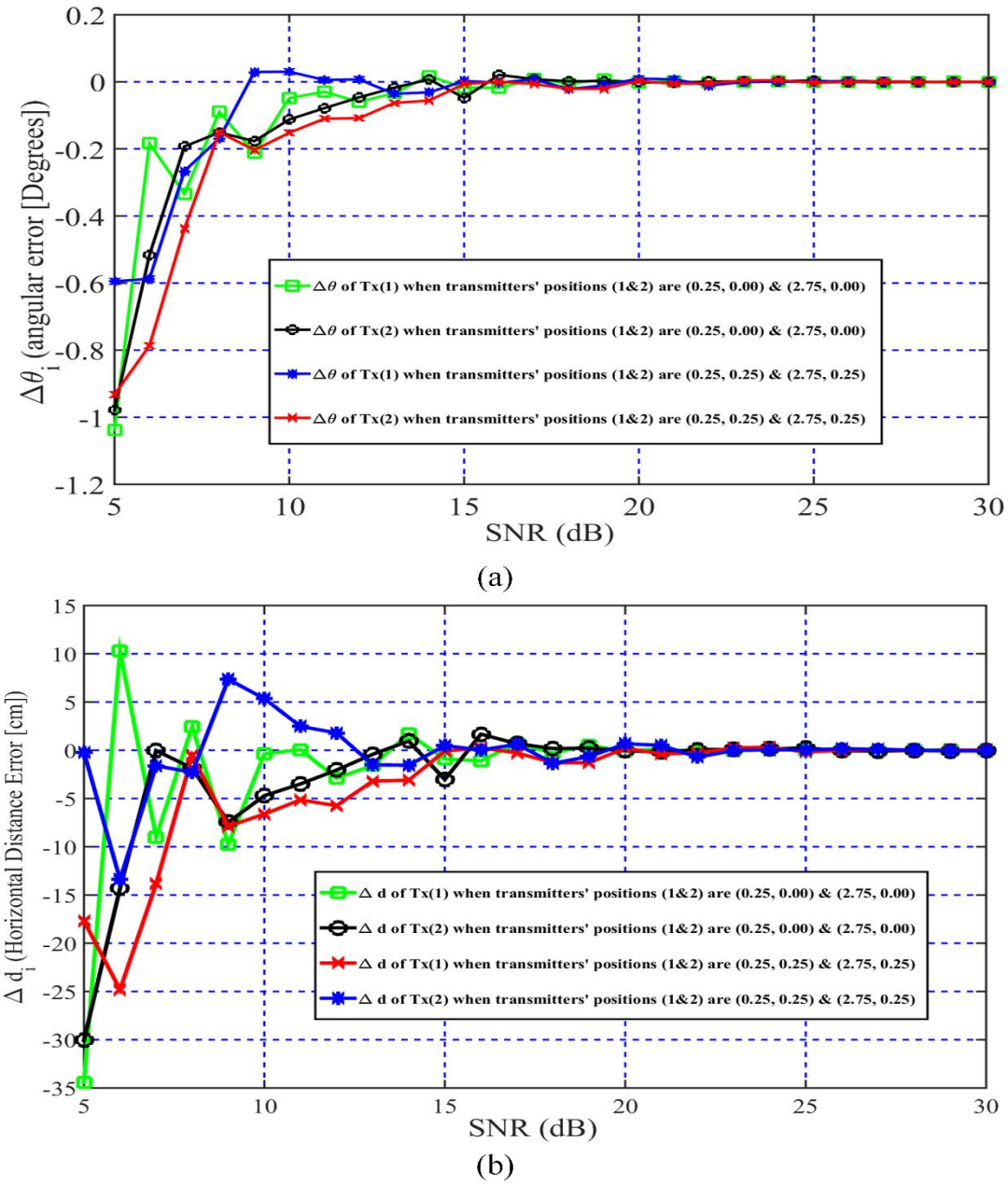


Fig. 4. 10 (a) The angular error vs SNR, (b) the horizontal distance error vs SNR for the optimum transmitter's positions for scenarios (1) and (2) when the receiver's position is (1.50m, 1.50m).

However, there is a clear distance error in the area under the transmitters in the best position of scenario (1) due to the directionality of Lambertian. On the other hand, a similar result is observed in the best position of scenario (2) but the distance error is slightly high in the area under the transmitters which also stems from to the directionality of Lambertian.

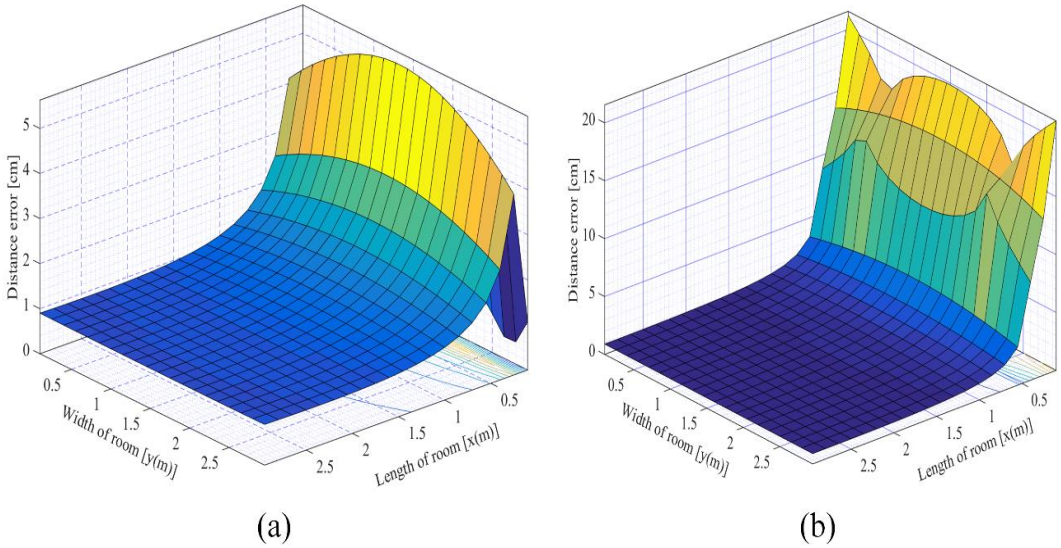


Fig. 4. 11 Spatial distribution of positioning error without considering noise for LOS scenario and when the transmitters' positions (1&2): (a) are (0.25m, 0m) & (2.75m, 0m) (b) are (0.25m, 0.25m) & (2.75m, 0.25m).

We have further investigated the system performance in the presence of noise. The simulations are at the two positions mentioned above. Firstly, the results presented here are the selected localization error distributions (depicted in Fig. 4.12) as well as the real vs estimated positions (plotted in Fig. 4.13) for the best position for scenario (1) (i.e. when the transmitters' positions (1&2) are (0.25m, 0m) and (2.75m, 0m)). These figures show the impact of noise on the positioning error distributions for different values of SNR (i.e. SNR of 10 dB, 15 dB, 20 dB and 30 dB) for the best position of scenario (1). For example, in Fig. 4.12 (b), the positioning error is less than 10 cm in all positions except the area that is under the transmitters when SNR = 15 dB. The maximum and minimum positioning errors, mean and standard deviation are summarized in Table 4.4. As can be clearly seen, there is a remarkable decline of the average positioning error when the SNR is increased. Furthermore, we also investigate the best position for scenario (2) using the LOS approach when the

transmitters' positions (1&2) are at (0.25m, 0.25m) and (2.75m, 0.25m). Fig.4.14 shows the positioning error distributions when the SNR is equal to 10 dB, 15 dB, and 20 dB, whereas Fig.4.15 presents the estimated and real positions among the four values of SNR which are 10 dB, 15 dB, and 20 dB. For instance, from Fig.4.14, we can see that the distance error is less than 10 cm in most locations in the typical room. The mean score for the distance error is around 12 cm. Table 4.4 provides the summary statistics for the positioning error. It can be observed that there is a significant decrease in the average positioning error when the SNR is increased especially for values higher than 15 dB. There are results from ROP distributions approach for positioning using two transmiters see Appendix C.

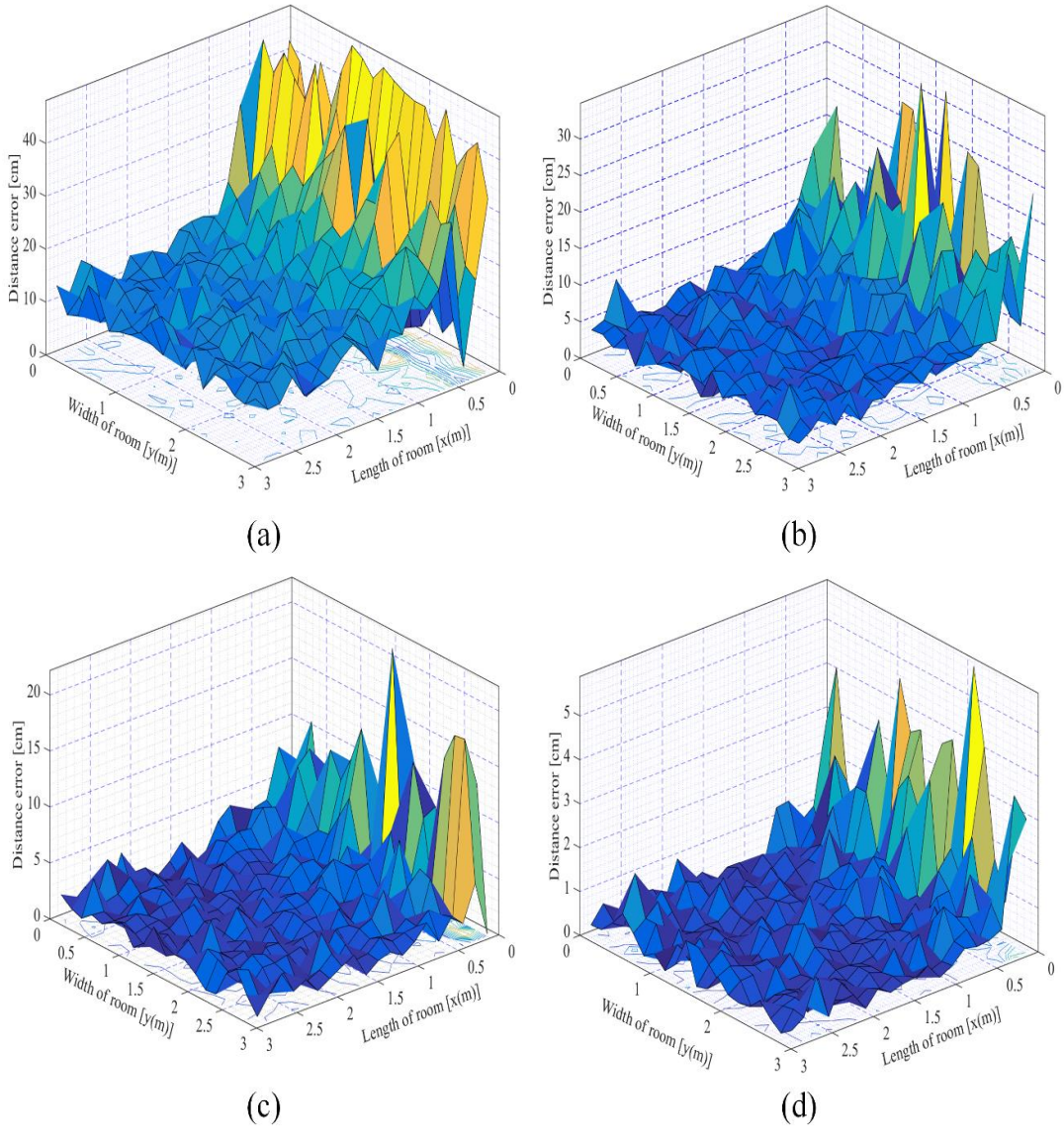


Fig. 4. 12 Positioning error distributions for the LOS scenario when the transmitters' positions (1&2) are (0.25m, 0m) & (2.75m, 0m) and (a) SNR = 10 dB, (b) SNR = 15 dB, (c) SNR = 20 dB and (d) SNR = 30 dB.

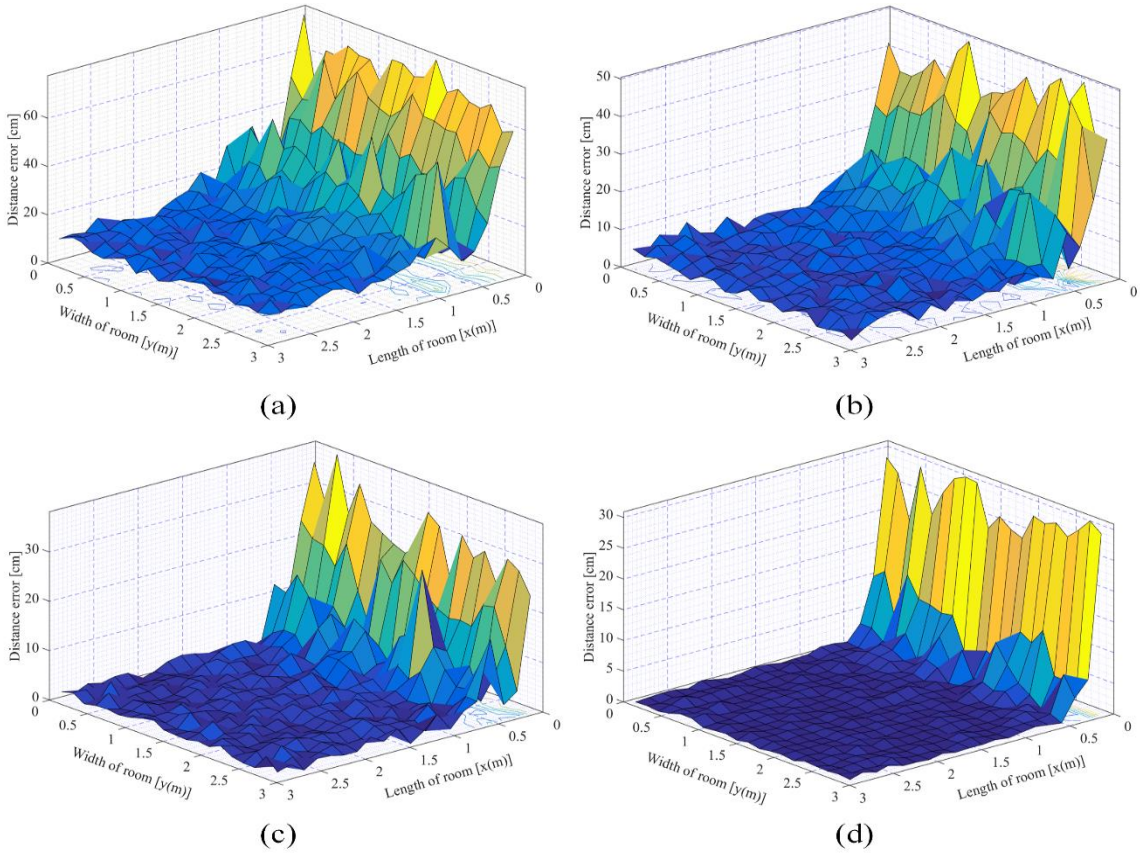


Fig. 4. 13 Positioning error distributions for the LOS scenario when the transmitters' positions (1&2) are (0.25, 0.25) & (2.75, 0.25) m and (a) SNR = 10 dB, (b) SNR = 15 dB, (c) SNR = 20 dB and (d) SNR = 30 dB.

Table 4. 4 Statistical standards of the positioning error for the LOS scenario.

| Positions of transmitters | SNR (dB) | Max. value (cm) | Min. value (cm) | The mean (cm) | Standard deviation (cm) |
|---|---|---|---|---|---|
| $Tx_1$ (0.25, 0)<br>$Tx_2$ (2.75, 0) | 0 | 153.432 | 7.851 | 85.180 | 30.638 |
| | 5 | 69.499 | 6.548 | 47.016 | 17.140 |
| | 10 | 59.773 | 3.119 | 21.712 | 10.414 |
| | 15 | 35.077 | 0.156 | 9.107 | 6.178 |
| | 20 | 21.025 | 0.716 | 4.424 | 3.725 |
| | 25 | 18.675 | 0.113 | 2.197 | 1.914 |
| | 30 | 7.019 | 0.150 | 1.522 | 1.130 |
| | 35 | 7.147 | 0.287 | 1.285 | 0.968 |
| | 40 | 5.009 | 0.014 | 1.167 | 0.842 |
| $Tx_1$ (0.25, 0.25)<br>$Tx_2$ (2.75,0.25) | 0 | 161.880 | 1.095 | 90.876 | 36.014 |
| | 5 | 118.046 | 1.460 | 53.260 | 23.735 |
| | 10 | 80.183 | 0.768 | 26.163 | 17.061 |
| | 15 | 55.126 | 0.841 | 12.392 | 11.455 |
| | 20 | 40.925 | 0.775 | 6.393 | 7.783 |
| | 25 | 34.191 | 0.205 | 4.189 | 6.195 |
| | 30 | 29.172 | 0.435 | 3.394 | 5.407 |
| | 35 | 25.659 | 0.366 | 3.182 | 5.101 |
| | 40 | 26.179 | 0.561 | 3.084 | 5.149 |

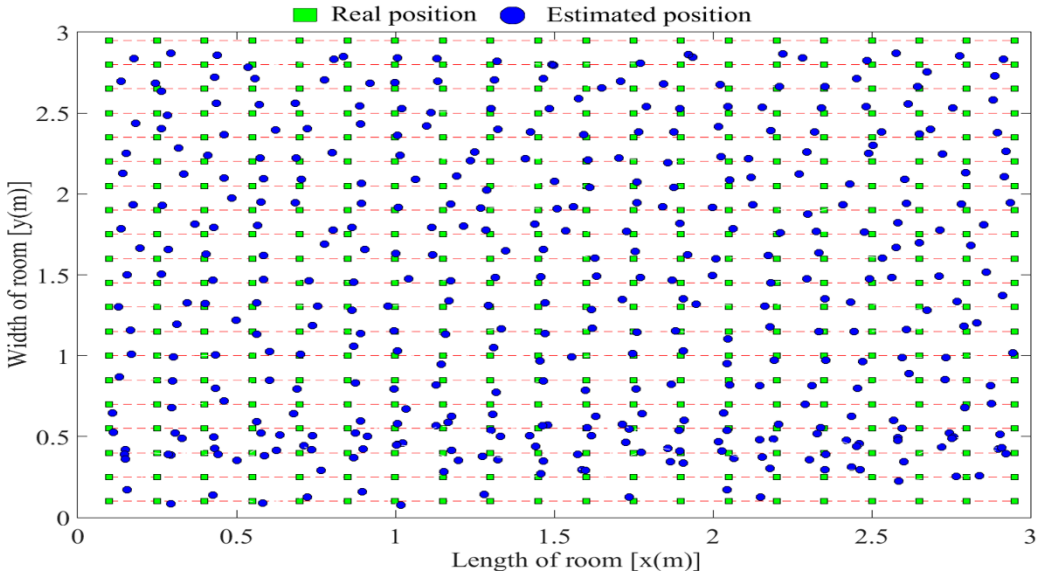


(a)

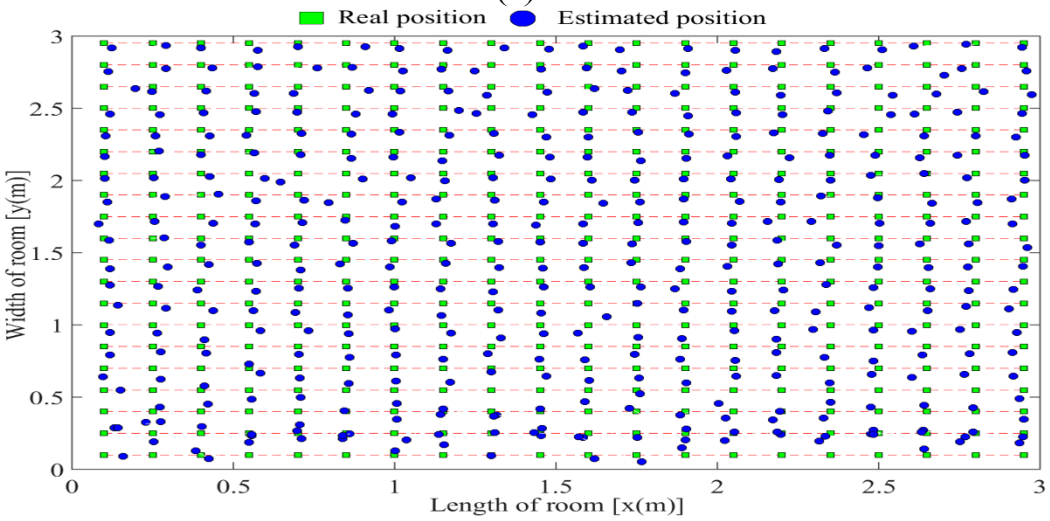


(b)

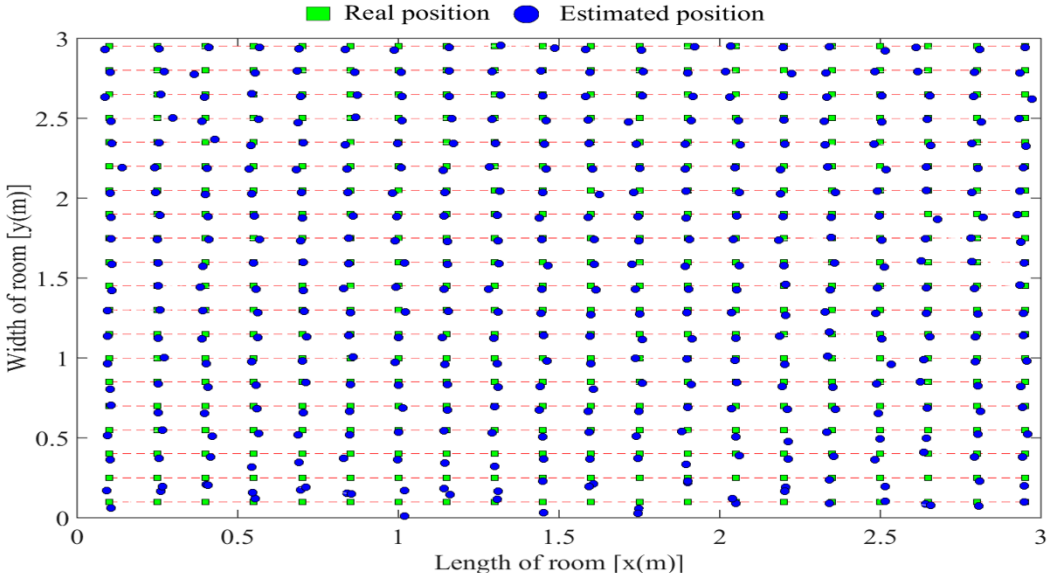


(c)

Fig. 4. 14 Estimated and real positions for the LOS scenario when the transmitters' positions (1&2) are (0.25m, 0m) & (2.75m, 0m) and (a) SNR = 10 dB, (b) SNR = 15 dB, (c) SNR = 20 dB.

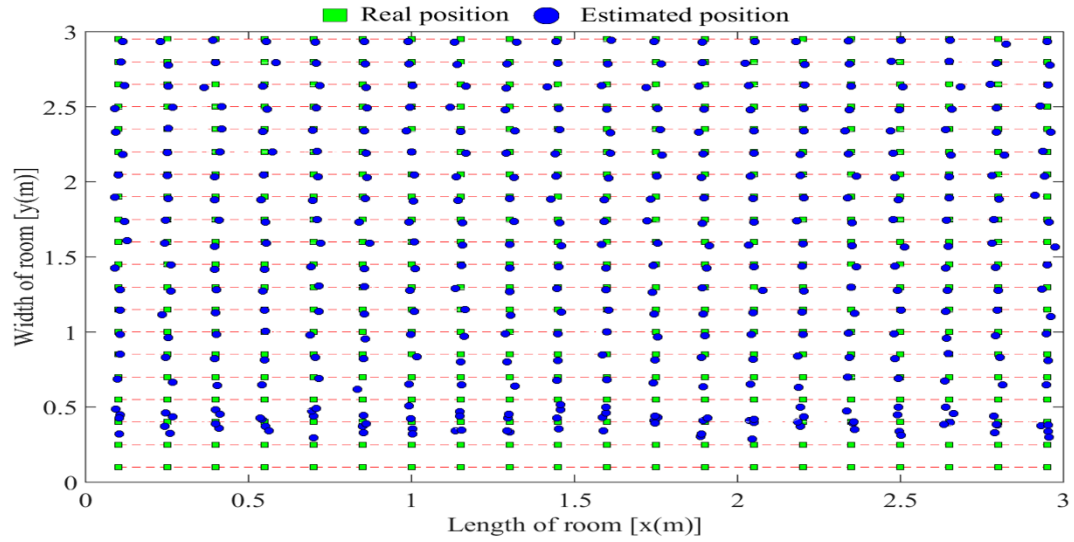


(a)

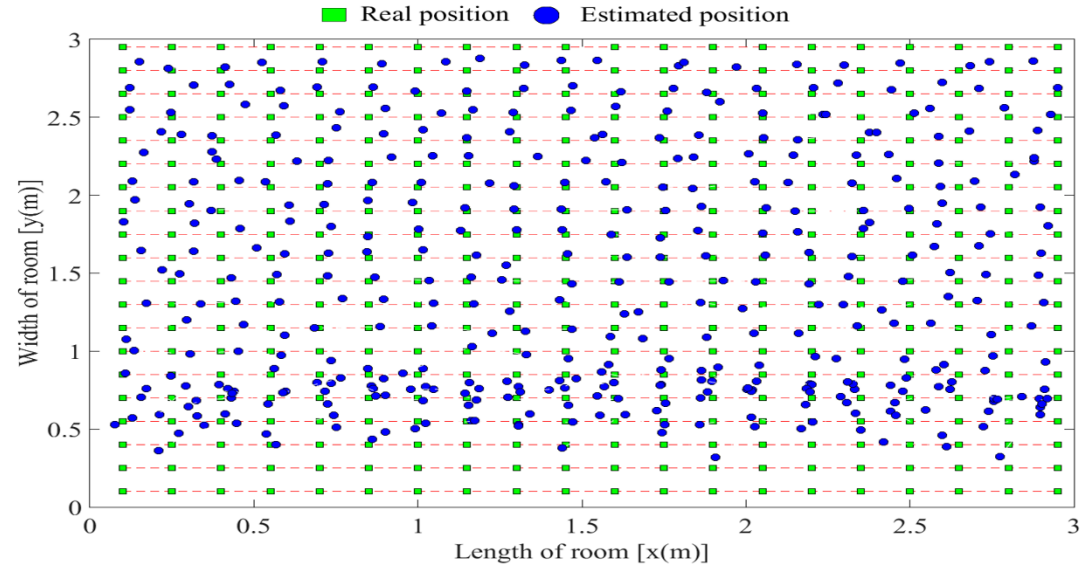


(b)

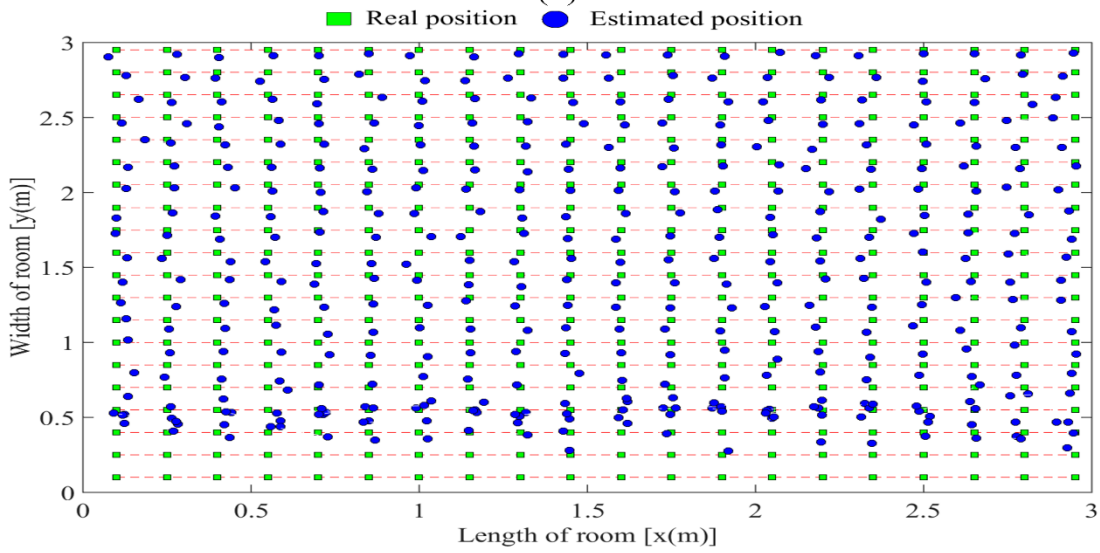


(c)

Fig. 4. 15 Estimated and real positions for the LOS scenario when the transmitters' positions (1 &2) are (0.25, 0.25) m & (2.75, 0.25) m and (a) SNR = 10 dB, (b) SNR = 15 dB, (c) SNR = 20 dB.

## 4.4.4.2. LOSNLOS Approach

This section presents an analysis of the system performance for a LOSNLOS approach. The positioning error was investigated under the effect of noise and without the presence of any noise in the positioning system (i.e. ideal system) to determine the effect of light reflections on the positioning error. Overall, there was no significant difference between the two approaches in the whole room except at the positions near the walls as shown in Fig.4.16. Figure 4.16 (a) provides the positioning error distribution for the best position of transmitters for scenario (1) where the mean is around 4.7 cm and the maximum is around 40 cm. The reason behind the disparity between the mean and the maximum values is due to the reflections of light. In addition, we have investigated the distance error for the best position for scenario (2) without considering any noise as shown in Fig.4.16 (b). Note that the mean in this case is approximately 8.4 cm while the maximum value is around 41 cm. This is also due to presence of light reflections as was the case for scenario (1) above.

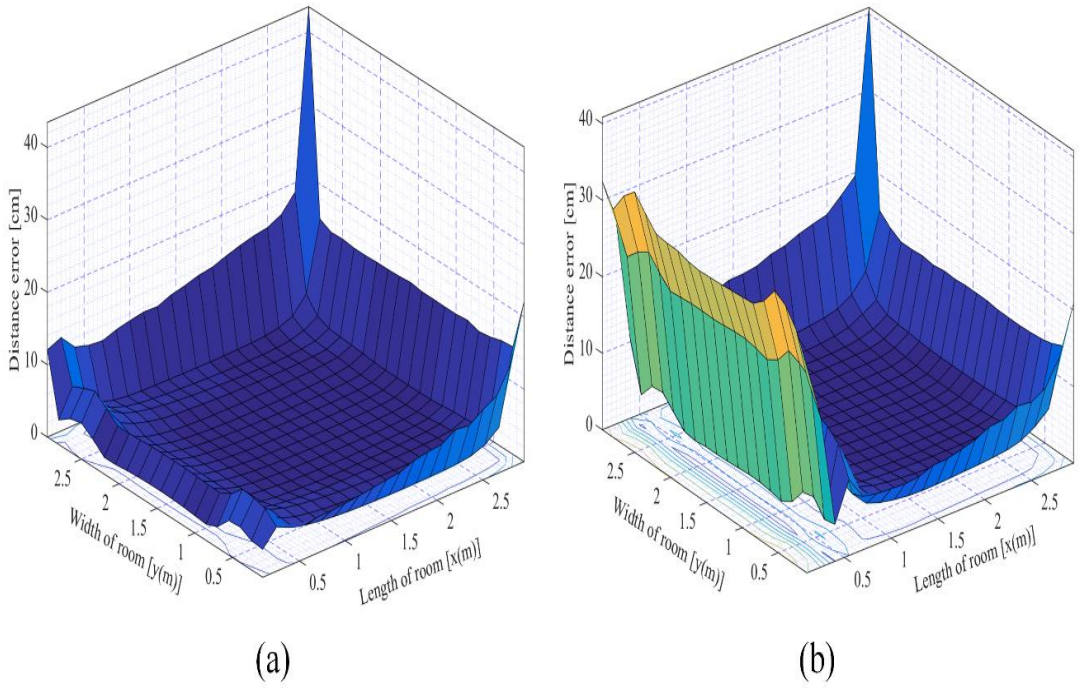


Fig. 4. 16 Spatial distribution of the positioning error without considering noise for the LOSNLOS scenario and when the transmitters' positions (1&2): (a) are (0.25m, 0m) & (2.75m, 0m) (b) are (0.25m, 0.25m) & (2.75m, 0.25m).

In the case of the presence of noise, we have simulated the LOSNLOS approach by following the same procedure adopted in the LOS approach above. The positioning error distributions for the best position of scenario (1) (i.e. when the transmitters' positions are (0.25m, 0m) & (2.75m, 0m)) are presented in Fig.4.17 at SNR values of 10 dB, 15 dB, 20 dB and 30 dB. The single most significant observation to emerge from the results is that the positioning error declines significantly but is slight high when the receiver approaches the walls. Fig. 4.18 shows the estimated and real positions when SNR = 10 dB, 15 dB, and 20 dB for the best position of scenario (1). From these sub-figures, we can see the effect of light reflections on the positioning error at wide range of SNR.

We have also simulated the best position for scenario (2) to determine the effect of the reflections on the positioning error when we have small blind area due to the same reason discussed above. Fig. 4.19 shows the results for the positioning error distributions obtained from the simulations to evaluate the indoor positioning system at different values of SNR. Fig. 4.19 (b) shows that the average of positioning error is less than 15 cm when the SNR is 15 dB. Fig. 4.20 depicts the estimated and real positions for the best position of scenario (2) for the proposed positioning system. Finally, Table 4.5 illustrates a summary of statistics for the positioning error (i.e. the maximum values, minimum values, the mean of positioning error and the standards deviation). Data from this table show that there is a significant decline in the positioning error average especially when the SNR is more than 15 dB.

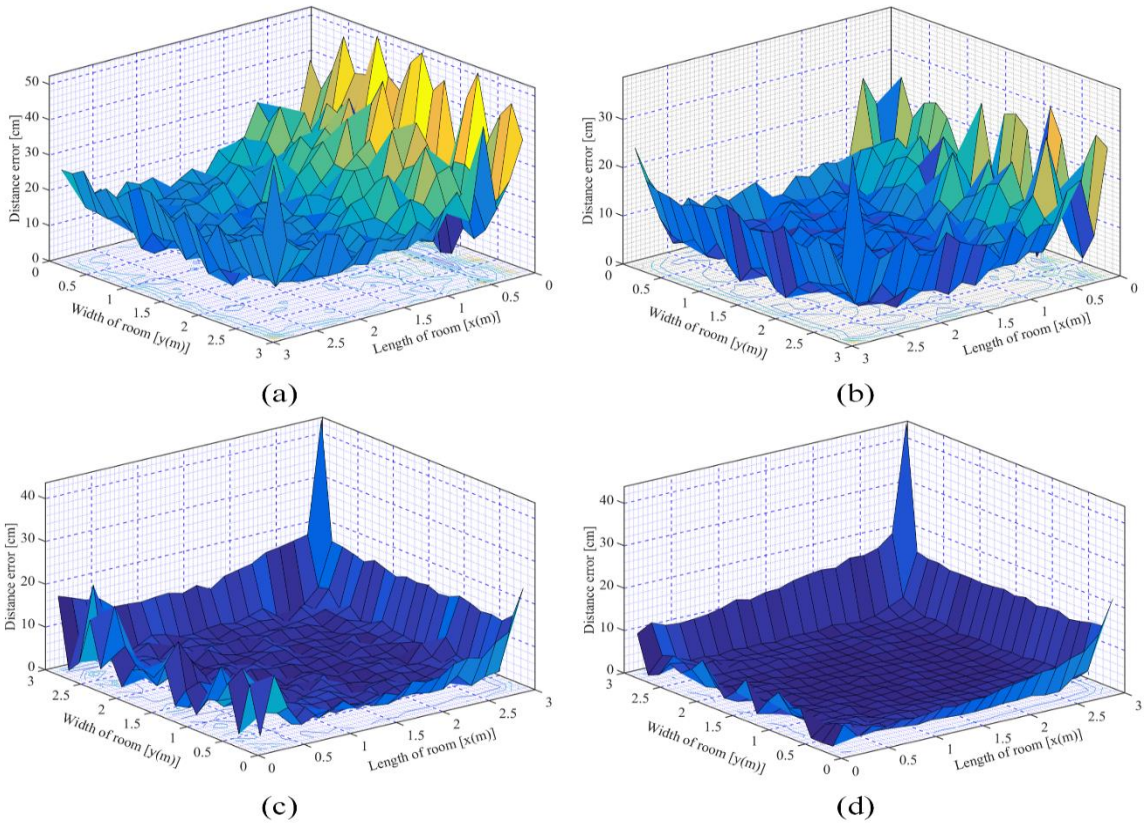


Fig. 4. 17 Positioning error distributions for the LOSNLOS scenario when the transmitters' positions (1&2) are (0.25m, 0m) & (2.75m, 0m) at (a) SNR = 10 dB, (b) SNR = 15 dB, (c) SNR = 20 dB and (d) SNR = 30 dB.

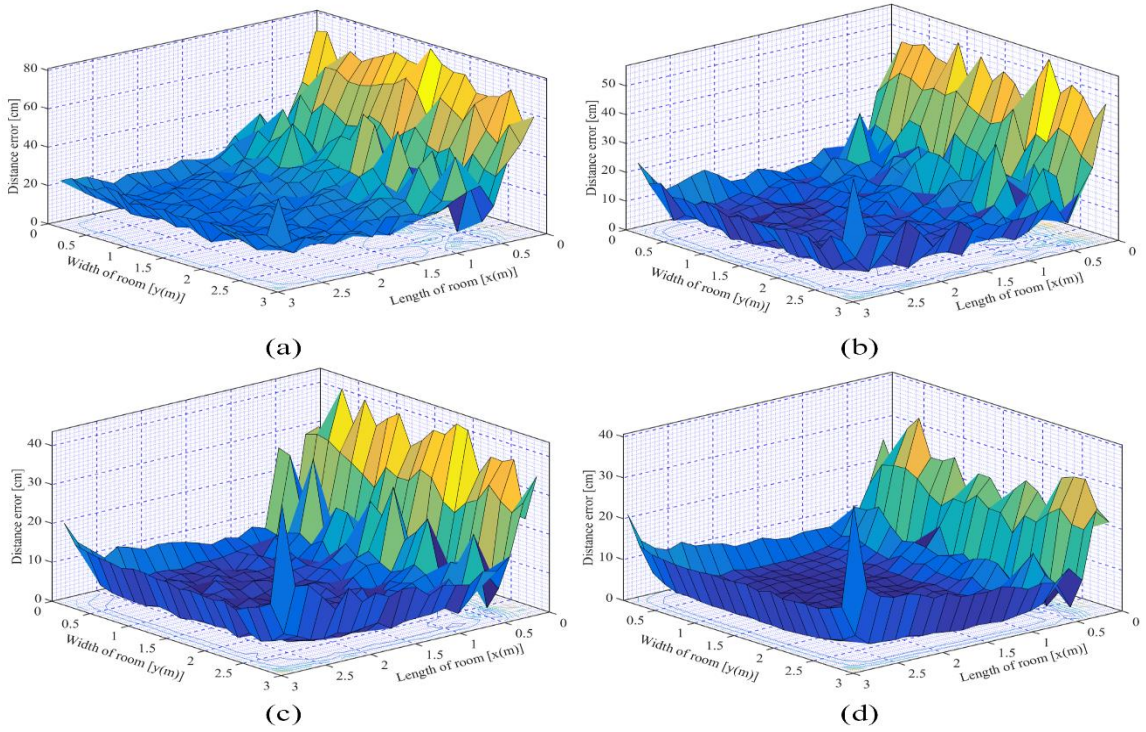


Fig. 4. 19 Positioning error distributions for the LOSNLOS scenario when the transmitters' positions (1&2) are (0.25, 0.25) & (2.75, 0.25) m and (a) SNR = 10 dB, (b) SNR = 15 dB, (c) SNR = 20 dB and (d) SNR = 30 dB.

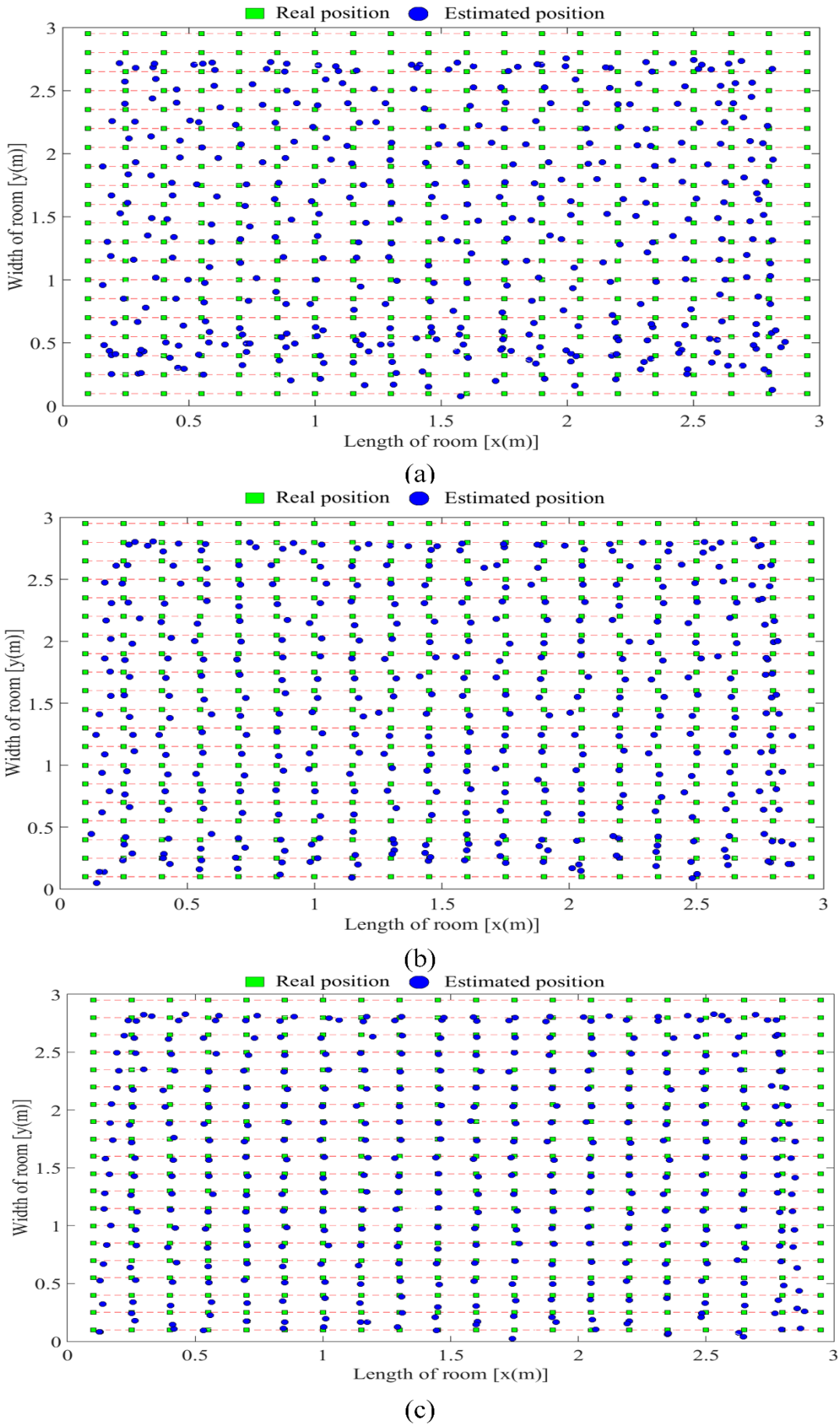


Fig. 4. 18 Estimated and real positions for the LOSNLOS scenario when the transmitters' positions (1&2) are (0.25m, 0m) & (2.75m, 0m) at (a) SNR = 10 dB, (b) SNR = 15 dB, and (c) SNR = 20 dB.

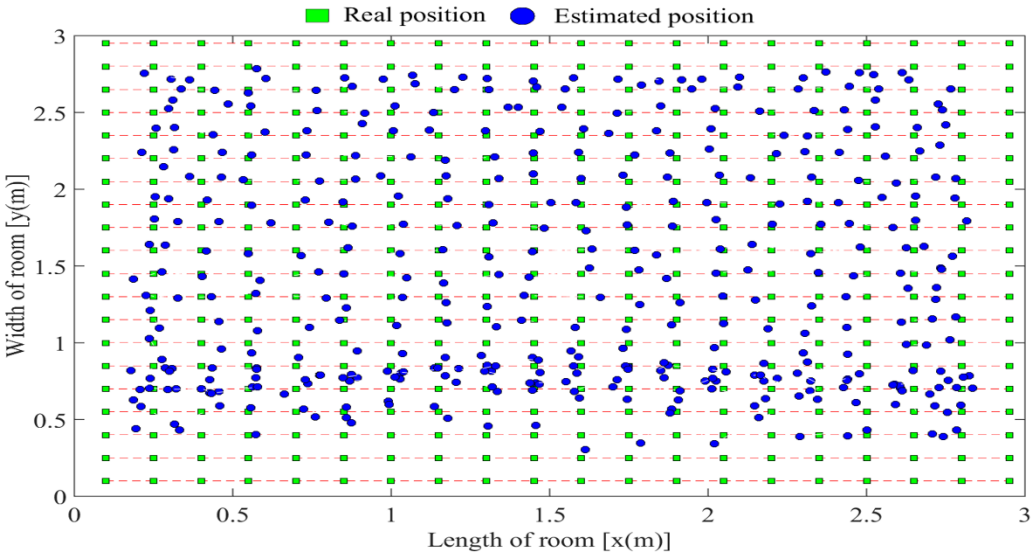


(a)

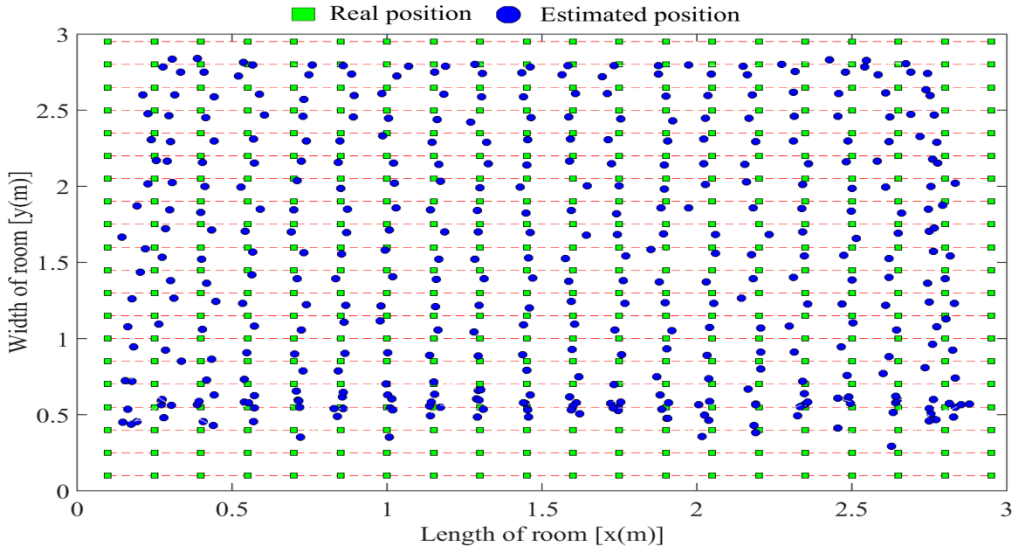


(b)

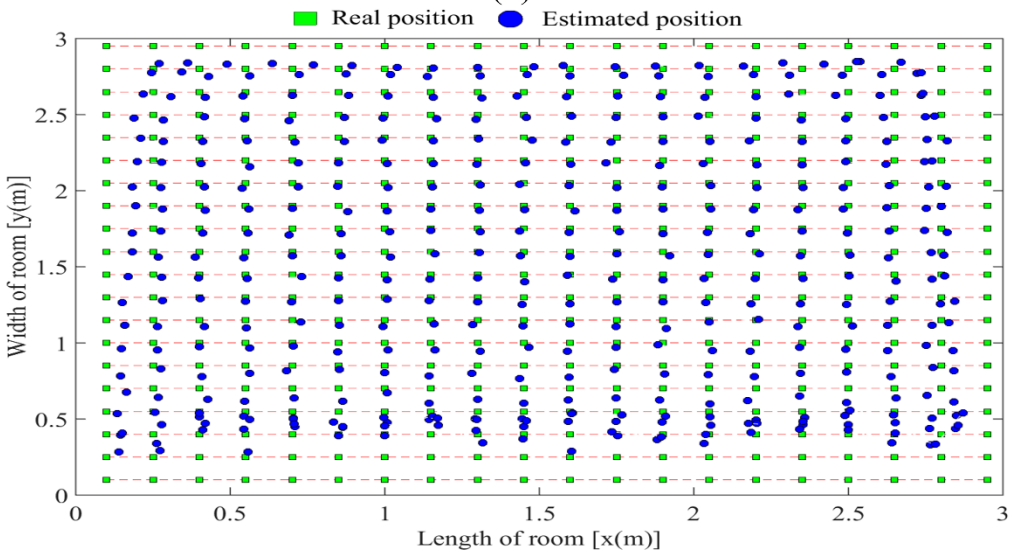


(c)

Fig. 4. 20 Estimated and real positions for the LOSNLOS scenario when the transmitters' positions (1 &2) are (0.25, 0.25) m & (2.75, 0.25) m and (a) SNR = 10 dB, (b) SNR = 15 dB, and (c) SNR = 20 dB.

Table 4. 5 Some statistical standards of the positioning error for the LOSNLOS scenario.

| Positions of transmitters | SNR (dB) | Max. value (cm) | Min. value (cm) | The mean (cm) | Standard deviation (cm) |
|---|---|---|---|---|---|
| $Tx_1$ (0.25, 0) $Tx_2$ (2.75, 0) | 0 | 158.503 | 6.261 | 86.938 | 31.607 |
| | 5 | 98.127 | 2.333 | 48.734 | 17.109 |
| | 10 | 65.883 | 3.174 | 23.509 | 10.752 |
| | 15 | 49.553 | 0.492 | 11.082 | 7.132 |
| | 20 | 43.243 | 1.068 | 6.335 | 5.014 |
| | 25 | 43.025 | 0.198 | 4.389 | 4.453 |
| | 30 | 44.160 | 0.752 | 3.670 | 4.358 |
| | 35 | 43.027 | 0.104 | 3.422 | 4.292 |
| | 40 | 43.237 | 0.182 | 3.377 | 4.282 |
| $Tx_1$ (0.25, 0.25) $Tx_2$ (2.75,0.25) | 0 | 161.533 | 4.503 | 93.127 | 36.703 |
| | 5 | 118.484 | 1.994 | 55.330 | 23.572 |
| | 10 | 82.399 | 1.643 | 28.629 | 16.672 |
| | 15 | 62.949 | 0.531 | 15.118 | 12.433 |
| | 20 | 44.760 | 2.100 | 10.227 | 9.763 |
| | 25 | 40.156 | 0.683 | 8.115 | 8.670 |
| | 30 | 40.499 | 1.256 | 7.149 | 7.799 |
| | 35 | 40.829 | 0.541 | 6.928 | 7.881 |
| | 40 | 40.918 | 1.095 | 6.820 | 7.737 |

# 4.5. Comparison with Previous Works

We have comparatively evaluated the proposed two-transmitters approach with the existing three-transmitters [46] one by studying their average errors as shown in Fig. 4.21 (a). It is observed that there is a small difference between the two transmitters and the three transmitters methods. Note that there are two different geometry setups for the three-transmitters system investigated here. The first setup (the green curve in Fig. 4.21(a)) uses four LEDs as illumination sources but two of these LEDs are also used in the two-transmitter system (the result is shown in the red curve of the Figure). Three of the LEDs are selected among four of them for localization. In the second setup we also use four LEDs but their positions are selected for the best illumination profile (i.e. the light intensity across the room is flat). The result obtained in this case is represented by the black curve.

We also note that the effect of the blind zone is small in the second scenario based on the best position (0.25, 0.25) and (0.25, 2.75) as shown in Fig. 4.21 (a) (red curve). The effect is in a small area underneath the two transmitters but in other areas of the room the positioning error is the same as shown in Fig. 4.21 (b). Fig. 4.21 (b) shows the estimated

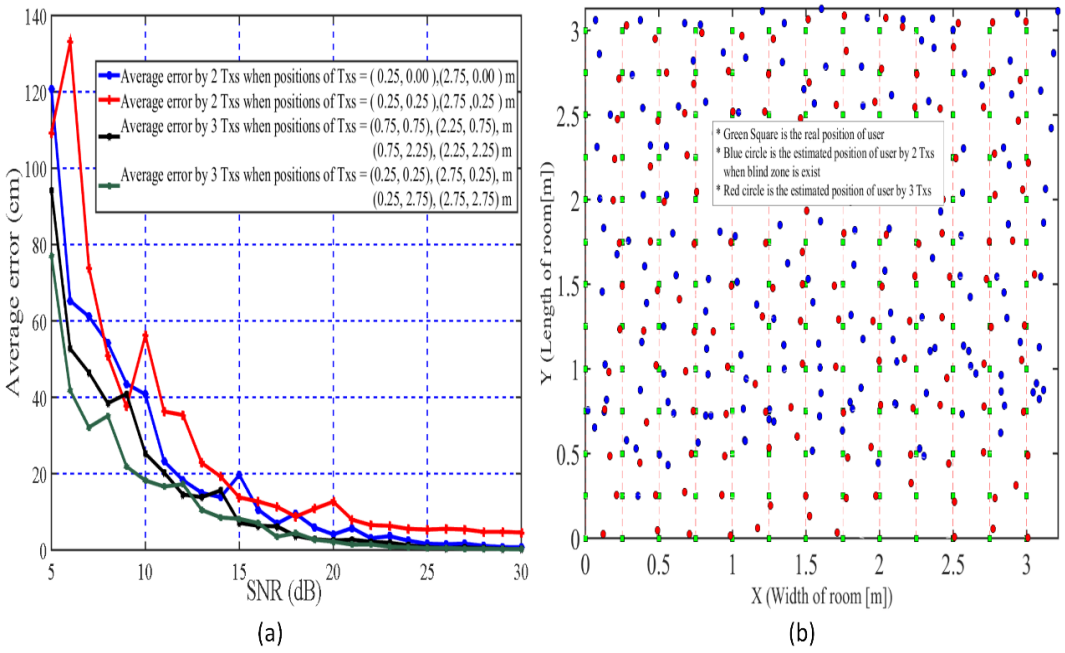


Fig. 4.21 (a) A comparison of the average error between the proposed positioning system using two transmitters (for two scenarios) and the positioning system using three transmitters (b) the distribution of the real position (green squares) and the estimated position for the positioning system using two transmitters (blue circles) and three transmitters (red circles). Note that there is no blue-dot in the blind zone in the two-transmitters case.

positions for both cases where the two transmitters are presented by blue circles, the three transmitters by red circles and the real position of the user by green squares.

# 4 .6. Summary

The proposed indoor 2D positioning was theoretically modelled and numerically evaluated. The investigation was based on the received optical power distributions as well as the RSSI technique using LED ceiling lamps as the transmitters. The approach used only two equations to estimate the user location (in a full 2D receiving plane) and its performance has been thoroughly explored. A comprehensive analysis of the angular error and the horizontal distance errors have been carried and verified through simulations. We have also investigated the balance of lighting distribution and its impact on the positioning performance as well as the optimised transmitted power. Statistical data have been obtained to carry out the evaluation. The study has also shown the power distributions map, distance estimation and position estimation with distance error in both the ideal and noisy conditions.

Note that this method does not require synchronization between the transmitters (LEDs) and the receiver. The simulation results of this system indicate that the device position estimation accuracy is acceptable. For LOS scenario, this positioning algorithm was able to determine the user position with an average error was between 9.1 and 21 of centimetres for the best position for scenario (1) whereas the average error was between 12.1 and 26.1 of centimetres for the best position for scenario (2) when the SNR is between 10 dB and 15 dB. For LOSNLOS scenario, the average error between 11 and 23.5 of centimetres for the best position for scenario (1) whereas the average error was between 15.1and 28.6 of centimetres for the best position for scenario (2) when the SNR is between 10 dB and 15 dB. The average error was much reduced when the SNR was increased.

Compared to a conventional three-transmitters scheme, the proposed system offers a simpler approach and can be readily applied to some cases. This offers a complementary method to existing trilateration to reduce the complexity when appropriate.

The next chapter will review information security and more details on cryptography. It will also investigate the impact of encryption on SISO VLC system performance with different cryptographic keys length for both LOS and LOSNLOS scenarios.

# Chapter Five

# Protection of VLC Systems

## 5.1. Introduction

The requirement of data security inside an organization has undergone two major changes in the recently time. Firstly, the need for automated tools for protecting information and other information stored on a computer became evident. Secondly, the need of network security measures are to protect information during transmission process. The process of security has six phases which can be detailed as follows:

1. **Identify your assets**: assets are the things or services that need protection such as computer hardware, financial data, and research activities etc.
2. **Analyse the risk of attack**: risks categorise anything that threaten the assets such as files damage in computers.
3. **Establish your security policy**: the security policy defines the protection needed to achieve the security goals and requirements. This policy works to balance the probability (the likelihood) of damage and assets.
4. **Implement your defences**: the previous phase establish the overall security policy needed. In this phase, this policy is implemented.
5. **Monitor your defences**: there are three famous operating systems (i.e. Windows, Linux, and Mac OS) that help monitor computer activities to collect full information and observe if the problem happens again.
6. **Recover from attacks**: if any attack occurred, a recovery process is carried out to assess the impact of the attack and to re-establish security defences.

There are three general properties of security, which are:

1. **Confidentiality:** the information must not be released to unauthorized persons.
2. **Integrity:** the information does not have to be modified during transmission to deliver it invalid.
3. **Availability**: the need to restore and use the information should be easy.

These properties are often referred to as the CIA properties and there exists security measures to maintain these properties. Confidentiality, integrity, availability, authentication and non-repudiation are security services which exist to preserve the CIA properties [42, 45, 164].

### 5.1.1. Threats to Information

In insecure channels, various individuals and/or organizations attempt to obtain the communicated information. In normal circumstances, the information (for example files) flow from the information source to the information destination as depicted in Fig. 5.1 (a). The other sub-figures show the following four classifications of attacks on communications networks:

- Interruption is any attack that causes a destruction of transmitted files or make such files unavailable. This type of attack targets the “availability”, which is one of the assets of the system as shown in Fig. 5.1 (b).
- Interception is any attack that is able to copy the transmitted files through an unauthorized user during the transmission process. This type of attack is on “confidentiality”, which is also an asset of the system as illustrated in Fig. 5.1 (c).
- Modification is any attack that is able to gain, modify and resend the transmitted files to an information destination by an unauthorized user. This attack targets the “integrity” asset of the system as depicted in Fig. 5.1 (d).

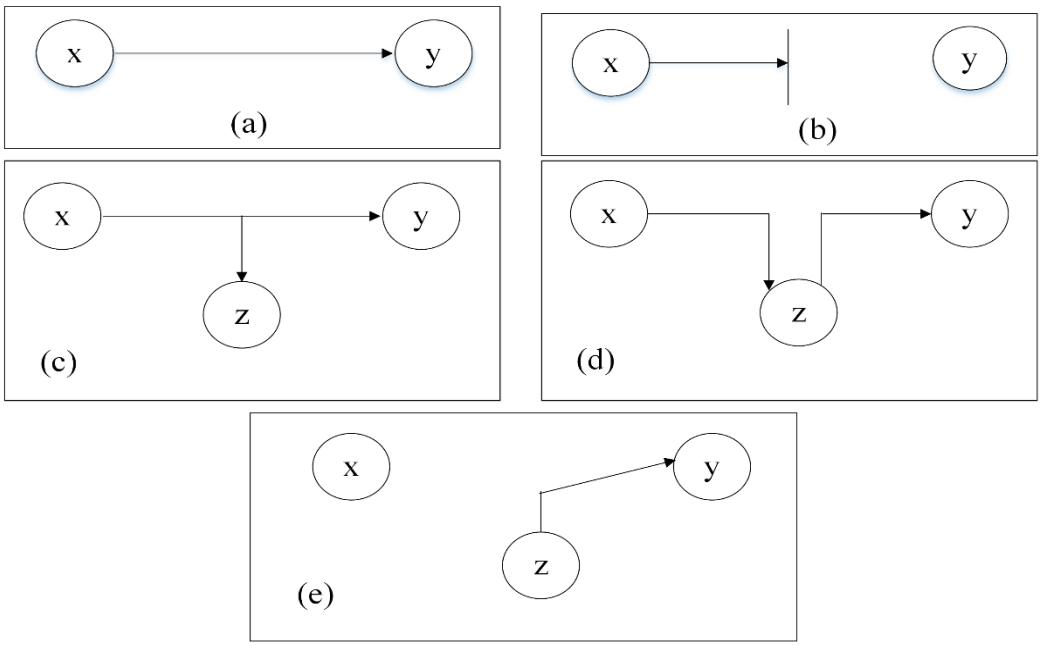


Fig.5.1 General classifications of attacks (a) Normal flow (b) Interruption (c) Interception (d) Modification (e) Fabrication. X represents an information source, y is an information destination and z is the attack entity.

- Fabrication is any attack that is able to generate files by an unauthorized user and send them to the information destination as legitimate transmission files. This attack targets the "authenticity" asset as illustrated in Fig. 5.1 (e).

However, another classification of types of security offenses is made in terms of the passive or active nature of the attacks. Passive attacks are divided into two types which are the relief of message fillings and traffic analyses. There is no alteration of the information as a result of passive attacks and as such, they are very difficult to detect. Active attacks on the other hand can be divided into four types of classifications: modification, replay, masquerade and denial of service [44, 45, 165].

## 5.1.2. Information Protection

There are numerous security products and policies that fit the needs of different security built on the requirements of the individual or the association. To achieve the security requirements, we need to address the requirements and approach the available security products and policies in a systematic way. For instance, for information security,

one must consider the security mechanism and the security service, whereas to provide the service, we often use one or more security mechanisms. To prevent loss of data availability or its recover, we can use authentication and encryption or some type of physical layer security.

We can protect the information using “access control”, which is defined as the ability to control any right of entry through communication links to limit access to operating systems and their applications and stop unauthorized use of a service. This control of each user access is achieved by identified or authenticated access rights.

On the other hand, there are often several security features that can be added to the software layer to protect the integrity and guarantee the privacy of data. Not all data can be safe as it is often available to public access or transmitted via email or web transactions and as a result, this data is susceptible to unauthorized access. Furthermore, data is sometimes susceptible to internal access as well. Cryptographic techniques are the most common methods to protect confidentiality of data from misuse by external or internal unauthorized users. The process of these techniques can convert the data into an unreadable format to be stored or transported. There are several security services but there is no single mechanism which can provide or implement all these services simultaneously. However, cryptography is one specific technique that motivates most of the security mechanisms in use. Encipherment or encryption is the most common mechanism to provide some of security services [43-45, 165-167].

## 5.2. A Review of Cryptography

Cryptology derives from two words of Greek: kryptós that means "hidden" and logos that means "by the word". Cryptology science is the knowledge which studies the security of information communication where every transmitter and receiver must be able to

transform plaintext into ciphertext using a secret key. Cryptology consists of two main parts which are cryptography part and cryptanalysis part.

Cryptography techniques offer the capability in that information can be hidden in ciphers and can only then be detected by the authorized users who have the valid secret key, thus making it impossible, very difficult or computationally infeasible for the message to be cracked by unauthorized recipients.

Furthermore, cryptanalysis also derives from two Greek words, namely, “kryptós” and analyein, which mean “to loosen” and “to untie” respectively. Cryptanalysis is the knowledge of studying methods and techniques that recover information from encryptions without any knowing of the secret key and the encryption details.

In cryptography, there are three main elements, namely, data encryption, data decryption and the key management unit as shown in Fig. 5.2. The encryption module (enciphering) includes the operations of converting the data stream into an unreadable form (i.e. cryptogram) to all except the intended recipient. At the receiver, the decryption module deciphers the encrypted message using the given which is akin to a password. It is the opposite of the encryption process or the unlock method of the locked message.

The key management system manages the generation, distribution, recognition and reception of the cryptographic keys, which is the most decisive element in any cryptographic system. The Encryption process uses a different system or algorithm to change the text of the original message (i.e.; plaintext) into an cryptogram form of the message (i.e.; ciphertext or enciphered). Cryptographic techniques (encrypted and decrypted keys as well as transition functions) equate individual letters in the original message using various keys, that are numbers or strings of characters. These cryptographic functions can be addressed as [43]:

The encryption process:

$$C_y = E_y(M_t, K_e) \tag{5. 1}$$

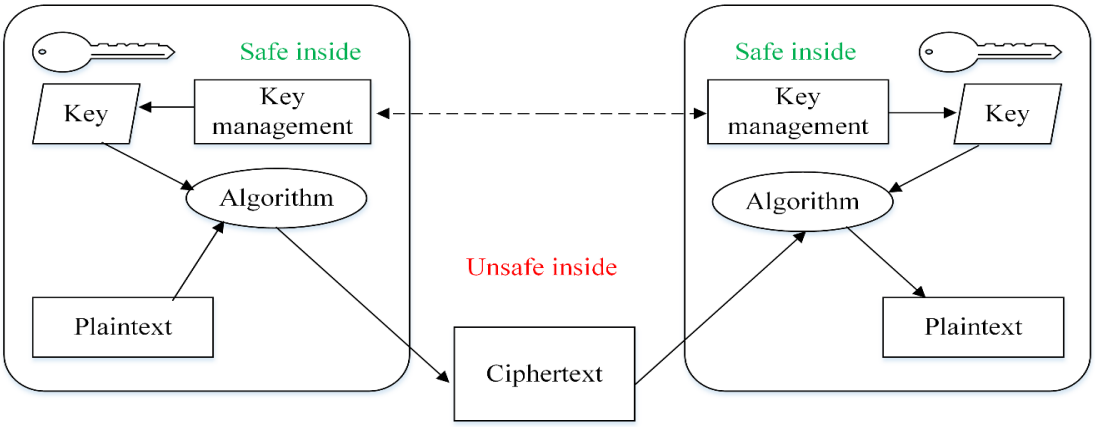


Fig.5.2 General cryptographic functions [37].

where $C_y$ is the cipher, ciphertext or unreadable text, $E_y$ is encryption algorithm that is based on the type of encryption key $K_e$ and $M_t$ is the transmitted message or plaintext.

The decryption process:

$$M_r = D_y(C_y, K_d) = D_y(E_y(M_t, K_e), K_d) \quad (5.2)$$

where that $M_r$ is the received message, $D_y$ is decryption algorithm that is based on the type of decryption key $K_d$. There are several goals of cryptography which cover the efforts to achieve a secure transmission channel and implement different aspects of confidentiality, data integrity, authentication and non-repudiation. At the same time, there are numerous methods to implement these goals such as physical protection, mathematical algorithms and the ability to prevent data manipulation by unauthorized users. The authenticated information delivered contains of origin, date of origin, transmitted data, time of sending… etc.[43, 45, 165-170].

## 5.2.1. Symmetric Ciphers

Symmetric ciphers are a format of cryptosystem in which use the same key to performed encryption and decryption processes. It is also known as single-key encryption or conventional encryption. Symmetric encryption converts the original message into encrypted text utilizing a single secret key and an encryption process in a transmitter side,

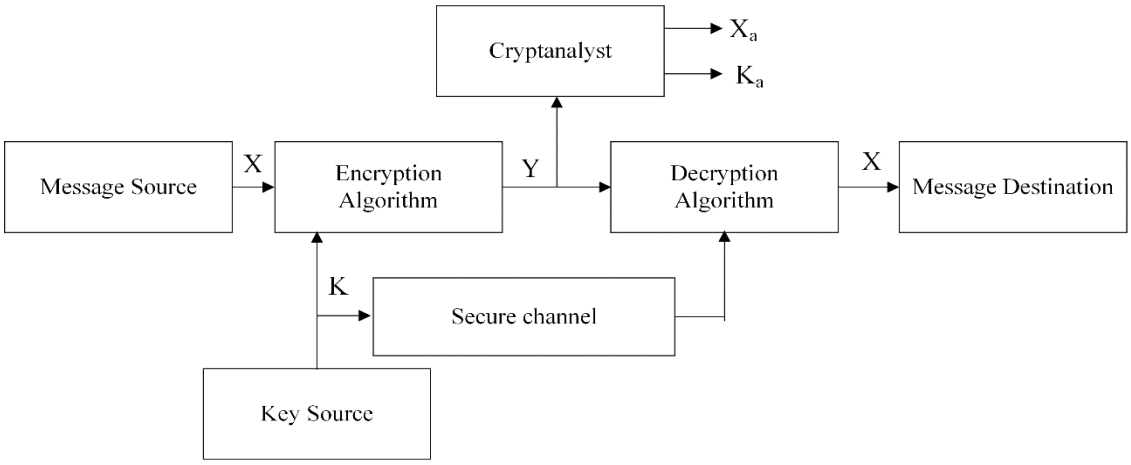


Fig.5. 3 Model of conventional cryptosystem.

whereas, the same single secret key and a decryption process use to recover the original data from the ciphertext in the receiver side. There are two types of attack on an encryption algorithm, thich are cryptanalysis science depending on the encryption algorithm possessions, and the second type is brute-force, that consists demanding all possible keys.

There are two necessities for the safe use of a traditional encryption: a robust encryption technique, as well as the providing of copies of the secret key to the transmitter and receiver using a secure method to distribute them. Fig. 5.3 shows the model of conventional cryptosystem [45, 164].

### 5.2.1.1 Substitution Techniques

In a substitution cipher algorithm, Each symbol in the original message is replaced for another different symbol in encrypted message. The receiver opposites the substitution process on the encrypted message to recover the original message. If theoriginal message is seen as a bits sequence, then the replacement process contains exchanging the bit patterns for plaintext with bit patterns for ciphertext. In traditional cryptography, the substitution ciphers have been divided into four types as follows:

- A simple substitution cipher, monoalphabetic cipher such as The Playfair.
- A homophonic substitution cipher.

- A polygram substitution cipher such as Hill cipher.
- A polyalphabetic substitution cipher such as Caesar cipher, Vernam cipher, one time key and a running-key cipher [45].

### 5.2.1.2. Transposition Techniques

In present, all the techniques observed contain the replacement of an encrypted text symbol for a symbol in the original message. A very various kind of mapping achieves using performing some types of permutation on the characters in the plaintext. This technique is known as a transposition cipher as well. In a pure transposition cipher, there are the same letter rates in plaintext and ciphertext as result, it is easily recognized. However, in columnar transposition, cryptanalysis science is obviously straightforward as well as it contains order out the ciphertext in a matrix and playing around utilizing the positions of letters in a column. Figure and trigram frequency tables can be suitable [45].

### 5.2.1.3. Product Ciphers

In the beings of manual cryptography, product ciphers were a convenient techniques for the cryptographer. In fact, double transposition ciphers on keyword-based matrices were vastly used. There were also fractionation systems that have been used as a particular class of product. In a fractionation system, a substitution is first made from characters in the original message to multiple different characters which are usually pairs in the ciphertext. In this case, it is known as a bilateral cipher, which is then super-encrypted using transposition techniques. The ADFGVX cipher is one of the most famous ciphers in fractionation systems. [43-45].

### 5.2.1.4. Block Ciphers

To the present, the most important encryption algorithm is the Data Encryption Standard (DES). A detailed study of DES gives an sympathetic of the basic used principles in the modern symmetric ciphers. The most used encryption schemes are based

on DES. The algorithm itself is also indicated to as the Data Encryption Algorithm (DEA). However, for DES, data is divided in 64-bit blocks and encrypted using a 56-bit key. The DES algorithm convert 64 bits from plaintext using series of steps into a 64-bit output as ciphertext. In transmitter side, the same steps and the same key are used in the decryption process. Triple DES uses three stages of the DES algorithm and uses two or three distinguished keys as well.

The most important outcome of this study is the approval of the Advanced Encryption Standard (AES). The designed symmetric encryption algorithm is to replace DES and triple DES and is likely to grow into the most Large-scale used symmetric encryption algorithm and RC4 as well [42, 164, 167, 169, 171].

## 5.2.2. Asymmetric Ciphers

In the entire cryptographic history, the public–key cryptography development is the greatest and possibly the only true revolution. Asymmetric cryptography is sometimes also pointed out as Public key cryptography. Public–key cryptography gives a radical dismissal from all that needed it. For one thing, public–key algorithms are depend on mathematical roles whereas traditional algorithms are based on permutation and substitution. Most importantly, public–key cryptography is including the use of two keys independently. In contrast to traditional encryption which uses only one key for encryption and decryption processes. The use of two keys has weighty results for authentication, confidentiality, and key distribution [45].

A cryptosystem involving a set of encryption transformations $E_e$ and a set of decryption transformations $D_d$. For each key pair [e, d], The encryption key e, and it is known as public key, that is made publicly available, whereas the decryption key d, called the private key, is kept secret. The cryptosystem must satisfy the property that it is computationally infeasible to calculate d from e. Public-key algorithms depend on one

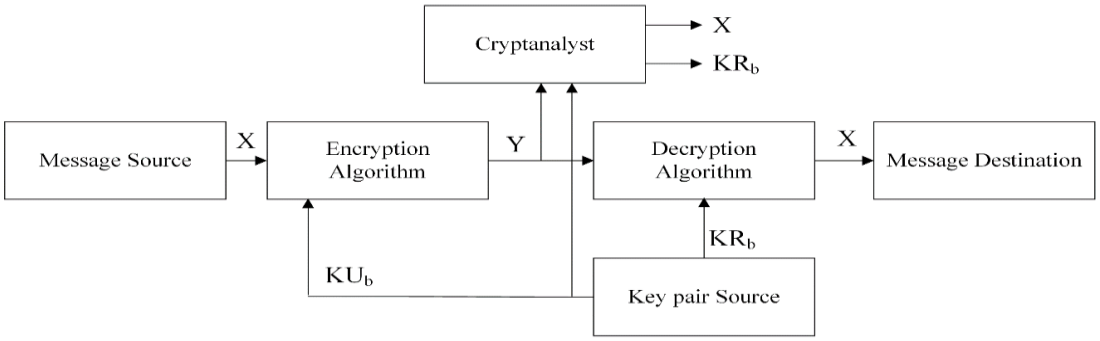


Fig.5. 4 Public-key cryptosystem to provide secrecy.

for enciphering and another different but related key for deciphering. These algorithms have some important characteristics as follows:

- It is computationally difficult to calculate the private key given only knowledge of the deciphering algorithm and the public key.
- Private key can be used for enciphering while public key can be used for decryption process.

Using the system in Fig. 5.4, we can provide confidentiality. The mesaage source produces a message in plaintext $X = (X_1, X_3, \ldots . X_M)$ whereas that $M$ elements of $X$ are letters with finite alphabet. The message is prepared for destination $B$. The destination $B$ generates a related pair of keys: a public key $KU_b$ and a private key $KR_b$. $KR_b$ is secret and known only to the distination $B$, whereas $KU_b$ is publicly available and therefore it is accessible by the source $A$. When the message $X$ and the encryption key $KU_b$ are inputs of the encryption algorithm, therefore, the outcome is the ciphertext $(Y_1, Y_2, \ldots \ldots, Y_N)$:

$$Y = E_{KU_b}(X) \tag{5. 3}$$

$$X = D_{KR_b}(Y) \tag{5. 4}$$

## 5.2.2.1. Applications for Public-Key Cryptosystems

One aspect of asymmetric cryptosystems worthy illumination is that asymmetric systems are distinguished by the use of algorithmic cryptographic type using two keys: One held private key and one obtainale publicly. Relying on the application, the

transmitter uses either the transmitter's private key or the receiver's public-key, or both to perform some type of the function of cryptography. In general terms, we can be able to classify the use of asymmtric cryptosystems into three classes:

- **Encryption and decryption:** the transmitter encrypts a message using the recipient's public key.
- **Digital signature:** the dispatcher "signs" a message using its private key. Signing is accomplished using an applied algorithm of cryptography to the message or to a small part of transmitted data which is a function of message.
- **Key exchange:** the sender and receiver participate to interchange a session key. there are possible several different approaches to achieve the exchange of private keys.

There are some asymmetric algorithms that are appropriate to achieve all three previous application [45, 168, 169]. There are two well-known public key algorithms: The RSA and the Elliptic curve cryptography (ECC). Though ECC is an emerging encryption algorithm.

## 5.2.2.2. The RSA Algorithm

RSA comes from the first character for each Rivest, Shamir and Adleman. It is an asymmetric cryptographic algorithm that does encryption and decryption using different key lengths. The use a long key for enhancing the security whereas a short key for to obtain the efficiency. The key of 512 bits for RSA algorithm is the most commonly used.

The block size of unencrypted data in RSA algorithm is variable and it must be smaller than the key length. The length of encrypted block will be the length of the key. The RSA algorithm is a block cipher in which the unencrypted data and ciphertext are integers between 0 and $n-1$ for some $n$. Where $n$ is 309 decimal digits or 1024 bits. The RSA algoritm makes use of an exponential expression. Data is encrypted in blocks, with each block having a value less than $n$. Where the block size must be less than or equal to $\log_2(n)$. Paractically, the block size is k bits ($2k < n \leq 2k+1$).

Both encryption and decryption processes need to know the value of $n$. The source knows the value of e and only the receiver knows the value of $d$. Thus, this an asymmetric encryption algorithm use a public-key of $KU = (e, n)$ and a private key of $KR = (d, n)$. For asymmetric encryption, the RSA algorithm is satisfactory.

#### 5.2.2.2.1. Key Generation Process

In RSA algorithm, public and private keys are created using mathematical steps as:

- Generate two large different prime numbers $p$ and $q$.
- Compute $n = p * q$.
- Calculate the Euler Totient Function: $f(n) = (p - 1)(q - 1)$.
- Select a random encryption key $e$, where $1 < e < f(n),\ gcd(e, f(n)) = 1$.
- Calculate the private exponent value for the decryption key $d$ such that;

  $d = (e - 1)\ mod\ (n)$.

Therefore, the private key consists of $(d, n)$ and the public key consists of $(e, n)$.

#### 5.2.2.2.2. Encryption/Decryption

The transmitted message $M_t$ $(0 \leq M_t < n)$ is encrypted by the public key at the sender by applying the following expression:

$$C = M^e (\text{mod}\ n) \tag{5. 5}$$

At the receiver, the original message will be recovered by [172]:

$$M = C^d \text{mod}\ n = (M^e)^d\ \text{mod}\ n = M^{ed}\ \text{mod}\ n \tag{5.6}$$

### 5.2.2.3. The Security of RSA

There three possible methodologies to attacking the RSA algorithm that can be smentioned as following:

1. Brute force: this includes trying all possibilities to find private keys.

2. Mathematical attacks: there several methodologies, all equivalent in effect to factoring the product of two primes.
3. Timing attacks: these rely on the running time of the decipher algorithm.

The protection of RSA algorithm from the brute force process is by a large keys as for other cryptosystems. Thus, more robust for the RSA algorithm against brute force is using the larger the number of bits in e and d. On the other side, there are huge calculations in encryption/decrytpion processes and key generation, that are more complex as a result, the system will be slower [172].

#### 5.2.2.3.1. The Factoring Problem

Recently, although the complexity has been reduced but the factoring is still a difficult problem for a large $n$. There are two threats of larger keys which are computing power and the continuing improvement of the factoring procedures. That the move to a various algorithm resulted in an incredible speedup have been seen recently. We can anticipate further improvements in the generalized number field sieve (GNFS), and the use of an even better algorithm. In fact, a related algorithm, the numbers can be factored using special number field sieve (SNFS) faster than the generalized number sieve with a specialized form considerably. For example, we need to be cautious in selecting a key length for RSA [43, 172, 173].

#### 5.2.2.3.2. Timing Attacks

Practically, The implementations of modular exponentiation do not include such excessive timing variations in which the enforcement time of a single iteration can be able to exceed the mean execution time of the full algorithm. Notwithstanding, there is enough divergence to make this timing attack practical. Though the timing attack is a dangerous threat, there are simple treatments against this threat which can be used as:

- Constant exponentiation time: we have to ensure that all exponentiation equation pick the same amount of time before returning a result. This is a simple resolve but it will degrade the performance of a system.
- Random delay: we can add a random delay to the exponentiation algorithm to achieve the best performance result to confuse the timing attack.
- Blinding: we can multiply a random number in the ciphertext before exponentiation process to prevent the attacker from knowing what ciphertext bits are being processed and therefore this prevents the bit-by-bit analysis of timing attack [45].

## 5.2.2.4. Advantages and Disadvantages of the RSA Technique

As mentioned earlier, the RSA algorithm is a public key technique. Therefore, it has the advantages and disadvantages of public key methods. In asymmetric encryption/ decryption, the public key is used to encrypt and it is different from the private key that is used to decrypt in the RSA encryption and decryption algorithms, respectively. The encryption key is available to the public, whereas the private key is kept secret by each individual person.

### 5.2.2.4.1. Advantages of Public-Key Cryptography

1. The private key must be kept a secret only, however, the authenticity of public key must be guaranteed.
2. Depending on the type of the use, we have ability able to unchanged the private and public keys for many sessions even several years.
3. The number of cryptographic keys may be smaller than in the traditional encryption scenario in a large networks.
4. There is no any restriction of shared secret keys between two users that need to contact with each other and therefore this is the idea behind asymmetric cryptography. The key which is shared between parties can be not used to communicate with another

party. In asymmetric encryption/decryption, Each party can be able to create a pair of keys where the public key is distributed to the other while the private key is kept. Each party is independent but the pair of keys created can be used to contact any other party.

5. The number of keys needed has been reduced extremely. In this system, for example, we need two million keys only for one million users, not half a billion as was the case in secret key encryption [173].

#### 5.2.2.4.2. Limitations of the RSA Method

The complexity problem is the most disadvantages of the public key technique. If the RSA technique is to be an effective method, we must have large prime numbers of $p$ and $q$. There are some of The RSA limitations as follows:

1. Speed of implementation: the process to convert the plaintext tociphertext using long keys takes long time. This is the main reason that public key encryption is not suitable for large text.
2. There must be the authentication for public key in RSA encryption: The sender must used a public key to encrypt the original message. Thus, the authenticated user can be participated in the encryption process.
3. Loss of private key threatens the security: private key is most important for RSA security in the decryption procedure that it is used to decrypt the original message. If one person who is unauthorized obtains on the private key, the whole RSA algorithm security is exposed.
4. Attacks on RSA: There are different attacks on the RSA cryptography, for example, the factorization problem, short message, common modulus, low decryption exponent, periodic attacks and so on. The security of RSA algorithm can breach using these types of attacks. To present, there is not proven to be unbreakable. The supercomputers are able to break this technique and have feature to work in a parallel

procedure. However, depending on the presumed difficulty of small set of numberic theoretic issues thus, the public key cryptography algorithms is still the most effective to protect the data [42, 43, 45, 167, 174].

### 5.2.2.5. Related Works

The RSA security depends on the large prime numbers but they are easily factorized and decomposed [175]. Ren and Miao have implemented a novel approach based on DES and RSA algorithms in Bluetooth Communication. That are using to encrypt transmitting data and the keys of DES, respectively [176]. In [175],a new approach RSA algorithm by Sonal Sharma et al, which uses modified Sum Cryptosystem based on subset sum of two numbers over RSA public key. In [177], Sami A. Nagar and Saad Alshamma have proposed the high speed implementation of RSA algorithm as well as they have modified keys exchange between Gateways using structured query language (SQL) server. B. Persis Urbana Ivy et al. have used 'n' number to generate public and private keys. That are not easily decomposed or factorized to getting high security and efficiency through a network [178].

# 5.3. Impact of Protection on the VLC Systems

## 5.3.1. VLC System Simulation Setup

The VLC system shown in Fig. 5.5 is adopted for a standard room of size 5×5×3 $m^3$ (width, length, height) where there are four transmitters with each transmitter consisting of several LEDs to provide good room illumination coverage. The receiver plane is 0.75m above the floor. The data signal is generated using a pseudo random bit stream (PRBS) of the length $(2^{10} - 1)$. The data is encrypted using the RSA technique which will be detailed in the next subsection. The transmitted data is modulated using OOK modulation via the SISO-TDM scheme. The IM/DD technique is employed to generate the transmission signal after it has been up-sampled by 10 times. The signal is convoluted

with the impulse response of the LED, which possesses the same impulse response as that discussed in (3.29) and Fig. 3.8 (a), Chapter 3. Here, in the encrypted VLC system, we have used the measured impulse response of OSRAM with LED, which has a raw bandwidth of 2.5 MHz (see Fig. 3.8 (a)). Here, we consider two scenarios to modulate the VLC channel: LOS scenario and LOSNLOS scenario. These are also detailed in subsections 3.4.1 and 3.4.2. of Chapter 3. The noise in the proposed VLC system is considered as AWGN due to ambient light sources, thermal noise and shot noise. The system is numerically simulated using MATLAB.

### 5.3.2. Proposed VLC Scheme with Encryption and Decryption

Without loss of generality, it is assumed that the public and private keys are provided at the transmitter and receiver (i.e. during the initialization session connections or presetting). Fig. 5.6 illustrates the system block diagram of the RSA algorithm adopted in the VLC system shown in Fig. 5.5 The binary stream (data) is converted into $k$-bit parallel blocks ($k = 8, 16, 32$), where $k$ is chosen to be of the same or a longer length as the key. These blocks are then converted into decimal values and encrypted by the pre-defined public key as described in (5.11). The encrypted data is passed through a parallel-to-serial converter with an output in OOK-NRZ format which is used to intensity-modulate the LED. At the receiver end, following optical detection, the reverse process of transmitter is implemented to recover the original data signal. The private key is employed for decryption as described in (5.12).

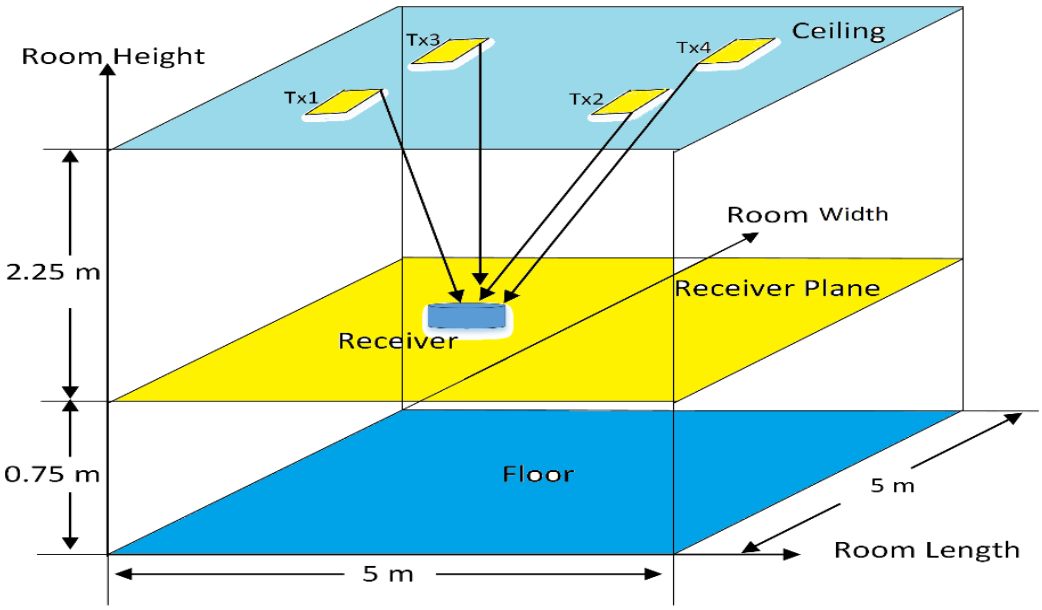


Fig.5. 5 A typical indoor VLC system environment.

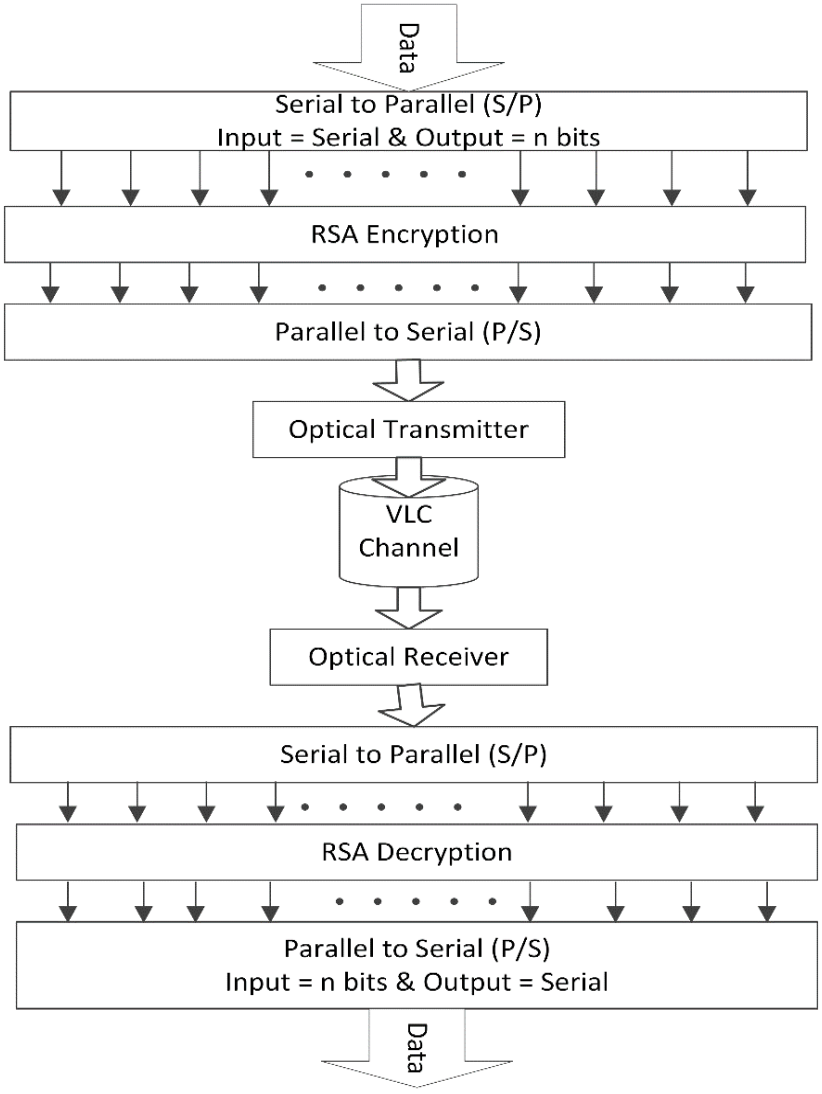


Fig.5. 6 Block diagram of RSA applied in a VLC system.

# 5.4. Results and Performance Evaluation

The secure VLC system is simulated using MATLAB to determine the impact of security implementation on the LED-based VLC system. The key simulation parameters are presented in Table 5.1. The key system performance indicators to investigate are the BER and the power penalty. The VLC model is based on the equations from (3.29) to (3.36) whereas the data encryption layer is implemented following the steps formulated in (5.6) to (5.12). In this chapter, the maximum encryption key length used for simulations is limited to several bits. This is due to the constraints of computational power of PC and the simulator. However, the same procedure can be adopted for longer key lengths as in practical applications. Furthermore, we have kept the ratio between input and output data to and from the RSA encryption block the same (see Fig. 5.6) (i.e.; the number of input bits is equal to the number of output bits). In other words, there is no extra data due to protection. For instance, if the input data in each block is 16 bits, then the output data from encryption is also 16 bits. However, the simulation results obtained are still valid for predicting the impact of encryption on VLC communications.

Table 5. 1 The simulation parameters of the secure VLC system

| Parameters | Values |
|---|---|
| Room size: Length, (X), Width, (Y), Height (Z) | 5m × 5m × 3m |
| Receive Plane above the floor | 0.75 m |
| LED half power angle $\phi_{1/2}$ | 70 deg. |
| Wall reflection coefficient $\rho$ | 0.7 |
| Number of reflections | 1 |
| Reflective area of wall $dA_{wall}$ | 0.02 $m^2$ |
| Transmitter coordinates (4 arrays of LEDs) | (1.25, 1.25) (3.75, 1.25)<br>(1.25, 3.75) (3.75, 3.75) |
| Transmitted data rate $R_B$ | 1 Mbps - 12 Mbps |
| Concentration lens refractive index at PD $n$ | 1.5 |
| Optical filter gain $T_s(\psi)$ | 1 |
| PIN detector FOV | 60 deg. |
| Active area ($A_R$) of receiver | $50\times10^{-6}$ $m^2$ |
| Transmit optical power $P_{tx}$ | 10 W |
| Data format | NRZ-OOK |
| LPF cut-off frequency | $R_B$ |
| Key length | 8 and 16 bits |
| Data block | 8 and 16 bits |

In these simulations, we transmit over one million bits over the channel and assume perfect synchronization between the transmitter and receiver. At the receiver end, following the capture of all transmitted bits, we have converted these bits into $k$-bit-parallel (8-bits, 16-bits or ……), we have called encrypted block or encrypted frame. These are the data patterns which are compared with the transmitted bits. For detection, we sample every bit at its centre and compare the sampled value with a threshold level set to half the mean signal amplitude. As only one million bits are sent with every iteration of the simulation, we know exactly where the encrypted code begins and ends, hence, there is no need for a preamble header and footer bits to be inserted into the code. However, in real practical applications, both pre- and post-ambles are required.

The subsequent figures represent the simulated BER performance against the received SNR for the VLC system with and without encryption. In Fig. 5.7 (a), the data rate is 2 Mbps which is well within the 3-dB bandwidth of LED (approx. 3 MHz). At a BER of $10^{-3}$, for the LOS scenario, power penalties $\Delta P$ of 1.05 dB and 1.64 dB are obtained compared to the back-to-back cases for encryption block lengths of 8 bits and 16 bits, respectively. On the other hand, for the LOSNLOS scenario, power penalties $\Delta P$ of 1.10 dB and 1.61 dB are recorded for encryption block lengths of 8 bits and 16 bits respectively. The power penalties are due to the block errors occurring in the encrypted VLC system rather than individual bit error in an unsecured VLC system. In secured VLCs, when an error occurs, the receiver cannot decrypt the whole block thus resulting in a block error. However, at lower data rates, the power penalties induced are much smaller i.e. < 1 dB.

In Fig. 5.7 (b), the data rate is 6 Mbps, which is much higher than the LED 3-dB modulation bandwidth. This test provides a good view of the excess power penalty due to "block error". For the same BER performance, the system requires slightly higher SNR (e.g. additional ~3 dB at a BER of $10^{-3}$). The power penalties for the LOS scenario have slightly increased to 1.21 dB and 1.68 dB for 8 bits and 16 bits of encryption block lengths

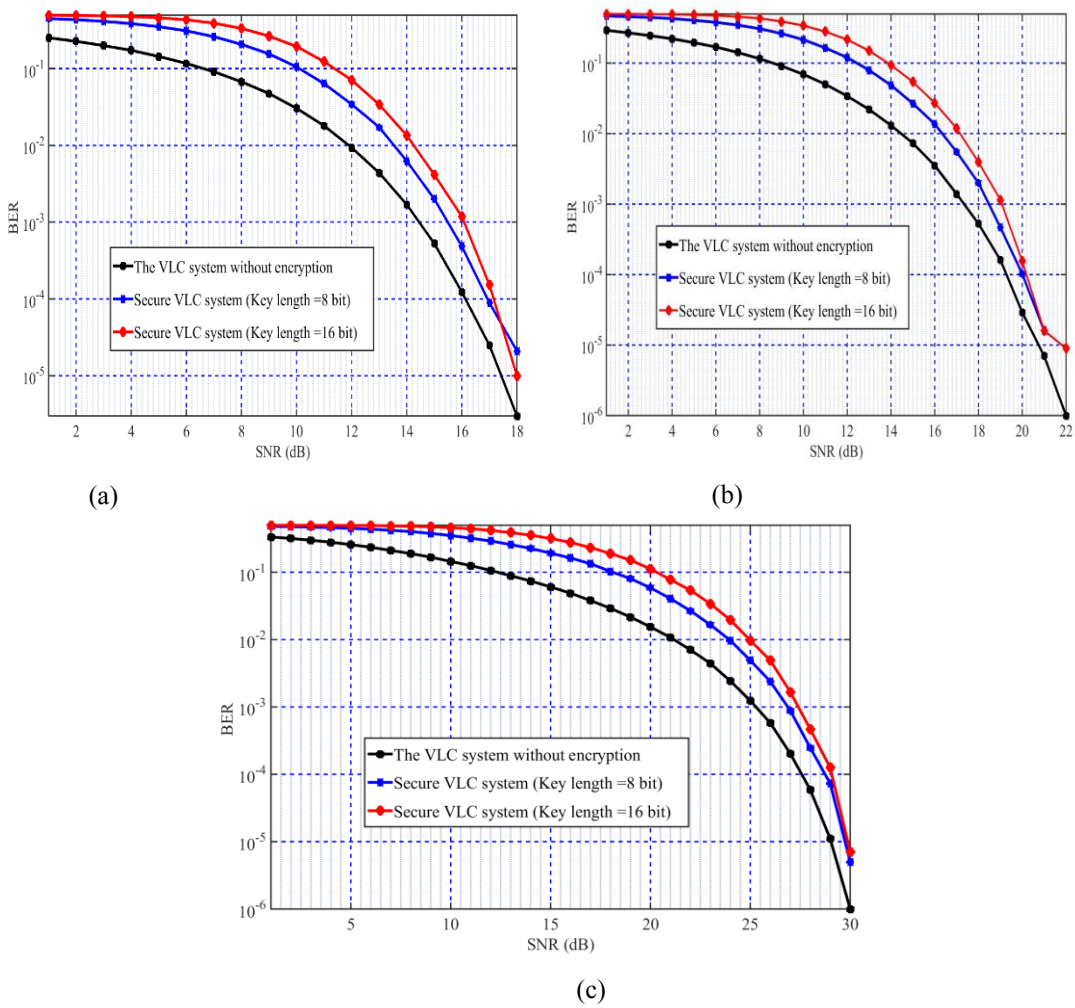


Fig.5. 7 BER vs. SNR of the received light beam for the back-to-back VLC and encrypted links at: (a) 2 Mbps, (b) 6 Mbps and (c) 10 Mbps when the receiver's position is in the middle of the room.

respectively, whereas for the LOSNLOS scenario, the penalties have also slightly increased to 1.42 dB and 2.13 dB for 8 bits and 16 bits, respectively.

In Fig.5.7 (c), the data rate is 10 Mbps and one can see that for the same BER performance, the system requires much higher SNR (i.e.; additional ~ 11 dB at a BER of $10^{-3}$). The power penalties for the LOS scenario have significantly increased to 1.68 dB and 2.12 dB for 8 bits and 16 bits of encryption block lengths respectively whereas for the LOSNLOS scenario, the power penalties also show significant increases to 1.79 dB and 3.15 dB for 8 bits and 16 bits, respectively.

We have further investigated the evaluation of the proposed VLC system with and without encryption when the position of the receiver is at the corner. The first set of analysis examines

the impact of the LOS and LOSNLOS on the BER performance. We have compared the results from the LOS scenario and the LOSNLOS scenario for four channels. We can note that the BER performance against SNR is different from one channel to another based on the distance between the transmitter and the receiver in the previous proposed model as shown in Fig. 5.8 and Fig. 5.9. In Fig. 5.8, when the data rate is 2 Mbps, the block length is 8 bits and the distance is shortest (between $Tx_1$ and Rx), the power penalty is approximately 1.5 dB for the LOS and the LOSNLOS scenarios and is 1 dB for the secure and unsecure VLC system as shown in Fig. 5.8 (a) for the same BER performance. In Fig. 5.8 (b) and (c), when the distance is slightly longer between Tx2 , Tx3 and Rx, the power penalty is around 1.2 dB for the secure and unsecure system but it is higher for the LOS and the LOSNLOS scenarios (around 2.75 dB at BER of $10^{-3}$). However, in Fig. 5.9 (d), the distance is much longer between Tx4 and Rx and the power penalty is 1.2 dB between the cases of with and without encryption for the LOS scenario whereas it is 1.7 dB for the LOSNLOS scenario. Furthermore, the power penalty is more than 5 dB between the LOS and the LOSNLOS scenarios.

In Fig. 5.9, when the data rate is 2 Mbps and the block length is 16 bits, there is clearly an increase in power penalty compared to 8 bits. Firstly, in Fig. 5.9 (a), when the distance is short (between Tx [1] and Rx), the power penalty is approximately 1.6 dB between the secure and unsecure cases for the LOS and the LOSNLOS scenarios, whereas it is 1.4 dB between the LOS and the LOSNLOS scenarios for secure or unsecure VLC system. Secondly, in Fig. 5.9 (b) and (c), the power penalty is around 1.6 dB between the secure and unsecure cases for the LOS scenario but it is around 2 dB for the LOSNLOS scenario. However, the power penalty is 2.7 dB between the LOS and the LOSNLOS scenarios in the absence of encryption and it is 3 dB in the presence of encryption. Finally, in Fig. 5.9 (d), the power penalty is 1.5 dB between the secure and unsecure cases for the LOS scenario whereas it is 2.7 dB for the LOSNLOS scenario. We also note from the same figure that power penalty increases

significantly between the LOS scenario and the LOSNLOS scenario. It is 4.7 dB and 5.9 dB for an unsecured and a secured VLC system respectively.

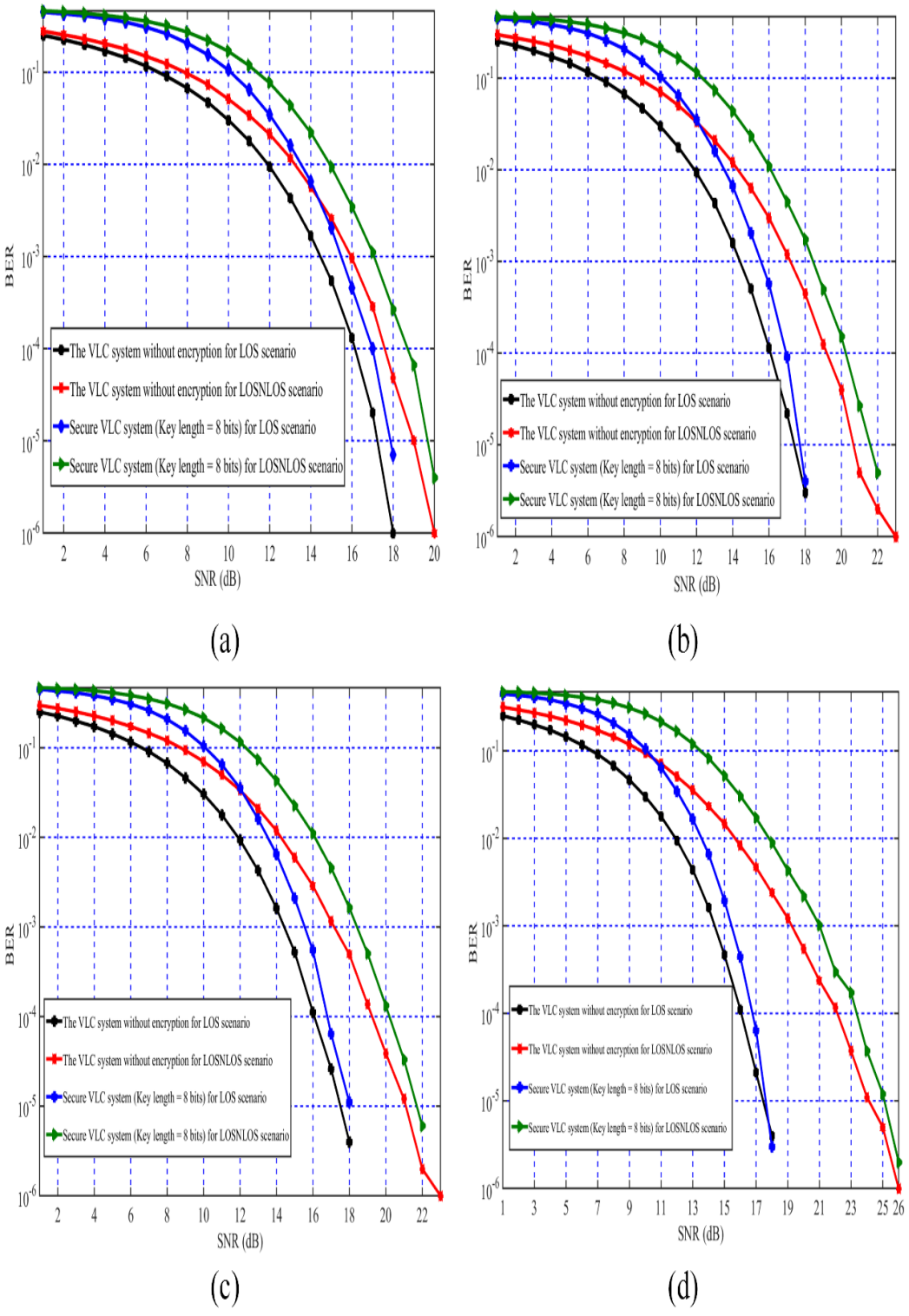


Fig.5. 8 Performance of BER against SNR of unsecure VLC system and secure VLC system with block length = 8 bits for (a) Channel [1] (b) Channel [2] (c) Channel [3] (d) Channel [4] for considering LOS scenario and LOSNLOS scenario when the Rx is in the corner of the room and data rate is 2 Mbps.

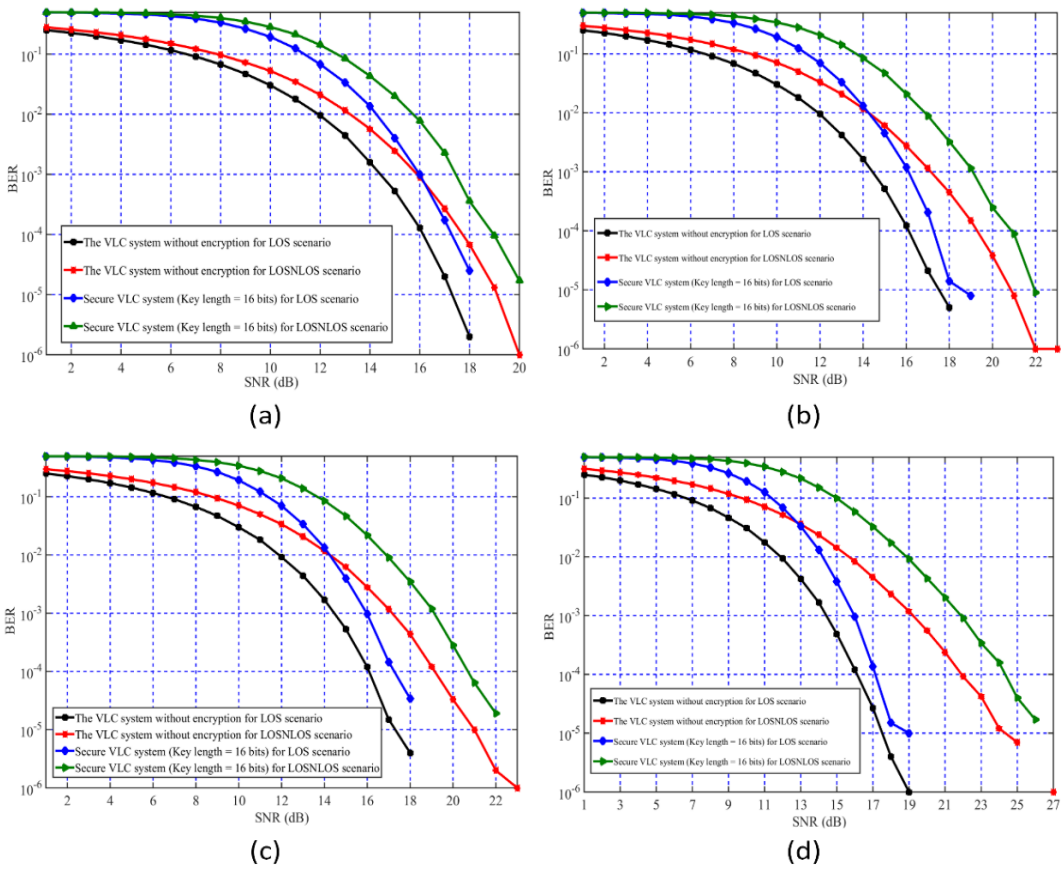


Fig.5. 9 The performance of BER against SNR for unsecure VLC system and secure VLC system when block length = 16 bits for (a) Channel [1] (b) Channel [2] (c) Channel [3] (d) Channel [4] when considering LOS and LOSNLOS scenarios, the Rx is in the corner of the room and data rate is 2 Mbps.

Figure 5.10 illustrates the power penalty against the data rate for 8 and 16 bits encryption block lengths at a BER of $10^{-3}$ for the LOS and LOSNLOS scenarios. Firstly, we consider the LOS scenario when the position of the receiver is in the middle of the room. For the 8-bit case (see Fig. 5.10, red curve), the power penalty is approximately 1 dB for data rates up to 7 Mbps increasing to over 1.5 dB at a data rate of 10 Mbps. For the 16-bit case (see Fig. 5.10, blue curve), the power penalty profile is similar to the 8-bit case but it is on average higher by 1.5-2.0 dB. Secondly, we consider the LOSNLOS scenario when the position of receiver is at the corner of the room. For the 8 bit encryption block (Fig. 5.10, green curve), the power penalty is between 1 dB and 1.5 dB for data rates up to 7 Mbps whereas it is increases to over 3 dB at 9 Mbps. On the other hand, for the 16 bit encryption block case (Fig. 5.10, black

curve), the power penalty is between 1.5 and 2 dB for data rates up to 6 Mbps, increasing to around 4 dB at for data rates of 9 Mbps.

Though the performance of a secured VLC system is heavily dependent on the encryption block lengths, it is noted that the redundancy is relatively small. As the encryption block length increases the redundancy is further minimized.

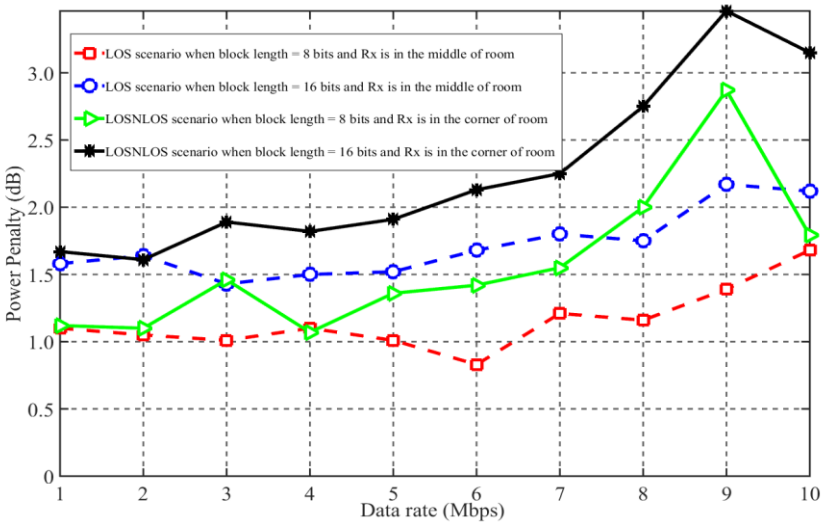


Fig.5. 10 Power penalty vs. the data rate for the LOS scenario of secure VLC system when the receiver's position is the middle of the room and the block lengths are 8 bits (red curve) and 16 bits (blue curve) as well as for LOSNLOS scenario when the receiver's position is the corner of the room and the block lengths are 8 bits (green curve) and 16 bits (black curve).

# 5.5. Summary

This chapter has fast reviewed information security with different techniques. We focused on cryptography and its techniques which were divided into symmetric and asymmetric ciphers. Furthermore, we also studied in detail the RSA technique.

The chapter has also investigated the VLC system performance with and without encryption in the MAC layer and physical layer for both the LOS and LOSNLOS scenarios. The results showed that the block error severely affects the system BER performance especially for the 16-bit encryption key length. The proposed secured VLC system requires more SNR to obtain the same BER performance. The power penalties observed ranged from 1 dB to 1.7 dB for the 8-bit encryption block length and 1.6 dB to 2.7 for the 16-bit encryption

block lengths and for different distances between Txs and Rx within the 3 dB LED bandwidth. We have also investigated the BER performance against SNR with different data rates for unsecured and secured VLC system. Overall, these results highlight the presence of power penalties between ~ 1 dB and ~3.5 dB for data rate from 1 Mbps to 10 Mbps, respectively, for both LOS and LOSNLOS scenarios.

Though the selected key lengths in this chapter were small mainly due to the limitation of the computer and the simulator computational powers, the results have generically indicated the trend of trading-off and error propagation as well as showing the minimum bandwidth loss of the secured VLC system.

The next chapter will discuss the design of a novel secure MIMO VLC system based on the position of the user and the RSA encryption in MAC layer with different key lengths and more ability to control the size of the encrypted VLC cell based on the user environment.

# Chapter Six

# Secure MIMO-VLC System

## 6.1. Introduction

The high data rates can readily be exploited to create optical MIMO communication systems. MIMO-VLC systems have thus become an attractive approach for increasing the channel capacity, particularly in an indoor environment. Such systems have already been demonstrated to achieve Gbps data rates and been reported in [66, 84, 85]. However, security in wireless telecommunication systems is a common concern, especially in MIMO VLC systems. What is known about security is largely based upon empirical studies that investigate how to implement the techniques to achieve a required purpose. RSA is more widely used in many security systems and still guarantees security of the system if the key length is long enough. [44, 45]. Several studies investigating RSA algorithm have been carried out on an improvement of security and overcome on the limitation in RSA method such as speed, computational cost, loss of private key sometimes result break the security and some types of attacks for example factorization problem or short message. Some of these studies have been mentioned in Chapter 5. Consequently, in this work, we have opted to adopt the RSA technique as outlined in subsequent sections.

Indeed and at the present time of writing, there are only a few number of researches that studied security in VLC systems as mentioned earlier in Chapter 5. Therefore, the main objectives of this chapter are three fold and can be summarized as follows: ($i$) development of a mathematical modell of positioning in non-imaging MIMO-VLC systems, ($ii$) design of novel secure MIMO-VLC system based on user's location and encryption without

affecting the efficiency in both ideal and real scenarios and ($iii$) deployment of RSA encryption at the MAC layer with no overhead data and with the ability to control the size of the encrypted VLC cells based on the user environment.

# 6.2. Positioning in MIMO VLC System

We have used the RSSI technique of indoor positioning using three transmitters with the trilateration method. The method recovers the channel characteristics from the incident light and estimates the receiver location by analytically solving the Lambertian equations.

## 6.2.1. Mathematical Modelling of Positioning Algorithm

The following algorithm calculates the path loss as a result of attenuation. From equations (2.36) and (3.33), which is a basic equation, one can calculate the power distribution in a VLC environment for any location inside a room. The received optical power at a distance $L$ utilizing (6.1) with the assumption of $\psi_{Lij} = \theta_{Lij}$ can be expressed as:

$$P_{\mathrm{PD},L_j}\left(\theta_{L_{ij}}, \psi_{L_{ij}}\right) = P_{\mathrm{tx}}.\frac{(m+1)}{2\pi {L_{ij}}^2}\,.\cos^m(\theta_{L_{ij}}).T_s\left(\psi_{L_{ij}}\right).g_s\left(\psi_{L_{ij}}\right).\cos\left(\psi_{L_{ij}}\right), \quad (6.\ 1)$$

Thus, the received optical power underneath the transmitter, i.e. at a distance $h$ as shown in Fig. 6.1. ( $\psi_{L_{ij}} = \theta_{L_{ij}} = 0$), is given as:

$$P_{\mathrm{PD},L_j}(0,0) = P_{\mathrm{tx}i}\,\frac{(m+1)}{2\pi h_j^2}\,. \quad (6.\ 2)$$

From equations (6.1) and (6.2), assuming $T_s(\psi).g_s(\psi) = 1$, (meaning that we do not have any attenuation or amplification for the received optical signal from these stages because of the employed positioning VLC technique here is RSSI technique which is depended on the received power level as well as $L_{ij} = {}^{h}/_{\cos\theta_{Lij}}$). Therefore, the mathematical model of RSSI technique can be written as:

$$P_{\mathrm{PD},Lij}(\theta_{Li}) = P_{\mathrm{PD},hij}(0).\cos^{m+\gamma+1}\left(\theta_{Lij}\right) \quad (6.\ 3)$$

where $i = j = 1,2,3\ or\ 4$ represents the number of transmitter and photodetectors in the room and $\gamma = 2$ is a path-loss exponent correction factor [31, 48, 93].

### 6.2.1.1. Horizontal Distance Estimation

From equation (6.3) we can measure the angle of irradiance $\left(\theta_{L_{ij}}\right)$ using measurements of the received power at a distance $h$ ($P_{\mathrm{PD,h}}(0)$) and store it at receiver which uses it along with the received power at distance $L_{ij}$ for all positions in the room. The final step calculates the horizontal distance estimation using simple trigonometry [48]:

$$d_{L_{ij}} = h.\tan\theta_{L_{ij}} \tag{6. 4}$$

### 6.2.1.2. Trilateration Method

The process of locating absolute or relative locations of targets by measuring the distances using the geometry of circles is shown in Fig. 6.2. As the figure illustrates, there are four power levels to be measured at the receiver. However, the receiver will select only the three maximum power levels that will be used in the positioning algorithm in order to determine the location of the user. So, we can use the RSSI algorithm to calculate $\theta_{Lij}$ (i.e., $\theta_{L1\mathrm{j}}$, $\theta_{L2\mathrm{j}}$ and $\theta_{L3\mathrm{j}}$) and then calculate $d_{L1\mathrm{j}}, d_{L2\mathrm{j}}$ and $d_{L3\mathrm{j}}$ using (6.3) and (6.4) respectively. Now, the trilateration method can be used to determine the position of user by obtaining the intersection point from the three following equations:

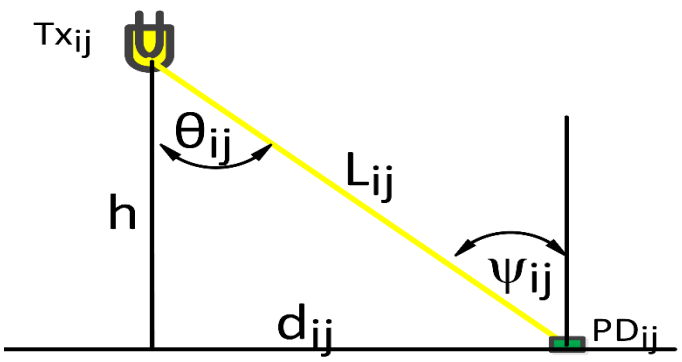


Fig. 6. 1 side view of 1-D indoor MIMOVLC system

$$\begin{cases} (x_{\mathrm{PD}_j} - x_{\mathrm{tx}_1})^2 + (y_{\mathrm{PD}_j} - y_{\mathrm{tx}_1})^2 = d_{L_{1j}}^2 \\ (x_{\mathrm{PD}_j} - x_{\mathrm{tx}_2})^2 + (y_{\mathrm{PD}_j} - y_{\mathrm{tx}_2})^2 = d_{L_{2j}}^2 \\ (x_{\mathrm{PD}_j} - x_{\mathrm{tx}_3})^2 + (y_{\mathrm{PD}_j} - y_{\mathrm{tx}_3})^2 = d_{L_{3j}}^2 \end{cases} \quad (6.5)$$

where $d_{L_{1j}}, d_{L_{2j}}$ and $d_{L_{3j}}$ are the horizontal distances between the transmitters and receivers and $(x_{\mathrm{tx}_1}, y_{\mathrm{tx}_1})$,$(x_{\mathrm{tx}_2}, y_{tx_2})$ and $(x_{\mathrm{tx}_3}, y_{\mathrm{tx}_3})$ are position coordinates of the transmitters; while $(x_{\mathrm{PD}_j}, y_{\mathrm{PD}_j})$ is the coordinates of the photodetector in the receiver array [110].

## 6.2.2. Centre of Receiver Calculations

The receiver array has two different designs based on the directional order of photodetectors as shown in Fig. 6.3. There are two configurations for designing the receiver array: $(i)$ anticlockwise configuration $(ii)$ clockwise configuration. If the coordinates of each of photodetector 1 $(x_{\mathrm{PD1}}, y_{\mathrm{PD1}})$ and photodetector 2 $(x_{\mathrm{PD2}}, y_{\mathrm{PD2}})$ are known, we can calculate the coordinates of both photodetectors 3 and 4 (in an anticlockwise configuration) from the following expressions:

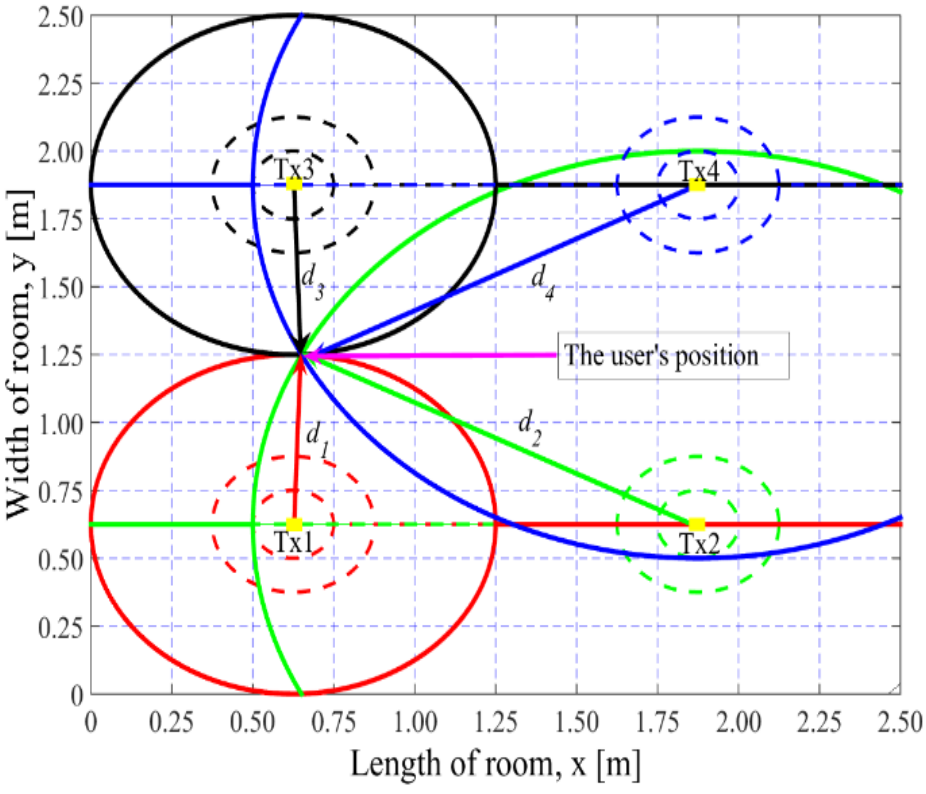


Fig. 6. 2 top view of 2-D system for positioning system using trilateration method

$$x_{\mathrm{PD3}} = x_{\mathrm{PD2}} \quad \text{and} \quad y_{\mathrm{PD3}} = y_{\mathrm{PD2}} + \Delta y \tag{6. 6}$$

$$x_{\mathrm{PD4}} = x_{\mathrm{PD1}} \quad \text{and} \quad y_{\mathrm{PD4}} = y_{\mathrm{PD1}} + \Delta y \tag{6. 7}$$

Note that in this proposed system, the requirement is to calculate the coordinates of the centre of the receiver (CORA) and not the coordinates of each photodetector in the receiver array. The estimation of the coordinates of CORA can be calculated using the following equations to reduce the positioning error:

$$x_{\mathrm{CORA}} = \frac{1}{N}\sum_{j=1}^{N}\left(x_{\mathrm{PDj}} + \begin{cases} \frac{\Delta x}{2} & \text{if } j = 1,4 \\ -\frac{\Delta x}{2} & \text{if } j = 2,3 \end{cases}\right) \tag{6. 8}$$

$$y_{\mathrm{CORA}} = \frac{1}{N}\sum_{j=1}^{N}\left(y_{\mathrm{PDj}} + \begin{cases} \frac{\Delta y}{2} & \text{if } j = 1,2 \\ -\frac{\Delta y}{2} & \text{if } j = 3,4 \end{cases}\right) \tag{6. 9}$$

# 6.3. Secure VLC-MIMO System Description

The security task in wireless communications has become a matter of concern due to the possibility of unauthorised access to transmitted data. This stems from the fact that all users use the same channel. However, in a VLC system, this issue is less pronounced because of the inability of light to through the walls. Recently, several types of researches have been proposed on security at the physical layer to encrypt the user's data [179, 180]. A typical MIMO-VLC system is designed to broadcast signals and hence any user in the VLC cell

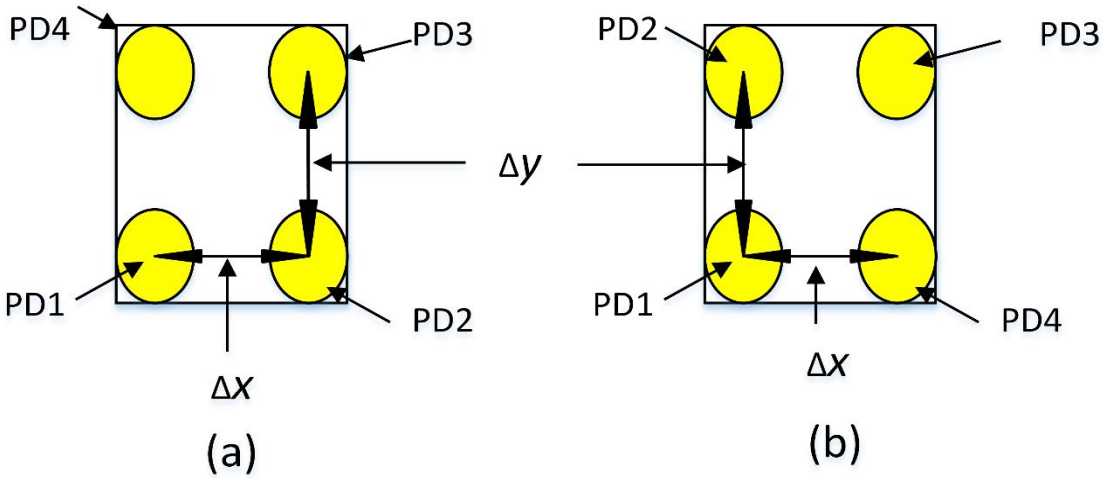


Fig. 6. 3 the receiver array (a) anticlockwise configuration (b) clockwise configuration.

range can receive the transmitted data inside the illumination coverage area. This communication system does not have a secured transmission link for each user.

### 6.3.1. Block Diagram of the Proposed Secure System

Figure 6.4 shows the block diagram of the proposed end-to-end secure MIMO-VLC system. It consists of a transmitter and a receiver, as well as 4 × 4 MIMO-VLC channels acting as the downlink and an RF or IR channel acting as the uplink due to the VLC system not possessing an uplink. This still presents the biggest challenge in VLC systems, and as such an RF/IR uplink was adopted. At the transmitter side, there is a coordinator that has the location codes of the transmitters' positions. We have considered two cases when (*i*) the user is new, and (*ii*) the user is not new and there is a possibility to move to a new location as follows:

Case I: the user is new, the coordinator sends locations codes only to the receiver via the MIMO-VLC channel. The receiver receives four signals using four photodetectors and recovers data by the MMSE equaliser. In the next stage, it calculates the user's location based on the RSSI technique that has been discussed in the previous section. The receiver can select the public and private keys from keys' store based on its location, and then sends the public key and power levels to the transmitter via the RF/IR channel. The transmitter subsequently receives them, and decides if the MIMO-VLC channel is suitable for data transmission.

Case II: the coordinator encrypts the user's data utilizing the public key and combines them with the location codes and sends the data via the MIMO-VLC channel. At the receiver side again, all four signals pass the photodetectors stage, the positioning stage and finally the decryption process using the private key to decrypt the data. In the positioning stage, if

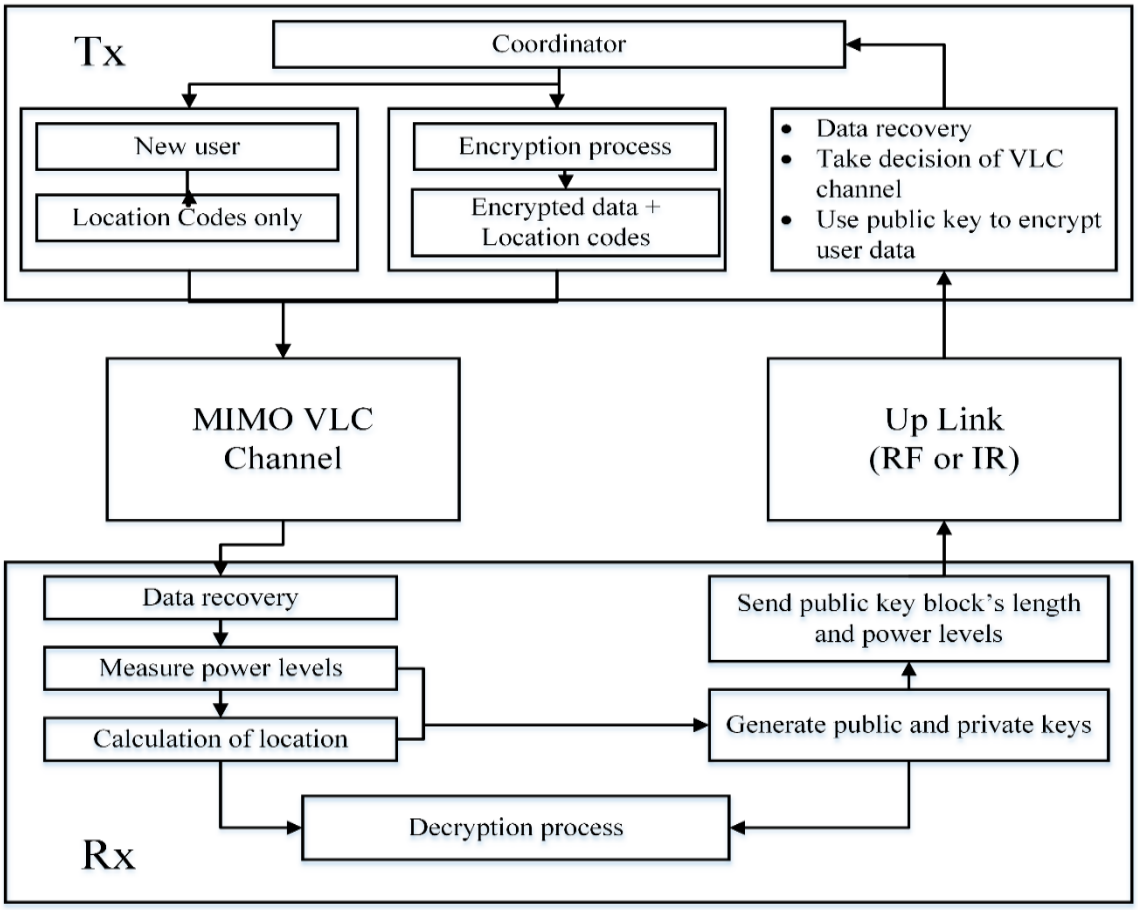


Fig. 6. 4 Bock diagram of a secure MIMO-VLC system.

the new location is not the same as the previous one, the receiver generates another key based on the new location using the cryptographic keys stage.

## 6.3.2. Modified RSA Algorithm and Encrypted Cells

In Fig. 6.4 there is a stage at the receiver side that generates public and private keys. In this section, we explain the modified RSA algorithm that produces a number of encryption/ decryption keys and distributes them on encrypted VLC cells. All frames from the transmitted data are divided into $k$-bit parallel blocks ($k$ = 8, 16, 32, 64,....), where k is chosen to be the same length as the key, which is generated by this modified RSA algorithm. The modified RSA algorithm is given in *Algorithm 1* below. We have modified the RSA algorithm for two main reasons; the first is the need to encrypt data without an increase in data length compared with plaintext data and as such to maintain the capacity of the channel. This means that the transmitted message per block $m_t(i)$ must not be more than $n$ ($0 < m_t <$

$n$). For instance, if we have a block of 8 bits then $n$ must be less than 255. However, there is a difficulty to find two prime numbers ($p$ and $q$) of which their multiplication result is exactly equal to $m$. Therefore, we select a percentage which is called maximum percentage of unencrypted data (MPUED) between data that is encrypted and data that cannot be encrypted (because it is more than $n$). The second reason is the requirement to generate a number of keys that are enough for every encrypted VLC cell. In the modified RSA technique, we are adding another level of ambiguity by not encrypting all transmitted data that is less than five percent. In this secure system, the problem of keys distribution has been solved using the generation of cryptographic keys in receiver (i.e.; at user) and sending the public key to transmitter only [173, 181-184].

The second process in this part relates to the distribution of the keys on the encrypted VLC cells. In Fig. 6.5, the standard VLC room has been divided into small square areas called the Encrypted VLC cells, where each encrypted cell has only one centre called the centre of encrypted cell (COEC). This means that every estimated user's location approaches the closest cell's centre due to the presence of a localization error based on positioning techniques and SNR. This approximation is the reason why it is difficult to make encrypted VLC cells smaller than this area. This system represents a flexible scheme in that it is able to control the size of encrypted cell.

In Fig. 6.5, we have three sub-figures which show three different sizes of the encrypted VLC cells. We have tested 4, 16 and 49 receivers for different lengths of cells, which are 0.50m, 1.00m and 1.50m, respectively. Therefore, all receivers in encrypted VLC cells have

Algorithm 1 Generation of public and private keys based on block's length.

- *Choose key's length* $m = 2^{k_l}$, *MPUED*
- *Generate prime numbers* $\left(P(:), Q(:)\right) \leq m$
- *Generate* $n(:) = P(:) * Q(:)$ , $\emptyset_n(:) = (P(:) - 1)(Q(:) - 1)$
- *If* $n(i) > m$ *or* $P(i) == Q(i)$ *or* $n(:) <= (n - percentage)$

  *delete* $P(i), Q(i)$ *and* $\emptyset_n(:)$
- *Generate prime numbers less than* $\emptyset_n(:)$ *to get public key (e(:), n(:))*
- *If* $gcd(e(i), \emptyset(i)) == 1$

  $e(:) \leftarrow e(i)$
- *Generate prime numbers less than* $\emptyset_n(:)$ *to get private key (d(:), n(:))*
- *If* $e(i) * d(i) mod\ \emptyset(i) == 1$

  $d(:) \leftarrow d(i)$
- *If* $e(i) \sim = d(i)$ *or* $e(i) * d(i) \sim = d(i) * e(i)$

  $e(:) \leftarrow e(i)$ *and* $d(:) \leftarrow d(i)$

only COEC (i.e., all positions inside cell approaches to one position which is COEC), and then all receivers have the same identification but they will take different public and private keys. Therefore, if one reduces the size of encrypted cells then the number of receivers will decrease as well. For example, if we decrease the length of encrypted VLC cell from 1.5 m to 1.0 m, at that point then, the number of receivers will decrease from 49 to 16 receivers as well. The reason being that we have assumed different environments such as convention hall, large office having approximately 16 users and small office has around four users. In a convention hall, the length of encrypted cell (LEC) is assumed 0.5m because the number of users is large and close to each other and every user has two or three devices. In addition, these devices have the same COEC due to its deployment/use by one user. In the proposed model, there will not be computational complexity because every receiver generates cryptographic keys based on its location and implements a decryption process as well.

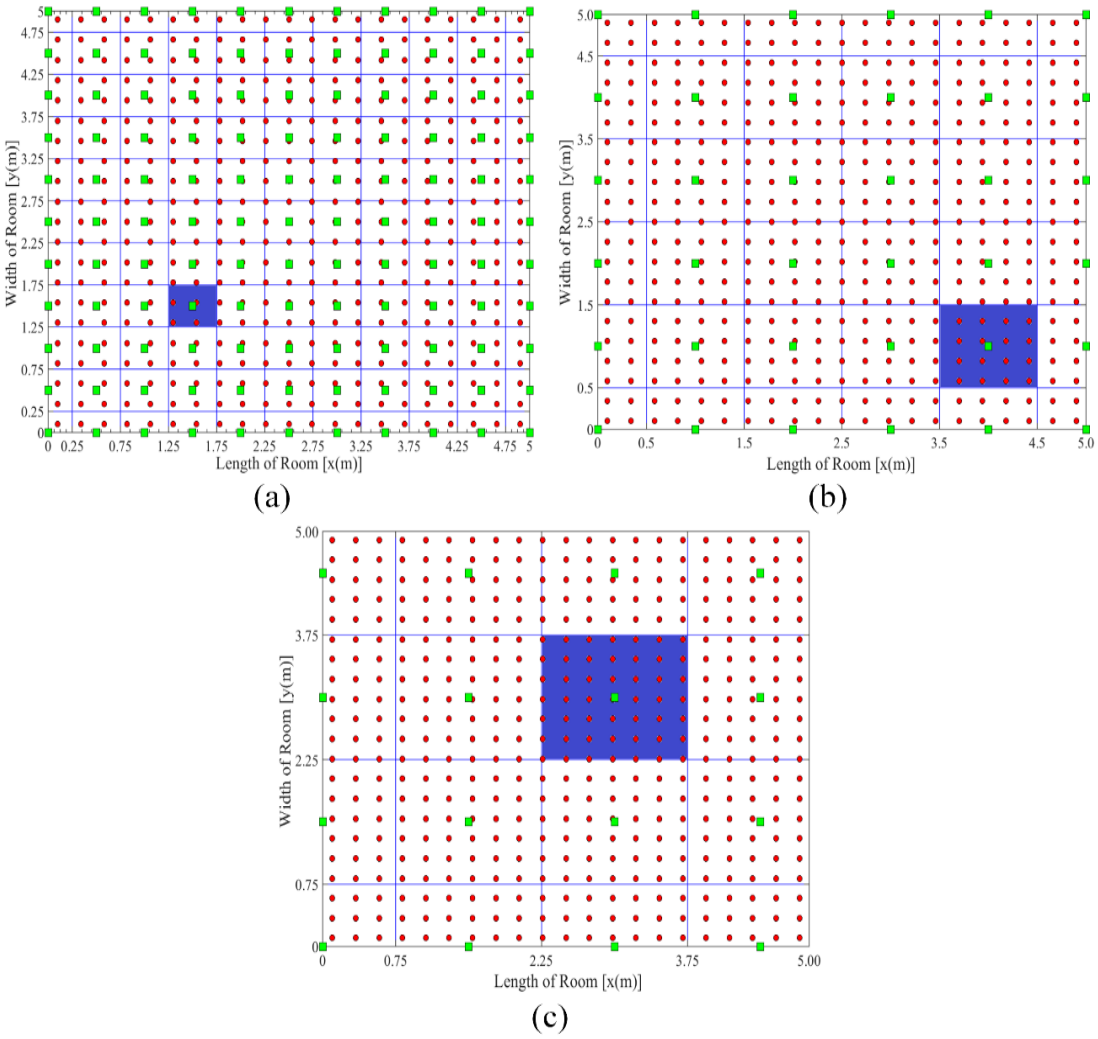


Fig. 6. 5 The encrypted VLC cells with the centers of encrypted cells (COECs). Green square is COEC, red circles are the positions of the users, and blue square areas are examples of encrypted VLC cell size for different length of encrypted cell (LEC) (a) LEC=0.50m (b) LEC=1.00m and (c) LEC=1.50m.

## 6.3.3. Encryption/Decryption in MIMO-VLC System

The receiver generates the public and private keys based on the user's location, and sends the public key only to the coordinator at the transmitter side by the RF/IR uplink channel. The coordinator converts the data (the binary stream) into $k$-bits parallel blocks ($k$ = 8, 12, 16, …) based on the public key's length which is generated and transmitted by the receiver. These blocks are then converted into decimal values and encrypted using the RSA encryption formula:

$$C = m_t^{e(i)} \, mod \, n(i) \qquad (6.\ 10)$$

where $(e(i), n(i), K_l)$ is the public key, $m_t$ is the parallel transmitted and it is function of $K_l$ and $C$ encrypted data, respectively. The parallel encrypted data is converted into serial data with an output in an OOK-NRZ format as shown in upper part of Fig. 6.6. The bottom part of the figure depicts a block diagram of the RSA decryption after recovering the original data signal. The receiver converts the data from serial to parallel blocks and applies the RSA decryption using the private key that already exists at the receiver side using the following formula:

$$m_r = C^{d(i)} \, mod \, n(i) \tag{6. 11}$$

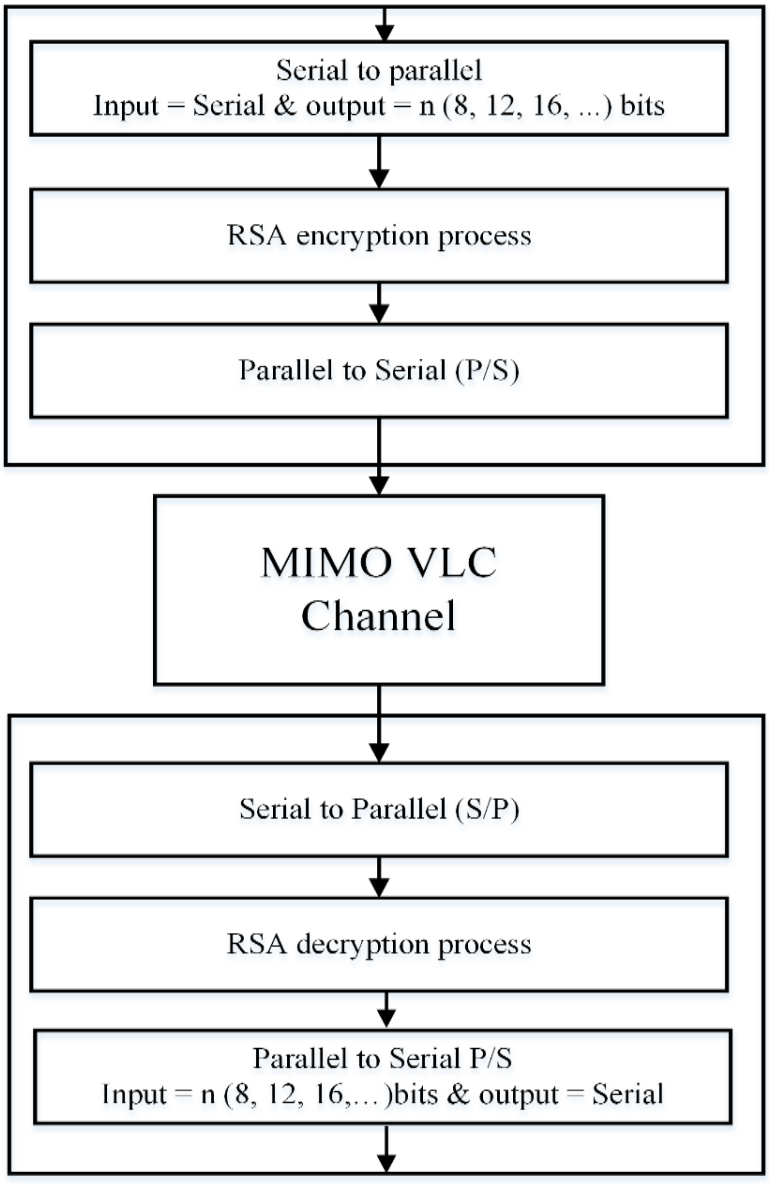


Fig. 6. 6 The RSA encryption/decryption applied in MIMO VLC system.

where $(d(i), n(i), K_l)$ is the private key and $C$ and $m_r$ are the parallel encrypted and received data, respectively. In the final stage in the process, all decrypted parallel data are converted into decrypted serial data and passed through the upper layers.

A comparison between the traditional RSA algorithm and the modified RSA algorithm is outlined in Table 6.1 and it has shown the security and speed of modified RSA algorithm are improved.

Table 6. 1 The comparison between the RSA algorithm and the modified RSA algorithm

| No. | The RSA Algorithm | The Modified RSA Algorithm |
|---|---|---|
| 1 | We must select $p$ and $q$ to determine common modulus $n$. | We have calculated $p$ and $q$ based on encryption block's lengths to get common modulus. |
| 2 | The large prime number only depends on two variables $p$ and $q$ to provide the strength of the algorithm. | The strength of the algorithm is based on three variables $p, q$ and $k_l$. Therefore, it is more difficult to break. |
| 3 | All parameters and calculations to select and generate p, q, e, d are at the time of data transmission. | All parameters and calculations to generate the number of public and private keys with different block's lengths are stored in database table at the receiver. |
| 4 | We have used $(e, n)$ as public key and $(d, n)$ as private key for encryption and decryption, processes, respectively. | We have used $(e(i), n(i), K_l)$ as public key and $(d(i), n(i), K_l)$ as private key for encryption and decryption processes, respectively. |
| 5 | We need to secure channel between Tx and Rx to exchange the keys, especially, private key. | We just need to send public key from Rx to Tx because the keys are generated at the receiver side based on the position of the user. |
| 6 | The user has just one public key and one private key and are changed based on the time period where it is sometimes longer. | The user has a number of public and private keys and are changed based on the position of the user and from time to time as well. |
| 7 | The RSA algorithm is applied in application layer. | The modified RSA algorithm is applied in MAC layer. |

# 6.4. Results and Analysis

## 6.4.1. Test Parameters

The proposed system described in the previous block diagrams of Fig. 6.4 and Fig. 6.6 is simulated and evaluated using MATLAB. The coordinator generates the location codes depending on the transmitter's positions on the ceiling and combines them to the transmitting data signal $x(t)$ to be sent to the receiver by an LED. The transmitted signal is modulated utilizing an OOK modulation scheme. Each transmitter contains a number of LEDs whose parameters are similar to typical commercially LED devices. There are two types of noise

associated with proposed system: thermal noise and shot noise. In this study, we have calculated the transmission matrix (CSI) from (2.36) which is then used to find y matrix from (2.35). Furthermore, at the receiver side, the transmission matrix is available and we have used this matrix to estimate the data using (2.48). we have considered that the noise in general is an additive white Gaussian noise (AWGN) added to the MIMO signals. The main parameters of the proposed system are presented in Table 6.2 below.

Table 6. 2 Simulation parameters for proposed secure MIMO VLC system

| Parameters | Values |
|---|---|
| Size of room | |
| Length (m) × width (m) × height (m) | 5×5×3 |
| Transmitters | |
| Number of LED-based transmitters | 4 |
| Transmitters Locations | (1.25,1.25), (1.25,3.75), (3.75,1.25), (3.75,3.75) |
| The LED's semi-angle at half power (FWHM) | 70 deg. |
| Transmitted power per Tx (watt) | 10, 100 |
| Optical Receivers | |
| Number of PD-based receivers | 4 |
| The dimensions of the receiver | 10 cm × 10 cm |
| Receiver plane above the floor | 0.75 m |
| Active area (AR) of receiver | $50\times10^{-6}$ $m^2$ |
| Half angle FOV of receiver | 70 deg. |
| Detector orientation: tilt horizontal (elevation) | 0 deg. |
| Detector orientation: tilt vertical (azimuth) | 0 deg. |
| Gain of the optical filter $T_s$ | 1 |
| Lens refractive index $n_r$ | 1.5 |
| Transmitted data rate $R_B$ | 0.5 Mb/s, 1 Mb/s |
| Receiver sensitivity (used with the AD8015 trans-impedance amplifier) | -36 dBm |
| LPF cut-off frequency | $0.7*R_B$ |
| X-Y sweep resolution | 0.25 × 0.25 m |
| Encryption/Decryption | |
| Encrypted VLC cells size | See Fig. 6.5 |
| Length of encrypted cell (LEC) (m) | 0.5, 1.0, 1.5 |
| The length of encrypted keys (bits) | 8, 12, 16 |
| Maximum percentage of unencrypted data (MPUED) | 0.05, 0.005, 0.0002 |

## 6.4.2. The Evaluation of MIMO-VLC System

We have also investigated the BER against a wide range of SNR in three different cases. Firstly, BER against SNR for single-input-single-output (SISO) VLC system was studied as shown in Fig. 6.7 (green curve) without the encryption. Secondly, we simulated a MIMO-VLC system (blue curve) without the encryption as well. Lastly, a BER against to SNR was simulated for a secure MIMO-VLC system using key lengths: 8 bits (red curve) and 16 bits (black curve) . In all cases, the receiver's position is in the middle of a standard room Rx's

position is (2.5, 2.5) m. This means that the distances are equal between the transmitters and receiver but the results in Fig. 6.1 have generated from the total bits that have sent to four channels. Note that at BER of $10^{-3}$ there is around 4 dB power penalty between the SISO-VLC and MIMO-VLC systems. However, the power penalty is around 1.4 dB for secure with key length =8 bits and unsecure MIMO-VLC system but it is approximately 0.7 dB between using key lengths 8 bits and 16 bits for secure MIMO-VLC system.

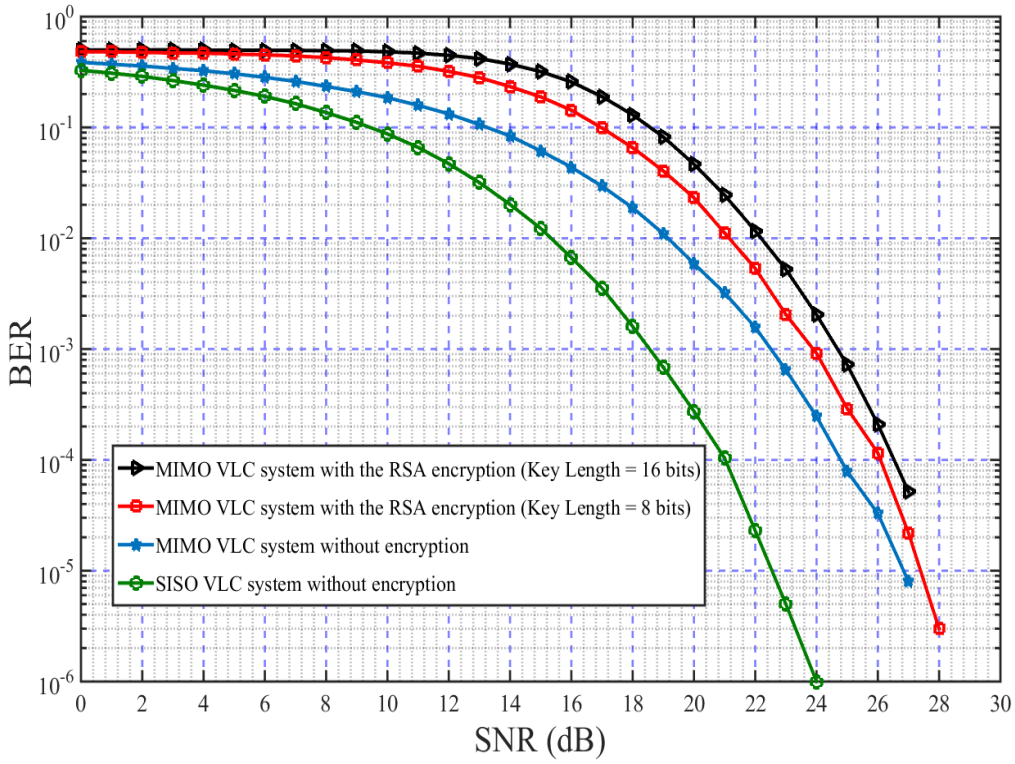


Fig. 6. 7 BER against SNR when the receiver is in the middle of typical room Rx (2.5, 2.5)m for a SISO-VLC system without encryption (Green curve), and a MIMO-VLC system without encryption (blue curve) and with encryption when the key length is 8 bits (red curve) and 16 bits (black curve).

## 6.4.3. Positioning Error Distributions

The proposed 2D indoor positioning system described in Fig. 6.1 and Fig. 6.2 is simulated and evaluated using MATLAB. The coordinator generates different location codes based on the positions of transmitters and send them after the full state information (CSI) stage. The receiver consists of four photodetectors and uses only two of the four signals to recover the location codes and hence determines the locations of the two photodetectors. Therefore, we

can calculate the positions of the other two photodetectors based on the size of Rx and the direction of the order of the photodetectors, (i.e. clockwise or anticlockwise as mentioned above). We have also investigated the localization error (The difference between the estimated position and the actual position). In the first approach, the system is considered an ideal system with no noise present at any stage in the aforementioned MIMO VLC system. The results are based on a LOS procedure and in the absence of any reflections from wells as shown in Fig. 6.8 (a). Furthermore, all statistical standards indicate there is a free error in the entire room. In the second approach, we further investigate the case when noise is existing. Here, the same positioning algorithm is applied but with the addition of noise to the received optical signal. The noise is modelled as an additive Gaussian distribution noise over an SNR range of 0 to 30 dB. The selected localization error distributions of the centre of the receiver at 15 dB and 20 dB are shown in Fig. 6.8 (b), and (c), respectively.

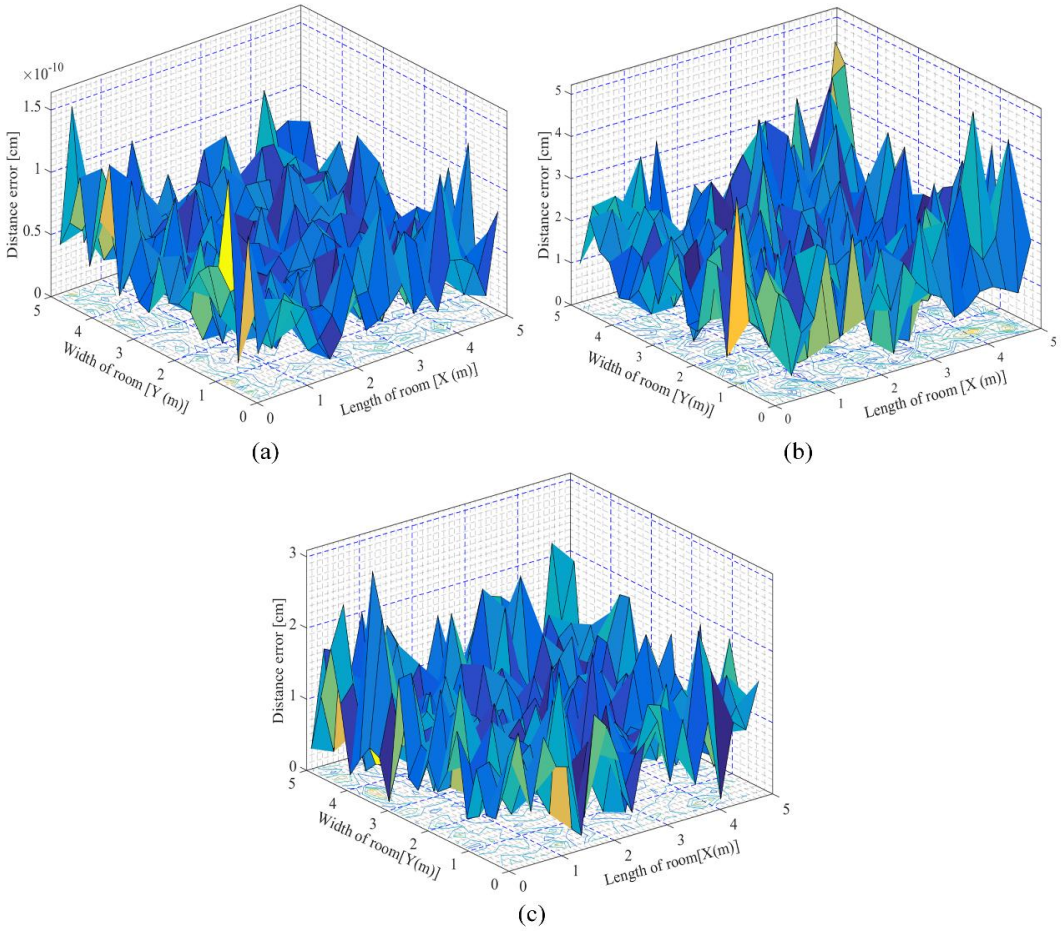


Fig. 6. 8 Spatial distribution of localization error for (a) ideal system (without noise) (b) when SNR = 15 dB (c) when SNR = 20 dB.

## 6.4.4. BER Distribution from Ideal System

We have also studied the BER distribution of the system using two scenarios. The first scenario is for an ideal system with no added noise. Fig. 6.9, plots sub-figures of the BER for a typical VLC room. We have tested authorised users for different encrypted VLC cells based on the size of the cell in different places in the VLC room (i.e.; up to 4, 16, and 49 users when LEC = 0.5, 1.0, 1.5 m, respectively). This means that the authorized users (4,16, 49 users) inside the cell have the same centre of the encrypted cell. Thus, they have the same public and private keys. As a result, they can receive the originally transmitted data while all users outside this cell cannot recover the data. For instance, in Fig. 6.9 (a) the centre of encrypted VLC cell is (1.5, 1.5) m so all users nearest to this centre are able to decrypt the data which was sent from the four transmitters for the whole room. Note that the BER is

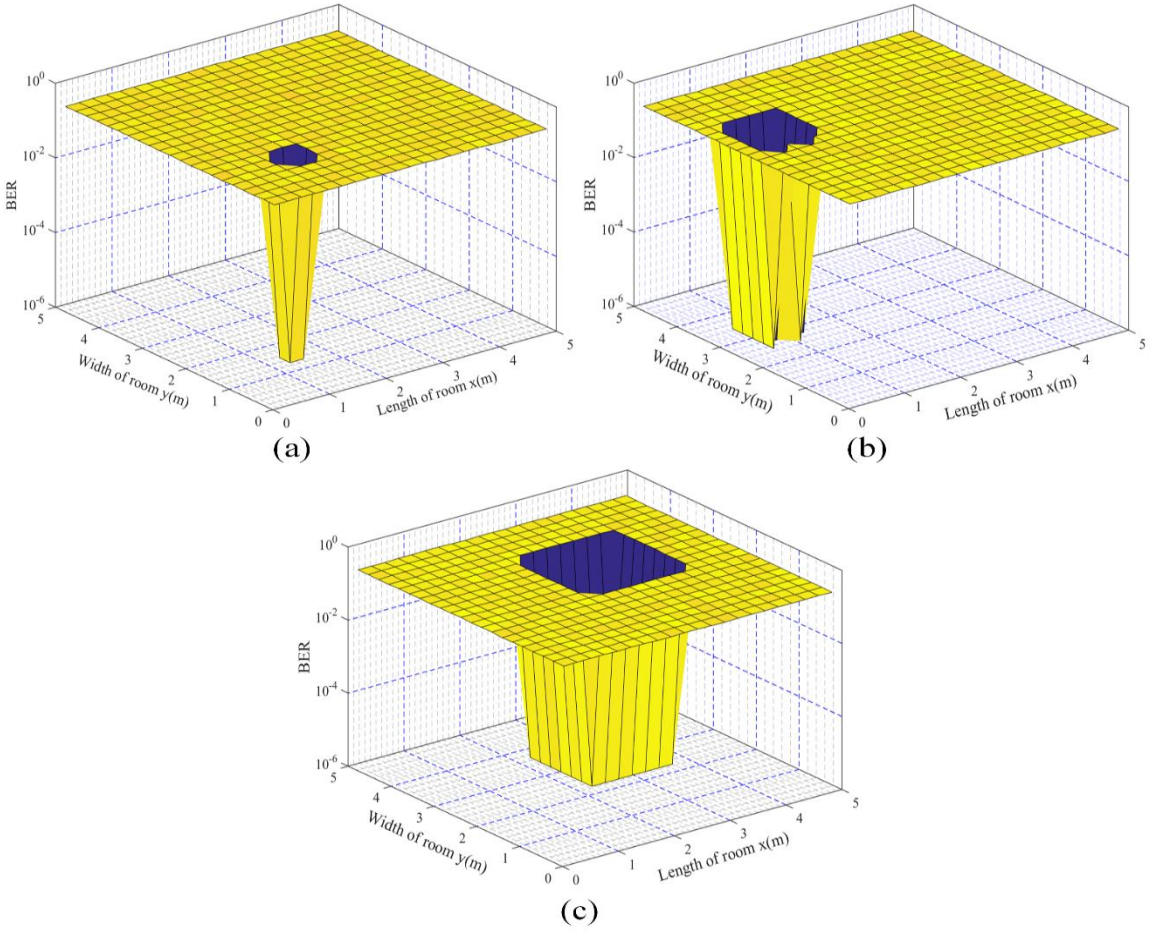


Fig. 6. 9 BER of an ideal MIMO-VLC system for different encrypted VLC cells when (a) COEC is (1.5, 1.5) m and LEC=0.5m (b) COEC is (1.0, 3.0) m and LEC= 1.0 m (c) COEC is (3.0, 3.0) m and LEC =1.5m.

free, but it is capped to $10^{-6}$ to clarify the difference between the authorised users and unauthorized users outside this cell. The cases in Fig. 6.9 (b), and (c) are similar to the previous example but with different COECs and different LEC.

## 6.4.5. BER Distribution from Real System

The second scenario studied is for a MIMO-VLC system with added noise which was modelled as an AWG noise for the wide range but we have selected only when SNR range of 20 dB. Fig. 6.10 (a) shows the comparison between BER distributions for authorized users inside the encrypted cell and all users outside this cell. Note that BER ~$10^{-3}$ for authorized users whereas unauthorized users cannot recover the transmitted data. Other BER distributions are also presented for different COECs and different length of encrypted cell (Fig. 6.10 (b) and (c)) as done in the previous scenario.

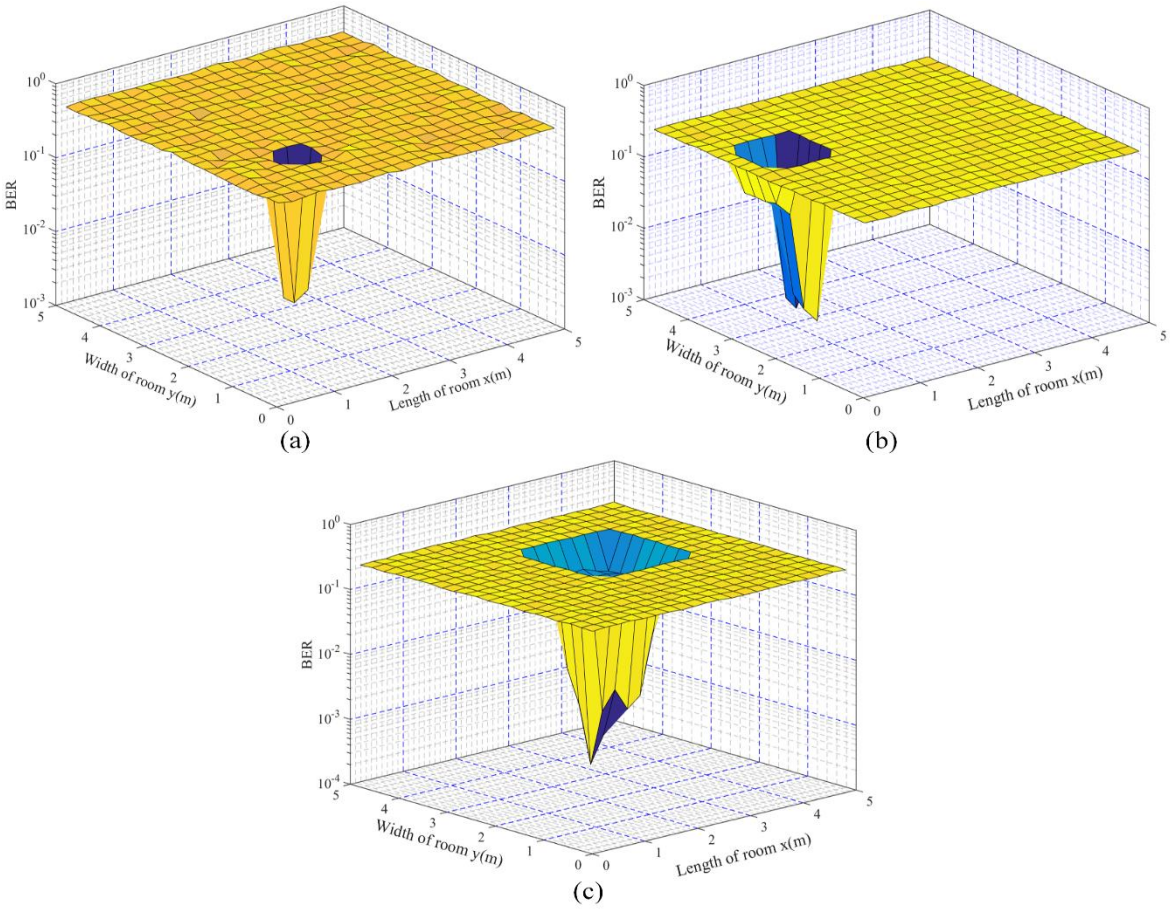


Fig. 6. 10 The BER of an MIMO-VLC system with noise when SNR = 20 dB for different encrypted VLC cells when (a) COEC is (1.5, 1.5) m and LEC=0.5m (b) COEC is (1.0, 3.0) m and LEC= 1.0 m (c) COEC is (3.0, 3.0) m and LEC =1.5 m.

## 6.5. Summary

In this chapter, we have discussed the design of a new secure MIMO-VLC system using a modified RSA technique to encrypt the transmitted data in the MAC layer based on the location of the user. One of the most important findings to emerge from this study is that the generation of a number of public and private keys with different lengths of keys are enough to distribute them on encrypted VLC cells that have different sizes. In this secure system, the problem of keys distribution has been solved by generating keys at the receiver and send the public key to transmitter only. The ability to control the size of the encrypted VLC cell (LEC) based on the user environment was also demonstrated. Furthermore, no extra data is needed due to the use of the cryptography process, thus maintaining the capacity of the channel. We have also shown that the positioning error was less than 5 cm when SNR=15 dB and have studied the distance error in both ideal and noisy conditions. Moreover, the paper has also presented a study on the BER distribution for authorized users in the encrypted VLC cell and unauthorized users (or eavesdropper) both in an ideal condition and when SNR = 20 dB. Finally, we investigated BER vs SNR for SISO-VLC and MIMO-VLC systems, which showed that the proposed system is working as expected.

# Chapter Seven

# Conclusion and Future Work

## 7.1. Conclusions

The main aim of this research was to explore methods and techniques to overcome challenges in indoor VLC positioning and security in VLC system. In the beginning of this investigation, an overview of indoor VLC systems, indoor MIMO VLC systems and indoor VLC positioning systems were provided. Additionally, several features of OWC systems were highlighted and compared to RF communication systems. Furthermore, some of challenges facing OWC systems were also explored and discussed. In particular, two of the most significant challenges facing current OWC technology are indoor positioning and indoor security in VLC systems, both of which were tackled in this thesis. In addition, it also set out to review all stages, from the source of data to its destination, of a VLC system. The advantages of LEDs and LDs were mentioned and a mathematical model of the transmitted optical power was investigated . Furthermore, a mathematical model of the impulse response of the VLC channel for both LOS and NLOS paths was studied as well. There are two common photodetectors deployed in OWC systems and are used in a wide range of applications, namely, PIN photodiode and APDs. In this study, PIN photodiode (PD) with a responsivity of -36 dBm (i.e. with a sensitivity, $\mathcal{R}$, of 0.6) was used because it is commercially available and relatively cheap. The majority of practical VLC systems employ the IM/DD scheme for both indoor and outdoor applications. As such, the main metrics of the OOK modulation scheme and the electrical PSD for OOK-NRZ and OOK-RZ were all studied. Three types of noise impacting the signal quality were also discussed in this overview which are dark noise, shot and thermal noises. Furthermore, the MIMO VLC

system was studied in order to provide illumination and high data transmission and the channel coefficients (i.e. CSI matrix) were calculated. To recover the data at receiver side, the ZF and MMSE equalizers were used. Finally, an overview of indoor positioning techniques was provided in this chapter along with the basic mathematical model of each technique. This thesis has proposed five contributions as follows:

Firstly, an indoor VLC system which employs two types of illuminations, using single and four cells configurations, has been proposed. The ROP distributions were evaluated when OLO was used and a semi-angle at half power was $70^{o}$. This study has found a number of relationships between the ROP, the semi-angle at half power of LED, the maximum horizontal distance and the transmitted power level at different levels of receiver sensitivity.

Secondly, the work has also proposed a 2D indoor positioning system using three transmitters and the trilateration method based on the RSSI technique. The positioning accuracy was not affected by using different location codes. The proposed positioning algorithm is able to determine the location of the user with an average error of 5 cm for the LOS scenario and 8 cm for the LOSNLOS scenario when the SNR is 15 dB. Furthermore, the average positioning error decreases dramatically when the SNR is increased above 15 dB. A comparison between the obtained results of the proposed positioning system and previous works was carried out and the results suggest that our technique outperforms offers. The thesis has also proposed the design and evaluation of a new scheme for recovering 4×4 MIMO VLC data with partial CSI knowledge (due to shadowing or blocking) for noisy and noiseless cases. The scheme was based on the location of the receiver using the RSSI technique.

Thirdly, a novel indoor VLC positioning scheme was theoretically modelled and evaluated based on the RSSI technique in a full 2D receiving plane and using only two LED ceiling lamps as transmitters. A comprehensive analysis of the angular and horizontal distance errors was carried out and validated through simulations. For the LOS scenario, the

positioning algorithm was able to determine the user position with an average error ranging from 9.1 to 21 of centimetres for the best position for scenario (1), whereas the average error was between 12.1 and 26.1 centimetres for the best position for scenario (2) when the SNR was between 10 dB and 15 dB. For the LOSNLOS scenario, an average error between 11 and 23.5 of centimetres for the best position for scenario (1) was obtained, whereas it was between 15.1and 28.6 centimetres for the best position for scenario (2) when the SNR was between 10 dB and 15 dB. The average error was substantially reduced when the SNR was increased to more than 15 dB. The final part of this work reported a comparison of the proposed VLC system and a conventional three-transmitter system. The proposed VLC positioning system offers a complementary method to existing trilateration to reduce the complexity when appropriate.

Fourthly, the impact of data encryption on VLC systems was investigated and the findings suggest that the proposed secure VLC system requires more SNR to obtain the same BER performance especially for long encryption key lengths. The power penalties observed ranged from 1 dB to 1.7 dB for the 8-bit encryption block length and 1.6 dB to 2.7 for the 16-bit encryption block length and for various distances between Txs and Rx within the 3 dB LED bandwidth. The more significant findings related to the presence of power penalties between ~ 1 dB and ~3.5 dB for data rates from 1 Mbps to 10 Mbps respectively for both the LOS and LOSNLOS scenarios.

Finally, another important contribution of this thesis, a new secure MIMO VLC system using an encryption based on the location of the user was proposed, designed and evaluated. The proposed design uses a modified RSA technique to encrypt the transmitted data in the MAC layer with no extra data needed, thus maintaining the capacity of the channel. Subsequently, the design focused on the generation of a number of public and private keys with different length of keys based on the encrypted block in the receiver. The demonstration of the proposed system ability to control the size of the encrypted VLC cell in different

environment was implemented. Following this, to determine the user's location, RSSI algorithm was used in the MIMO VLC system with a trilateration method. The results of this technique show that the positioning error was less than 5 cm when SNR=15 dB. Furthermore, an analysis of the BER distribution performance for authorized users in the encrypted VLC cell and unauthorized users out of the encrypted VLC cell for noisy and noiseless cases was given. This analysis along with a study of the relationship between BER vs SNR have shown that the proposed secure MIMO VLC system is working as intended.

## 7.2. Recommendations for future work

Although the aims and objectives set out in Chapter 1 of this thesis have all been accomplished, it is essential to recommend a few suggestions for future work which is necessary to make the accomplishments of this thesis more efficient and effective. In the following, we suggest a number of recommendations for future work:

- Indoor VLC positioning system using three transmitters was simulated and evaluated in Chapter 3, but only one modulation scheme, OOK modulation, was used. We recommend the use of other modulation schemes such as M-PPM, PAM, OFDM, and m-CAP and evaluate the positioning accuracy for both LOS and LOSNLOS scenarios. Furthermore, it might be necessary to perform this work experimentally and compare the experimental results with those obtained from simulation and subsequently implement a self-correcting MIMO VLC system using localization experimentally with different modulation schemes.
- In Chapter 4, an indoor VLC positioning system using two transmitters was proposed, designed and simulated. As a future work, it would be interesting to implement this system experimentally with different modulation schemes, positioning techniques and environments. Furthermore, the technique can be implemented in a Wi-Fi environment to realise indoor positioning using two transmitters to reduce the complexity.

- In Chapter 5, a secure SISO VLC system based on the TDM scheme was proposed and evaluated. However, this system was implemented using RSA technique. It would be interesting to implement this system using different encryption techniques such as AES and one-time key to possibly achieve further enhancements for the speed of implementation and power penalties.
- A secure MIMO VLC system based on the location of the user was proposed and validated in Chapter 6 for various environments. We recommend implementing this proposed secure system experimentally. Furthermore, the proposed secure system could also be implemented in a Wi-Fi environment.
- We recommend a comprehensive investigation on the speed impact of RSA technique in MAC layer and the complexity.
- In this thesis, there is no mobility of the receiver which has only one orientation (i.e.; the irradiance angle ($\psi$)= the incidence angle ($\theta$), as the transmitter and the receiver are assumed to be in parallel planes). Therefore, the mobility is the most challenge in the VLC systems and it is still an open research issue.
- In Chapter 3 and Chapter 4, the positioning error slightly increases near the walls due to the directionality of Lambertian. It would be interesting to analyse the effect of directionality of Lambertian on the positioning errors in an indoor positioning VLC system.
- In Chapter 6, we have divided the typical room into a number of encrypted VLC cells. However, we did not consider the user mobility for different speeds between these cells. Therefore, the user mobility in secure VLC systems is still an open research challenge.

# Appendices

# Appendix A:

## The VLC Channel Modelling Based on ROP Distributions

The relationship between the transmitted optical power, $P_{\mathrm{Tx}}$, and the received optical power, $P_{\mathrm{Rx}}$, is been given in equation (3.33) of Chapter 2. We propose to rewrite the channel gain as follows [185]:

$$H(0) = \sum_{\mathrm{i}}(H_{\mathrm{ch,LOS}_i}(0) + \int_{walls} dH_{\mathrm{ch,NLOS}_i}(0)), \tag{A.1}$$

where $i$ is the index of the $i^{\mathrm{th}}$ transmitter, LOS is the line-of-sight and $\mathrm{ch,NLOS}_i$ is the diffused configurations (non-LOS). The system here is used for localisation and as result we only consider low data rates (i.e. kbps) for the identification (ID) of LEDs). Therefore, the bit duration is much larger than the channel delay spread for both LOS and NLOS. For the LOS configuration, the received optical power is given by [55]:

$$P_{\mathrm{Rx},L_i}(\theta_{L_i},\psi_{L_i}) = \begin{cases} \frac{m+1}{2\pi L^2} P_{\mathrm{Tx}} A_R \cos^m(\theta_{L_i}) \cos(\psi_{L_i}) \mathrm{T_s}(\psi_{L_i}) \mathrm{g}(\psi_{L_i}); & 0 \le \Psi \le \mathrm{FOV} \\ 0; & \text{otherwise} \end{cases}, \tag{A.2}$$

where $\theta_{L_i}$ is the angle of irradiance of the $\mathrm{Tx_i}$, $\Psi_{L_i}$ is the angle of incidence at the Rx, $\mathrm{T_s}(\psi_{L_i})$ is the gain of an optical filter, $\mathrm{g}(\psi_{L_i})$ is the gain of an optical concentrator, $A_R$ is the PD effective area, FOV is the field of view of the Rx and $m$ is the order of Lambertian emission defined in (2.10). Here $\mathrm{T_s}\left(\psi_{L_i}\right)$ and $\mathrm{g}\left(\psi_{L_i}\right)$ are assumed to be unity in our investigation as we use bare PD (i.e. without the optics). On the other hand, the received optical power from NLOS is given as [55]:

$$P_{\mathrm{Rx},L_i}(\theta_{L_i},\psi_{L_i}) = \begin{cases} \frac{m+1}{2\pi^2 L_1^2 L_2^2} P_{\mathrm{Tx}} \rho dA_{wall} \cos^m(\theta_{L_i}) \cos(\psi_{L_i}) \cos(\alpha) \cos(\beta) \mathrm{T_s}(\psi_{L_i}) \mathrm{g}(\psi_{L_i}); & 0 \le \Psi \le \mathrm{FOV} \\ 0; & \text{otherwise} \end{cases}, \tag{A.3}$$

where $\rho$ is the reflectance factor and $dA_{wall}$ is a reflective area of small region. We have used (A.2) and (A.3) to generate the following results.

# Appendix B

Results of an indoor VLC positioning system using three transmitters from ROP distributions approach.

## Appendix.B.1

Spatial distribution of the localization error of the positioning VLC system for noiseless LOS scenario from ROP distributions approach.

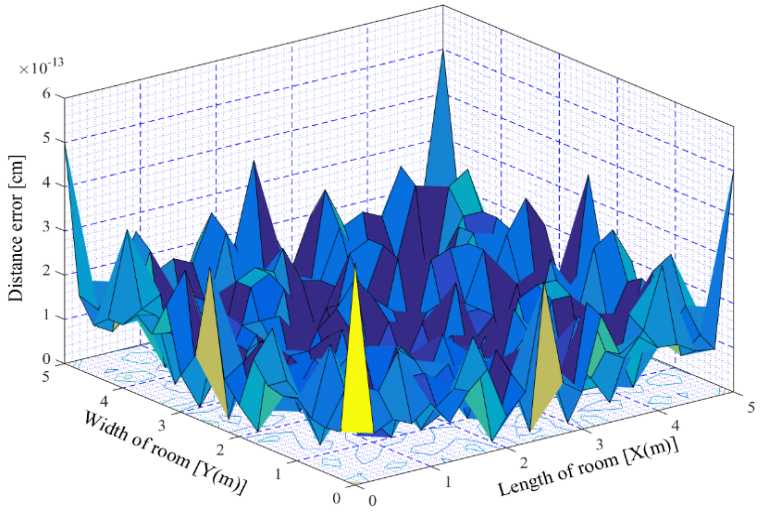


## Appendix.B.2

Spatial distribution of the localization error of the positioning VLC system for the noisy LOS scenario when SNR = 15 dB from ROP distributions approach.

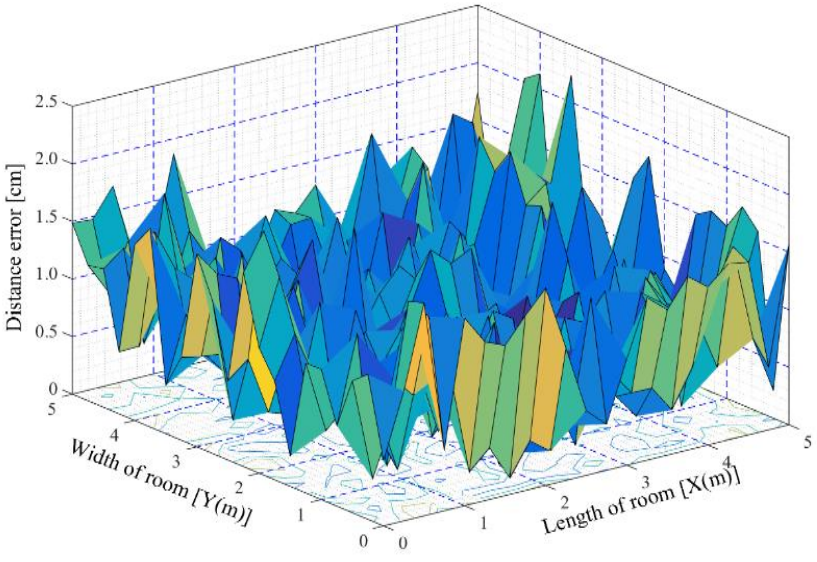

## Appendix.B.3

Estimated (blue circles) and real positions (green squares) for the real system at SNR=15 dB from ROP distributions approach.

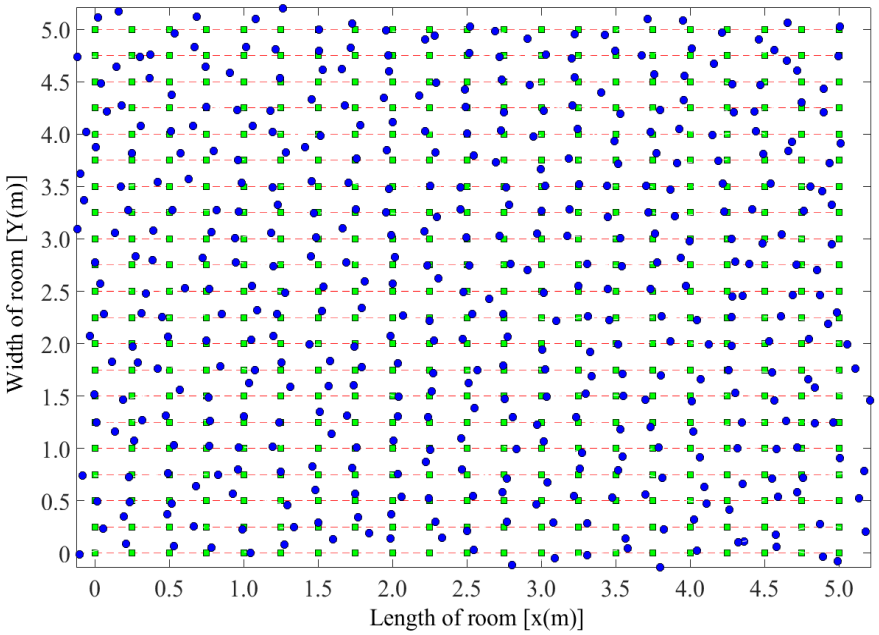


## Appendix.B.4

The relationship between the positioning error average and the SNR from ROP distributions approach for LOS scenario.

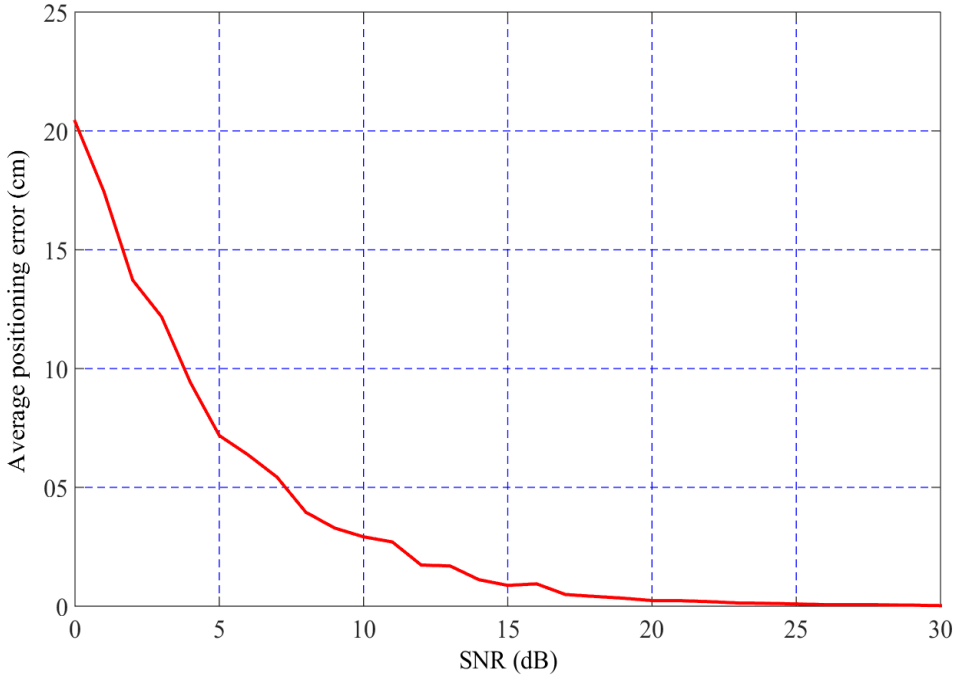

## Appendix.B.5

The statistical standards for the LOS scenario from ROP distributions approach.

| SNR (dB) | Max. (cm) | Mean (cm) | Standard Deviation |
|---|---|---|---|
| 0 | 62.04 | 20.39 | 11.31 |
| 5 | 21.56 | 7.52 | 4.05 |
| 10 | 7.35 | 2.41 | 1.25 |
| 15 | 2.23 | 0.83 | 0.43 |
| 20 | 1.01 | 2.5e-1 | 1.48e-1 |
| 25 | 2.21e-1 | 7.6e-3 | 4.09e-2 |
| 30 | 7.58e-2 | 2.66e-2 | 1.35e-2 |

# Appendix C :

## Appendix.C.1

The average position errors against the SNR of LOS scenario for four procedures and different transmitters' locations: (a) procedure (1) with $y_{\mathrm{Tx}_i}$ = 0 cm, (b) procedure (2) with $y_{\mathrm{Tx}_i}$= 25 cm, (c) procedure (3) with $x_{\mathrm{Tx}_i}$= $y_{\mathrm{Tx}_i}$, and (d) procedure (4) with $x_{\mathrm{Tx}_i}$= 0 from the extending proposed positioning system (End-to-end proposed positioning system)

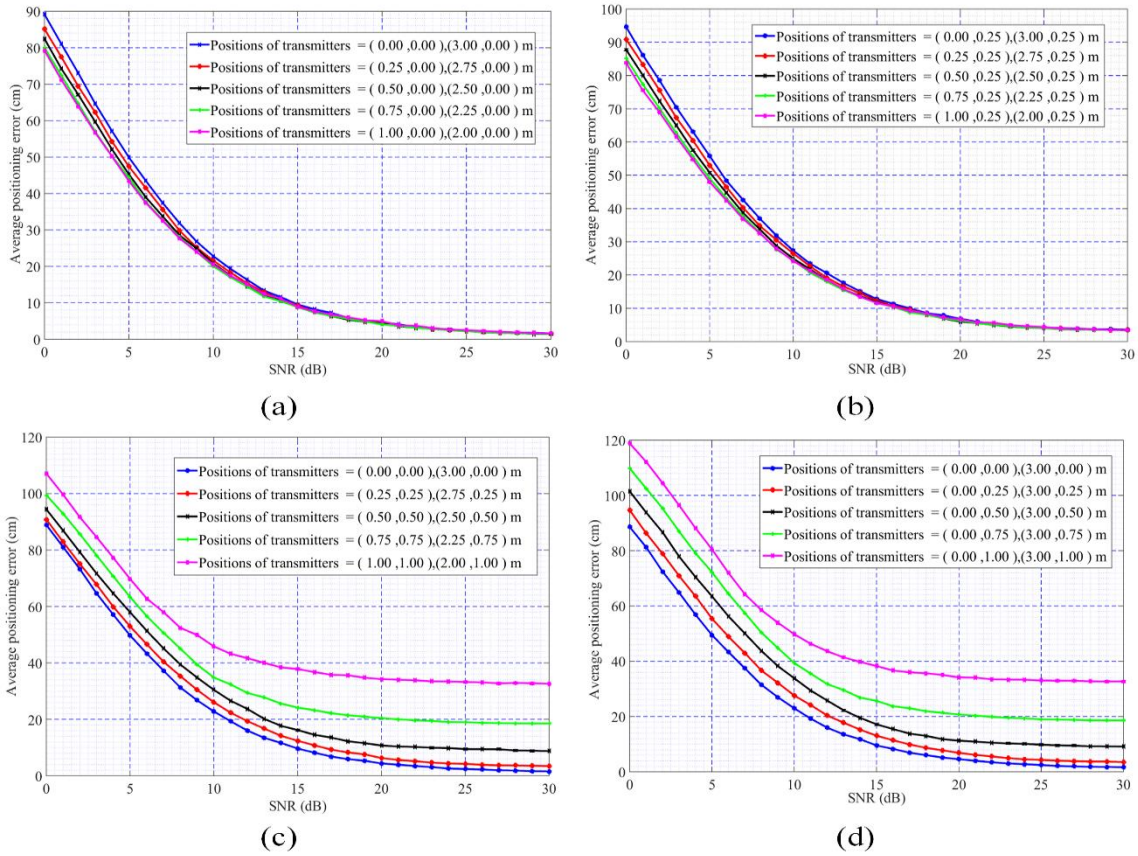

## Appendix.C.2

The average position errors against the SNR of LOS scenario for four scenarios and different transmitters' locations: (a) scenario (1) with $y_{\mathrm{Tx}_i}$ = 0 cm, (b) scenario (2) with $y_{\mathrm{Tx}_i}$= 25 cm, (c) scenario (3) with $x_{\mathrm{Tx}_i}$= $y_{\mathrm{Tx}_i}$, and (d) scenario (4) with $x_{\mathrm{Tx}_i}$= 0 from ROP distributions approach.

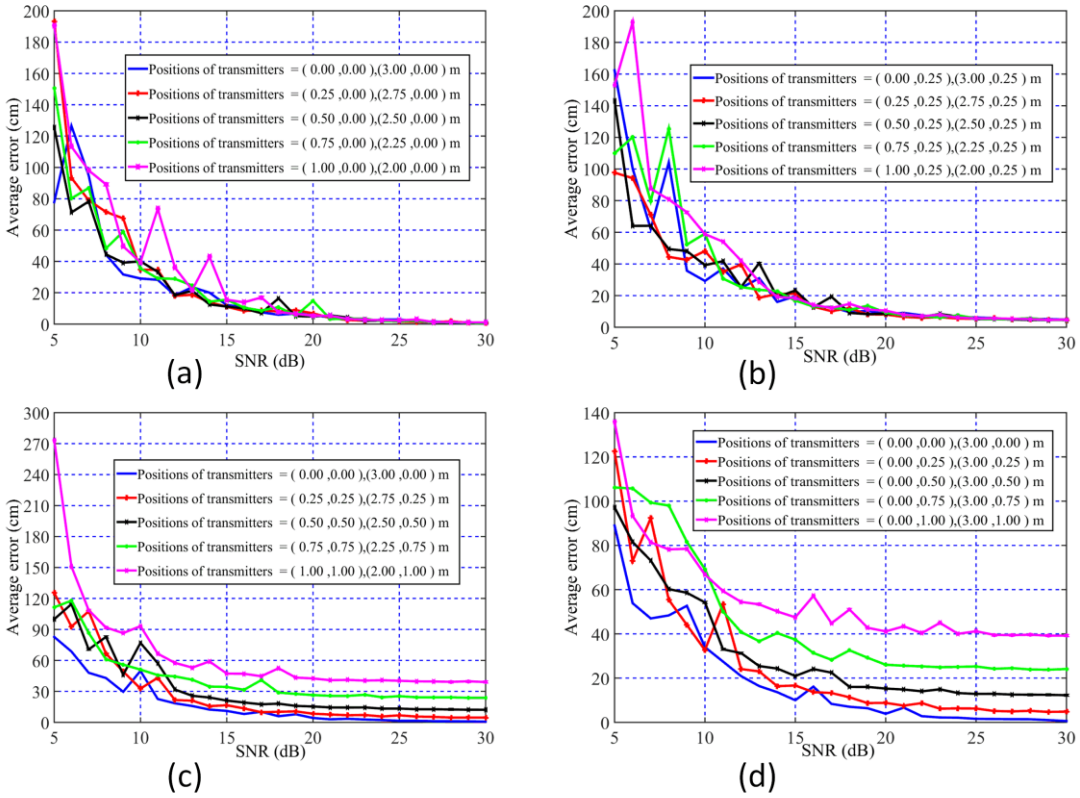


## Appendix.C.3

Spatial distribution of localization error without considering noise when the transmitters' positions (1&2): (a) are (0.25m, 0m) & (2.75m, 0m) (b) are (0.25m, 0.25m) and (2.75m, 0.25m) from ROP distributions approach.

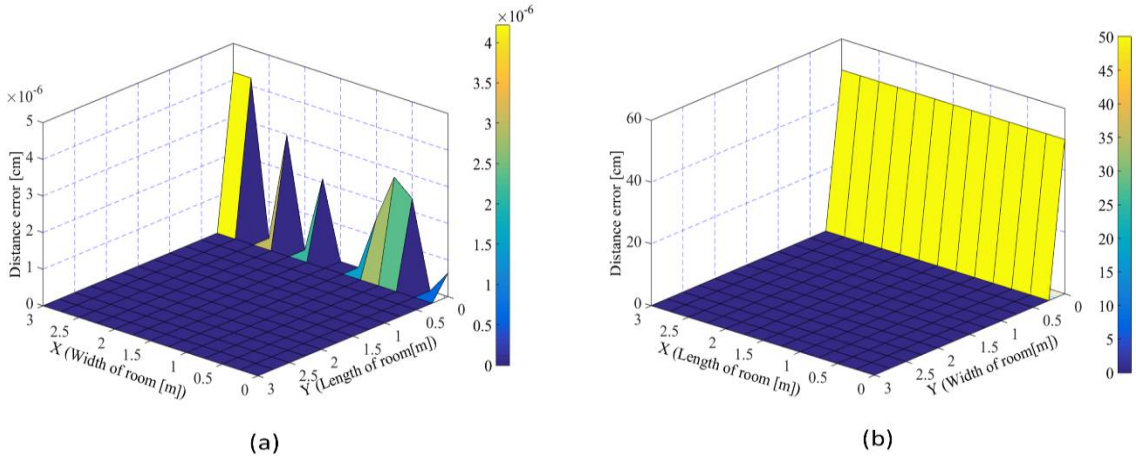

## Appendix.C.4

(a) Positioning error distribution when the transmitters' positions (1&2) are (0.25m, 0m) & (2.75m, 0m) at SNR = 15 dB. (b) Estimated and real positions when the transmitters' positions (1&2) are (0.25m, 0m) & (2.75m, 0m) at SNR = 15 dB from ROP distributions approach.

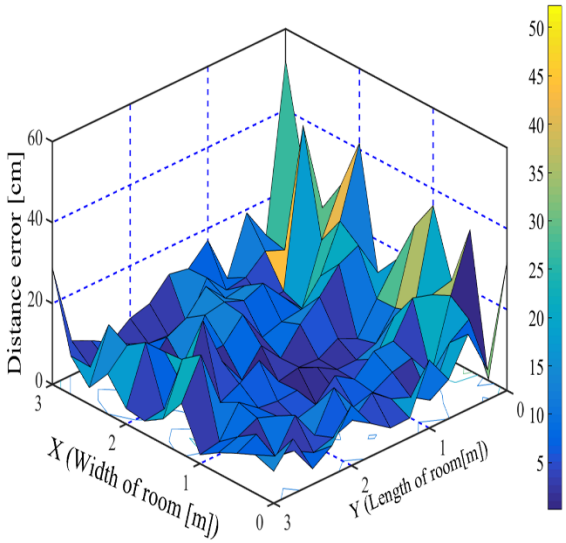


(a)

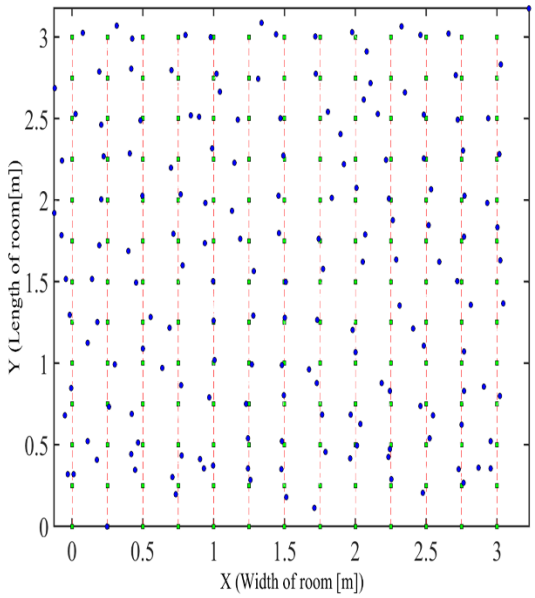


(b)

## Appendix.C.5

(a) Positioning error distribution when the transmitters' positions (1&2) are (0.25, 0.25) & (2.75, 0.25) m and SNR =15 dB. (b) Estimated and real positions when the transmitters' positions (1 &2) are (0.25, 0.25) m & (2.75, 0.25) m and SNR = 15 dB from ROP distributions approach.

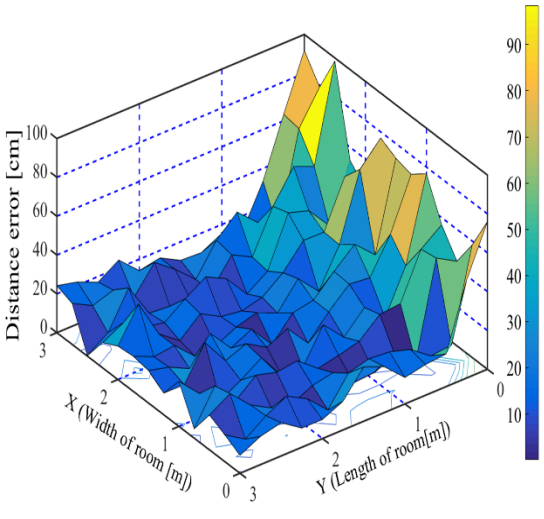


(a)

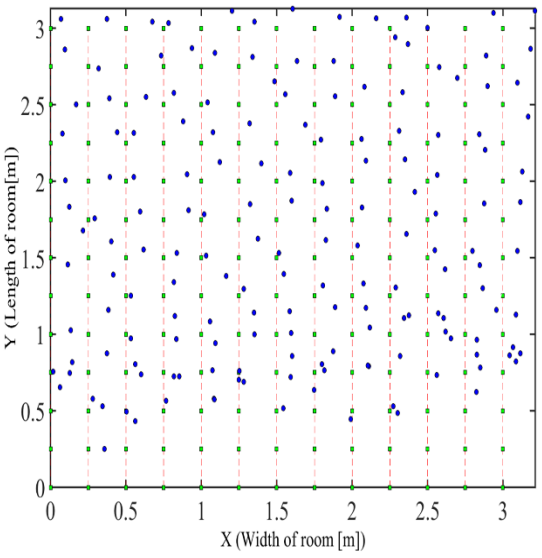


(b)

# Appendix.C.6

Table shows some statistical standards for positioning error from ROP distributions approach.

| Positions of transmitters | SNR (dB) | Max. value (cm) | The mean (cm) | Standard deviation (cm) |
|---|---|---|---|---|
| $Tx_1$ (0.25, 0) $Tx_2$ (2.75, 0) | 10 | 142.57 | 40.12 | 26.20 |
| | 15 | 82.95 | 13.28 | 12.14 |
| | 20 | 36.70 | 4.420 | 5.740 |
| | 25 | 14.36 | 1.390 | 2.27 |
| $Tx_1$ (0.25, 0.25) $Tx_2$ (2.75,0.25) | 10 | 135.70 | 36.38 | 26.38 |
| | 15 | 119.79 | 28.77 | 21.43 |
| | 20 | 62.36 | 7.500 | 13.40 |
| | 25 | 53.68 | 5.41 | 13.45 |

# References


[1] J. M. Kahn and J. R. Barry, "Wireless infrared communications," *Proceedings of the IEEE,* vol. 85, pp. 265-298, 1997.

[2] H. S. Kim, D. R. Kim, S. H. Yang, Y. H. Son, and S. K. Han, "Mitigation of inter-cell interference utilizing carrier allocation in visible light communication system," *IEEE Communications Letters,* vol. 16, pp. 526-529, 2012.

[3] IEEE, "IEEE Standard for Local and Metropolitan Area Networks Part 15.7: Short-range wireless optical communication using visible light," in *IEEE Std 802.15.7-2011*, ed, 2011, pp. 1-309.

[4] P. A. Haigh, "Using equalizers to increase data rates in organic photonic devices for visible light communications systems," Northumbria University, July 2014.

[5] S. H. Lee, S. Y. Jung, and J. K. Kwon, "Modulation and coding for dimmable visible light communication," *IEEE Communications Magazine,* vol. 53, pp. 136-143, 2015.

[6] T. Komine and M. Nakagawa, "Fundamental analysis for visible-light communication system using LED lights," *IEEE Transactions on Consumer Electronics,* vol. 50, pp. 100-107, 2004.

[7] P. Lou, H. Zhang, X. Zhang, M. Yao, and Z. Xu, "Fundamental analysis for indoor visible light positioning system," in *2012 1st IEEE International Conference on Communications in China Workshops (ICCC)*, 2012, pp. 59-63.

[8] S. Zvanovec, P. Chvojka, P. A. Haigh, and Z. Ghassemlooy, "Visible light communications towards 5G," *Radioengineering,* vol. 24, p. 9, APRIL 2015

[9] A. Sewaiwar, S. V. Tiwari, and Y. H. Chung, "Mobility support for full-duplex multiuser bidirectional VLC networks," *IEEE Photonics Journal,* vol. 7, pp. 1-9, 2015.

[10] G. Cossu, A. M. Khalid, P. Choudhury, R. Corsini, and E. Ciaramella, "3.4 Gbit/s visible optical wireless transmission based on RGB LED," presented at the ECOC, Amsterdam, Holland, 2012.

[11] L. Hanzo, H. Haas, S. Imre, D. O. Brien, M. Rupp, and L. Gyongyosi, "Wireless myths, realities, and futures: From 3G/4G to optical and quantum wireless," *Proceedings of the IEEE,* vol. 100, pp. 1853-1888, 2012.

[12] J. Armstrong, Y. A. Sekercioglu, and A. Neild, "Visible light positioning: a roadmap for international standardization," *IEEE Communications Magazine,* vol. 51, pp. 68-73, 2013.

[13] M. Kavehrad, "Broadband room service by light encoded light transmissions can provide the wireless devices in a room with multimedia web services such as videoconferencing, movies on demand and more," *Sci Am,* vol. 297, pp. 82-7, Jul 2007.

[14] H. Haas, L. Yin, Y. Wang, and C. Chen, "What is LiFi?," *Journal of Lightwave Technology,* vol. 34, pp. 1533-1544, 2016.

[15] Y. Wang, "Indoor localization based on visible light communication " MSc. thesis, Lehigh University 2017

[16] J. Ziyan, "A Visible light communication based hybrid positioning method for wireless sensor networks," in *Second International Conference on Intelligent System Design and Engineering Application (ISDEA),*, 2012, pp. 1367-1370.

[17] M. Bilgi, M. Yuksel, and N. Pala, "3-D Optical wireless localization," in *IEEE Globecom Workshops*, 2010, pp. 1062-1066.

[18] T. Nguyen and Y. M. Jang, "Highly accurate indoor three-dimensional localization technique in visible light communication systems," *http://dx.doi.org/10.7840/kics.2013.38C.9.775,* vol. 38C, p. 6, 2013.

[19] G. del Campo-Jimenez, J. M. Perandones, and F. J. Lopez-Hernandez, "A VLC-based beacon location system for mobile applications," in *International Conference on Localization and GNSS (ICL-GNSS),* , 2013, pp. 1-4.

[20] T.-H. Do and M. Yoo, "An in-depth survey of visible light communication based positioning systems," *Sensors,* vol. 16, p. 678, 2016.

[21] H. Liu, H. Darabi, P. Banerjee, and J. Liu, "Survey of wireless indoor positioning techniques and systems," *IEEE Transactions on Systems, Man, and Cybernetics, Part C (Applications and Reviews),* vol. 37, pp. 1067-1080, 2007.

[22] Widyawan, M. Klepal, and D. Pesch, "Influence of predicted and measured fingerprint on the accuracy of RSSI-based indoor location systems," in *Proceedings of 4th Workshop on Positioning, Navigation, and Communication (WPNC'07)* 2007 pp. pp.145-151.

[23] J. Yim, S. Jeong, K. Gwon, and J. Joo, "Improvement of Kalman filters for WLAN based indoor tracking," *Expert Systems with Applications,* vol. 37, pp. 426-433, 2010.

[24] M. A. Youssef, A. Agrawala, and A. Udaya Shankar, "WLAN location determination via clustering and probability distributions," in *Pervasive Computing and Communications, 2003. (PerCom 2003). Proceedings of the First IEEE International Conference on*, 2003, pp. 143-150.

[25] Teemu Roos, Petri Myllyma¨ki, Henry Tirri, Pauli Misikangas, and J. Sieva¨nen, "A Probabilistic approach to WLAN user location estimation," *International Journal of Wireless Information Networks,* vol. 9, July 2002.

[26] H. Fonseca, A. Nogueira, and P. Salvador, "Localization system for wireless networks," in *IEEE International Conference onCommunications Workshops (ICC),*, 2013, pp. 988-993.

[27] P. M. P. Kontkanen, T. Roos, H. Tirri, K. Valtonen, and H. Wettig,, "Topics in probabilistic location estimation in wireless networks,," *in Proceedings of the 15th IEEE Symp. Pers,* vol. 2, p. 5, 2004.

[28] M. K. Zhou Zhou, Peng Deng, "Indoor positioning algorthim using light-emitting diode visible light communications," *Optical Engineering,* vol. 51, p. 6, August 2012 2012.

[29] M. S. Islam and R. Klukas, "Indoor positioning through integration of optical angles of arrival with an inertial measurement unit," in *IEEE/ION Position Location and Navigation Symposium (PLANS)*, 2012, pp. 408-413.

[30] W. S. Jang and M. J. Skibniewski, "Wireless network system for automated tracking of construction materials on project sites," *Journal of Civil Engineering and Management* vol. 14 pp. 11–19, 2008.

[31] G. Cossu, M. Presi, R. Corsini, P. Choudhury, A. M. Khalid, and E. Ciaramella, "A Visible light localization aided optical wireless system," in *IEEE GLOBECOM Workshops (GC Wkshps)*, 2011, pp. 802-807.

[32] S.-Y. Jung, S. Hann, and C.-S. Park, "TDOA-based optical wireless indoor localization using LED ceiling lamps," *IEEE Transactions on Consumer Electronics,* vol. 57, pp. 1592-1597, 2011.

[33] A. M. Vegni and M. Biagi, "An indoor localization algorithm in a small-cell LED-based lighting system," in *International Conference on Indoor Positioning and Indoor Navigation (IPIN)*, 2012, pp. 1-7.

[34] H.-S. Kim, D.-R. Kim, S.-H. Yang, Y.-H. Son, and S.-K. Han, "An indoor visible light communication positioning system using a RF carrier allocation technique," *Journal of Lightwave Technology,* vol. 31, pp. 134-144, 2013.

[35] Y.-Y. Won, S.-H. Yang, D.-H. Kim, and S.-K. Han, "Three-dimensional optical wireless indoor positioning system using location code map based on power distribution of visible light emitting diode," *IET Optoelectronics,* vol. 7, pp. 77-83, 2013.

[36] J. Zhu, "Physical layer security in massive MIMO systems," PhD diss., The University of British Columbia, 2016.
[37] A. Mostafa, "Physical-Layer Security for Visible-Light Communication Systems," PhD diss., THE UNIVERSITY OF BRITISH COLUMBIA, April 2017.
[38] H.-K. Lo, M. Curty, and K. Tamaki, "Secure quantum key distribution," *Nature Photonics,* vol. 8, pp. 595-604 2014.
[39] H. Xu, S. Wijesekera, and D. Sharma, "Implementation of Quantum Key Distribution in Wi-Fi (IEEE 802.11) Wireless Networks," in *Advanced Communication Technology, 2008. ICACT 2008. 10th International Conference on*, 2008, pp. 865-870.
[40] L. Zhiqiang, S. Xiaoxin, D. Changbin, and D. Qun, "Hardware design and implementation of Wi-Fi technology based encryption system," in *International Conference on Sensor Network Security Technology and Privacy Communication System (SNS & PCS)*, 2013, pp. 144-147.
[41] J. A. Rabadan, S. T. Perez, R. Perez, F. A. Delgado, and M. A. Bacallado, "Wireless optical spread spectrum communications data security improvement in wireless links," in *39th Annual 2005 International Carnahan Conference on Security Technology (CCST)*, 2005, pp. 168-170.
[42] O. O. Khalifa, M. R. Islam, S. Khan, and M. S. Shebani, "Communications cryptography," in *Proceedings in RF and Microwave Conference (RFM 2004)*, 2004, pp. 220-223.
[43] A. J. Menezes, S. A. Vanstone, P. C., and V. Oorschot, *Handbook of applied cryptography* FL, USA CRC Press, 1996.
[44] D. R. Stinson, *Cryptography: theory and practice*, 2nd ed. London : Chapman Boca Raton, Fla. , 1995.
[45] W. Stallings, *Cryptography and network security: Principles and practice* 5th ed.: Prentice Hall, 2010.
[46] F. I. K. Mousa, N. Almaadeed, K. Busawon, A. Bouridane, R. Binns, and I. Elliot, "Indoor visible light communication localization system utilizing received signal strength indication technique and trilateration method," vol. 57, p. 10, 2018.
[47] H. L. Minh, Z. Ghassemlooy, A. Burton, F. Mousa, S. Biswas, A. T. Pham*, et al.*, "Self-correcting multiple input multiple output visible light communications system using localization," presented at the IEEE International Conference on Communication Workshop (ICCW), London, 2015.
[48] F. I. K. Mousa, H. Le-Minh, Z. Ghassemlooy, X. Dai, S. T. Tran, A. C. Boucouvalas*, et al.*, "Indoor localization system utilizing two visible light emitting diodes," *Optical Engineering,* vol. 55, pp. 116114-116114, 2016.
[49] F. Mousa, T. T. Son, A. Burton, H. L. Minh, Z. Ghassemlooy, T. Q. Duong*, et al.*, "Investigation of data encryption impact on broadcasting visible light communications," in *9th International Symposium on Communication Systems, Networks & Digital Sign (CSNDSP)*, 2014, pp. 390-394.
[50] F. I. K. Mousa, N. A. Maadeed, K. Busawon, A. Bouridane, and R. Binns, "Secure MIMO visible light communication system based on user's location and encryption," *Journal of Lightwave Technology,* vol. 35, pp. 5324-5334, 2017.
[51] Y. Tanaka, S. Haruyama, and M. Nakagawa, "Wireless optical transmissions with white colored LED for wireless home links," in *11th IEEE International Symposium on Personal, Indoor and Mobile Radio Communications (PIMRC 2000)*, 2000, pp. 1325-1329 vol.2.
[52] S. Dimitrov and H. Haas, *Principles of LED light communications: towards networked Li-Fi* vol. First published University Printing House, Cambridge CB2 8BS, United Kingdom: Cambridge University Press 2015.

[53] H.-S. Kim, D.-R. Kim, S.-H. Yang, Y.-H. Son, and S.-K. Han, "Indoor positioning system based on carrier allocation visible light communication," presented at the Quantum Electronics Conference & Lasers and Electro-Optics (CLEO/IQEC/PACIFIC RIM), 2011.
[54] S. Hranilovic, *Wireless Optical Communication Systems*: Springer, 2006.
[55] Z. Ghassemlooy, W. O. Popoola, and S. Rajbhandari, *Optical wireless communications system and channel modelling with Matlab*: CRC publisher, 2012.
[56] B. He and R. Schober, "Bit-interleaved coded modulation for hybrid RF/FSO systems," *IEEE Transactions on Communications,* vol. 57, pp. 3753-3763, 2009.
[57] P. H. Pathak, X. Feng, P. Hu, and P. Mohapatra, "Visible Light Communication, Networking, and Sensing: A Survey, Potential and Challenges," *IEEE Communications Surveys & Tutorials,* vol. 17, pp. 2047-2077, 2015.
[58] K. Cui, G. Chen, Q. He, and Z. Xu, "Indoor optical wireless communication by ultraviolet and visible light," *Proc. of SPIE,* vol. 7464, 2009.
[59] H. L. M. D. O'Brien, L. Zeng, G. Faulkner, K. Lee, D. Jung, Y. Oh, and E. T. Won, "Indoor visible light communications: challenges and prospects," *Proc. of SPIE,,* vol. vol. 7091, 2008.
[60] A. M. Khalid, G. Cossu, R. Corsini, M. Presi, and E. Ciaramella, "Hybrid radio over fiber and visible light (RoF-VLC) communication system," in *37th European Conference and Exhibition on Optical Communication*, 2011, pp. 1-3.
[61] D. C. O. Brien, L. Zeng, H. Le-Minh, G. Faulkner, J. W. Walewski, and S. Randel, "Visible light communications: Challenges and possibilities," in *IEEE 19th International Symposium on Personal, Indoor and Mobile Radio Communications*, 2008, pp. 1-5.
[62] T. Cevik and S. Yilmaz, "An overview of visible light communication systems," *CoRR,* vol. abs/1512.03568, 2015.
[63] L. Chen and D. Chen, "Study of gigabit indoor wireless optical communication system," presented at the International Conference on Computer Science and Network Technology (ICCSNT), 2011.
[64] J. Armstrong, "OFDM for optical communications," *Journal of Lightwave Technology,* vol. 27, pp. 189-204, 2009.
[65] F. M. Wu, C. T. Lin, C. C. Wei, C. W. Chen, Z. Y. Chen, H. T. Huang*, et al.*, "Performance comparison of OFDM signal and CAP signal over high capacity RGB-LED-based WDM visible light communication," *IEEE Photonics Journal,* vol. 5, pp. 7901507-7901507, 2013.
[66] A. H. Azhar, T. Tran, and D. O'Brien, "A Gigabit/s indoor wireless transmission using MIMO-OFDM visible light communications," *IEEE Photonics Technology Letters,* vol. 25, pp. 171-174, 2013.
[67] H. Chun, S. Rajbhandari, G. Faulkner, D. Tsonev, E. Xie, J. J. D. McKendry*, et al.*, "LED based wavelength division multiplexed 10 Gb/s visible light communications," *Journal of Lightwave Technology,* vol. 34, pp. 3047-3052, 2016.
[68] T. Komine. (2005). *Visible light wireless communications and its fundamental study*. Available: http://iroha.scitech.lib.keio.ac.jp:8080/sigma/handle/10721/12/browse?type=dateissued&order=DESC
[69] H. L. Minh, D. O. Brien, G. Faulkner, O. Bouchet, M. Wolf, L. Grobe*, et al.*, "A 1.25-Gb/s indoor cellular optical wireless communications demonstrator," *IEEE Photonics Technology Letters,* vol. 22, pp. 1598-1600, 2010.
[70] K. Wang, A. Nirmalathas, C. Lim, and E. Skafidas, "High-speed optical wireless communication system for indoor applications," *IEEE Photonics Technology Letters,* vol. 23, pp. 519-521, 2011.

[71] F. R. Gfeller and U. Bapst, "Wireless in-house data communication via diffuse infrared radiation," *Proceedings of the IEEE,* vol. 67, pp. 1474-1486, 1979.
[72] J. B. Carruther and J. M. Kahn, "Angle diversity for nondirected wireless infrared communication," *IEEE Transactions on Communications,* vol. 48, pp. 960-969, 2000.
[73] S. Arnon, J. Barry, G. Karagiannidis, R. Schober, and M. Uysal, *Advanced optical wireless communication systems*. Cambridge: Cambridge University Press, 2012.
[74] J. Spragins, *Data communications, computer networks and open systems* vol. 10, 1996.
[75] S. Rajagopal, R. D. Roberts, and S. K. Lim, "IEEE 802.15.7 visible light communication: modulation schemes and dimming support," *IEEE Communications Magazine,* vol. 50, pp. 72-82, 2012.
[76] A. Nuwanpriya, S. W. Ho, J. A. Zhang, A. J. Grant, and L. Luo, "PAM-SCFDE for optical wireless communications," *Journal of Lightwave Technology,* vol. 33, pp. 2938-2949, 2015.
[77] S. Rajbhandari. (2009). *Application of wavelets and artificial neural network for indoor optical wireless communication systems*. Available: http://nrl.northumbria.ac.uk/1933/
[78] M. S. Islim and H. Haas, "Modulation techniques for Li‐Fi," *ZTE Communications,* vol. 14, April 2016 2016.
[79] L. Seongsu and J. Sung-Yoon, "Location awareness using angle-of-arrival based circular-PD-array for visible light communication," presented at the 18th Asia-Pacific Conference on Communications (APCC), 2012.
[80] L. Wang, C. Wang, X. Chi, L. Zhao, and X. Dong, "Optimizing SNR for indoor visible light communication via selecting communicating LEDs," *Optics Communications,* vol. 387, pp. 174-181, 2017.
[81] A. M. Cailean, B. Cagneau, L. Chassagne, V. Popa, and M. Dimian, "Evaluation of the noise effects on visible light communications using Manchester and Miller coding," presented at the International Conference on Development and Application Systems (DAS), 2014.
[82] L. Seok-Ju and J. Sung-Yoon, "A SNR analysis of the visible light channel environment for visible light communication," in *2012 18th Asia-Pacific Conference on Communications (APCC)*, 2012, pp. 709-712.
[83] D. Svilen and H. Harald, *Principles of LED light communications towards networked Li-Fi*, 1st ed.: Cambridge University Press 2015.
[84] H. Le-Minh, Z. Ghassemlooy, A. Burton, F. Mousa, S. Biswas, P. Anh Tuan, *et al.*, "Self-correcting MIMO visible light communications system using localization," in *IEEE International Conference on Communication Workshop (ICCW)*, 2015, pp. 1362-1367.
[85] Z. Lubin, D. O'Brien, M. Hoa, G. Faulkner, L. Kyungwoo, and J. Daekwang, "High data rate multiple input multiple output (MIMO) optical wireless communications using white led lighting," *IEEE Journal Selected Areas in Communications,* vol. 27, pp. 1654-1662, 2009.
[86] M. Biagi, A. M. Vegni, and T. D. C. Little, "LAT indoor MIMO-VLC: Localize, access and transmit," in *International Workshop on Optical Wireless Communications (IWOW)*, 2012, pp. 1-3.
[87] L.-M. Hoa, D. O'Brien, G. Faulkner, Z. Lubin, L. Kyungwoo, J. Daekwang, *et al.*, "100-Mb/s NRZ Visible Light Communications Using a Postequalized White LED," *Photonics Technology Letters, IEEE,* vol. 21, pp. 1063-1065, 2009.
[88] W. D. Zhong, C. Chen, D. Wu, and Z. Ghassemlooy, "MIMO visible light communications system using imaging receiver with angle diversity detectors," in

*2016 15th International Conference on Optical Communications and Networks (ICOCN)*, 2016, pp. 1-3.

[89] K. D. Kulat and D. Shalke, "Performance analysis of ZF and MMSE receiver algorithm," *International Journal of Research in Engineering and Applied Sciences,* vol. 03, p. 10, Jan 2015 2015.

[90] T. Komine and M. Nakagawa, "Fundamental analysis for visible-light communication system using LED lights," *IEEE Transactions on Consumer Electronics,* vol. 50, pp. 100-107, 2004.

[91] J. G. Proakis, M. Salehi, N. Zhou, and X. Li, *Communication systems engineering* vol. 2: Prentice Hall New Jersey, 1994.

[92] N. Kaur and L. Kansal, "Performance comparison of MIMO systems over AWGN and Rician channels with Zero Forcing receivers," *International Journal of Wireless & Mobile Networks (IJWMN)* vol. 5, p. 12, February 2013.

[93] S. Adnan, N. U. Rehman, and M. I. Zahoor, "Effect of different modulation techniques comparison of linear MIMO receivers," *International Journal of Computer Applications* vol. 121, p. 5, July 2015.

[94] P. Bahl and V. N. Padmanabhan, "RADAR: an in-building RF-based user location and tracking system," in *Nineteenth Annual Joint Conference of the IEEE Computer and Communications Societies (INFOCOM 2000)*, 2000, pp. 775-784.

[95] D. Niculescu and B. Nath, "VOR base stations for indoor 802.11 positioning," in *Proceedings of the 10th annual international conference on Mobile computing and networking*, 2004, pp. 58-69.

[96] G. Roussos, "Location sensing technologies and applications," *School of Computer Science and Information Systems, Birkbeck College, University of London,* 2002.

[97] A. Stefio Yosse, E. Joelianto, A. Widyotriatmo, and W. Adiprawita, "Low cost vision-based 3D localization system for indoor unmanned aerial vehicles," in *International Conference on Robotics, Biomimetics, Intelligent Computational Systems*, 2013, pp. 237-241.

[98] G. Félix, M. Siller, and E. N. Álvarez, "A fingerprinting indoor localization algorithm based deep learning," in *Eighth International Conference on Ubiquitous and Future Networks (ICUFN)*, 2016, pp. 1006-1011.

[99] T. V. Haute, E. D. Poorter, F. Lemic, V. Handziski, A. Behboodi, A. Wolisz*, et al.*, "D2.2 Report on experiments without interference," EVARILOS, http://www.evarilos.eu/deliverables.phpOct 2013-July 2014.

[100] R. Murai, T. Sakai, H. Kawano, Y. Matsukawa, Y. Kitano, Y. Honda*, et al.*, "A novel visible light communication system for enhanced control of autonomous delivery robots in a hospital," in *2012 IEEE/SICE International Symposium on System Integration (SII)*, 2012, pp. 510-516.

[101] X. Liu, H. Makino, S. Kobayashi, and Y. Maeda, "Research of Practical Indoor Guidance Platform Using Fluorescent Light Communication," *IEICE Transactions on Communications,* vol. E91.B, pp. 3507-3515, 2008.

[102] L. Xiaohan, H. Makino, and Y. Maeda, "Basic study on indoor location estimation using Visible Light Communication platform," in *30th Annual International Conference of the IEEE Engineering in Medicine and Biology Society (EMBS 2008)* 2008, pp. 2377-2380.

[103] T. Q. Wang, Y. A. Sekercioglu, A. Neild, and J. Armstrong, "Position accuracy of time-of-arrival based ranging using visible light with application in indoor localization systems," *Journal of Lightwave Technology,* vol. 31, pp. 3302-3308, 2013.

[104] C. Yiu-Tong, T. Wing-Yue, S. Hing-Cheung, and C. Pak-chung, "Time-of-arrival based localization under NLOS conditions," *IEEE Transactions on Vehicular Technology,* vol. 55, pp. 17-24, 2006.

[105] J. H. Y. Nah, R. Parthiban, and M. H. Jaward, "Visible light communications localization using TDOA-based coherent heterodyne detection," in *IEEE 4th International Conference on Photonics (ICP)*, 2013, pp. 247-249.
[106] C. Young Hoon, P. In Hwan, K. Yoon Hyun, and J. Y. Kim, "Novel LBS technique based on visible light communications," in *IEEE International Conference on Consumer Electronics (ICCE)*, 2012, pp. 576-577.
[107] G. B. Prince and T. D. C. Little, "A two phase hybrid RSS/AoA algorithm for indoor device localization using visible light," in *IEEE Global Communications Conference (GLOBECOM)*, 2012, pp. 3347-3352.
[108] I. M. S. and K. R., "Indoor positioning through integration of optical angles of arrival with an inertial measurement unit," in *Position Location and Navigation Symposium (PLANS)* 2012, pp. 408-413.
[109] A. Behboodi, P. Crombez, J. J. d. l. Heras, V. H. Eli De Poorter, F. Lemić, I. Moerman*, et al.*, "Evaluation of RF-based indoor localization solutions for the future internet," Lisbon, Portugal, 2013.
[110] S. Yamaguchi, V. V. Mai, T. C. Thang, and A. T. Pham, "Design and performance evaluation of VLC indoor positioning system using optical orthogonal codes," in *IEEE Fifth International Conference on Communications and Electronics (ICCE)*, 2014, pp. 54-59.
[111] E. M. Jeong, S. H. Yang, H. S. Kim, and S. K. Han, "Tilted receiver angle error compensated indoor positioning system based on visible light communication," *Electronics Letters,* vol. 49, pp. 890-892, 2013.
[112] Y.-S. Kuo, P. Pannuto, K.-J. Hsiao, and P. Dutta, "Luxapose: indoor positioning with mobile phones and visible light," presented at the Proceedings of the 20th annual international conference on Mobile computing and networking, Maui, Hawaii, USA, 2014.
[113] S.-Y. Jung, "Indoor localization based on optical wireless transmission technique using light emitting diodes for illumination," MSc. thesis, Gwangju Institute of Science and Technology, 2012.
[114] W. Zhang, "Indoor optical positioning system," PhD diss., The Pennsylvania State University, 2014.
[115] L. Li, P. Hu, C. Peng, G. Shen, and F. Zhao, "Epsilon: A visible light based positioning system," in *Proceedings of the 11th USENIX Conference on Networked Systems Design and Implementation (NSDI 14)*, 2014, pp. 331-343.
[116] Y. Hu, Y. Xiong, W. Huang, X. Y. Li, Y. Zhang, X. Mao*, et al.*, "Lightitude: Indoor positioning using ubiquitous visible lights and COTS devices," in *IEEE 35th International Conference on Distributed Computing Systems (ICDCS)*, 2015, pp. 732-733.
[117] S. H. Yang, D. R. Kim, H. S. Kim, Y. H. Son, and S. K. Han, "Visible light based high accuracy indoor localization using the extinction ratio distributions of light signals," *Microwave and Optical Technology Letters $V 55,* pp. 1385-1389, 2013.
[118] S. H. Yang, E. M. Jeong, D. R. Kim, H. S. Kim, Y. H. Son, and S. K. Han, "Indoor three-dimensional location estimation based on LED visible light communication," *Electronics Letters,* vol. 49, pp. 54-56, 2013.
[119] Y. Se-Hoon, K. Deok-Rae, K. Hyun-Seung, S. Yong-Hwan, and H. Sang-Kook, "Indoor positioning system based on visible light using location code," in *Fourth International Conference on Communications and Electronics (ICCE)* 2012, pp. 360-363.
[120] C. Sertthin, T. Ohtsuki, and M. Nakagawa, "6-Axis sensor assisted low complexity high accuracy visible light communication based indoor positioning system," *IEICE,* vol. E93-B, pp. 1745-1345, 2010.

[121] C. Sertthin, E. Tsuji, M. Nakagawa, S. Kuwano, and K. Watanabe, "A switching estimated receiver position scheme for visible light based indoor positioning system," in *4th International Symposium on Wireless Pervasive Computing (ISWPC 2009)*, 2009, pp. 1-5.

[122] C. Sertthin, T. Ohtsuki, and M. Nakagawa, "6-Axis sensor assisted low complexity high accuracy visible light communication based indoor positioning system " *IEICE,* vol. E93-B, pp. 1745-1345, November 2010.

[123] D. Iturralde, I. Soto, D. Fuentealba, J. Bravo, and N. Becerra, "A new system based on web services and RFID for tracking people in a pervasive mining environment," in *2013 IEEE Latin-America Conference on Communications*, 2013, pp. 1-5.

[124] J. Soo-Yong, C. Chang-Kuk, H. Sang Hu, L. Seong Ro, and P. Chang-Soo, "Received signal strength ratio based optical wireless indoor localization using light emitting diodes for illumination," in *IEEE International Conference on Consumer Electronics (ICCE)*, 2013, pp. 63-64.

[125] H. Swook, K. Jung-Hun, J. Soo-Yong, and P. Chang-Soo, "White LED ceiling lights positioning systems for optical wireless indoor applications," in *36th European Conference and Exhibition on*, *Optical Communication (ECOC),* 2010, pp. 1-3.

[126] Y. Se-Hoon, J. Eun-Mi, and H. Sang-Kook, "Indoor location estimation based on LED visible light communication using multiple optical receivers," *IEEE Communications Letters,* vol. 17, pp. 1834-1837, 2013.

[127] W. Gu, M. Kavehrad, and M. Aminikashani, "Three dimensional indoor light positioning algorithm based on nonlinear estimation," *SPIE Opt. Eng.,* vol. 9772, pp. 97720-1-97720-6, 2016.

[128] D. Iturralde, C. Azurdia-Meza, N. Krommenacker, I. Soto, Z. Ghassemlooy, and N. Becerra, "A new location system for an underground mining environment using visible light communications," presented at the 9th International Symposium on Communication Systems, Networks & Digital Signals Processing (CSNDSP), 2014.

[129] K. Wang, A. Nirmalathas, C. Lim, and E. Skafidas, "Experimental demonstration of a novel indoor optical wireless localization system for tracking multiple users," in *Proceedings of the International Quantum Electronics Conference and Conference on Lasers and Electro-Optics*, Sydney, 2011, p. C556.

[130] K. Wang, A. Nirmalathas, C. Lim, and E. Skafidas, "Experimental demonstration of a centralized optical wireless indoor localization system for high-speed communications in personal areas," in *18th OptoElectronics and Communications Conference held jointly with International Conference on Photonics in Switching (OECC/PS)*, 2013, pp. 1-2.

[131] K. Wang, A. Nirmalathas, C. Lim, and E. Skafidas, "Indoor optical wireless localization system for high-speed personal area networks," in *IEEE Photonics Society Summer Topical Meeting Series*, 2012, pp. 78-79.

[132] M. Saadi, L. Wuttisittikulkij, Z. Yan, K. Panlek, K. Woradit, and P. Sangwongngam, "Performance analysis of optical wireless communication system using pulse width modulation," in *10th International Conference on Electrical Engineering/ Electronics, Computer, Telecommunications and Information Technology (ECTI-CON)*, 2013, pp. 1-5.

[133] W. Zhang and M. Kavehrad, "A 2-D indoor localization system based on visible light LED," in *IEEE Photonics Society Summer Topical Meeting Series*, 2012, pp. 80-81.

[134] W. Zhang, M. I. S. Chowdhury, and M. Kavehrad, "Asynchronous indoor positioning system based on visible light communications," *Optical Engineering,* vol. 53, pp. 045105-045105, 2014.

[135] P. Luo, M. Zhang, X. Zhang, G. Cai, D. Han, and Q. Li, "An indoor visible light communication positioning system using dual-tone multi-frequency technique," in

*2013 2nd International Workshop on Optical Wireless Communications (IWOW)*, 2013, pp. 25-29.

[136] J. Lim, "Ubiquitous 3D positioning systems by led-based visible light communications," *IEEE Wireless Communications,* vol. 22, pp. 80-85, 2015.

[137] B. Lin, X. Tang, Z. Ghassemlooy, Y. Li, and S. Zhang, "An indoor VLC positioning system based on OFDMA," in *Asia Communications and Photonics Conference* Wuhan, 2016, p. AS1B.5.

[138] W. Gu, M. A. Kashani, and M. Kavehrad, "Multipath reflections analysis on indoor visible light positioning system," *arXiv preprint arXiv:1504.01192,* 2015.

[139] W. Gu, M. Aminikashani, and M. Kavehrad, " Impact of multipath reflections on the performance of indoor visible light positioning systems," *arXiv* vol. arXiv:1505.07534v1, p. 10, 2015.

[140] M. A. Elkarim, N. A. Mohammed, and M. H. Aly, "Exploring the performance of indoor localization systems based on VLC-RSSI, including the effect of NLOS components using two light-emitting diode lighting systems," *Opt. Eng.,* vol. 54, p. 9, 2015.

[141] K. Y. Yi, D. Y. Kim, and K. M. Yi, "Development of a localization system based on VLC technique for an indoor environment," *J. Electr. Eng. Technol,* vol. 10, pp. 436-442, 2015.

[142] Z. Zhou, M. Kavehrad, and P. Deng, "Indoor positioning algorthim using light-emitting diode visible light communications," *Optical Engineering,* vol. 51, p. 6, August 2012.

[143] M. Aminikashani, W. Gu, and M. Kavehrad, "Indoor location estimation with optical-based OFDM communications," *arXiv preprint arXiv:1506.07571,* 2015.

[144] W. G. Mohammadreza A. Aminikashani , Mohsen Kavehrad, "Indoor Positioning in High Speed OFDM Visible Light Communications," *CoRR,* vol. abs/1505.01811, 2015.

[145] W. Xu, J. Wang, H. Shen, H. Zhang, and X. You, "Indoor positioning for multiphotodiode device using visible light communications," *IEEE Photonics Journal,* vol. 8, pp. 1-11, 2016.

[146] J. Ding, Z. Huang, and Y. Ji, "Evolutionary algorithm based power coverage optimization for visible light communications," *IEEE Communications Letters,* vol. 16, pp. 439-441, 2012.

[147] D. Wu, Z. Ghassemlooy, M. H. Le, S. Rajbhandari, and C. Lu, "Channel characteristics analysis of diffuse indoor cellular optical wireless communication systems," *Proc. of SPIE,* vol. 8309, 2011.

[148] T. Borogovac, M. Rahaim, and J. B. Carruthers, "Spotlighting for visible light communications and illumination," in *IEEE Globecom Workshops*, 2010, pp. 1077-1081.

[149] D. Wu, "Cellular indoor optical wireless communication system," PhD, Physical ans Electrical, Northumbria university, 2013.

[150] T. Borogovac, M. B. Rahaim, M. Tuganbayeva, and T. D. C. Little, ""Lights-off" visible light communications," in *IEEE GLOBECOM Workshops (GC Wkshps)*, 2011, pp. 797-801.

[151] D. Wu, Z. Ghassemlooy, W. d. Zhong, and C. Chen, "Cellular indoor OWC systems with an optimal lambertian order and a handover algorithm," in *7th International Symposium on Telecommunications (IST)* 2014, pp. 777-782.

[152] D. Wu, Z. Ghassemlooy, W.-D. Zhong, M. A. Khalighi, H. L. Minh, C. Chen*, et al.*, "Effect of optimal lambertian order for cellular indoor optical wireless communication and positioning systems," *Optical Engineering,* vol. 55, pp. 066114-066114, 2016.

[153] A. C. Boucouvalas, "IEC 825-1 eye safety classification of some consumer electronic products," in *IEE Colloquium on Optical Free Space Communication Links*, 1996, pp. 13/1-13/6.
[154] I. E. Commission, "Standard: IEC 60825-1: safety of laser products-part 1: equipment classification and requirements," ed, 2014, p. 224.
[155] Findchips. (1996, 10/01/2017). *155 MBPS Transimpedance Amplifier*. Available: https://www.digchip.com/datasheets/parts/datasheet/041/AD8015.php
[156] A. Tsiatmas, C. P. M. J. Baggen, F. M. J. Willems, J. P. M. G. Linnartz, and J. W. M. Bergmans, "An illumination perspective on visible light communications," *IEEE Communications Magazine,* vol. 52, pp. 64-71, 2014.
[157] A. T. Hussein, M. T. Alresheedi, and J. M. H. Elmirghani, "20 Gb/s mobile indoor visible light communication system employing beam steering and computer generated holograms," *Journal of Lightwave Technology,* vol. 33, pp. 5242-5260, 2015.
[158] K. Cui, G. Chen, Z. Xu, and R. D. Roberts, "Line-of-sight visible light communication system design and demonstration," in *7th International Symposium on Communication Systems, Networks & Digital Signal Processing (CSNDSP 2010)*, 2010, pp. 621-625.
[159] P. Chvojka, S. Zvanovec, P. A. Haigh, and Z. Ghassemlooy, "Channel characteristics of visible light communications within dynamic indoor environment," *Journal of Lightwave Technology,* vol. 33, pp. 1719-1725, 2015.
[160] Z. Ghassemlooy, W. O. Popoola, and S. Rajbhandari, *Optical wireless communications-system and channel modelling with Matlab,*: CRC publisher, 2012.
[161] C. Mekhiel and X. Fernando, "LED beam steering for Li-Fi communications," in *IEEE 21st International Workshop on Computer Aided Modelling and Design of Communication Links and Networks (CAMAD)*, 2016, pp. 237-241.
[162] A. Burton, M. Hoa Le, Z. Ghassemlooy, E. Bentley, and C. Botella, "Experimental demonstration of 50-Mb/s visible light communications using 4x4 MIMO," *IEEE Photonics Technology Letters,* vol. 26, pp. 945-948, 2014.
[163] D. Tsonev, S. Sinanovic, and H. Haas, "Practical MIMO capacity for indoor optical wireless communication with white LEDs," in *IEEE 77th Vehicular Technology Conference (VTC Spring)*, 2013, pp. 1-5.
[164] A. J. Menezes, S. A. Vanstone, and P. C. V. Oorschot, *Handbook of Applied Cryptography*: CRC Press, Inc., 1996.
[165] B. Lynn Margaret, "Introduction," in *Public key cryptography: Applications and attacks*, 1st ed: Wiley-IEEE Press, 2013, pp. 1-11.
[166] B. A. John and J. Rolf, "Cryptology: Fubswrorjb," in *Understanding Information Transmission*, 1st ed: Wiley-IEEE Press, 2005, pp. 211-240.
[167] B. Schneier, *Applied cryptography: Protocols, algorithms and Source Code in C*, 1st ed.: Wiley, 2015.
[168] R. E. Blahut, *Cryptography and Secure Communication*, 1 ed. New York: Cambridge University Press, 2014.
[169] R. D. Dorothy Elizabeth, *Cryptography and Data security*. Boston, MA, USA: Addison-Wesley Longman 1983.
[170] R. A. Mollin, *An introduction to cryptography*, 1 ed. Boca Raton: Chapman & Hall/CRC, 2007.
[171] N. A. Boudriga, *Security of mobile communications*, 1 ed. Boca Raton, Fla: Auerbach Publications Boston, MA, USA, 2010.
[172] B. Lynn Margaret, "Congruence equations," in *Public Key Cryptography: Applications and Attacks*, 1st ed: Wiley-IEEE Press, 2013, pp. 13-43.

[173] A. Al Hasib and A. M. Haque, "A comparative study of the performance and security issues of AES and RSA cryptography," in *Third International Conference on Convergence and Hybrid Information Technology ( ICCIT '08)*, 2008, pp. 505-510.
[174] R. Patidar and R. Bhartiya, "Modified RSA cryptosystem based on offline storage and prime number," in *IEEE International Conference on Computational Intelligence and Computing Research*, 2013, pp. 1-6.
[175] S. Sharma, P. Sharma, and R. S. Dhakar, "RSA algorithm using modified subset sum cryptosystem," in *2nd International Conference on Computer and Communication Technology (ICCCT-2011)*, 2011, pp. 457-461.
[176] W. Ren and Z. Miao, "A hybrid encryption algorithm based on DES and RSA in bluetooth communication," in *Second International Conference on Modeling, Simulation and Visualization Methods*, 2010, pp. 221-225.
[177] S. A. Nagar and S. Alshamma, "High speed implementation of RSA algorithm with modified keys exchange," in *6th International Conference on Sciences of Electronics, Technologies of Information and Telecommunications (SETIT)*, 2012, pp. 639-642.
[178] B. P. U. Ivy, P. Mandiwa, and M. Kumar, "A modified RSA cryptosystem based on 'n' prime numbers," *International Journal Of Engineering And Computer Science (ISSN),* vol. 1, p. 4, Nov. 2012.
[179] F. Mousa, S. Tran The, A. Burton, M. Hoa Le, Z. Ghassemlooy, T. Q. Duong*, et al.*, "Investigation of data encryption impact on broadcasting visible light communications," in *9th International Symposium on Communication Systems, Networks & Digital Signal Processing (CSNDSP)*, 2014, pp. 390-394.
[180] C. H. Lin, S. H. Tsai, and Y. P. Lin, "Secure MIMO transmission via compressive sensing," in *IEEE International Conference on Communications (ICC)*, 2015, pp. 7383-7387.
[181] N. Muhammad, J. M. Zain, and M. Y. Mohd Saman, "Loop-based RSA key generation algorithm using string identity," in *13th International Conference on Control, Automation and Systems (ICCAS)*, 2013, pp. 255-258.
[182] E. Poonguzhali, A. Priyadarsini, P. Magnifique, and S. Asvini, "A security model for timing attack in cloud environment," in *International Conference on Innovations in Information, Embedded and Communication Systems (ICIIECS)*, 2015, pp. 1-5.
[183] H. Dahui and D. Zhiguo, "An improved Kerberos protocol based on fast RSA algorithm," in *IEEE International Conference on Information Theory and Information Security*, 2010, pp. 274-278.
[184] B. Lynn Margaret, "The RSA scheme," in *Public key cryptography: Applications and attacks*, ed: Wiley-IEEE Press, 2013, pp. 59-79.
[185] L. Li, P. Hu, C. Peng, G. Shen, and F. Zhao, "Epsilon: A visible light based positioning system," in *Proceedings of the 11th USENIX Conference on Networked Systems Design and Implementation* 2015, pp. 331-343